Numéro d'ordre: 2016LYSEC41 **Année: 2016**

Ecole Centrale de Lyon

Ecole Doctorale MEGA
(Mécanique, Energétique, Génie Civil et Acoustique)

THESIS

Elastic wave propagation in periodic structures through numerical and analytical homogenization techniques

Xiangkun Sun

en vue d'obtenir le titre de

DOCTEUR DE L'ECOLE CENTRALE DE LYON

Spécialité: **Génie Mécanique**

Devant le jury composé de

Abdelkhalak EL HAMI	Professeur, INSA de Rouen	Rapporteur
Mohamed FARHLOUL	Professeur, Université de Moncton, Canada	Rapporteur
Michel MASSENZIO	Professeur, IUT Lyon 1	Président
Olivier BAREILLE	Maitre de conférence, LTDS, ECL	Examinateur
Mohamed ICHCHOU	Professeur, LTDS, ECL	Directeur
Abdel-malek ZINE	Maitre de conférence, ICJ, ECL	Co-directeur
Jean-pierre LAINE	Maitre de conférence, LTDS, ECL	Co-encadrant

Acknowledgements

Three years of Ph.D life have been pasted. During the last three years, what I have gained are not only the research results, but also the priceless memory in France and the precious friendship at Ecole Centrale de Lyon.

First of all, I would like to express my deepest gratitude to my thesis advisor Mohammed Ichchou and Abdel-Malek Zine. Prof. Ichchou, he managed the whole thesis for me, he guided me out of the research difficulties, and he pushed me forward with his rigorous research attitude. Dr. Zine, he helped me a lot in mathematics, he showed me a great example of rigorous mathematician with his kindness and patience. Without their help, I can never finish my Ph.D study. I am really appreciated for their help. Secondly, my sincere thanks goes to all the members of the jury for their gentleness of being the jury of my Ph.D defence, especially for the two reviewers. Thanks them for the patient reading of my thesis, for their approval of my job, and for their precious advice in amelioration of my work. Thirdly, I am grateful to Dr. Lainé. Even he is not my official supervisor, he was present during my regular research reports, we discussed together frequently, and he helped me a lot in correcting my defence power-point and defence speech.

I am also very fortunate to have so many amazing colleagues in LTDS. Zhou Changwei, as I worked in the analytical aspect of structure vibration, her work in numerical field provides me the reference to compare with. Fan Yu, he taught me numerous techniques in dealing with different structures, and gave me an abundant supply of study resources. Zakaria, Omar, Anna-Rita, Régis, they make me feel comfortable, and we formed an enjoyable working atmosphere. And the other friends in LTDS: Huang Xingrong, Yi Kaijun, Yang Yifan, Shen Zihan, Chai Wenqi, Meng Han, Hui Yi, Zhu guang, You Weizhen, Liu Jiuzhou, thanks them for their help in preparing my defence. And of course many other friends at ECL: Qu Bo, Xie Baolin, Li Bo, Zhou Lu, Zhang Lu, etc. I would like to express my thankfulness to all of my friends.

A particular acknowledgement has to be made to my dear parents. They trust me, encourage me, and support me, even I haven't been back home during the whole three years. I would also express my thanks to my girlfriend Zhao Xin. Her company makes my life more wonderful and makes me different.

At last, I gratefully acknowledge Chinese Scholarship Council (CSC) for providing the funding source to support my Ph.D work.

Abstract

In this work, the multi-scale homogenization method, as well as various non homogenization methods, will be presented to study the dynamic behaviour of periodic structures. The multi-scale method starts with the scale-separation, which indicates a micro-scale to describe the local behaviour and a macro-scale to describe the global behaviour. According to the homogenization theory, the long-wave assumption is used, and the unit cell length should be much smaller than the characteristic length of the structure. Thus, the valid frequency range of homogenization is limited to the first propagating zone. The traditional homogenization model makes use of material properties' mean values, but the practical validity range is far less than the first Bragg band gap. This deficiency motivated the development of new enriched homogenized models. Compared to traditional homogenization model, higher order homogenized wave equations are proposed to provide more accuracy homogenized models.

Two multi-scale methods are introduced: the asymptotic expansion method, and the homogenization of periodic discrete media method (HPDM). These methods will be applied sequentially in longitudinal wave cases in bi-periodic rods and flexural wave cases in bi-periodic beams. Same higher order models are obtained by the two methods in both cases. Then, the proposed models are validated by investigating the dispersion relation and the frequency response function. Analytical solutions and wave finite element method (WFEM) are used as references. Parametric studies are carried out in the infinite case while two different boundary conditions are considered in the finite case.

Afterwards, the HPDM and the CWFEM are employed to study the longitudinal and transverse vibrations of framed structures in 1D case and 2D case. The valid frequency range of the HPDM is re-evaluated using the wave propagation feature identified by the CWFEM. The relative error of the wavenumber by HPDM compared to CWFEM is illustrated in the function of frequency and scale ratio. Parametric studies on the thickness of the structure is carried out through the dispersion relation. The dynamics of finite structures are also investigated using the HPDM and CWFEM.

keyword: multi-scale homogenization, periodic structure, framed structure, longitudinal vibration, transverse vibration.

Résumé

Dans ce travail, la méthode homogénéisation de multi-échelle, ainsi que diverses méthodes non homogénéisation, seront présentés pour étudier le comportement dynamique des structures périodiques. La méthode de multi-échelle commence par la séparation d'échelles. Dans ce cas, une échelle microscopique pour décrire le comportement local et une échelle macroscopique pour décrire le comportement global sont introduites. D'après la théorie de l'homogénéisation, la longueur d'onde est supposée grande, et la longueur de la cellule doit être beaucoup plus petite que la longueur caractéristique de la structure. Ainsi, le domaine d'homogénéisation est limité à la première zone de propagation. Le modèle d'homogénéisation traditionnel utilise des valeurs moyennes des éléments, mais le domaine de validité pratique est beaucoup plus petit que la première bande interdite. Alors, le développement de nouveaux modèles homogénéisés est beaucoup motivé par cet inconvénient. Par rapport au modèle d'homogénéisation traditionnel, équations d'ordre supérieur sont proposées pour fournir des modèles homogénéisation plus précises.

Deux méthodes multi-échelles sont introduites: la méthode de développement asymptotique, et la méthode de l'homogénéisation des milieux périodiques discrètes (HMPD). Ces méthodes seront appliquées de façon séquentielle dans le cas d'onde longitudinale et le cas d'onde transversale. Les mêmes modèles d'ordre supérieur sont obtenus par les deux méthodes dans les deux cas. Ensuite, les modèles proposés sont validés en examinant la relation de dispersion et de la fonction de réponse fréquentielle. Des solutions analytiques et la méthode des ondes éléments finis(WFEM) sont utilisés pour donner les références. Des études paramétriques sont effectuées dans le cas infini, et deux différentes conditions aux limites sont prises en compte dans le cas fini.

Ensuite, le HMPD et CWFEM sont utilisés pour étudier les vibrations longitudinales et transversales des structures réticulées dans le cas 1D et 2D. Le domaine de validité du HPDM est réévalué à l'aide de la fonction de propagation identifiée par le CWFEM. L'erreur relative au nombre d'onde obtenue par HPDM est illustré sur la fonction de la fréquence et le rapport d'échelle. Des études paramétriques sur l'épaisseur de la structure sont réalisées par la relation de dispersion. La dynamique des structures finies sont également étudiés en utilisant la HPDM et CWFEM.

keyword: multi-échelle homogénéisation, structure périodique, structure réticulées, vibration longitudinales, vibration transversale.

Contents

List of Figures

List of Tables

Abbreviations

1D	One Dimensional
IBZ	Irreducible Brillouin Zone
PWE	Plane-Wave Expansion method
TMM	Transfer Matrix Method
FEM	Finite Element Method
WFEM	Wave Finite Element Method
CWFEM	Condensed Wave Finite Element Method
DOF	Degree of Freedom
HPDM	Homogenization of Periodic Discrete Media
HOH1	Higher Order Homogenized model One
HOH2	Higher Order Homogenized model Two
TH	Traditional Homogenized model
PDE	Partial Differential Equation
MAC	Modal Assurance Criterion

Introduction

The periodic structure, which consists of a number of identical elements repeatedly joined together in one dimension or two dimensions, possess very rich dynamic behaviour. It may consist of rods, beams, flat plates with different support boundary conditions. The simplest structures transmit vibrational energy by only one type wave, while in other wave-guides, the energy may be carried by combined waves. When encountering a discontinuity in the periodic structure, the various propagating waves reflect and interact between each other. The changeable wave propagation process leads to abundant dynamic behaviour. Because of the rich dynamic behaviour, the periodic structure are widely employed in the industry domains, such as aeronautics, civil engineering, material science and biomechanics. In recent years, the periodic structure has experienced a recovery with the introduction of phononic crystals [1–4], and the study of acoustic metamaterials [5]. Besides, the technique developed for the treatment of damping in structural dynamics provides a rich resource for application of wave propagation in periodic structures.

The most known characteristic of periodic structures is the non propagating frequency range caused by wave reflection at the periodic interface. The periodicity makes the material impedance mismatches. Thus, the analysis of periodic structures are relatively more difficult and onerous due to anisotropy and heterogeneity when compared with isotropic and homogeneous structures. Thus, efforts have been made to develop effective homogeneous models.

The homogenization theory aims at averaging out the global material properties without much local details. The research about the theory starts with [6, 7]. Based on these works, a number of different perspectives on the averaging process have been motivated, such as the multi-scale asymptotic expansion (which will be discussed in this work), the idea of compensated compactness [8, 9], the variational method, the method of two-scale convergence [10] and the periodic unfolding technique [11]. In classical homogenization theory, the physical parameters are expanded into power series of the scale separation. The leading order, which is called the homogenized solution, is used to determine the macroscopic behaviour. In this case, the solution flux (stress) depends on the gradient (strain) only. However, when the contrast of the material properties

of the given periodic structure varies, higher order solutions are needed to describe correctly the contrast change. In this work, the higher order homogenization models for longitudinal waves and flexural waves in periodic structures are given by two different methods. The two different methods prove each other by obtaining the same higher order models. Then more complicated 1D and 2D framed structures are also discussed.

Outlines of the thesis

In chapter 1, the results of conducted literature review are presented. The survey concerns the filter characteristic of periodic structures. Existing analytical techniques, numerical tools to study periodic structures are then introduced. Afterwards, some traditional homogenization ideas are presented, and the existing homogenized models at low frequency and high frequency are discussed. At last, the technique of HPDM is presented in the uniform structure case.

In chapter 2, longitudinal waves in bi-periodic rod is discussed. Both HPDM and multi-scale asymptotic expansion method are applied in this case to deduce higher order homogenization models. The two methods lead to the same homogenized models. Afterwards, these models are validated through comparing the dispersion relation, where the references are analytical solution or numerical WFEM solution. At last, some implementations of these models in finite case are discussed and a more accurate homogenized model for the longitudinal case is given.

In chapter 3, flexural waves in bi-periodic beam is discussed. The same higher order homogenized models are deduced by HPDM and multi-scale asymptotic expansion method. With the higher order models, the associated dispersion relations are used to valid the enriched models. By comparing with the WFEM results, validity ranges of these models are given during the parametric study. Then, these models are applied in finite cases. The variational approach formulates appropriate weak forms for these models. Different boundary conditions are considered in different beam cases. At last, a more accurate homogenized model is recommended to simulate the transversal vibration in periodic beams.

In chapter 4, the analytical method HPDM to study the longitudinal and transverse vibrations of a 1D reticulated beam is explained. The homogenized vibration equations

and associated boundary conditions for longitudinal and transverse movement are given. Then, an overview of the numerical CWFEM is discussed and a specified structure is studied by both HPDM and CWFEM. Three different kinds of waves, longitudinal wave, transverse wave, and gyration mode wave, are obtained in the infinite case. The validity range of HPDM are re-evaluated in the finite case.

In chapter 5, the analytical method HPDM implemented on 2D framed structures is presented. Two different characterise frequency ranges are discussed. Pure shear waves at the first frequency range propagate only in the element orientation directions. At the next specific frequency range, pure compressive waves exist only in the orientation direction, while the diagonal waves are shear-compressive waves. Subsequently, an overview of the numerical CWFEM on 2D case is given, and a specified square unit cell formed infinite structure is studied by both CWFEM. The efficiency of HPDM theory is discussed through wave shapes and dispersion relations.

At last, conclusions and perspectives are discussed in chapter 6.

Chapter 1

Literature Review

1.1 Introduction

A periodic structure is a material or structural system which consists of a number of identical elements in space. These periodic elements possess the same internal geometry, the same constituent and they are coupled together in the same way to form the whole system. Some typical examples of periodic structures are composite sandwich panels, airplane fuselage, and phonic crystals. It is Newton's work [12] about the sound propagation in the air and Rayleigh's early study [13] of continuous periodic structures which begin the nearly 300 years' history for the study of periodic materials. From then on, a great quantity of work has been achieved on the theory, the conception and the analysis techniques for the study of periodic structures. During the 1900s, the two most motivating applications of periodic structures are composite materials [14, 15] and aircraft structures [16]. Other areas related to mechanical and civil engineering include multiblade turbines [17–19], impact resistant foam cellular materials [20–23], periodic foundations for buildings [24], and multistory buildings and multispan bridges [25].

The purpose of this chapter is to present the fundamental filter characteristic of periodic structures, which is the band diagram. Then, some brief introduction of the existing methods is represented, such as plane-wave expansion method, transfer matrix method, wave finite element method, and some homogenization methods.

1.2 Filter characteristic of periodic structure

The filter characteristic of periodic structures, which is also called the band diagram, is the most important wave propagation characteristics in periodic structures. The associated dispersion diagram represents the change in frequency with the wavenumber. It is also called dispersion relation describing the nature of free wave propagation in an elastic medium. Here is a classical example, the one-dimensional periodic lattice with two different types of particles.

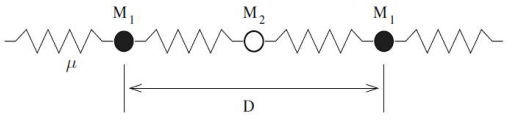

FIGURE 1.1: the 1D "bi-atomic" periodic structure

This typical structure consists of two types of masses, M_1 and M_2, the stiffness of the string is μ , and D is the period. In this elementary cell,u_n and v_n denote the displacement of M_1 and M_2 respectively. The equation of motion for the two particles are as follows:

$$M_1 \frac{\partial^2 u_n}{\partial t^2} - \mu(v_n + v_{n-1} - 2u_n) = 0 \tag{1.1}$$

$$M_2 \frac{\partial^2 v_n}{\partial t^2} - \mu(u_n + u_{n-1} - 2v_n) = 0 \tag{1.2}$$

The Bloch-Floquet theory is largely employed in this kind of periodic structure problem. According to the theory, the solution of the equation satisfies the condition:

$$\begin{aligned} u_{s+n} &= u_s e^{inK} \\ v_{s+n} &= v_s e^{inK} \end{aligned} \tag{1.3}$$

And the solution is referred to as the Bloch-Floquet wave. K is said to be the Bloch parameter, s and n denote the integer. Supposing the solution is time harmonic, then:

$$\begin{aligned} u_n &= U e^{i(nKD-\omega t)} \\ v_n &= V e^{i(nKD-\omega t)} \end{aligned} \tag{1.4}$$

Substituting Eq. (1.4) into Eq. (1.1) and (1.2), we have:

$$\begin{aligned}(\omega^2\mu^{-1}M_1 - 2)U + (1 + e^{-iKD})V = 0\\ (1 + e^{iKD})U + (\omega^2\mu^{-1}M_2 - 2)V = 0\end{aligned} \tag{1.5}$$

This is a linear algebraic equation system with respect to U and V, and it can be conveniently expressed in the following matrix form:

$$MX = 0 \tag{1.6}$$

where

$$M = \begin{bmatrix} \omega^2\mu^{-1}M_1 - 2 & 1 + e^{-iKD} \\ 1 + e^{iKD} & \omega^2\mu^{-1}M_2 - 2 \end{bmatrix} \quad X = \begin{pmatrix} U \\ V \end{pmatrix} \tag{1.7}$$

This equation system has a non-trivial solution if and only if the $Det(M) = 0$, which yields:

$$\frac{M_1M_2}{\mu^2}\omega^4 - \frac{2(M_1 + M_2)}{\mu}\omega^2 + 2(1 - cos(KD)) = 0 \tag{1.8}$$

This is the dispersion equation providing the relation between ω and K. The explicit solution is:

$$\omega^2 = \mu\frac{M_1 + M_2 \pm \sqrt{(M_1 + M_2)^2 - 2M_1M_2(1 - cos(KD))}}{M_1M_2} \tag{1.9}$$

This is the explicit relation between ω and K, and the expression suggests that the corresponding dispersion curve has two branches, as shown in Fig 1.2

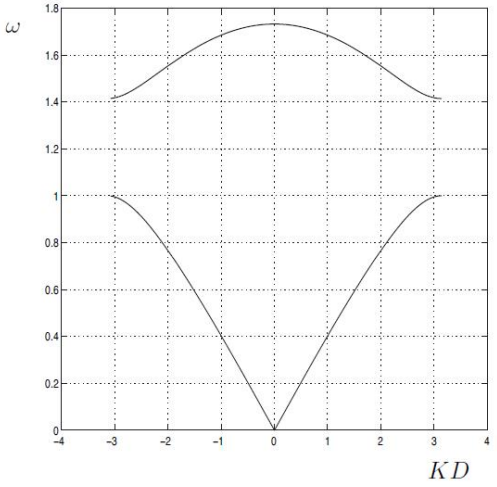

FIGURE 1.2: Dispersion curve for the "bi-atomic" structure, with $M_1 = 1, M_2 = 2, \mu = 1$

From the figure 1.2, we note that there is a separation between the two branches of the dispersion curve, which is called stop band. The Bloch-Floquet wave doesn't exist in the stop band, i.e. the wave possessing the frequency in the interval of stop band cannot propagate in the bi-atomic structure. When the period of the structure is D, the period for the dispersion curve becomes $2\pi/D$. The interval $(-\pi/D, \pi/D)$ is known as the Irreducible Brillouin Zone (IBZ). The width of the stop band can be computed by evaluating the frequency at the boundary of the Brillouin zone, where $K = \pm\pi/D$. Assuming that $M_1 < M_2$, one can deduce that the width of the band gap is $\sqrt{2\mu/M_1} - \sqrt{2\mu/M_2}$. For the bi-atomic periodic system, the Bloch-Floquet waves exist only within the pass band intervals $(0, \sqrt{2\mu/M_2})$ and $(\sqrt{2\mu/M_1}, \sqrt{2\mu(M_1+M_2)/(M_1M_2)})$, and the size of the stop band can be controlled by changing the stiffness of springs and the masses of particles.

The method presented here is a typical analytical approach to study the periodic structure. In fact, during the development history of the methods to study periodic structures, there exist also many other methods. Some of them are analytical, for instance the plane-wave expansion method (PWE), the transfer matrix method (TMM), while some others are numerical, such as the wave finite element method (WFEM). They are the mostly employed method to obtain the dispersion relation of the periodic structure.

1.3 Analytical method to study the periodic structure

1.3.1 Plane-wave expansion method

The plane wave method (PWM) is often used for photonic crystal modelling since it can yield accurate and reliable results [26]. For a one-dimensional periodic structure, the solution is a Bloch wave, which possesses the following form:

$$u(x, k, t) = U(x)e^{i(kx-\omega t)} \tag{1.10}$$

$U(x)$ is the unit-cell Bloch displacement function, and it is periodic over the unit cell. Supposing D the period of the structure, $U(x)$ is a function of period D. Then, it is

expanded into a Fourier series representing the superposition of plane waves of wavenumber $2\pi l/D$, where l is an integer. These plane waves are defined in the reciprocal lattice space of the periodic structure. The main idea of the plane-wave expansion method for continuous systems is to expand the solution field and the material properties into a Fourier series. Then according to the orthogonality of the basis function of Fourier series, an eigenvalue problem is deduced to produce the dispersion relation between the frequency and the wavenumber. The principal idea of the method can be clearly illustrated for an one-dimensional continuous system. In the one-dimensional case, the governing wave equation is as follows:

$$\rho\frac{\partial^2 u}{\partial t^2} = \frac{\partial}{\partial x}(E\frac{\partial u}{\partial x}) \tag{1.11}$$

where $u(x,t)$ denotes the displacement field, $\rho(x)$ denotes the density, and $E(x)$ denotes the Young's Modulus. The material properties $\rho(x)$ and $E(x)$ are assumed to vary periodically with periodicity D. Then one can deduce the expansion of $u(x,t), \rho(x)$ and $E(x)$:

$$u(x,t) = e^{i(kx-\omega t)}\sum_l u_l e^{i\frac{2\pi l}{D}x} \tag{1.12}$$

$$\rho(x) = \sum_m \rho_m e^{i\frac{2\pi m}{D}x} \tag{1.13}$$

$$E(x) = \sum_n E_n e^{i\frac{2\pi n}{D}x} \tag{1.14}$$

Where the l, m, n denote the integer, i denotes the complex number. Substituting these expansion series into Eq. (1.11) leads to:

$$\begin{aligned}&(-\omega^2)\left(\sum_m \rho_m e^{i\frac{2\pi m}{D}x}\right)\cdot\left(\sum_l u_l e^{i\frac{2\pi l}{D}x}\right)\\ =&\sum_n\sum_l -\left(\frac{2\pi l}{D}+k\right)\cdot\left(\frac{2\pi(l+n)}{D}+k\right)\cdot\left(E_n e^{i\frac{2\pi n}{D}x}\right)\cdot\left(u_l e^{i\frac{2\pi l}{D}x}\right)\end{aligned} \tag{1.15}$$

Eq.(1.15) can be simplified by employing the orthogonality of the basis function of Fourier series. For both sides of the equation, forming the product with $e^{-i2\pi qx/D}$, where $q \in I$, and integrating over one spatial period, one can deduce:

$$\sum_l \left(-\omega^2\rho_{q-l} + (k+\frac{2\pi l}{D})(k+\frac{2\pi q}{D})E_{q-l}\right)u_l = 0 \tag{1.16}$$

The expression above is obtained due to the fact that the only nonzero terms in the product are those satisfying $m + l = q$ and $n + l = q$. This is a well-posed eigenvalue problem results. Because the resulting equation system is homogeneous, and the evaluation of non-trivial roots requires the solution of an eigenvalue problem. It can also be expressed in a matrix form as:

$$Mu_l = 0 \tag{1.17}$$

where:

$$M_{q,l} = -\omega^2 \rho_{q-1} + (k + \frac{2\pi l}{D})(k + \frac{2\pi q}{D}) E_{q-l} \tag{1.18}$$

the ρ_{q-l} and E_{q-l} are the Fourier coefficients. Given a value of k in the first Brillouin zone , the solution of the above eigenvalue problem gives the value of ω, which defines the dispersion relations of the considered structure.

1.3.2 Transfer matrix method

Transfer matrix methods are an excellent tool for accurately analysing the wave transmission in periodic media [27]. It has been applied extensively in periodic and quasi-periodic multi-layer media. The method can be well illustrated through a simple one-dimensional periodic structure, as shown in figure (1.3). The periodic structure is form by an infinite repetition of a unit cell with length d. The density of the unit cell is ρ, and the Young's modulus is E.

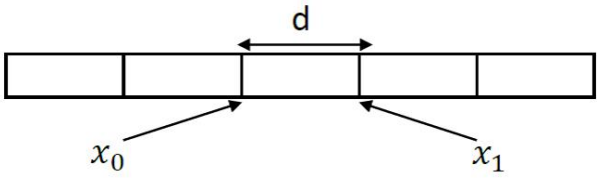

FIGURE 1.3: one-dimensional periodic structure

For each unite cell, the governing equation of such a periodic structure is as follows:

$$\rho \frac{\partial^2 u}{\partial t^2} - E \frac{\partial^2 u}{\partial x^2} = 0 \tag{1.19}$$

with the time-harmonic motion of frequency ω, we have $u(x,t) = U(x)e^{-i\omega t}$. Then the equation can be expressed as follows:

$$\frac{\partial^2 U}{\partial x^2} + \frac{\rho}{E}\omega^2 U = 0 \tag{1.20}$$

The solution of this equation can be written in the following form:

$$U(x) = Aexp(ikx) + Bexp(-ikx) \tag{1.21}$$

with

$$k = \omega c, \quad c = \sqrt{\rho/E} \tag{1.22}$$

Then for each unit cell, we want to find a matrix between the state vectors of the two endpoints. The state vector include the displacement and traction. So, our aim is to find the matrix M in the following expression.

$$\begin{pmatrix} U(x_1) \\ E\frac{\partial U}{\partial x}(x_1) \end{pmatrix} = M \begin{pmatrix} U(x_0) \\ E\frac{\partial U}{\partial x}(x_0) \end{pmatrix} \tag{1.23}$$

With $x_1 = x_0 + d$. According to the solution form of the equation, we have:

$$M = \begin{bmatrix} cos(kd) & \frac{sin(kd)}{Ek} \\ -Eksin(kd) & cos(kd) \end{bmatrix} \tag{1.24}$$

According to the Bloch theory, for 1D periodic structures, the state vectors at the endpoints of a unit cell satisfy the following condition:

$$\begin{pmatrix} U(x_1) \\ E\frac{\partial U}{\partial x}(x_1) \end{pmatrix} = \lambda \begin{pmatrix} U(x_0) \\ E\frac{\partial U}{\partial x}(x_0) \end{pmatrix} \tag{1.25}$$

Substituting the Bloch wave condition (1.25) into Eq.(1.23) leads to the following eigenvalue problem:

$$(M - \lambda I) \begin{pmatrix} U(x_0) \\ E\frac{\partial U}{\partial x}(x_0) \end{pmatrix} = 0 \tag{1.26}$$

The eigenvalue is linked to the wavenumber $\lambda = exp(-ikd)$, and the associated eigenvector is the corresponding wave shape. The caluclation presented here corresponds to the definition of the Bloch wave solution: when a free wave travels along the periodic

structure, the state vector of the two boundaries are related by a propagation constant kd, where k is the Block parameter and d is the period of the structure. Then, with a given interested frequency range, the wave number or the Block parameter k can be deduced by solving the eigenvalue problem of the transfer matrix. The method has been applied to analyse the wave characteristics of periodic Timoshenko beam [28], nonsymmetrical axially loaded thin-walled Euler-Bernoulli beams [29] and periodic structures with local resonators [30, 31].

1.4 Numerical method to study the periodic structure

1.4.1 Wave finite element method(WFEM)

Wave finite element method (WFEM) is a combination of conventional finite element method (FEM) and the Floquet-Bloch theorem which converts the study of a periodic structure into a single unit cell. The method has been applied in various examples, such as thin-wall structures [32, 33], fluid-filled pipes [34] and curved members [35]. A segment of the structure, or the unit cell, can be easily modelled using conventional FE methods, with a commercial FE package. In FEM analysis for wave propagation, the element in the model has to be small enough to make sure that no artificial reflection may occur due to the change in mesh size. Compared to the standard FEM, where the whole structure is meshed, the computational cost of the WFEM is much lower, because only a small segment of the structure, the unit cell, has to be meshed. WFEM takes the advantage of the periodicity condition in the model for structural vibration analysis.

The unit cell of a periodic structure can be various. The criterion for the choice of unit cell is to minimize the number of coupling coordinates, in which case the computational size will be decreased [36, 37]. We consider an one-dimensional structure represented by a finite or infinite number of cells and assume that a single cell is cut from the structure and meshed with an equal number of nodes on the left and right sides. For free wave propagation, there is no external forces being acted on the structure. With the existing FEM procedures, one can obtain explicitly the stiffness matrix, $\mathbf{K}$, the mass matrix, $\mathbf{M}$, and damping matrix, $\mathbf{C}$, of the unit cell. Assuming time-harmonic behaviour

and neglecting damping, the motion equation of the unit cell becomes as follows:

$$(\mathbf{K} - \omega^2 \mathbf{M})\mathbf{q} = \mathbf{f} \tag{1.27}$$

Where $\mathbf{q}$ is the displacement vector, and $\mathbf{f}$ is the loading vector. Introducing the dynamic stiffness matrix $\mathbf{D} = \mathbf{K} - \omega^2 \mathbf{M}$, and decomposing the matrix into boundary and interior degree of freedom, the motion equation results in the following matrix form:

$$\begin{bmatrix} \mathbf{D_{bd}} & \mathbf{D_{bdI}} \\ \mathbf{D_{Ibd}} & \mathbf{D_I} \end{bmatrix} \begin{pmatrix} \mathbf{q_{bd}} \\ \mathbf{q_I} \end{pmatrix} = \begin{pmatrix} \mathbf{f_{bd}} \\ 0 \end{pmatrix} \tag{1.28}$$

$\mathbf{q_{bd}}, \mathbf{q_I}$ are the displacement of the boundary points and interior points. $\mathbf{f_{bd}}$ is the force on boundary from adjacent unit cells. The interior displacement can be condensed using the second row of the expression above:

$$\mathbf{q_I} = -\mathbf{D_I^{-1}} \mathbf{D_{Ibd}} \mathbf{q_{bd}} \tag{1.29}$$

Then the first row of Eq.(1.28) becomes:

$$(\mathbf{D_{bd}} - \mathbf{D_{bdI}} \mathbf{D_I^{-1}} \mathbf{D_{Ibd}}) \mathbf{q_{bd}} = \mathbf{f_{bd}} \tag{1.30}$$

For simplicity, Eq.(1.30) can be rewrite in an equivalent form:

$$\begin{bmatrix} \mathbf{D_{ll}} & \mathbf{D_{lr}} \\ \mathbf{D_{rl}} & \mathbf{D_{rr}} \end{bmatrix} \begin{pmatrix} \mathbf{q_l} \\ \mathbf{q_r} \end{pmatrix} = \begin{pmatrix} \mathbf{f_l} \\ \mathbf{f_r} \end{pmatrix} \tag{1.31}$$

The induce r, l means right boundary and left boundary. According to the Bloch theorem, for free wave propagation, we have:

$$\mathbf{q_r} = \lambda \mathbf{q_l}; \quad \mathbf{f_r} = -\lambda \mathbf{f_l} \tag{1.32}$$

with

$$\lambda = exp(-ikd) \tag{1.33}$$

k is the wavenumber or the Bloch parameter, d is the period of the periodic structure. With equation (1.31) and (1.32), one can deduce a relation between the left state vector

and the right state vector [38]:

$$\mathbf{S}\begin{pmatrix}\mathbf{q_l}\\ \mathbf{f_l}\end{pmatrix}=\begin{pmatrix}\mathbf{q_r}\\ -\mathbf{f_r}\end{pmatrix}=\lambda\begin{pmatrix}\mathbf{q_l}\\ \mathbf{f_l}\end{pmatrix} \tag{1.34}$$

where

$$\mathbf{S}=\begin{pmatrix}-\mathbf{D_{lr}^{-1}D_{ll}} & \mathbf{D_{lr}^{-1}}\\ -\mathbf{D_{rl}}+\mathbf{D_{rr}D_{lr}^{-1}D_{ll}} & -\mathbf{D_{rr}D_{lr}^{-1}}\end{pmatrix} \tag{1.35}$$

Thus, the wavenumber and the frequency are associated to the eigenvalue problem of S. The eigenvalues of S are related to wavenumbers by the equation (1.33). By choosing the interested frequency range, we can obtain the corresponding wavenumber value. Then the dispersion relation in the first Brillouin zone is obtained. The process presented in this section is called the directed form of WEFM in 1D case. The direct form can be used to study the damped structure and the forced response of the structure [39]. THe details of the method for free wave propagation in smiple waveguides with simply-supported edges are preseted in [40]. For complex cross-section, the eigenvalue problem may be poor conditioned. In this case, other alternative formulations are proposed in [41, 42].

1.4.2 Condensed wave finite element method(CWFEM)

When the DOFs are enormous, numerical errors appears and the calculation efficiency is slowed down. To overcome this deficiency, reduced models for the unit cells can be used. The reduced model can be built form modes of the unit cells [43, 44] or waves of other frequencies [39, 45–47], or both [48]. The condensed wave finite element method is actually a combination of the typical wave finite element method [49] and the model order reduction techniques [50, 51]. The model order reduction techniques have been widely used to predict wave propagation characteristics in periodic structure. Especially, when the structure is large-scale, the involved eigenvalue problem becomes much more complex, and the computational effort are badly increased. Thus, several techniques have been developed to speed up band structure calculation, such as the fixed interface component mode synthesis method [51], the free boundary component mode synthesis method [52] and the branch mode method [53] etc. Here the fixed interface component mode synthesis method is chosen to be combined with the wave finite element method. One the one hand, the mode order reduction speeds up the calculation of unite cell

eigenvalue problem. On the other hand, the wave element finite method makes full use of the periodicity of the structure which makes the behaviour of the whole structure can be obtained by transfer relations. By combining these advantages, the condensed wave finite element method makes the associated computation more efficient.

The fixed interface component mode synthesis, which is also known as the Craig-Bampton method, projects internal physical DOFs onto a fixed boundary mode basis. Then the reduced model dynamic stiffness is used in WFEM to study the wave propagation characteristic. With the conventional FEM, the equation of motion can be written in the following manner:

$$\begin{bmatrix} M_{LL} & M_{LR} & M_{LI} \\ M_{RL} & M_{RR} & M_{RI} \\ M_{IL} & M_{IR} & M_{II} \end{bmatrix} \begin{pmatrix} \ddot{q}_L \\ \ddot{q}_R \\ \ddot{q}_I \end{pmatrix} + \begin{bmatrix} K_{LL} & K_{LR} & K_{LI} \\ K_{RL} & K_{RR} & K_{RI} \\ K_{IL} & K_{IR} & K_{II} \end{bmatrix} \begin{pmatrix} q_L \\ q_R \\ q_I \end{pmatrix} = \begin{pmatrix} F_L \\ F_R \\ 0 \end{pmatrix} \tag{1.36}$$

where M and K are mass and stiffness matrices. q_L, q_R, q_I denote the physical DOFs of the left boundary, right boundary and internal nodes. The physical DOFs q_I are then reformulated to a reduced modal basis of modal DOFs, with generalized coordinate P_c. Then a matrix B is used to form the relation between the physical coordinates and the Craig-Bampton hybrid coordinates:

$$\begin{pmatrix} q_L \\ q_R \\ q_I \end{pmatrix} = B \begin{pmatrix} q_L \\ q_R \\ P_c \end{pmatrix} \tag{1.37}$$

with

$$B = \begin{bmatrix} I_n & 0 & 0 \\ 0 & I_n & 0 \\ \Psi_L & \Psi_R & \Psi_c \end{bmatrix} \tag{1.38}$$

Ψ_L, Ψ_R are the boundary mode with

$$\Psi_L = -K_{II}^{-1} K_{IL}, \quad \Psi_R = -K_{II}^{-1} K_{IR} \tag{1.39}$$

Fixed boundary modes Ψ_I are calculated with $q_L = q_R = 0$.

$$[K_{II} - \omega_0^2 M_{II}]\Psi_I = 0 \tag{1.40}$$

Matrix Ψ_c is a reduced basis in Ψ_I with n_I rows and n_c columns. Then the equation of motion can be reduced in the following form:

$$\begin{bmatrix} M^*_{LL} & M^*_{LR} & M^*_{LI} \\ M^*_{RL} & M^*_{RR} & M^*_{RI} \\ M^*_{IL} & M^*_{IR} & M^*_{II} \end{bmatrix} \begin{pmatrix} \ddot{q}_L \\ \ddot{q}_R \\ \ddot{P}_c \end{pmatrix} + \begin{bmatrix} K^*_{LL} & K^*_{LR} & K^*_{LI} \\ K^*_{RL} & K^*_{RR} & K^*_{RI} \\ K^*_{IL} & K^*_{IR} & K^*_{II} \end{bmatrix} \begin{pmatrix} q_L \\ q_R \\ P_c \end{pmatrix} = \begin{pmatrix} F_L \\ F_R \\ 0 \end{pmatrix} \tag{1.41}$$

The new mass matrix as well as the stiffness matrix can be written in the following manner:

$$\begin{bmatrix} M^*_{LL} & M^*_{LR} & M^*_{LI} \\ M^*_{RL} & M^*_{RR} & M^*_{RI} \\ M^*_{IL} & M^*_{IR} & M^*_{II} \end{bmatrix} = B^T \begin{bmatrix} M_{LL} & M_{LR} & M_{LI} \\ M_{RL} & M_{RR} & M_{RI} \\ M_{IL} & M_{IR} & M_{II} \end{bmatrix} B \tag{1.42}$$

The generalized force remains the same:

$$\begin{pmatrix} F^*_L \\ F^*_R \\ 0 \end{pmatrix} = B^T \begin{pmatrix} F_L \\ F_R \\ 0 \end{pmatrix} = \begin{pmatrix} F_L \\ F_R \\ 0 \end{pmatrix} \tag{1.43}$$

Assuming harmonic response, the new reduced equation can be solved with the same method which is mentioned in the last section.

1.5 Homogenization method to study the periodic structure

Homogenization is finding the macroscopic properties of a material that has inhomogeneity on the microscopic scale or more generally, homogenization of a heterogeneous material is a process leading to its macroscopic description with fewer parameters than those needed for a full description of the object. There exists a large number of homogenization methods to study the heterogeneous materials: the equivalent strain energy method [54–56], the mode-based method [57–62], the wave-based method [63], the asymptotic homogenization method, the homogenization of periodic discrete media (HPDM). The main idea of these methods is to find a homogeneous structure with equivalent material properties.

1.5.1 Traditional homogenization method

The equivalent strain energy method aims to replace the periodic structure by an equivalent homogenized model with the same volume. Besides, the stress and the strain tensors of the homogeneous medium are equivalent to the average stress and strain of the unit cell. The average stress and strain of the homogenized model follow the Hooke's law.

$$\bar{\sigma} = D^H \bar{\epsilon} \tag{1.44}$$

where D^H is the effective elastic tensor of the material, σ and ϵ are the average stress and strain of the unit cell. The strain energy stored in the periodic structure and the homogenized model have to be equal. The strain energy of the periodic structure can be computed by numerical method, while the strain energy of the homogenized model can be expressed by σ and ϵ. One can chose some specific boundary conditions to identify the effective elastic tensor. Thus, the effective material properties are determined.

The mode-based method is to determine equivalent model of periodic structures. Firstly, develop a finite element model for some homogeneous solid structures. Secondly, perform the modal analysis for the structure with original properties. Thirdly, compare the frequencies and determine the ratio of frequencies of the structure to those of homogeneous solid structure. At last, find the multipliers of Young's modulus of homogeneous solid structure in order to match the frequencies of the original structure using the relationship between the frequency and Young's modulus.

The wave-based methods is designed to find equivalent flexural and shear stiffness of composite panels. Following classic or modern plate theories, the propagating flexural and shear wavenumber can be expressed as a function of the mechanical characteristics of the structure. With the WFEM, one can calculate the values of propagating wavenumbers for a wide frequency range and then derived the expressions for the equivalent dynamic mechanical characteristics. By comparing the numerical dispersion relation with the equivalent homogeneous expression, one can deduce the equivalent flexural and shear stiffness of the structure.

1.5.2 Low frequency homogenization of 1D periodic structure

Many structures are constructed from composites with periodic, or doubly periodic variations in material parameters. Thus, there is considerable interest in modelling wave propagation in the periodic structure. The wave propagation properties of composite structures has been used in a great number of applications, for example the photonic crystals and the metamaterial. Homogenization is an analytical method to study the periodic structure. The aim is to obtain an equivalent homogeneous material with effective material parameters. The traditional homogenization techniques of asymptotic homogenization is limited to low frequency situations. And the traditional homogenization theory is only capable of describing the fundamental Bloch wave at low frequencies. It can't fully reproduce high frequency dynamic behaviours characteristic of periodic structures, such as strong dispersion, the presence of band gaps or negative refraction. Then the high frequency homogenization method is needed. In this section, both the low frequency homogenization method and the high frequency homogenization method will be illustrated through a one-dimensional structure. And there will be a comparison between the numerical result obtained by WFEM, and the analytical formulation obtained by homogenization methods.

The asymptotic homogenization method is an analytical method, which is also called long wave approximation method. Because at low frequency, the wavelength is large, and the wavenumber tends to zero. The method will be illustrated in a one-dimensional structure show as in figure 1.4 The periodic beam consists of a repetition of section A of

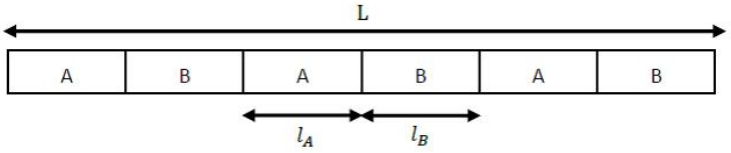

FIGURE 1.4: the binary periodic beam

FIGURE 1.5: the unit cell of periodic beam

length l_A and section B of length l_B. So the period of the structure is l_A+l_B. The length of the whole beam is L. Then the longitudinal motion $u(X,t)$ and the transverse motion

$\omega(X,t)$ of the beam is described by the following set of partial differential equations:

$$\frac{\partial}{\partial X}\left(K(X)\frac{\partial}{\partial X}u(X,t)\right) - m(X)\frac{\partial^2}{\partial t^2}u(X,t) = 0 \tag{1.45}$$

$$\frac{\partial^2}{\partial X^2}\left(D(X)\frac{\partial^2}{\partial X^2}\omega(X,t)\right) + m(X)\frac{\partial^2}{\partial t^2}\omega(X,t) = 0 \tag{1.46}$$

The equation (1.45) is the motion equation of longitudinal wave, and the equation (1.46) is the motion equation of bending wave. $K(X)$, $D(X)$ respectively denote the axial stiffness and the bending stiffness of the beam, while $m(X)$ is the linear mass. According to the configuration of figure 1.4, the generic physical property of the beam $P(X)$ can be expressed as a piecewise function of period $p = l_A + l_B$, ie:

$$P(X) = P(X+p) \tag{1.47}$$

Over a period centred at $x = 0$, $P(X)$ can be expressed as:

$$P(X) = \begin{cases} P_A & -l_A < X < 0 \\ P_B & 0 < X < l_B \end{cases} \tag{1.48}$$

For the unit cell of figure 1.5, we have:

$$\begin{aligned} m(X) &= \begin{cases} \rho_A S_A & -l_A < X < 0 \\ \rho_B S_B & 0 < X < l_B \end{cases} \\ K(X) &= \begin{cases} E_A S_A & -l_A < X < 0 \\ E_B S_B & 0 < X < l_B \end{cases} \\ D(X) &= \begin{cases} E_A J_A & -l_A < X < 0 \\ E_B J_B & 0 < X < l_B \end{cases} \end{aligned} \tag{1.49}$$

where ρ_A and ρ_B are the density of A and B. S_A and S_B are the crosses sectional area of A and B. E_A and E_B are the Young's modulus of A and B. J_A and J_B are the inertia moment of A and B. Then, the state vector z can be defined as:

$$z(X) = (u, \omega, \frac{\partial \omega}{\partial x}, N, M, Q)^T \tag{1.50}$$

where

$$\begin{aligned} N &= k(X)\frac{\partial u}{\partial X} \\ M &= D(X)\frac{\partial^2 \omega}{\partial X^2} \\ Q &= -\frac{\partial M}{\partial X} \end{aligned} \tag{1.51}$$

N is the axial stress, M is the bending moment, and Q is the shear force at location X. Then the equation (1.45) and (1.46) can be combined in the following first order system:

$$A(X)\frac{\partial}{\partial X}z(X) = B(X)z(X) \tag{1.52}$$

where

$$A(X) = diag([K(X), 1, D(X), 1, -1, 1]) \tag{1.53}$$

$$B(X) = \begin{bmatrix} 0 & 0 & 0 & 1 & 0 & 0 \\ 0 & 0 & 1 & 0 & 0 & 0 \\ 0 & 0 & 0 & 0 & 1 & 0 \\ -\omega^2 m(X) & 0 & 0 & 0 & 0 & 0 \\ 0 & 0 & 0 & 0 & 0 & 1 \\ 0 & -\omega^2 m(X) & 0 & 0 & 0 & 0 \end{bmatrix} \tag{1.54}$$

Equation (1.52) can also be rewritten as:

$$\frac{\partial}{\partial X}z(X) = C(X)z(X) \tag{1.55}$$

where

$$C(X) = A(X)^{-1}B(X) \tag{1.56}$$

$C(X)$ is a periodic matrix, because $A(X)$ and $B(X)$ are composed of the periodic physical properties: $K(X)$, $D(X)$ and $m(X)$. Under the long wavelength approximation, the deduction of effective properties starts with the introducing of two scales. We introduce $x = X$ and $y = x/\epsilon$, $u(X) = u(x, y)$ is no longer x-periodic . The second scale y describes the periodicity of u, with the definition $\epsilon = p/L$, where p is the period of the structure, L is the length of the structure. Accordingly, equation (1.55) is expressed as:

$$\frac{\partial}{\partial X}z(x, y) = C(x, y)z(x, y) \tag{1.57}$$

In the long wavelength approximation, however, there exist a large number of unit cell

in a wavelength. So, the properties of the beam can be considered as homogeneous, i.e. $C(x, y)$ depends no longer on x.

$$C(x, y) \approx C(y) \tag{1.58}$$

Next, the state vector is expanded according to the two-scale expansion:

$$z(X) = z_0(x, y) + \epsilon z_1(x, y) + \epsilon^2 z_2(x, y) + \dots \tag{1.59}$$

and the spatial derivative in equation (1.57) is rewritten as:

$$\frac{\partial}{\partial X} = \frac{\partial}{\partial x} + \frac{1}{\epsilon}\frac{\partial}{\partial y} \tag{1.60}$$

Substituting equation (1.59) and (1.60) in equation (1.57) gives:

$$\frac{1}{\epsilon}\frac{\partial}{\partial y}z_0 + \frac{\partial}{\partial x}z_0 + \frac{\partial}{\partial y}z_1 + \epsilon\frac{\partial}{\partial x}z_1 + \dots = C(y)(z_0 + \epsilon z_1 + \dots) \tag{1.61}$$

Which leads to the following set of ordered equations:

$$\epsilon^{-1} : \frac{\partial}{\partial y}z_0 = 0 \tag{1.62}$$

$$\epsilon^{0} : \frac{\partial}{\partial x}z_0 + \frac{\partial}{\partial y}z_1 = C(y)z_0 \tag{1.63}$$

$$\epsilon^{1} : \frac{\partial}{\partial x}z_1 + \frac{\partial}{\partial y}z_2 = C(y)z_1 \tag{1.64}$$

$$\dots\dots$$

Equation (1.62) implies that:

$$z_0(x, y) = z_0(x) \tag{1.65}$$

Then integrating both side of equation (1.63) with respect to y over a period p. In the example of figure 1.5, we have $p = l_A + l_B$ and $y \in [-l_A, l_B]$, then one can deduce:

$$p\frac{\partial}{\partial x}z_0(x) + \int_{-l_A}^{l_B}\frac{\partial}{\partial y}z_1 dy = \int_{-l_A}^{l_B} C(y)dy z_0(x) \tag{1.66}$$

Because of the fact that the integral of the derivative of a periodic function over its period equals to zero, the second term in the left side of equation (1.66) vanish, and the

equation can be rewritten as:

$$\frac{\partial}{\partial x} z_0(x) = C_{eq} z_0(x) \tag{1.67}$$

This is the governing equation for a beam whose equivalent homogeneous properties are given by:

$$C_{eq} = \frac{1}{p} \int_{-l_A}^{l_B} C(y) dy \tag{1.68}$$

Considering the piece-wised nature of our structure, C_{eq} is given by:

$$C_{eq} = \frac{l_A}{p} C_A + \frac{l_B}{p} C_B \tag{1.69}$$

After calculating the matrix C_{eq}, we obtain the expression of C_{eq}:

$$C_{eq} = \begin{bmatrix} 0 & 0 & 0 & K_{eq}^{-1} & 0 & 0 \\ 0 & 0 & 1 & 0 & 0 & 0 \\ 0 & 0 & 0 & 0 & D_{eq}^{-1} & 0 \\ -\omega^2 m_{eq} & 0 & 0 & 0 & 0 & 0 \\ 0 & 0 & 0 & 0 & 0 & -1 \\ 0 & -\omega^2 m_{eq} & 0 & 0 & 0 & 0 \end{bmatrix} \tag{1.70}$$

where m_{eq},K_{eq},D_{eq} are the equivalent linear mass, axial and bending stiffness of the beam. The expression of these quantities are as follows:

$$\begin{aligned} m_{eq} &= \frac{l_A}{p} m_A + \frac{l_B}{p} m_B \\ \frac{p}{K_{eq}} &= \frac{l_A}{K_A} + \frac{l_B}{K_B} \\ \frac{p}{D_{eq}} &= \frac{l_A}{D_A} + \frac{l_B}{D_B} \end{aligned} \tag{1.71}$$

The result is incidentally a classical one, and does not require any particular homogenization technique to prove it. It is the same as the relation obtained through the application of the rule of mixture for composite materials.

Here is a specific example to verify the homogenization method. The binary periodic structure is composed of Epoxy in section A and Aluminium in section B. The lengths l_A,l_B are both $1m$, then the period p equals to $2m$, as shown in figure 1.6. The properties of the material can be found in table 1.1.

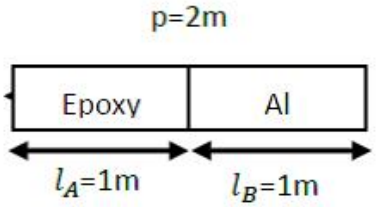

FIGURE 1.6: the specific unit cell of periodic beam

Materials	Young's Modulus: $E(Gpa)$	Density: $\rho(kg/m3)$
Epoxy	4.35	1183
Aluminium	77.56	2730

TABLE 1.1: material properties

The aim is to compare the dispersion relation obtained by the homogenization method with the dispersion relation obtained by WFEM. The former is an analytical result while the latter is a numerical one. For the homogeneous one-dimensional periodic structure, one can deduce the analysis formula of the dispersion relation.

For the longitudinal wave, we have:

$$k = \frac{\omega}{c} \quad c = \sqrt{\frac{k}{m}}$$

For the flexural wave, we have:

$$k^2 = \sqrt{\frac{m}{D}}\omega$$

The figure (1.7) represents the comparison between the two different results for longitudinal wave. From the figure (1.7), it can be seen that, for longitudinal wave, the first band gap appears at about $380Hz$. But the homogenized dispersion curve can't predict the band gap. What's more, the difference between the two curves is very small before $200Hz$, which proves that before $200Hz$, or at low frequency, the homogenized method is valid.

The figure (1.8) shows the comparison between the two different results for flexural wave. From the figure (1.8), we can see that, for flexural wave, the first band gap appears at about $10Hz$. But the homogenized dispersion curve can't predict the band gap. The difference between the two curves is very small before $10Hz$, which is the

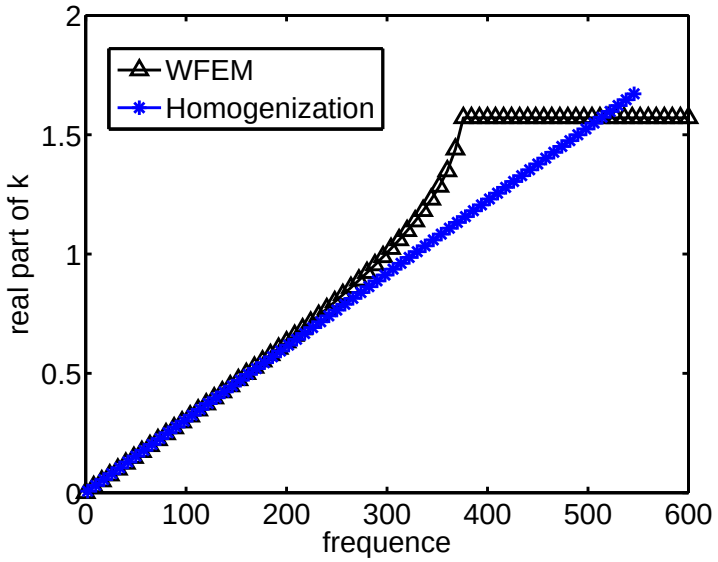

FIGURE 1.7: comparison between numerical and homogenized dispersion curve of longitudinal wave

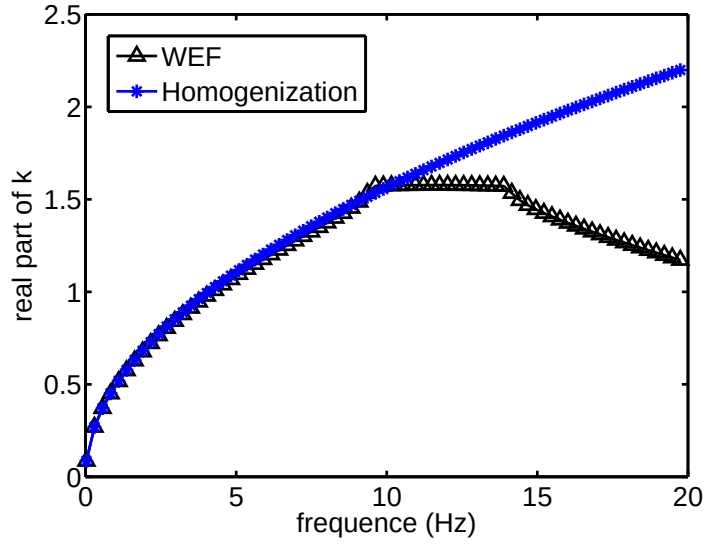

FIGURE 1.8: comparison between numerical and homogenized dispersion curve of flexural wave

critical frequency of the first band gap. The result proves that, at low frequency, the homogenized method is valid.

From the above results, we know that the homogenization method at low frequency is valid. But, it doesn't work anymore at high frequency. In other word, the homogenized dispersion curve can't predict the band gap which is the filtering property of periodic structures. So, another homogenization method to simulate the behaviour of wave at high frequency is proposed. In the following, the new homogenization method

in longitudinal case will be discussed. And the comparison between the homogenized result and the numerical result will be presented to verify the feasibility of the method.

1.5.3 High frequency Homogenization of 1D periodic structure

At high frequency, the behaviour of the periodic structure becomes unpredictable. The strong dispersion, the presence of band gaps or negative refraction can no longer be predicted by homogenization models. For periodic structures, the interest lies often in identifying the Bloch spectra and stop band structure. The Bloch spectra at the edges of the irreducible Brillouin zone corresponds to standing waves. Here is a method to develop a high-frequency asymptotic procedure based upon perturbing about these standing wave solutions occurring at particular frequencies across a periodic structure [64, 65].

The method will be illustrated with the same periodic structure shown in figure 1.4. Specifically, we have $l_A = l_B = l$, the period is $2l$, and $\epsilon = l/L$. For the piece-wise periodic structure, the governing equation for longitudinal wave is:

$$E(X)\frac{\partial^2 u(X,t)}{\partial X^2} - \rho(X)\frac{\partial^2 u(X,t)}{\partial t^2} = 0 \tag{1.72}$$

Where $E(X)$ is the Young's modulus, $\rho(X)$ is the density. With the assumption that u is time-harmonic, the equation can be expressed as:

$$\frac{\partial^2 u(X)}{\partial X^2} + \frac{\rho(X)\omega^2}{E(X)}u(X) = 0 \tag{1.73}$$

The two independent non-dimensional variables are defined as:

$$x = \frac{X}{L}, \quad y = \frac{X}{l}$$

Thus, the solution $u(x, y)$ will be periodic in y, but not necessarily in x. And the equation (1.73) becomes:

$$\frac{\partial^2 u}{\partial y^2} + 2\epsilon\frac{\partial^2 u}{\partial y \partial x} + \epsilon^2\frac{\partial^2 u}{\partial x^2} + \frac{\rho\omega^2 l^2}{E}u = 0 \tag{1.74}$$

This equation will be solved subject to either y-periodic conditions: $u(x,-1) = u(x,1)$ and $u_y(x,-1) = u_y(x,1)$ where $u_y \equiv \partial u/\partial y$, or the anti-periodic conditions $u(x,-1) =$

$-u(x,1)$ and $u_y(x,-1) = -u_y(x,1)$. These two cases correspond to standing waves that are either in-phase or completely out-of-phase at the end of each unit cell. According to Floquet-Bloch theory, the wavenumber of the two situations situated at the ends of the Brillouin zone. The wave speed $C = \sqrt{E/\rho}$. We introduce the non-dimensional wave speed c, so $C(y) = c_0 c(y)$, where c_0 is the characteristic wave speed. Then we note $\lambda^2 = \omega^2 l^2/c_0^2$, here the λ is a non-dimensional frequency. Then we adopt the expansion:

$$\begin{aligned} u(x,y) &= u_0(x,y) + \epsilon u_1(x,y) + \epsilon^2 u_2(x,y) + \dots \\ \lambda^2 &= \lambda_0^2 + \epsilon\lambda_1^2 + \epsilon^2\lambda_2^2 + \dots \end{aligned} \tag{1.75}$$

Our aim is to obtain the dispersion relation between the frequency and the wavenumber. Substituting the equation (1.75) into (1.74), and equating to zero the coefficients of individual powers of ϵ, we obtain a hierarchy of equations for $u_i(x,y)$ and λ_i with associated boundary conditions from the periodicity in y. The leading order equation is as follows:

$$u_{0yy} + \frac{\lambda_0^2}{c^2} u_0 = 0 \tag{1.76}$$

This is a typical wave equation, and the solution to be found is in the following form:

$$u_0(x,y) = f_0(x) U_0(y) \tag{1.77}$$

With the periodic boundary conditions:

$$U_0(-1) = U_0(1), \quad U_{0y}(-1) = U_{0y}(1) \tag{1.78}$$

Or anti-periodic boundary conditions:

$$U_0(-1) = -U_0(1), \quad U_{0y}(-1) = -U_{0y}(1) \tag{1.79}$$

The equation (1.76) gives rise to a discrete spectrum of eigenvalues λ_0^2 for which there is no phase shift cross a period of the structure and standing wave is formed. This leading order solution is exactly periodic on the cell. Generally, the leading order problem would need to be solved numerically, as is in the case of classical homogenization. We continue with the hierarchy to find the corrections λ_1^2, λ_2^2 and the function $f_0(x)$.

At next order, the equation for $u_1(x, y)$ is :

$$u_{1yy} + \frac{\lambda_0^2}{c^2} u_1 = -2u_{0xy} - \frac{\lambda_1^2}{c^2} u_0 \tag{1.80}$$

Multiplying the (1.80) by U_0, and integrating over the periodic cell in y, one can obtain:

$$\int_{-1}^{1} \left(u_{1yy} + \frac{\lambda_0^2}{c^2} u_1 \right) U_0 dy = -\int_{-1}^{1} \left(2u_{0xy} + \frac{\lambda_1^2}{c^2} u_0 \right) U_0 dy \tag{1.81}$$

Substituting the equation (1.77) into (1.81), we have:

$$\int_{-1}^{1} \left(u_{1yy} + \frac{\lambda_0^2}{c^2} u_1 \right) U_0 dy = -2f_{0x} \int_{-1}^{1} U_{0y} U_0 dy - f_0 \lambda_1^2 \int_{-1}^{1} \frac{U_0^2}{c^2} u_0 dy \tag{1.82}$$

What's more

$$2\int_{-1}^{1} U_{0y} U_0 dy = U_0^2(1) - U_0^2(-1) \tag{1.83}$$

The first integral on the right-hand side vanishes, because the U_0 is y-periodic. Then the equation (1.82) becomes:

$$\int_{-1}^{1} \left(u_{1yy} + \frac{\lambda_0^2}{c^2} u_1 \right) U_0 dy = -f_0 \lambda_1^2 \int_{-1}^{1} \frac{U_0^2}{c^2} u_0 dy \tag{1.84}$$

Next, we multiple the equation (1.76) by u_1/f_0, and integrate it over the cell, we get:

$$\int_{-1}^{1} \left(U_{0yy} + \frac{\lambda_0^2}{c^2} U_0 \right) u_1 dy = 0 \tag{1.85}$$

Subtracting the (1.85) from (1.84) results in:

$$\int_{-1}^{1} \left(u_{1yy} U_0 - U_{0yy} u_1 \right) dy = -f_0 \lambda_1^2 \int_{-1}^{1} \frac{U_0^2}{c^2} dy \tag{1.86}$$

And

$$\int_{-1}^{1} \left(u_{1yy} U_0 - U_{0yy} u_1 \right) dy = \left[u_{1y} U_0 - u_1 U_0 y \right]_{-1}^{1} = 0 \tag{1.87}$$

Because of the y- periodicity, the left-hand side integral of (1.86) vanishes too. And we get:

$$f_0 \lambda_1^2 \int_{-1}^{1} \frac{U_0^2}{c^2} dy = 0 \tag{1.88}$$

According to (1.88), λ_1 must be zero. The equation (1.80) becomes:

$$u_{1yy} + \frac{\lambda_0^2}{c^2} u_1 = -2 f_{0x} U_{0y} \tag{1.89}$$

Then we need to find the solution u_1 with the same method used for u_0, the separation of variables.

$$u_1(x, y) = f_1(x) U_1(y) \tag{1.90}$$

Then the equation (1.89) becomes:

$$U_{1yy} + \frac{\lambda_0^2}{c^2} U_1 = -2 \frac{f_{0x}}{f_1} U_{0y} \tag{1.91}$$

This is a second order differential equation, and the variation of parameters method is applied to solve the equation.

Here is a brief introduction of the variation of parameters method. The general second order differential equation is in the following form:

$$g'' + m(x) g' + n(x) g = l(x) \tag{1.92}$$

We suppose that g_1 and g_2 are two independent solutions of the homogeneous equation, and the solution $g(x)$ that we need is in the following form:

$$\begin{cases} g(x) = \alpha(x) g_1(x) + \beta(x) g_2(x) \\ g'(x) = \alpha(x) g_1'(x) + \beta(x) g_2'(x) \end{cases} \tag{1.93}$$

From the equation (1.93), one can deduce a linear equation system of $\alpha(x)$ and $\beta(x)$:

$$\begin{cases} \alpha'(x) g_1(x) + \beta'(x) g_2(x) = 0 \\ \alpha'(x) g_1'(x) + \beta'(x) g_2'(x) = l(x) \end{cases} \tag{1.94}$$

The first equation of (1.94) is obtained by substituting the expression of $g(x)$ in $g'(x)$, and the second equation of (1.94) is obtained by substituting the expression of $g(x)$ and

$g^{'}(x)$ in equation (1.92). Then we have the derive of $\alpha(x)$ and $\beta(x)$:

$$\alpha^{'} = \frac{\begin{vmatrix} 0 & g_2 \\ l & g_2^{'} \end{vmatrix}}{\begin{vmatrix} g_1 & g_2 \\ g_1^{'} & g_2^{'} \end{vmatrix}} = \frac{-g_2 l}{g_1 g_2^{'} - g_1^{'} g_2} \tag{1.95}$$

$$\beta^{'} = \frac{\begin{vmatrix} g_1 & 0 \\ g_1^{'} & l \end{vmatrix}}{\begin{vmatrix} g_1 & g_2 \\ g_1^{'} & g_2^{'} \end{vmatrix}} = \frac{g_1 l}{g_1 g_2^{'} - g_1^{'} g_2} \tag{1.96}$$

According to the variation of parameter method, the solution of equation 1.91 is in the following form:

$$U_1 = A_1(y)cos(\delta y) + B_1(y)sin(\delta y) \tag{1.97}$$

with

$$\begin{aligned} \delta &= \frac{\lambda_0}{c} \\ A_{1y} &= \frac{2f_{0x}}{\delta f_1} sin(\delta y) U_{0y} \\ B_{1y} &= -\frac{2f_{0x}}{\delta f_1} cos(\delta y) U_{0y} \end{aligned} \tag{1.98}$$

With $U_0 = asin(\delta y) + bcos(\delta y)$, one can deduce the expression of $A(y)$ and $B(y)$:

$$\begin{aligned} A_1 &= \frac{f_{0x}}{f_1}\left(\frac{sin(\delta y)}{\delta} U_0 - by + C_3\right) + C_1 \\ B_1 &= \frac{f_{0x}}{f_1}\left(-\frac{cos(\delta y)}{\delta} U_0 - ay + C_4)\right) + C_2 \end{aligned} \tag{1.99}$$

Where C_1, C_2, C_3, C_4 are the integrate constants. And the expression of U_1 is obtained:

$$U_1 = C_1 cos(\delta y) + C_2 sin(\delta y) + \frac{f_{0x}}{f_1}(C_3 cos(\delta y) + C_4 sin(\delta y) - yU_0) \tag{1.100}$$

As U_1 is the solution of the non-homogeneous equation (1.91), U_1 can also be considered as the combination of the associated homogeneous equation's general solution and a specific solution of the non-homogeneous equation. Considering that U_0 is the periodic general solution of the homogeneous equation, the solution of U_1 can be transformed as

follows:

$$U_1 = U_0 + \frac{f_{0x}}{f_1}(AW_1(y) - yU_0) \tag{1.101}$$

where U_0 performs as the general solution of the associated homogeneous equation, and the rest part serves as a specific solution for equation (1.91). Here, $W_1(y) = (C_3 cos(\delta y) + C_4 sin(\delta y))/A$ is a non-periodic solution of equation (1.76), and

$$A = \frac{2U_0(1)}{W_1(1) \mp W_1(-1)} \tag{1.102}$$

guarantees the periodicity of U_1 with the upper sign; and the anti-periodicity with the lower sign. Then, the solution of equation (1.89) can be expressed in the following form:

$$u_1(x, y) = f_{0x}(AW_1 - yU_0) + f_1(x)U_0 \tag{1.103}$$

At next order:

$$u_{2yy} + \frac{\lambda_0^2}{c^2}u_2 = -\frac{\lambda_2^2}{c^2}u_0 - u_{0xx} - 2u_{1xy} \tag{1.104}$$

Multiplying the (1.104) by U_0, and integrating over the periodic cell with respect to y, one can obtain:

$$\int_{-1}^{1}(u_{2yy} + \frac{\lambda_0^2}{c^2}u_2)U_0 dy = -\int_{-1}^{1}(\frac{\lambda_2^2}{c^2}u_0 + u_{0xx} + 2u_{1xy})U_0 dy \tag{1.105}$$

According to (1.103), we have:

$$u_{1xy} = f_{0xx}(AW_{1y} - U_0 - yU_{0y}) + f_{1x}U_{0y} \tag{1.106}$$

Then

$$\begin{aligned}
&\int_{-1}^{1} u_{1xy}U_0 dy \\
=&f_{0xx}A\int_{-1}^{1} W_{1y}U_0 dy - f_{0xx}\int_{-1}^{1}(U_0 + yU_{oy})U_0 dy + f_{1x}\int_{-1}^{1} U_{0y}U_0 dy \\
=&f_{0xx}A\int_{-1}^{1} W_{1y}U_0 dy - f_{0xx}\int_{-1}^{1}\frac{U_0^2}{2}dy - f_{0xx}\int_{-1}^{1}(\frac{U_0^2}{2} + yU_{0y}U_0)dy \\
&+ \frac{f_{1x}}{2}(U_0^2(1) - U_0^2(-1)) \\
=&f_{0xx}A\int_{-1}^{1} W_{1y}U_0 dy - f_{0xx}\int_{-1}^{1}\frac{U_0^2}{2}dy - \frac{f_{0xx}}{2}[yU_0^2]_{-1}^{1} \\
=&f_{0xx}A\int_{-1}^{1} W_{1y}U_0 dy - f_{0xx}\int_{-1}^{1}\frac{U_0^2}{2}dy - f_{0xx}U_0^2(1)
\end{aligned}$$

Then the right-hand side of equation (1.105) becomes:

$$\begin{aligned}
&-\int_{-1}^{1}(\frac{\lambda_2^2}{c^2}u_0+u_{0xx}+2u_{1xy})U_0dy\\
=&-\lambda_2^2 f_0\int_{-1}^{1}\frac{U_0^2}{c^2}dy-f_{0xx}\int_{-1}^{1}U_0^2dy\\
&-2\left(f_{0xx}A\int_{-1}^{1}W_{1y}U_0dy-f_{0xx}\int_{-1}^{1}\frac{U_0^2}{2}dy-f_{0xx}U_0^2(1)\right)\\
=&-\lambda_2^2 f_0\int_{-1}^{1}\frac{U_0^2}{c^2}dy-2f_{0xx}\left(A\int_{-1}^{1}W_{1y}U_0dy-U_0^2(1)\right)
\end{aligned}$$

And the equation (1.105) becomes:

$$\begin{aligned}
&\int_{-1}^{1}(u_{2yy}+\frac{\lambda_0^2}{c^2}u_2)U_0dy\\
=&-\lambda_2^2 f_0\int_{-1}^{1}\frac{U_0^2}{c^2}dy-2f_{0xx}\left(A\int_{-1}^{1}W_{1y}U_0dy-U_0^2(1)\right)
\end{aligned}\tag{1.107}$$

Next, we multiple the equation (1.76) by u_2/f_0, and integrate it over the cell, we get:

$$\int_{-1}^{1}\left(U_{0yy}+\frac{\lambda_0^2}{c^2}U_0\right)u_2dy=0\tag{1.108}$$

Subtracting the (1.108) from (1.107) results in:

$$\begin{aligned}
&\int_{-1}^{1}\left(u_{2yy}U_0-U_{0yy}u_2\right)dy\\
=&-\lambda_2^2 f_0\int_{-1}^{1}\frac{U_0^2}{c^2}dy-2f_{0xx}\left(A\int_{-1}^{1}W_{1y}U_0dy-U_0^2(1)\right)
\end{aligned}\tag{1.109}$$

For the left side of (1.109), we have:

$$\int_{-1}^{1}\left(u_{2yy}U_0-U_{0yy}u_2\right)dy=\left[u_{2y}U_0-U_{0y}u_2\right]_{-1}^{1}=0\tag{1.110}$$

Because of the y- periodicity, the left-hand side integral of (1.109) vanishes. And we get:

$$-\lambda_2^2 f_0\int_{-1}^{1}\frac{U_0^2}{c^2}dy-2f_{0xx}\left(A\int_{-1}^{1}W_{1y}U_0dy-U_0^2(1)\right)=0\tag{1.111}$$

The equation (1.111) can be simplified as:

$$Tf_{0xx}+\lambda_2^2 f_0=0\tag{1.112}$$

With:

$$T = \frac{2\left(A\int_{-1}^{1} W_{1y}U_0 dy - U_0^2(1)\right)}{\int_{-1}^{1}\frac{U_0^2}{c^2}dy} \tag{1.113}$$

Now we have λ_2^2. The next is the solution u_2. The main idea is always the same:

$$u_2(x,y) = f_2(x)U_2(y) \tag{1.114}$$

Then equation (1.104) can be expressed as:

$$f_2(U_{2yy} + \frac{\lambda_0^2}{c^2}U_2) = -(\frac{\lambda_2^2}{c^2}f_0 + f_{0xx})U_0 - 2u_{1xy} \tag{1.115}$$

Subsisting (1.106) into (1.115) gives:

$$U_{2yy} + \frac{\lambda_0^2}{c^2}U_2 = \frac{1}{f_2}\left(-(\frac{\lambda_2^2}{c^2}f_0 - f_{0xx})U_0 - 2f_{0xx}AW_{1y} - 2f_{1x}U_{0y} + 2f_{0xx}yU_{0y}\right) \tag{1.116}$$

Noting:

$$M = (\frac{\lambda_2^2}{c^2}f_0 - f_{0xx})/f_2$$

$$N = 2f_{0xx}A/f_2$$

$$P = 2f_{1x}/f_2$$

$$Q = -2f_{0xx}/f_2$$

Then, we have:

$$U_{2yy} + \frac{\lambda_0^2}{c^2}U_2 = -MU_0 - NW_{1y} - PU_{0y} - QyU_{0y} \tag{1.117}$$

With the same idea of finding the solution u_1, we have the expression of U_2:

$$U_2 = U_0 + U_{2p1} + U_{2p2} + U_{2p3} + U_{2p4} \tag{1.118}$$

Where

U_0 is the solution of homogeneous equation.

U_{2p1} is a particular solution of $U_{2yy} + \frac{\lambda_0^2}{c^2}U_2 = -MU_0$,

U_{2p2} is a particular solution of $U_{2yy} + \frac{\lambda_0^2}{c^2}U_2 = -NW_{1y}$,

U_{2p3} is a particular solution of $U_{2yy} + \frac{\lambda_0^2}{c^2}U_2 = -PU_{0y}$,

U_{2p4} is a particular solution of $U_{2yy} + \frac{\lambda_0^2}{c^2}U_2 = -QyU_{0y}$.

Using the variation of parameters method, we can find these four solutions of different equations.

$$\begin{cases} U_{2p1} = M(\dfrac{yU_{0y} - U_0}{2\delta^2} + D_1 W_1(y)) \\ U_{2p2} = N(-\dfrac{yW_1}{2} + D_2 W_1(y))) \\ U_{2p3} = P(-\dfrac{yU_0}{2} + D_3 W_1(y)) \\ U_{2p4} = Q(-\dfrac{y^2 U_0}{4} - \dfrac{yU_{0y}}{4\delta^2} + D_4 W_1(y)) \end{cases} \tag{1.119}$$

Here, we use the periodic condition(for the anti-periodic, the calculate is the same):

$$U_2(-1) = U_2(1)$$

Then, we have

$$\begin{cases} D_1 = -\dfrac{2U_{0y}(1)}{2\delta^2(W_1(1) - W_1(-1))} \\ D_2 = \dfrac{W_1(1) + W_1(-1)}{2(W_1(1) - W_1(-1))} \\ D_3 = \dfrac{U_0(1)}{W_1(1) - W_1(-1)} \\ D_4 = \dfrac{U_{0y}(1)}{2\delta^2(W_1(1) - W_1(-1))} \end{cases} \tag{1.120}$$

Hence, the solution of U_2 can be expressed as:

$$\begin{aligned} U_2 =& U_0 + M(\frac{yU_{0y} - U_0}{2\delta^2} + D_1 W_1(y)) + N(-\frac{yW_1}{2} + D_2 W_1(y)) \\ &+ P(-\frac{yU_0}{2} + D_3 W_1(y)) + Q(-\frac{y^2 U_0}{4} - \frac{yU_{0y}}{4\delta^2} + D_4 W_1(y)) \end{aligned} \tag{1.121}$$

Now we have λ_2 and u_2. The expression of u_2 is quite complicated, which explains somehow why we stop at equation of second order. Besides, because of the Floquet-Bloch conditions, $u(x + 2\epsilon, y) = exp(2ik\epsilon)u(x, y)$. As $u_0(x, y) = f_0(x)U_0(y)$, these two relations force $f_0(X) = exp(ikX)$. Thus, according to equation (1.112), $\lambda_2^2 = Tk^2$.

We suppose that for the piecewise periodic structure, the wave speed varies as follows:

$$c(y) = \begin{cases} 1 & -1 \leq y < 0 \\ \dfrac{1}{r} & 0 < y \leq 1 \end{cases} \tag{1.122}$$

Then we can find a solution of leading order equation (1.76):

$$U_0(y) = \begin{cases} rsin(\lambda_0 y) + pcos(\lambda_0 y) & -1 \leq y < 0 \\ sin(r\lambda_0 y) + pcos(r\lambda_0 y) & 0 < y \leq 1 \end{cases} \tag{1.123}$$

With

$$p = \frac{rsin(\lambda_0) \pm sin(\lambda_0)}{cos(\lambda_0) \mp cos(r\lambda_0)}$$

The upper signs for periodic boundary condition, while the lower signs for the anti-periodic condition. Besides, we also need W_1 to finish our calculation. Here is a possible solution of W_1:

$$W_1(y) = \begin{cases} rsin(\lambda_0 y) & -1 \leq y < 0 \\ sin(r\lambda_0 y) & 0 < y \leq 1 \end{cases} \tag{1.124}$$

With these solutions, we can obtain the formula of T:

$$T = 4\lambda_0 \frac{sin(\lambda_0) sin(r\lambda_0)}{(rsin(\lambda_0) \mp sin(r\lambda_0))(cos(\lambda_0) \mp cos(r\lambda_0))} \tag{1.125}$$

The upper signs for periodic boundary condition, while the lower signs for the anti-periodic condition.

At last, we deduce the dispersion relation:

$$\begin{aligned} \lambda^2 &= \lambda_0^2 + \epsilon\lambda_1^2 + \epsilon^2\lambda_2^2 + \dots \\ &= \lambda_0^2 + \epsilon^2\lambda_2^2 + \left(\frac{\epsilon^2\lambda_2^2}{2\lambda_0}\right)^2 + \dots \\ &= \left(\lambda_0 + \frac{\epsilon^2\lambda_2^2}{2\lambda_0}\right)^2 + \dots \end{aligned} \tag{1.126}$$

So, in the periodic case, we have:

$$\lambda \approx \lambda_0 + \frac{\epsilon^2\lambda_2^2}{2\lambda_0} + \dots = \lambda_0 + \frac{T(\epsilon k)^2}{2\lambda_0} \tag{1.127}$$

And in the anti-periodic case, we have:

$$\lambda \approx \lambda_0 + \frac{T(\epsilon k - \pi)^2}{2\lambda_0} \tag{1.128}$$

Then with the same material as show in figure 1.6, we will compare the dispersion

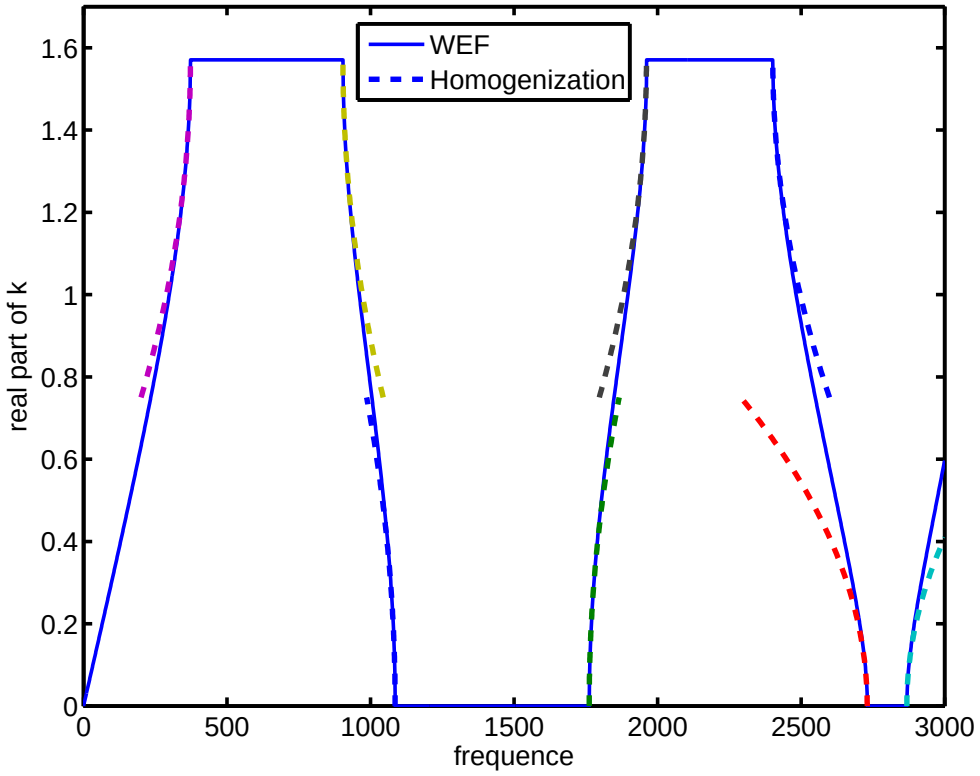

FIGURE 1.9: the comparison between the numerical result and the homogenized method.

relation obtain by the numerical method, WFEM, with the homogenized result. The comparison is depicted in figure 1.9. In the figure 1.9, the solid line is obtained by WFEM, while the dash line is the homogenized dispersion relation. We can see that, the approximation is better at the endpoint of band gap. But, when it is far from the endpoint, the difference between the two curves grows great. So the correlation of λ is not good enough if we stop at the second order equation. With further correlation, the dispersion curve maybe better.

The main idea of the high-frequency homogenization method is to develop an approximation procedure based upon perturbing about these standing waves solution which occur at particular frequencies across a periodic structure. All the equations are constructed on the macro-scale which is valid for frequencies in the vicinity of the standing wave. In low frequency homogenization, according to the equation (1.62), the leading order of z, z_0 is independent of y. But in high frequency homogenization, the conclusion in not valid. The leading order u_0 depends on the macroscopic scale x, the following order of u, is the correlation of the u_0. with these correlation terms, the dispersion, or

the band gaps appears. From the example, we can see that by perturbing away from the standing wave solutions, the Bloch spectra is identified through a simple differential eigenvalue problem, whose coefficient involves the integrations over the periodic cell. The main difference is that the integrated quantities are longer simply averaged wave speed or simple averaged quantities.

1.5.4 Homogenization of periodic discrete media (HPDM)

HPDM, which stands for homogenization of periodic discrete media, is a method to study the reticulated structures. Based on continuum mechanics, the method leads to an analytical continuous description of the framed structure, which is a repetition of the same material in one direction (1D case) shown in figure (1.10(a)) or two directions (2D case) shown in figure (1.10(b)). In the method, a scale ratio which involves the length of unit cell and the characterized length of the structure leads to an asymptotic expansion of differential operator and solutions. By solving equations of dominant order and higher orders, a continuous structure model is derived from the discrete description.

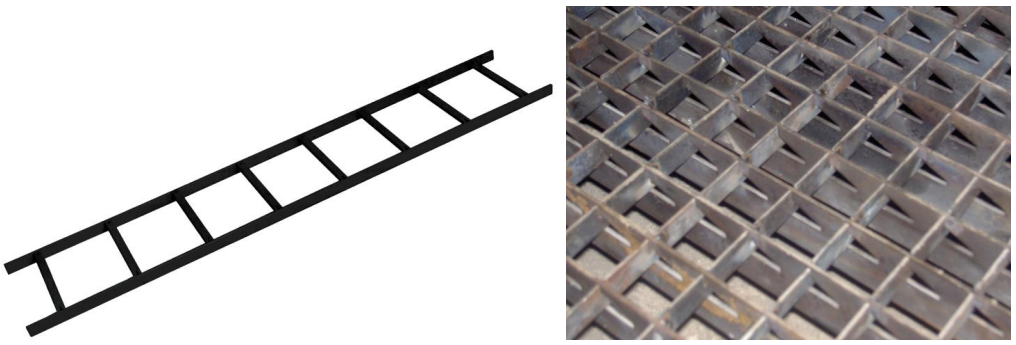

(a) 1D periodic discrete structure (b) 2D periodic discrete structure

FIGURE 1.10: Periodic discrete structures

The method is composed of two parts: discretization and homogenization. As the studied structure is composed of interconnected beam or plate, the dynamic balance of the whole structure can be expressed in a discrete form by the element balance and nodal balance. The discretization starts with the local balance of each element. The longitudinal force, transversal force and bending moment at extremities can be expressed explicitly by the displacement and rotation of these points. At last, the discrete balance equation is rigorously derived from nodal force balance equations. After discretization,

the homogenization process needs the scale ratio. According to the homogenization theory, the scale ratio should be small enough to ensure little dynamic behavior distinction between adjoining unit cell. In this case, the discrete dynamic variables at each node can be considered as specific values of a continuous function, and these dynamic variables of neighboring nodes can be connected by Taylor's Series. With all these dynamic variables developed in Taylor's Series with respect to the scale ratio, a sequence of balance equation at various order can be derived by nodal balance equation. At last, the variation of element properties contrast leads to different kinds of homogenized models

Here are two examples of this method applied on homogeneous structures. As mentioned before, the first step is discretization. And the dynamic balance of the Euler-Bernoulli beam elements are expressed by considering the displacements and rotations at their endpoints as boundary conditions shown in figure (1.11). The u_B, u_E denote the longitudinal displacements, $v_B, v_E, \theta_B, \theta_E$ denote the transversal displacements and rotations. $N^B, N^E, T^B, T^E, M^B, M^E$ represent the axial force, shear force and moment. The superscripts B, E mean begin and end.

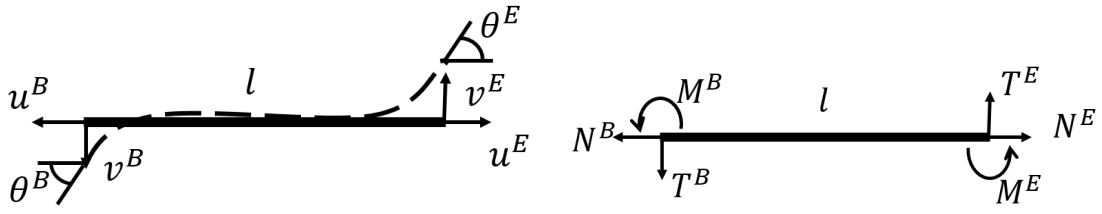

FIGURE 1.11: Element notation

In the longitudinal case, the wave equation is

$$E\frac{\partial^2 u(x,t)}{\partial x^2} - \rho\frac{\partial^2 u(x,t)}{\partial t^2} = 0$$

where E, ρ are respectively the Young's Modulus and the density of the uniform structure. By considering the harmonic wave solution, the equation becomes: $u''(x) + k_L^2 u(x) = 0$, where $k_L = \sqrt{\rho\omega^2/E}$. The associated solution is $u(x) = c_1 sin(k_L x) + c_2 cos(k_L x)$. Knowing the boundary conditions: $u(0) = u^B$ and $u(l) = u^E$, we have the equation system to deduce the solution of the wave equation:

$$\begin{cases} c_2 = u^B \\ c_1 sin(k_L l) + c_2 cos(k_L l) = u^E \end{cases} \tag{1.129}$$

Then the solution writes:

$$u(x) = \frac{u^E - u^B cos(k_L l)}{sin(k_L l)} sin(k_L x) + u^B cos(k_L x) \tag{1.130}$$

The axial forces at the endpoints can be deduced:

$$\begin{cases} N^B = -ESu'(0) = ESk_L \dfrac{u^B cos(k_L l) - u^E}{sin(k_L l)} \\ N^E = -ESu'(l) = -ESk_L \dfrac{u^E cos(k_L l) - u^B}{sin(k_L l)} \end{cases} \tag{1.131}$$

where S is the section area. In the homogeneous case, the unit cell length can be chosen as infinitesimal ($l \to 0$). Note that

$$N(u_1, u_2) = ESk_L \frac{u_1 cos(k_L l) - u_2}{sin(k_L l)}$$

then $N^B = N(u^B, u^E), N^E = -N(u^E, u^B)$, and the series expansion with respect to l is:

$$N(u_1, u_2) = \frac{ES}{l}(u_1 - u_2 - \frac{2u_1 + u_2}{6} k_L^2 l^2 - \frac{8u_1 + 7u_2}{360} k_L^4 l^4 + O(l^6)) \tag{1.132}$$

At present, the element dynamic balance is verified. And, the next step is the nodal balance of the whole structure. The nodal balance equation at the endpoint of two unit cells shown in figure (1.12) writes:

$$N_n^E = N_{n+1}^B$$

.

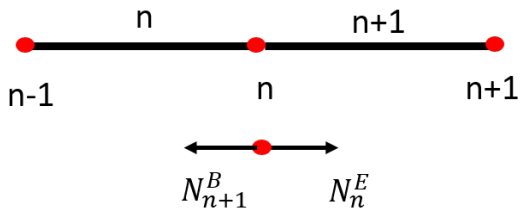

FIGURE 1.12: Longitudinal vibration nodal balance

According to equation (1.132),

$$N_n^E = -N(u_n, u_{n-1}) = -\frac{ES}{l}(u_n - u_{n-1} - \frac{2u_n + u_{n-1}}{6}k_L^2 l^2 - \frac{8u_n + 7u_{n-1}}{360}k_L^4 l^4)$$

$$N_{n+1}^B = N(u_n, u_{n+1}) = \frac{ES}{l}(u_n - u_{n+1} - \frac{2u_n + u_{n+1}}{6}k_L^2 l^2 - \frac{8u_n + 7u_{n+1}}{360}k_L^4 l^4)$$

Then, the nodal balance equation becomes:

$$(u_{n-1} + u_{n+1})(1 + \frac{k_L^2 l^2}{6} + \frac{7k_L^4 l^4}{360}) - 2u_n(1 - \frac{k_L^2 l^2}{3} - \frac{k_L^4 l^4}{45}) = 0 \tag{1.133}$$

According to the homogenization theory, scale ratio between the unit cell length l and characteristic length L of the whole structure should be small enough, $\epsilon = l/L \ll 1$. By introducing the scale separation, ϵ is used for the expansion of the displacement.

$$u_n(x) = u_{n0}(x) + \epsilon u_{n1}(x) + \epsilon^2 u_{n2}(x) + \epsilon^3 u_{n3}(x) + ... \tag{1.134}$$

where u_{ni} is the ith order displacement of u_n. Since the unit cell length l is a small increment for the variable x, the discrete displacement varies slowly from one node to the next and it can be considered as specific values of a continuous function: $u_n(x) = u(x = nl)$. The displacements of node n-1 and node n+1 can also be related to the node n by using Taylor's series:

$$\begin{aligned} u_{n+1} &= u_n + u_n' l + \frac{u_n''}{2}l^2 + \frac{u_n'''}{6}l^3 + \frac{u_n''''}{24}l^4 + ... \\ &= u_n + \epsilon L u_n' + \epsilon^2 L^2 \frac{u_n''}{2} + \epsilon^3 L^3 \frac{u_n'''}{6} + \epsilon^4 L^4 \frac{u_n''''}{24} + ... \end{aligned}$$

Then inserting equation (1.134) into the above equation and rewriting it according to the order of ϵ, the u_{n+1} becomes:

$$\begin{aligned} u_{n+1} =& u_{n0} + \epsilon(u_{n1} + Lu_{n0}') + \epsilon^2(u_{n2} + Lu_{n1}' + \frac{L^2}{2}u_{n0}'') \\ &+ \epsilon^3(u_{n3} + Lu_{n2}' + \frac{L^2}{2}u_{n1}'' + \frac{L^3}{6}u_{n0}''') + ... \end{aligned} \tag{1.135}$$

Similarly for u_{n-1}, we have

$$\begin{aligned} u_{n-1} =& u_{n0} + \epsilon(u_{n1} - Lu_{n0}') + \epsilon^2(u_{n2} - Lu_{n1}' + \frac{L^2}{2}u_{n0}'') \\ &+ \epsilon^3(u_{n3} - Lu_{n2}' + \frac{L^2}{2}u_{n1}'' - \frac{L^3}{6}u_{n0}''') + ... \end{aligned} \tag{1.136}$$

which induces that

$$u_{n-1} + u_{n+1} = 2u_{n0} + \epsilon(2u_{n1}) + \epsilon^2(2u_{n2} + L^2u''_{n0}) + \epsilon^3(2u_{n3} + L^2u''_{n1}) + ... \quad (1.137)$$

Inserting equation (1.134) and (1.137) into equation (1.133), and using the relation $l = \epsilon L$, a series of equation for u_{ni} are obtained by identifying the terms with the equal power of ϵ:

Order $O(\epsilon^0)$: $2u_{n0} - 2u_{n0} = 0$

Order $O(\epsilon^1)$: $2u_{n1} - 2u_{n1} = 0$

Order $O(\epsilon^2)$:

$$2u_{n0}\frac{(Lk_L)^2}{6} + (2u_{n2} + L^2u''_{n0}) - u_{n0}(-\frac{2}{3}(Lk_L)^2) - 2u_{n2} = 0 \Rightarrow u''_{n0} + k_L^2u_{n0} = 0$$

Order $O(\epsilon^3)$:

$$2u_{n1}\frac{(Lk_L)^2}{6} + (2u_{n3} + L^2u''_{n1}) - u_{n1}(-\frac{2}{3}(Lk_L)^2) - 2u_{n3} = 0 \Rightarrow u''_{n1} + k_L^2u_{n1} = 0$$

Order $O(\epsilon^4)$:

$$\begin{aligned} &2u_{n0}\frac{7(Lk_L)^4}{360} + (2u_{n2} + L^2u''_{n0})\frac{(Lk_L)^2}{6} + (2u_{n4} + L^2u''_{n2} + \frac{L^4}{12}u''''_{n0}) \\ &-u_{n0}(-\frac{2}{45}(Lk_L)^4) - u_{n2}(-\frac{2}{3}(Lk_L)^2) - 2u_{n4} = 0 \\ &\Rightarrow u''_{n2} + k_L^2u_{n2} = 0 \end{aligned}$$

At the first two orders, the results are trivial equations. But, from the second order on, the result equations are the classical longitudinal wave equations for u_{n-2}, which corresponds to the beginning wave equation.

In the transversal case, the wave equation is

$$EI\frac{\partial^4 v(x,t)}{\partial x^4} + \rho S\frac{\partial^2 v(x,t)}{\partial t^2} = 0$$

where E, ρ, I, S are respectively the Young's Modulus, the density, the inertia moment and the section area of the uniform structure. The wave solution is always harmonic, and the wave equation becomes: $v''''(x) - k_T^4 v(x) = 0$, where $k_T = \sqrt[4]{\rho S\omega^2/EI}$. The affiliated solution is $v(x) = d_1 sin(k_T x) + d_2 cos(k_T x) + d_3 sinh(k_T x) + d_4 cosh(k_T x)$. As the displacement and rotation at the endpoints are known boundary conditions:

$v(0) = v^B, v(l) = v^E$ and $v'(0) = \theta(0) = \theta_B, v'(l) = \theta(l) = \theta_E$, the equation system to solve writes:

$$\begin{cases} d_2 + d_4 = v^B \\ d_1 sin(k_T l) + d_2 cos(k_T l) + d_3 sinh(k_T l) + d_4 cosh(k_T l) = v^E \\ d_1 + d_3 = \dfrac{\theta^B}{k_T} \\ d_1 cos(k_T l) - d_2 sub(k_T l) + d_3 cosh(k_T l) + d_4 sinh(k_T l) = \dfrac{v^E}{k_T} \end{cases} \tag{1.138}$$

With the solution of $v(x)$ being obtained, the moment and the shear force at the end-points deduce by the following expression:

$$M = -EI\frac{\partial^2 v}{\partial x^2}; \qquad T = EI\frac{\partial^3 v}{\partial x^3}$$

If we note

$$\begin{aligned} M(v_1, v_2, \theta_1, \theta_2) = -\frac{EI}{l^2}(&\frac{v_1 sin(k_T l) sh(k_T l) + v_2(cos(k_T l) - ch(k_T l))}{cos(k_T l)ch(k_T l) - 1}(k_T l)^2 \\ &+ l\frac{\theta_1(ch(k_T l)sin(k_T l) - sh(k_T l)cos(k_T l)) - \theta_2(sin(k_T l) - sh(k_T l))}{cos(k_T l)ch(k_T l) - 1}(k_T l)) \end{aligned}$$

$$\begin{aligned} &T(v_1, v_2, \theta_1, \theta_2) \\ =& -\frac{EI}{l^3}(\frac{v_1(ch(k_T l)sin(k_T l) + sh(k_T l)cos(k_T l)) - v_2(sin(k_T l) + sh(k_T l))}{cos(k_T l)ch(k_T l) - 1}(k_T l)^3 \\ &+ l\frac{\theta_1 sin(k_T l)sh(k_T l) - \theta_2(cos(k_T l) - ch(k_T l))}{cos(k_T l)ch(k_T l) - 1}(k_T l)^2) \end{aligned}$$

then

$$\begin{cases} M^B = M(v^B, v^E, \theta^B, \theta^E) \\ M^E = M(v^E, v^B, -\theta^E, -\theta^B) \\ T^B = T(v^B, v^E, \theta^B, \theta^E) \\ T^E = -T(v^E, v^B, -\theta^E, -\theta^B) \end{cases} \tag{1.139}$$

And the related series expansion with respect to l are:

$$M(v_1, v_2, \theta_1, \theta_2) = \frac{2EI}{l^2}(3(v_1 - v_2) + l(2\theta_1 + \theta_2) - \frac{22v_1 + 13v_2 + l(4\theta_1 - 3\theta_2)}{840}(k_T l)^4 + O(l^8))$$

$$T(v_1, v_2, \theta_1, \theta_2) = \frac{6EI}{l^3}(2(v_1 - v_2) + l(\theta_1 + \theta_2) - \frac{156v_1 + 54v_2 + l(22\theta_1 - 13\theta_2)}{2520}(k_T l)^4 + O(l^8))$$

The element dynamic balance for transversal vibration is verified. In the transversal

case, the nodal balance is composed of two parts: the moment balance and the shear force balance, shown in figure (1.13). The corresponding equations are in the following form:

$$M_n^E = M_{n+1}^B; \qquad T_n^E = T_{n+1}^B$$

where $M_n^E = M(v_n, v_{n-1}, -\theta_n, -\theta_{n-1}); M_{n+1}^B = M(v_n, v_{n+1}, \theta_n, \theta_{n+1});$
$T_n^E = -T(v_n, v_{n-1}, -\theta_n, -\theta_{n-1}); T_{n+1}^B = T(v_n, v_{n+1}, \theta_n, \theta_{n+1}).$

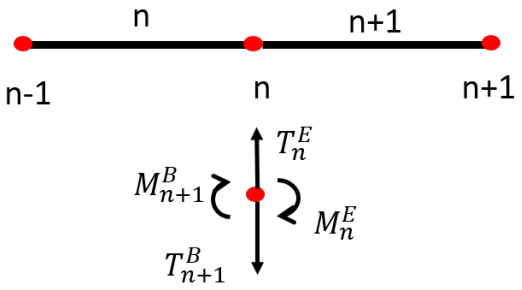

FIGURE 1.13: Longitudinal vibration nodal balance

Substituting the series expansion of $M_n^E, M_{n+1}^B, T_n^E, T_{n+1}^B$ into the balance equation, the moment balance equation writes:

$$(v_{n+1} - v_{n-1})(3 + \frac{13}{840}(k_T l)^4) - l\theta_n(4 - \frac{8}{840}(k_T l)^4) - l(\theta_{n+1} + \theta_{n_1})(1 + \frac{3}{840}(k_T l)^4) = 0 \tag{1.140}$$

the shear force balance equation writes:

$$(v_{n+1} + v_{n-1})(12 + \frac{9}{70}(k_T l)^4) + v_n(-24 + \frac{26}{35}(k_T l)^4) - l(\theta_{n+1} - \theta_{n_1})(6 + \frac{13}{420}(k_T l)^4) = 0 \tag{1.141}$$

The equation (1.135) and (1.136) give the expression of $v_{n+1} - v_{n-1}$ by changing u to v:

$$v_{n+1} - v_{n-1} = \epsilon(2Lv'_{n0}) + \epsilon^2(2Lv'_{n1}) + \epsilon^3(2Lu'_{n2} + \frac{L^3}{3}u'''_{n0}) + \epsilon^4(2Lu'_{n3} + \frac{L^3}{3}u'''_{n1}) + ... \tag{1.142}$$

As for the other series expansion, such as $\theta_{n+1} + \theta_{n-1}$, the expression can be obtained by changing the associated variables. Then inserting these series expansion into the transversal vibration balance equation, and using the relation $l = \epsilon L$, a series of equations for v_i are obtained by identifying the terms with the equal power of ϵ. The result are shown in the following table.

Moment balance equation	$M_n^E = M_{n+1}^B$
Order $O(\epsilon^1)$	$v'_{n0} - \theta_{n0} = 0$
Order $O(\epsilon^2)$	$v'_{n1} - \theta_{n1} = 0$
Order $O(\epsilon^3)$	$6L(v'_{n2} - \theta_{n2}) - L^3(\theta''_{n0} - v'''_{n0}) = 0$
Order $O(\epsilon^4)$	$6L(v'_{n3} - \theta_{n3}) - L^3(\theta''_{n1} - v'''_{n1}) = 0$
Order $O(\epsilon^5)$	$L^5(\frac{13}{420}v'_{n0}(k_T l)^4 + \frac{1}{20}v^{(5)}_{n0} + \frac{1}{420}\theta_{n0}(k_T l)^4 - \frac{1}{12}\theta^{(4)}_{n0}) +$ $6L(v'_{n4} - \theta_{n4}) - L^3(\theta'''_{n2} - v^{(4)}_{n2}) = 0$

TABLE 1.2: Moment balance equation at various orders

Shear force balance equation	$T_n^E = T_{n+1}^B$
Order $O(\epsilon^2)$	$v''_{n0} - \theta'_{n0} = 0$
Order $O(\epsilon^3)$	$v''_{n1} - \theta'_{n1} = 0$
Order $O(\epsilon^4)$	$L^4(v_{n0}(k_T l)^4 + v^{(4)}_{n0} - 2\theta'''_{n0}) + 12L^2(v''_{n2} - \theta'_{n2}) = 0$
Order $O(\epsilon^5)$	$L^4(v_{n1}(k_T l)^4 + v^{(4)}_{n1} - 2\theta'''_{n1}) + 12L^2(v''_{n3} - \theta'_{n3}) = 0$
Order $O(\epsilon^6)$	$L^6(\frac{9}{70}v''_{n0}(k_T l)^4 + \frac{1}{30}v^{(6)}_{n0} - \frac{13}{210}\theta'_{n0}(k_T l)^4 - \frac{1}{10}\theta^{(5)}_{n0}) +$ $L^4(v_{n2}(k_T l)^4 + v^{(4)}_{n2} - 2\theta'''_{n2}) + 12L^2(v''_{n4} - \theta'_{n4}) = 0$

TABLE 1.3: Shear force balance equation at various orders

After some simplification, the two series balance equations together deduce the homogenized wave equation at various orders, and the homogenized equation are shown in table (1.4):

$M_n^E = M_{n+1}^B$	$T_n^E = T_{n+1}^B$
$v'_{n0} - \theta_{n0} = 0$	$v''_{n0} - \theta'_{n0} = 0$
$v'_{n1} - \theta_{n1} = 0$	$v''_{n1} - \theta'_{n1} = 0$
$v'_{n2} - \theta_{n2} = 0$	$v''''_{n0} - k_T^4 v_{n0} = 0$
$v'_{n3} - \theta_{n3} = 0$	$v''''_{n1} - k_T^4 v_{n1} = 0$
$v'_{n4} - \theta_{n4} = 0$	$v''''_{n2} - k_T^4 v_{n2} = 0$

TABLE 1.4: Homogenized wave equation at various orders

From the result, it can be seen that the moment balance equation provides the definition of rotation and the shear force balance equation provides the wave equations at various orders which are the same as beginning wave equation.

In a word, although the HPDM is a method to study framed structure, it can deduce the classical wave equation for both longitudinal vibration and transversal vibration in the uniform structures. The result proves that the method is efficient and it will be implemented in periodic structures. The implementation details of this method on longitudinal waves and flexural waves in 1D periodic structures will be discussed in chapter 2 and chapter 3.

1.6 Conclusion

The literature review in this chapter is guided on three aspects: the wave propagation characteristic of periodic structures, the numerical method and the analytical method to study the periodic structure. The dispersion curve of 1D periodic structure, or the band diagram of 2D periodic structure is the essential properties. To obtain these properties, the plane-wave expansion method, the transfer matrix method, the wave finite element method, and the condensed wave finite element method are explained. These method are all validated by plenty of works. However, the main points of our work focus on the homogenization, which is also a kind of analytical method. In this chapter, two homogenization methods are presented, as well as the comparison of the result before homogenization and after homogenization. The results shows that some more work are needed to obtain more precise simulation models.

Numerical method can deal with complex structures. However, the computational cost can be high and parametrization or scaling of the model requires repeated computations. As for the analytical methods, although often limited to simple structures, it provides a full insight into the behaviour of modelled periodic structures with obtained solutions parametrized and fully scalable. The homogenization method for the periodic structures, which allows to obtain analytical solutions of the model, combines the advantages of numerical method and analytical method. This method will help us to get a better understanding about the periodic structure's behaviour.

Chapter 2

Homogenization of longitudinal waves in 1 dimensional periodic structures

2.1 Introduction

Composite structures are widely spread in various industry domains. Especially, periodic composite structures also attract new motivations in recent years. The main characteristics of periodic structures are the specific wave dispersion effect which means different harmonic waves propagate with a different velocity, and the stop bands which indicate the non propagating frequency range. Many investigations concerning wave propagation in periodic structures have been conducted [66–68]. According to the theory of Floquet-Bloch [69–71], the study of a periodic structure can be converted to the study of its unit cell. Based on this theory, plenty of methods have been developed, such as receptance method [72], transfer matrix method (TMM) [73] and space-harmonic method [74]. When the structure becomes complex, the heterogeneity or the anisotropy makes the affiliated analysis more arduous. In this case, the wave finite element method (WFEM), which takes full advantage of finite element modelling of the unit cell, has been applied in various studieds [75–77].

Another alternative option to study periodic structures is to find their homogenized models with equivalent parameters or equivalent equilibrium equations. The traditional

homogenization method aims for the determination of homogenized equivalent parameters. With these effective parameters, the original heterogeneous structure can be simulated as a homogeneous one. The homogenization models are based on the long-wave assumption, which indicates that the wavelength in a studied case should be larger than the unit cell length. Consequently, the frequency valid domain is limited to the frequency range before the first Bragg band gap. However, the practical validity range of traditional homogenization models is far less than the first Bragg band gap. When the frequency approaches the first Bragg band gap, the wave-microstructure interaction becomes important, and the traditional homogenization model can no longer predict correctly the structure's dynamic behaviour. Therefore, new homogenized models which can provide more accuracy simulations of the structure's dynamic behaviour at a larger validity range in the first propagating zone are needed. Similar limitation appears in the classical continuum mechanics. Thus, the so-called gradient elasticity theory has been developed [78–82] to derive enriched continuum models. Motivated by the gradient elasticity theory, multi-scale asymptotic homogenization method is developed to overcome the deficiency. Firstly proposed in [83–85], more recently in [86, 87], multi-scale homogenization method is an averaging tool to study the physical processes in composite media. Then, based on the idea of multi-scale asymptotic expansion, several other discussions about homogenization appeared, such as two-scale convergence [88], the periodic unfolding technique [89]. An overview of these discussions are presented in [90].

According to the multi-scale asymptotic homogenization method, a homogenized wave equation rather than the effective parameters will be established. Some implementations of this method can be found in [91–93]. In [91, 92], the free vibration of a periodic structure under the clamped-free boundary condition is investigated. With an initial disturbance in displacement, the time-varying displacement of the structure is presented to validate the method. Factors related to the validity range have been identified. However, only one initial/boundary value problem is studied. And some explanations about the determination of boundary conditions need to be supplemented. In [93], the dispersion relation of an infinite periodic structure is derived. But some more discussions about the dispersion relation, for instance the influence of the material parameter contrast, are still needed. Besides, studies concerning forced vibration of a finite periodic structure are not presented in this work.

In this chapter, the multi-scale expansion method is used to derive higher order homogenization models for longitudinal waves propagating in one-dimensional periodic structures. Some details of the homogenization process are presented, and higher order homogenization models are established. The validation of these models is carried out in the infinite case. A parametric study of the dispersion relation is also investigated to exhibit further discussions about the validity range. Some implementations of these models are achieved in the finite case, where boundary conditions need to be considered. A variational approach is used to formulate the appropriate boundary conditions, and the forced vibration under different boundary conditions is investigated to display the robustness of the higher order homogenization model. The calculations by analytical formulation and numerical WFEM are also conducted to give reference results. The outline of this chapter is as follows. The formulations of longitudinal wave theory are gave in section 2.2. In section 2.3, the application of HPDM on periodic rod is discussed. Section 2.4 presents the derivation of higher order homogenization models by using the multi-scale asymptotic homogenization method. Afterwards, section 2.5 discusses the comparison and validation of these models through the dispersion relation. In section 2.6, some implementations of these models are carried out. At last, some conclusions are made in section 2.7.

2.2 Problem statement

We consider the longitudinal wave propagating in a periodic composite rod, which is composed of two different materials A and B (figure 2.1). The governing wave equation is as follows:

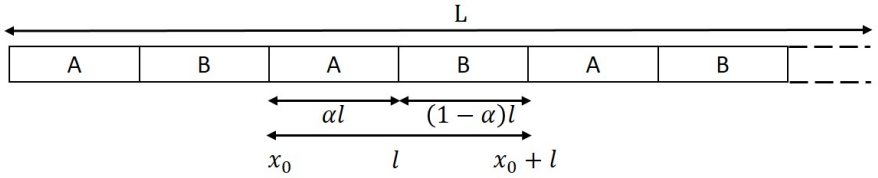

FIGURE 2.1: A bi-laminate periodic rod

$$\frac{\partial}{\partial x}\left(E(\frac{x}{\epsilon})\frac{\partial u(x,t)}{\partial x}\right) - \rho(\frac{x}{\epsilon})\frac{\partial^2 u(x,t)}{\partial t^2} = 0 \tag{2.1}$$

where the $u(x,t)$ denotes the displacement field, $\rho(x/\epsilon)$ the mass density, $E(x/\epsilon)$ the Young's Modulus. $\epsilon = l/L$, L is the characteristic length, and l is the period unit cell

length. The stress at the interface is defined as:

$$\sigma = E(\frac{x}{\epsilon})\frac{\partial u}{\partial x} \tag{2.2}$$

In order to proceed the multi-scale homogenization, two scales are introduced: the macroscale $X = x$ and the microscale $y = x/\epsilon$. The scale X represents the global behaviour of the structure, while the scale y represents the heterogeneity or the periodicity of the structure. Thus, the object is to establish an effective wave equation which involves only the macroscale X. Meanwhile, the heterogeneity of the structure is approximated by some homogenized new term in the effective wave equation.

2.3 HPDM homogenization process

In this section, the implementation of HPDM on the periodic rod will be discussed. According to the HPDM, the first step is the discretization of the element dynamic balance. The element of the periodic rod is shown in figure (2.2), and the dynamic balance will be expressed by considering the displacement at $x = -\alpha l$ and $x = (1-\alpha)l$ as known boundary conditions. Together with the continuity conditions at $x = 0$, the axial force at the endpoints will be deduced.

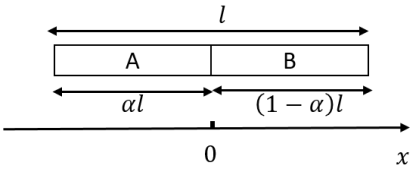

FIGURE 2.2: Rod element chosen for HPDM

The wave equations for material A and material B are :

$$E_a\frac{\partial^2 u}{\partial x^2} - \rho_a\frac{\partial^2 u}{\partial t^2} = 0; \quad E_b\frac{\partial^2 u}{\partial x^2} - \rho_b\frac{\partial^2 u}{\partial t^2} = 0$$

where E_a, E_b, ρ_a, ρ_b are the Young's modulus and the density of material A and B. As the studied displacement is harmonic, the wave equation becomes:

$$u'' + k_a^2 u = 0; \quad u'' + k_b^2 u = 0$$

with $k_a = \sqrt{\rho_a\omega^2/E_a}, k_b = \sqrt{\rho_b\omega^2/E_b}$. The solution is in the following form:

$$u = \begin{cases} c_1 sin(k_a x) + c_2 cos(k_a x) & -\alpha l < x < 0 \\ c_3 sin(k_b x) + c_4 cos(k_b x) & 0 < x < (1-\alpha)l \end{cases}$$

with the associated conditions:

$$\begin{cases} u(-\alpha l) = u^B \\ u((1-\alpha)l) = u^E \\ u(0^-) = u(0^+) \\ E_a \dfrac{\partial u}{\partial x}(0^-) = E_b \dfrac{\partial u}{\partial x}(0^+) \end{cases}$$

Then, the solution of u can be deduced by solving the equation system, which provides the axial force at the endpoints.

$$\begin{cases} N^B = -E_a S u'(-\alpha l) = -Sp \dfrac{qu^E + (psin(ml)sin(nl) - qcos(ml)cos(nl))u^B}{pcos(ml)sin(nl) + qsin(ml)cos(nl)} \\ N^E = -E_b S u'((1-\alpha)l) = -Sq \dfrac{-pu^B + (pcos(ml)cos(nl) - qsin(ml)sin(nl))u^E}{pcos(ml)sin(nl) + qsin(ml)cos(nl)} \end{cases}$$

with $p = E_a k_a, q = E_b k_b, m = \alpha k_a, n = (1-\alpha)k_b$, and S is the section area. The nodal balance equation in this periodic case reminds unchanged as before: $N_n^E = N_{n+1}^B$. For the homogenization of periodic structures, the long-wave approximation is used. This means that the unit cell length l is much more small compared to the characteristic size L. Thus, the scale ratio $\epsilon = l/L \ll 1$ is introduced, and the displacement at node n, n-1 and n+1 is expanded in power of ϵ, as is shown in equation (1.134), (1.135), (1.136).

$$\begin{aligned} u_n =& u_{n0} + \epsilon u_{n1} + \epsilon^2 u_{n2} + \epsilon^3 u_{n3} + ... \\ u_{n+1} =& u_{n0} + \epsilon(u_{n1} + Lu'_{n0}) + \epsilon^2(u_{n2} + Lu'_{n1} + \frac{L^2}{2}u''_{n0}) \\ &+\epsilon^3(u_{n3} + Lu'_{n2} + \frac{L^2}{2}u''_{n1} + \frac{L^3}{6}u'''_{n0}) + ... \\ u_{n-1} =& u_{n0} + \epsilon(u_{n1} - Lu'_{n0}) + \epsilon^2(u_{n2} - Lu'_{n1} + \frac{L^2}{2}u''_{n0}) \\ &+\epsilon^3(u_{n3} - Lu'_{n2} + \frac{L^2}{2}u''_{n1} - \frac{L^3}{6}u'''_{n0}) + ... \end{aligned}$$

With the relation $l = \epsilon L$, the axial force can also be expanded with respect to ϵ. The details are present in the appendix (A). Then inserting the expansion of displacement in the nodal balance equation, and identifying the terms with equal power of ϵ, the

homogenized equation at various orders are obtained.

Order $O(\epsilon^0)$:

$$2u_{n0}\frac{pq}{mq+np} - \frac{2pq}{mq+np}u_{n0} = 0$$

Order $O(\epsilon^1)$:

$$2u_{n1}\frac{pq}{mq+np} - \frac{2pq}{mq+np}u_{n1} = 0$$

Order $O(\epsilon^2)$:

$$u''_{n0} + (m^2+n^2+(p^2+q^2)\frac{mn}{pq})u_{n0} = 0$$

with

$$m^2+n^2+(p^2+q^2)\frac{mn}{pq} = (\alpha\rho_a+(1-\alpha)\rho_b)\frac{\alpha E_b+(1-\alpha)E_a}{E_aE_b}\omega^2 = \frac{\rho_0}{E_0}\omega^2$$

Then the homogenized wave equation can be simplified as:

$$E_0u''_{n0} + \rho_0\omega^2u_{n0} = 0 \tag{2.3}$$

where $E_0 = E_aE_b/\alpha E_b + (1-\alpha)E_a, \rho_0 = \alpha\rho_a + (1-\alpha)\rho_b$.

Order $O(\epsilon^3)$:

$$u''_{n1} + (m^2+n^2+(p^2+q^2)\frac{mn}{pq})u_{n1} = 0$$

which can be simplified as:

$$E_0u''_{n1} + \rho_0\omega^2u_{n1} = 0 \tag{2.4}$$

Order $O(\epsilon^3)$:

$$u''_{n2} + (m^2+n^2+(p^2+q^2)\frac{mn}{pq})u_{n2} + \frac{(p-q)^2(p+q)^2m^2n^2}{12p^2q^2}\frac{L^2u''''_{n0}}{k_0^4} = 0$$

with

$$\frac{(p-q)^2(p+q)^2m^2n^2}{12p^2q^2} = \frac{\alpha^2(1-\alpha)^2(E_a\rho_a-E_b\rho_b)^2}{12E_a^2E_b^2}\omega^4, \quad k_0 = \sqrt{\frac{\rho_0\omega^2}{E_0}}$$

Then the homogenized wave equation can be simplified as:

$$E_0u''_{n2} + \rho_0\omega^2u_{n2} + \frac{\alpha^2(1-\alpha)^2(E_a\rho_a-E_b\rho_b)^2E_0L^2}{12\rho_0^2((1-\alpha)E_a+\alpha E_b)^2}u''''_{n0} = 0 \tag{2.5}$$

Similar results to the homogeneous case in the section introduction can be obtained: the

first two equations are trivial relation; from the second order on, the obtained equations are the homogenized equations for u_{n-2}.

2.4 Multi-scale asymptotic homogenization process

To obtain the effective wave equation, we assume that the macro length of the structure L is much larger than the period l, i.e. $\epsilon = l/L << 1$. With the macroscale $X = x$ and the microscale $y = x/\epsilon$, one can begin the asymptotic homogenization with the expansion of displacement u:

$$u(x,t) \equiv u(X,y,t) = u_0(X,y,t) + \epsilon u_1(X,y,t) + \epsilon^2 u_2(X,y,t) + ... \tag{2.6}$$

where $x \in [0,L]$, $X \in [0,L]$, $y \in [0,L/\epsilon]$. The derivative of x becomes:

$$\frac{\partial}{\partial x} = \frac{\partial}{\partial X} + \frac{1}{\epsilon}\frac{\partial}{\partial y} \tag{2.7}$$

As the scale X represents the global behaviour of the structure, while the scale y represents the heterogeneity or the periodicity of the structure, the displacement u and the stress σ are periodic in y with the period L, but not necessarily in X. For one unit cell, the periodicity of the structure implies the periodic conditions with respect to y:

$$\begin{aligned} u(X,0,t) &= u(X,L,t) \\ E(y)\frac{\partial u}{\partial x}(X,0,t) &= E(y)\frac{\partial u}{\partial x}(X,L,t) \end{aligned} \tag{2.8}$$

And the wave equation (2.1) becomes:

$$\left(\frac{\partial}{\partial X} + \frac{1}{\epsilon}\frac{\partial}{\partial y}\right)\left(E(y)\left(\frac{\partial}{\partial X} + \frac{1}{\epsilon}\frac{\partial}{\partial y}\right)u(X,y,t)\right) = \rho(y)\frac{\partial^2 u(X,y,t)}{\partial t^2} \tag{2.9}$$

In order to make the following calculate more clear, we rewrite the equation (2.9) according to the the power of ϵ:

$$\begin{aligned} \frac{1}{\epsilon^2}\frac{\partial}{\partial y}\left(E(y)\frac{\partial u}{\partial y}\right) + \frac{1}{\epsilon}\left(\frac{\partial}{\partial X}\left(E(y)\frac{\partial u}{\partial y}\right) + \frac{\partial}{\partial y}\left(E(y)\frac{\partial u}{\partial X}\right)\right) \\ + \frac{\partial}{\partial X}\left(E(y)\frac{\partial u}{\partial X}\right) = \rho(y)\frac{\partial^2 u}{\partial t^2} \end{aligned} \tag{2.10}$$

Then inserting the expansion of u into equation (2.10), and identifying the terms with the equal power of ϵ, a series of equations for u_i are obtained. For simplicity, the dependence of time is omitted.

2.4.1 Asymptotic calculation of $O(\epsilon^{-2})$ order equation

At $O(\epsilon^{-2})$, we have:

$$\frac{\partial}{\partial y}\left(E(y)\frac{\partial u_0}{\partial y}\right) = 0 \tag{2.11}$$

Integrating the equation in y, one can obtain:

$$E(y)\frac{\partial u_0}{\partial y} = a_0(X) \tag{2.12}$$

The general solution of u_0 can be obtained by integrating again equation (2.12) with respect to y over the unit cell domain:

$$u_0(X,y) = a_0(X)\int_0^y \frac{1}{E(\tau)}\,d\tau + b_0(X) \tag{2.13}$$

where $a_0(X)$ and $b_0(X)$ are integration constants. Because of the periodicity of the displacement over the unit cell, we have $u_0(X,0) = u_0(X,L)$ which implies that $a_0(X) = 0$. Then, here is the first important conclusion:

$$u_0(X,y) = b_0(X) = U_0(X) \tag{2.14}$$

u_0 the leading order displacement depends only on the macroscale X.

2.4.2 Asymptotic calculation of $O(\epsilon^{-1})$ order equation

At $O(\epsilon^{-1})$, the wave equation becomes:

$$\frac{\partial}{\partial X}\left(E(y)\frac{\partial u_0}{\partial y}\right) + \frac{\partial}{\partial y}\left(E(y)(\frac{\partial u_0}{\partial X} + \frac{\partial u_1}{\partial y})\right) = 0 \tag{2.15}$$

Thanks to (2.14), the above equation can be simplified as:

$$\frac{\partial}{\partial y}\left(E(y)(\frac{\partial u_0}{\partial X} + \frac{\partial u_1}{\partial y})\right) = 0 \tag{2.16}$$

Integrating the above equation gives:

$$\frac{\partial u_1}{\partial y} = \frac{a_1(X)}{E(y)} - \frac{\partial u_0}{\partial X} \tag{2.17}$$

Integrating again and the general solution of u_1 is obtained:

$$u_1(X,y) = a_1(X)\int_0^y \frac{1}{E(\tau)}\,d\tau - \frac{\partial u_0}{\partial X}(y+b_1) + c_1(X) \tag{2.18}$$

With the periodic condition $u_1(X,0) = u_1(X,L)$, one can obtain:

$$a_1(X)\int_0^L \frac{1}{E(y)}\,dy - \frac{\partial u_0}{\partial X}L = 0 \tag{2.19}$$

For simplicity, an averaging operator $< f >= \frac{1}{L}\int_0^L f(y)dy$ is defined. Substituting the expression of $a_1(X)$ in equation (2.18), the simplified formula of u_1 is obtained:

$$\begin{aligned} u_1(X,y) &= \frac{\partial u_0}{\partial X}\frac{L}{\int_0^L \frac{1}{E(y)}\,dy}\int_0^y \frac{1}{E(\tau)}\,d\tau - \frac{\partial u_0}{\partial X}(y+b_1) + c_1(X) \\ &= c_1(X) + \left(\frac{\int_0^y \frac{1}{E(\tau)}\,d\tau}{< \frac{1}{E(y)} >} - y - b_1\right)\frac{\partial u_0}{\partial X} \\ &\equiv U_1(X) + H(y)\frac{\partial u_0}{\partial X} \end{aligned}$$

where

$$< \frac{1}{E(y)} >= \frac{1}{L}\int_0^L \frac{1}{E(y)}\,dy$$

$$H(y) = \frac{\int_0^y \frac{1}{E(\tau)}\,d\tau}{< \frac{1}{E(y)} >} - y - b_1$$

u_1 is composed of two parts: one part (global behaviour) depends only on X, and the other (local behaviour) depends on both X and y. $H(y)$ reminds to be determined. As shown in figure (2.1), the unit cell is composed of two different materials. Then

$$< \frac{1}{E(y)} >= \frac{\alpha}{E_a} + \frac{1-\alpha}{E_b}$$

For the material A

$$\begin{aligned} H_a(y) &= \frac{\frac{y}{E_a}}{\frac{\alpha}{E_a}+\frac{1-\alpha}{E_b}} - y - b_{1a} \\ &= \frac{E_b y}{(1-\alpha)E_a + \alpha E_b} - y - b_{1a} \\ &= \frac{(1-\alpha)(E_b - E_a)}{(1-\alpha)E_a + \alpha E_b} y - b_{1a} \end{aligned}$$

For the material B

$$\begin{aligned} H_b(y) &= \frac{\frac{y}{E_b}}{\frac{\alpha}{E_a}+\frac{1-\alpha}{E_b}} - y - b_{1b} \\ &= \frac{E_a y}{(1-\alpha)E_a + \alpha E_b} - y - b_{1b} \\ &= \frac{\alpha(E_a - E_b)}{(1-\alpha)E_a + \alpha E_b} y - b_{1b} \end{aligned}$$

In order to determine the two constant b_{1a}, b_{1b},we have

Periodicity condition: $u_1(X,0) = u_1(X,L) \Rightarrow H_a(0) = H_b(L)$

Continuity condition: $u_1(X,\alpha L^-) = u_1(X,\alpha L^+) \Rightarrow H_a(\alpha L^-) = H_b(\alpha L^+)$

The periodicity condition has been used before in (2.19). So we need one normalization condition to ensure the uniqueness of the two constant, which means:

$$< u_1(X,y) >= U_1(X) \Rightarrow < H(y) >= 0$$

Here is the calculate:

$$\begin{aligned} H_a(\alpha L^-) = H_b(\alpha L^+) &\Rightarrow \frac{(1-\alpha)(E_b - E_a)}{(1-\alpha)E_a + \alpha E_b}\alpha L - b_{1a} = \frac{\alpha(E_a - E_b)}{(1-\alpha)E_a + \alpha E_b}\alpha L - b_{1b} \\ &\Rightarrow b_{1b} = b_{1a} + \frac{E_a - E_b}{(1-\alpha)E_a + \alpha E_b}\alpha L \end{aligned}$$

$$\begin{aligned} < H(y) >= 0 &\Rightarrow \frac{1}{L}\left(\int_0^{\alpha L} H_a(y)\,dy + \int_{\alpha L}^{L} H_b(y)\,dy\right) = 0 \\ &\Rightarrow \frac{(1-\alpha)(E_b - E_a)}{(1-\alpha)E_a + \alpha E_b}\frac{(\alpha L)^2}{2} - b_{1a}\alpha L \\ &+ \frac{\alpha(E_a - E_b)}{(1-\alpha)E_a + \alpha E_b}\frac{(1-\alpha^2)L^2}{2} - b_{1b}(1-\alpha)L = 0 \\ &\Rightarrow b_{1b} = -\frac{\alpha}{1-\alpha}b_{1a} + \frac{E_a - E_b}{2((1-\alpha)E_a + \alpha E_b)}\alpha L \end{aligned}$$

With these two equations, we get b_{1a}, b_{1b}

$$\begin{cases} b_{1a} = \dfrac{(1-\alpha)(E_b - E_a)}{(1-\alpha)E_a + \alpha E_b}\dfrac{\alpha L}{2} \\ b_{1b} = \dfrac{\alpha(E_a - E_b)}{(1-\alpha)E_a + \alpha E_b}\dfrac{(1+\alpha)L}{2} \end{cases} \tag{2.20}$$

And the expression of $H(y)$

$$H(y) = \begin{cases} \dfrac{(1-\alpha)(E_b - E_a)}{(1-\alpha)E_a + \alpha E_b}\left(y - \dfrac{\alpha L}{2}\right) & 0 < y < \alpha L \\ \dfrac{\alpha(E_a - E_b)}{(1-\alpha)E_a + \alpha E_b}\left(y - \dfrac{(1+\alpha)L}{2}\right) & \alpha L < y < L \end{cases} \tag{2.21}$$

where E_a, E_b denote respectively the Young's Modulus of material A and B. The expression of $H(y)$ being obtained, some useful conclusions about the $\mathrm{O}(\epsilon^0)$ order stress should be noted:

$$u_1(X, y) = U_1(X) + H(y)\frac{\partial U_0}{\partial X} \tag{2.22}$$

$$E(y)(\frac{\partial u_0}{\partial X} + \frac{\partial u_1}{\partial y}) = E(y)(1 + \frac{\partial H(y)}{\partial y})\frac{\partial U_0}{\partial X} = E_0\frac{\partial U_0}{\partial X} \tag{2.23}$$

where

$$E_0 = \frac{E_\mathrm{a}E_\mathrm{b}}{(1-\alpha)E_\mathrm{a} + \alpha E_\mathrm{b}}$$

2.4.3 Asymptotic calculation of $\mathrm{O}(\epsilon^0)$ order equation

From $O(\epsilon^0)$ order on, the homogenized wave equation is generated because of the appearance of dynamic terms in the wave equation. The main calculation process consists of two parts shown in figure (2.3): the left part aims to obtain the homogenized wave equation at order $O(\epsilon^n)$; the right part's target is the solution of u_{n+2} which is a necessary element to derive the $O(\epsilon^{n+1})$ order homogenized equation.

The left part: homogenized wave equation at order $O(\epsilon^0)$.

$$\frac{\partial}{\partial X}\left(E(y)(\frac{\partial u_0}{\partial X} + \frac{\partial u_1}{\partial y})\right) + \frac{\partial}{\partial y}\left(E(y)(\frac{\partial u_1}{\partial X} + \frac{\partial u_2}{\partial y})\right) = \rho(y)\frac{\partial^2 u_0}{\partial t^2} \tag{2.24}$$

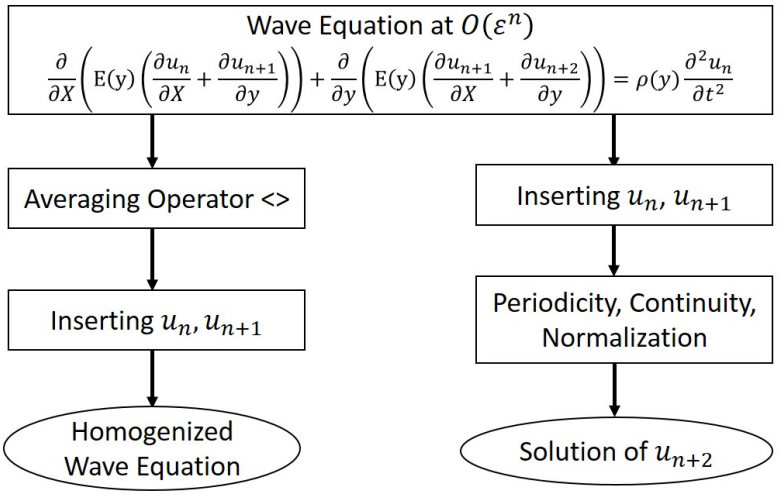

FIGURE 2.3: Calculation process of $O(\epsilon^n)$ order equation $n = 0, 1, 2...$

Applying the averaging operator to the equation (2.24), and because of the periodic force condition $\sigma_1(0) = \sigma_1(L)$, we have the following equation:

$$\frac{1}{L}\int_0^L \left(\frac{\partial}{\partial X}\left(E(y)(\frac{\partial u_0}{\partial X}+\frac{\partial u_1}{\partial y})\right)\right) dy = \frac{1}{L}\int_0^L \rho(y)\, dy \frac{\partial^2 u_0}{\partial t^2} \tag{2.25}$$

we note $\rho_0 =< \rho(y) >= \alpha\rho_a + (1-\alpha)\rho_b$ and substitute the equation (2.22) into the equation (2.25).

$$\frac{1}{L}\int_0^L \left(E(y)(1+\frac{\partial H(y)}{\partial y})\right) dy \frac{\partial^2 u_0}{\partial X^2} = \rho_0 \frac{\partial^2 u}{\partial t^2} \tag{2.26}$$

Since we have the exact expression of $H(y)$,

$$\begin{aligned}
&\frac{1}{L}\int_0^L \left(E(y)(1+\frac{\partial H(y)}{\partial y})\right) dy \\
=&\frac{1}{L}\int_0^{\alpha L} \left(E_a(1+\frac{\partial H_a(y)}{\partial y})\right) dy + \frac{1}{L}\int_{\alpha L}^{L} \left(E_b(1+\frac{\partial H_b(y)}{\partial y})\right) dy \\
=&\frac{E_a}{L}\int_0^{\alpha L} \left(1+\frac{(1-\alpha)(E_b-E_a)}{(1-\alpha)E_a+\alpha E_b}\right) dy + \frac{E_b}{L}\int_{\alpha L}^{L} \left(1+\frac{\alpha(E_a-E_b)}{(1-\alpha)E_a+\alpha E_b}\right) dy \\
=&\alpha E_a \frac{E_b}{(1-\alpha)E_a+\alpha E_b} + (1-\alpha)E_b\frac{E_a}{(1-\alpha)E_a+\alpha E_b} \\
=&\frac{E_a E_b}{(1-\alpha)E_a+\alpha E_b} = E_0
\end{aligned}$$

Finally, from the equation of order ϵ^0, equation (2.24), we get the homogenized equation for u_0:

$$E_0 \frac{\partial^2 u_0}{\partial X^2} = \rho_0 \frac{\partial^2 u_0}{\partial t^2} \tag{2.27}$$

where $\rho_0 =< \rho(y) >= \alpha\rho_\mathrm{a} + (1-\alpha)\rho_\mathrm{b}$. ρ_a, ρ_b represent the mass density of material A

and B. This is the traditional homogenized wave equation where the periodic structure is considered as a homogeneous one with equivalent parameters E_0, ρ_0. As mentioned before, equation (2.27) can not predict the dispersive effect of longitudinal waves in periodic structures. Thus, higher order equations are needed to provide a more precise wave equation.

The right part: solution of u_2, which is indispensable to obtain the $O(\epsilon^1)$ order homogenized equation. Owing to (2.22), the equation (2.24) becomes:

$$\frac{\partial^2 u_0}{\partial X^2}\left(E(y)(1+\frac{\partial H(y)}{\partial y})\right)+\frac{\partial}{\partial y}\left(E(y)(\frac{\partial U_1}{\partial X}+H(y)\frac{\partial^2 u_0}{\partial X^2}+\frac{\partial u_2}{\partial y})\right)=\rho(y)\frac{\partial^2 u_0}{\partial t^2} \quad (2.28)$$

For material A:

$$E(y)(1+\frac{\partial H(y)}{\partial y})=E_a(1+\frac{(1-\alpha)(E_b-E_a)}{(1-\alpha)E_a+\alpha E_b})=\frac{E_aE_b}{(1-\alpha)E_a+\alpha E_b}=E_0$$

For material B:

$$E(y)(1+\frac{\partial H(y)}{\partial y})=E_b(1+\frac{\alpha(E_a-E_b)}{(1-\alpha)E_a+\alpha E_b})=\frac{E_aE_b}{(1-\alpha)E_a+\alpha E_b}=E_0$$

So, for the whole structure, we always have

$$E(y)(1+\frac{\partial H(y)}{\partial y})=\frac{E_aE_b}{(1-\alpha)E_a+\alpha E_b}=E_0$$

Then the equation (2.28) becomes:

$$\frac{\partial}{\partial y}\left(E(y)(\frac{\partial U_1}{\partial X}+H(y)\frac{\partial^2 u_0}{\partial X^2}+\frac{\partial u_2}{\partial y})\right)=\rho(y)\frac{\partial^2 u_0}{\partial t^2}-E_0\frac{\partial^2 u_0}{\partial X^2}$$

Besides, according to equation (2.27), we have

$$\frac{\partial^2 u_0}{\partial t^2}=\frac{E_0}{\rho_0}\frac{\partial^2 u_0}{\partial X^2}$$

Then we have the equation to determine the expression of u_2:

$$\frac{\partial}{\partial y}\left(E(y)(\frac{\partial u_2}{\partial y}+\frac{\partial U_1}{\partial X}+H(y)\frac{\partial^2 u_0}{\partial X^2})\right)=E_0(\theta(y)-1)\frac{\partial^2 u_0}{\partial X^2} \quad (2.29)$$

with $\theta(y)=\rho(y)/\rho_0$.

By analogy to u_1, due to equation (2.29), the solution of u_2 should be in the following form:

$$u_2(X,y) = U_2(X) + H(y)\frac{\partial U_1}{\partial X} + P(y)\frac{\partial^2 u_0}{\partial X^2} \tag{2.30}$$

where $H(y)$ is the same as in the last section, and $P(y)$ needs to be determined. In order to find $P(y)$, substituting equation (2.30) into equation (2.29)

$$\frac{\partial}{\partial y}\left(E(y)\frac{\partial U_1}{\partial X}(\frac{\partial H(y)}{\partial y}+1) + E(y)\frac{\partial^2 u_0}{\partial X^2}(\frac{\partial P(y)}{\partial y}+H(y))\right) = E_0(\theta(y)-1)\frac{\partial^2 u_0}{\partial X^2} \tag{2.31}$$

we rewrite the equation (2.31)

$$\frac{\partial U_1}{\partial X}\frac{\partial}{\partial y}\left(E(y)(\frac{\partial H(y)}{\partial y}+1)\right) + \frac{\partial^2 u_0}{\partial X^2}\frac{\partial}{\partial y}\left(E(y)(\frac{\partial P(y)}{\partial y}+H(y))\right) = E_0(\theta(y)-1)\frac{\partial^2 u_0}{\partial X^2} \tag{2.32}$$

As $E(y)(1+H(y)_{,yy}) = E_0$, where $u_{,y}$ means the derivative with respect to y, the first term in the left side of the equation vanishes. And according to the equation (2.27), $u_{0,XX} \neq 0$. The equation (2.32) becomes:

$$\frac{\partial}{\partial y}\left(E(y)(\frac{\partial P(y)}{\partial y}+H(y))\right) = E_0(\theta(y)-1) \tag{2.33}$$

For the material A,

$$\begin{aligned}&\frac{\partial}{\partial y}\left(E_a(\frac{\partial P_a(y)}{\partial y}+H_a(y))\right) = E_0(\frac{\rho_a}{\rho_0}-1)\\ \Rightarrow &E_a(\frac{\partial P_a(y)}{\partial y}+H_a(y)) = E_0(\frac{\rho_a}{\rho_0}-1)(y+a_{2a})\end{aligned}$$

For the material B,

$$\begin{aligned}&\frac{\partial}{\partial y}\left(E_b(\frac{\partial P_b(y)}{\partial y}+H_b(y))\right) = E_0(\frac{\rho_b}{\rho_0}-1)\\ \Rightarrow &E_b(\frac{\partial P_b(y)}{\partial y}+H_b(y)) = E_0(\frac{\rho_b}{\rho_0}-1)(y+a_{2b})\end{aligned}$$

According to the displacement periodicity condition, we have:

$$u_2(X,0) = u_2(X,L) \Rightarrow P(0) = P(L) \Rightarrow < \frac{\partial P(y)}{\partial y} + H(y) >= 0$$

As for the order $O(\epsilon^1)$ stress:

$$\begin{aligned}\sigma_1 &= E(y)(\frac{\partial u_1}{\partial X}+\frac{\partial u_2}{\partial y})\\ &= E(y)(\frac{\partial U_1}{\partial X}+H(y)\frac{\partial^2 u_0}{\partial X^2})+E(y)(\frac{\partial H(y)}{\partial y}\frac{\partial U_1}{\partial X}+\frac{\partial P(y)}{\partial y}\frac{\partial^2 u_0}{\partial X^2})\\ &= E(y)(1+\frac{\partial H(y)}{\partial y})\frac{\partial U_1}{\partial X}+E(y)(H(y)+\frac{\partial P(y)}{\partial y})\frac{\partial^2 u_0}{\partial X^2}\end{aligned} \tag{2.34}$$

the continuity condition $\sigma_{1a}(X,\alpha L)=\sigma_{1b}(X,\alpha L)$ leads to

$$E_a(H_a(\alpha L)+\frac{\partial P_a(\alpha L)}{\partial y})=E_b(H_b(\alpha L)+\frac{\partial P_b(\alpha L)}{\partial y})$$

In summary, we have

$$\begin{cases} <\frac{\partial P(y)}{\partial y}+H(y)>=0\\ E_a(H_a(\alpha L)+\frac{\partial P_a(\alpha L)}{\partial y})=E_b(H_b(\alpha L)+\frac{\partial P_b(\alpha L)}{\partial y})\end{cases}$$

$$\Rightarrow\begin{cases}\int_0^{\alpha L}\frac{E_0}{E_a}(\frac{\rho_a}{\rho_0}-1)(y+a_{2a})\,dy+\int_{\alpha L}^{L}\frac{E_0}{E_b}(\frac{\rho_b}{\rho_0}-1)(y+a_{2b})\,dy=0\\ E_0(\frac{\rho_a}{\rho_0}-1)(\alpha L+a_{2a})=E_0(\frac{\rho_b}{\rho_0}-1)(\alpha L+a_{2b})\end{cases}$$

$$\Rightarrow\begin{cases}a_{2a}=-\frac{\alpha}{2}L\\ a_{2b}=-\frac{1+\alpha}{2}L\end{cases}$$

Then

$$\frac{\partial P(y)}{\partial y}+H(y)=\begin{cases}\frac{E_0}{E_a}(\frac{\rho_a}{\rho_0}-1)(y-\frac{\alpha}{2}L) & 0<y<\alpha L\\ \frac{E_0}{E_b}(\frac{\rho_b}{\rho_0}-1)(y-\frac{1+\alpha}{2}L) & \alpha L<y<L\end{cases}$$

which means

$$\begin{aligned}&\frac{\partial P(y)}{\partial y}\\ &=\begin{cases}\left(\frac{E_0}{E_a}(\frac{\rho_a}{\rho_0}-1)-\frac{(1-\alpha)(E_b-E_a)}{(1-\alpha)E_a+\alpha E_b}\right)\left(y-\frac{\alpha L}{2}\right) & 0<y<\alpha L\\ \left(\frac{E_0}{E_b}(\frac{\rho_b}{\rho_0}-1)-\frac{\alpha(E_a-E_b)}{(1-\alpha)E_a+\alpha E_b}\right)\left(y-\frac{(1+\alpha)L}{2}\right) & \alpha L<y<L\end{cases}\end{aligned} \tag{2.35}$$

We note that

$$c_{2a}=\frac{E_0}{E_a}(\frac{\rho_a}{\rho_0}-1)-\frac{(1-\alpha)(E_b-E_a)}{(1-\alpha)E_a+\alpha E_b}$$

$$c_{2b} = \frac{E_0}{E_b}(\frac{\rho_b}{\rho_0} - 1) - \frac{\alpha(E_a - E_b)}{(1-\alpha)E_a + \alpha E_b}$$

Then

$$\frac{\partial P(y)}{\partial y} = \begin{cases} c_{2a}\left(y - \dfrac{\alpha L}{2}\right) & 0 < y < \alpha L \\ c_{2b}\left(y - \dfrac{(1+\alpha)L}{2}\right) & \alpha L < y < L \end{cases}$$

which deduces that

$$P(y) = \begin{cases} c_{2a}\left(\dfrac{y^2}{2} - \dfrac{\alpha L}{2}y\right) + d_{2a} & 0 < y < \alpha L \\ c_{2b}\left(\dfrac{y^2}{2} - \dfrac{(1+\alpha)L}{2}y\right) + d_{2b} & \alpha L < y < L \end{cases}$$

where d_{2a}, d_{2b} needs to be determined. This is the same question as the one to determine the $H(y)$:two parameters, two conditions.

Periodicity condition: $u_2(X,0) = u_2(X,L) \Rightarrow P(0) = P(L)$

Normalization condition: $< u_2(X,y) >= U_2(X) \Rightarrow < P(y) >= 0$

These two conditions lead to:

$$\begin{cases} d_{2a} = -c_{2b}\dfrac{\alpha L^2}{2} + d_{2b} \\ \displaystyle\int_0^{\alpha L}\left(c_{2a}\left(\frac{y^2}{2} - \frac{\alpha L}{2}y\right) + d_{2a}\right)dy + \int_{\alpha L}^{L}\left(c_{2b}\left(\frac{y^2}{2} - \frac{1+\alpha L}{2}y\right) + d_{2b}\right)dy = 0 \end{cases}$$

After simplification, one can deduce that

$$\begin{cases} d_{2a} = -c_{2b}\dfrac{\alpha L^2}{2} + d_{2b} \\ d_{2a}\alpha L + d_{2b}(1-\alpha)L = c_{2a}\dfrac{\alpha^3 L^3}{12} + c_{2b}\dfrac{L^3}{12}(\alpha^3 + 3\alpha^2 - 3\alpha - 1) \end{cases}$$

Finally, the two parameters are obtained

$$\begin{cases} d_{2a} = c_{2a}\dfrac{\alpha^3 L^2}{12} + c_{2b}\dfrac{L^2}{12}(\alpha^3 - 3\alpha^2 + 3\alpha - 1) \\ d_{2b} = c_{2a}\dfrac{\alpha^3 L^2}{12} + c_{2b}\dfrac{L^2}{12}(\alpha^3 - 3\alpha^2 - 3\alpha - 1) \end{cases}$$

And the exact expression of $P(y)$ can be expressed as:

$$P(y) = \begin{cases} c_{2a}\left(\frac{y^2}{2} - \frac{\alpha L}{2}y\right) + d_{2a} & 0 < y < \alpha L \\ c_{2b}\left(\frac{y^2}{2} - \frac{(1+\alpha)L}{2}y\right) + d_{2b} & \alpha L < y < L \end{cases} \tag{2.36}$$

with four constants

$$\begin{cases} c_{2a} = \frac{E_0}{E_a}(\frac{\rho_a}{\rho_0} - 1) - \frac{(1-\alpha)(E_b - E_a)}{(1-\alpha)E_a + \alpha E_b} \\ c_{2b} = \frac{E_0}{E_b}(\frac{\rho_b}{\rho_0} - 1) - \frac{\alpha(E_a - E_b)}{(1-\alpha)E_a + \alpha E_b} \\ d_{2a} = c_{2a}\frac{\alpha^3 L^2}{12} - c_{2b}\frac{L^2}{12}(\alpha^3 - 3\alpha^2 + 3\alpha - 1) \\ d_{2b} = c_{2a}\frac{\alpha^3 L^2}{12} - c_{2b}\frac{L^2}{12}(\alpha^3 - 3\alpha^2 - 3\alpha - 1) \end{cases} \tag{2.37}$$

The expression of $P(y)$ being deduced, an useful conclusion about the $\mathrm{O}(\epsilon^1)$ order stress should be noted:

$$E(y)(\frac{\partial u_1}{\partial X} + \frac{\partial u_2}{\partial y}) = E_0\frac{\partial U_1}{\partial X} + E(y)(H(y) + \frac{\partial P(y)}{\partial y})\frac{\partial^2 U_0}{\partial X^2} \tag{2.38}$$

2.4.4 Asymptotic calculation of $\mathrm{O}(\epsilon^1)$ order equation

At $O(\epsilon^1)$, the wave equation is:

$$\frac{\partial}{\partial X}\left(E(y)(\frac{\partial u_1}{\partial X} + \frac{\partial u_2}{\partial y})\right) + \frac{\partial}{\partial y}\left(E(y)(\frac{\partial u_2}{\partial X} + \frac{\partial u_3}{\partial y})\right) = \rho(y)\frac{\partial^2 u_1}{\partial t^2} \tag{2.39}$$

Applying the averaging operator to the equation (2.39), and because of the periodic stress condition $\sigma_2(0) = \sigma_2(L)$, we have the following equation:

$$\frac{1}{L}\int_0^L \left(\frac{\partial}{\partial X}\left(E(y)(\frac{\partial u_1}{\partial X} + \frac{\partial u_2}{\partial y})\right)\right) dy = \frac{1}{L}\int_0^L \rho(y)\frac{\partial^2 u_1}{\partial t^2}\, dy \tag{2.40}$$

Subsisting equation (2.34) into the left side of above equation

$$\begin{aligned} &\frac{1}{L}\int_0^L \left(\frac{\partial}{\partial X}\left(E(y)(\frac{\partial u_1}{\partial X} + \frac{\partial u_2}{\partial y})\right)\right) dy \\ =&\frac{1}{L}\int_0^L \left(\frac{\partial}{\partial X}\left(E(y)(1 + \frac{\partial H(y)}{\partial y})\frac{\partial U_1}{\partial X} + E(y)(H(y) + \frac{\partial P(y)}{\partial y})\frac{\partial^2 u_0}{\partial X^2}\right)\right) dy \\ =&< E(y)(1 + \frac{\partial H(y)}{\partial y}) > \frac{\partial^2 U_1}{\partial X^2} + < E(y)(H(y) + \frac{\partial P(y)}{\partial y}) > \frac{\partial^3 u_0}{\partial X^3} \end{aligned}$$

we have obtained that

$$\frac{\partial P(y)}{\partial y} + H(y) = \begin{cases} \frac{E_0}{E_a}(\frac{\rho_a}{\rho_0} - 1)(y - \frac{\alpha}{2}L) & 0 < y < \alpha L \\ \frac{E_0}{E_b}(\frac{\rho_b}{\rho_0} - 1)(y - \frac{1+\alpha}{2}L) & \alpha L < y < L \end{cases}$$

Thus,

$$\begin{aligned} &< E(y)(H(y) + \frac{\partial P(y)}{\partial y}) > \\ =&E_0(\frac{\rho_a}{\rho_0} - 1)\frac{1}{L}\int_0^{\alpha L}(y - \frac{\alpha}{2}L)\,dy + E_0(\frac{\rho_b}{\rho_0} - 1)\frac{1}{L}\int_{\alpha L}^{L}(y - \frac{1+\alpha}{2}L)\,dy \\ =&0 \end{aligned}$$

As $E(y)(1 + H(y)_{,y}) = E_0$, equation (2.40) becomes

$$E_0\frac{\partial^2 U_1}{\partial X^2} = \frac{1}{L}\int_0^L \rho(y)\frac{\partial^2 u_1}{\partial t^2}\,dy \tag{2.41}$$

Substituting the equation (2.22) into the right side of above equation

$$\frac{1}{L}\int_0^L \rho(y)\frac{\partial^2 u_1}{\partial t^2}\,dy = \frac{1}{L}\int_0^L \rho(y)\,dy\frac{\partial^2 U_1}{\partial t^2} + \frac{1}{L}\int_0^L \rho(y)H(y)\,dy\frac{\partial^2}{\partial t^2}\left(\frac{\partial u_0}{\partial X}\right)$$

As the exact expression of $H(y)$ has been deduced, the second term in the above expression can be simplified

$$\begin{aligned} &\frac{1}{L}\int_0^L \rho(y)H(y)\,dy \\ =&\frac{1}{L}\rho_a\frac{(1-\alpha)(E_b - E_a)}{(1-\alpha)E_a + \alpha E_b}\int_0^{\alpha L}\left(y - \frac{\alpha L}{2}\right)dy + \\ &\frac{1}{L}\rho_b\frac{\alpha(E_a - E_b)}{(1-\alpha)E_a + \alpha E_b}\int_{\alpha L}^{L}\left(y - \frac{(1+\alpha)L}{2}\right)dy \\ =&0 \end{aligned}$$

Finally, the homogenized equation at $O(\epsilon^1)$ order reads:

$$E_0\frac{\partial^2 U_1}{\partial X^2} = \rho_0\frac{\partial^2 U_1}{\partial t^2} \tag{2.42}$$

Then, similar to the previous section, the solution of u_3, which is essential to obtain the $O(\epsilon^2)$ order homogenized equation, should be deduced from equation (2.39). Substituting the expression of u_1, u_2 in equation (2.39), the second term in the left side of the

equation becomes

$$\begin{aligned}&\frac{\partial}{\partial y}\left(E(y)(\frac{\partial u_2}{\partial X}+\frac{\partial u_3}{\partial y})\right)\\=&\frac{\partial}{\partial y}\left(E(y)(\frac{\partial u_3}{\partial y}+\frac{\partial U_2}{\partial X}+H(y)\frac{\partial^2 U_1}{\partial X^2}+P(y)\frac{\partial^3 u_0}{\partial X^3})\right)\end{aligned}$$

The first term in the left side of equation (2.39) becomes

$$\begin{aligned}&\frac{\partial}{\partial X}\left(E(y)(\frac{\partial u_1}{\partial X}+\frac{\partial u_2}{\partial y})\right)\\=&\frac{\partial}{\partial X}\left(E(y)(\frac{\partial U_1}{\partial X}+H(y)\frac{\partial^2 u_0}{\partial X^2}+\frac{\partial H(y)}{\partial y}\frac{\partial U_1}{\partial X}+\frac{\partial P(y)}{\partial y}\frac{\partial^2 u_0}{\partial X^2})\right)\\=&E(y)(1+\frac{\partial H(y)}{\partial y})\frac{\partial^2 U_1}{\partial X^2}+E(y)(H(y)+\frac{\partial P(y)}{\partial y})\frac{\partial^3 u_0}{\partial X^3}\\=&E_0\frac{\partial^2 U_1}{\partial X^2}+E(y)(H(y)+\frac{\partial P(y)}{\partial y})\frac{\partial^3 u_0}{\partial X^3}\end{aligned}$$

The right side term of equation (2.39) becomes

$$\rho(y)\frac{\partial^2 u_1}{\partial t^2}=\rho(y)\frac{\partial^2 U_1}{\partial t^2}+\rho(y)H(y)\frac{\partial^2}{\partial t^2}(\frac{\partial u_0}{\partial X})$$

According to equation (2.27) and equation (2.42), we have

$$\frac{\partial^2 U_1}{\partial t^2}=\frac{E_0}{\rho_0}\frac{\partial^2 U_1}{\partial X^2}$$

$$\frac{\partial^2}{\partial t^2}(\frac{\partial u_0}{\partial X})=\frac{\partial}{\partial X}(\frac{\partial^2 u_0}{\partial t^2})=\frac{\partial}{\partial X}(\frac{E_0}{\rho_0}\frac{\partial^2 u_0}{\partial X^2})=\frac{E_0}{\rho_0}\frac{\partial^3 u_0}{\partial X^3}$$

then the right side of equation (2.39) becomes:

$$\rho(y)\frac{\partial^2 u_1}{\partial t^2}=E_0\frac{\rho(y)}{\rho_0}\frac{\partial^2 U_1}{\partial X^2}+E_0H(y)\frac{\rho(y)}{\rho_0}\frac{\partial^3 u_0}{\partial X^3}=E_0\theta(y)\frac{\partial^2 U_1}{\partial X^2}+E_0H(y)\theta(y)\frac{\partial^3 u_0}{\partial X^3}$$

We replace all the term in equation (2.39):

$$\begin{aligned}&E_0\frac{\partial^2 U_1}{\partial X^2}+E(y)(H(y)+\frac{\partial P(y)}{\partial y})\frac{\partial^3 u_0}{\partial X^3}+\\&\frac{\partial}{\partial y}\left(E(y)(\frac{\partial u_3}{\partial y}+\frac{\partial U_2}{\partial X}+H(y)\frac{\partial^2 U_1}{\partial X^2}+P(y)\frac{\partial^3 u_0}{\partial X^3})\right)\\=&E_0\theta(y)\frac{\partial^2 U_1}{\partial X^2}+E_0H(y)\theta(y)\frac{\partial^3 u_0}{\partial X^3}\end{aligned}$$

The above equation can be rewritten in the following form:

$$\begin{aligned}&\frac{\partial}{\partial y}\left(E(y)(\frac{\partial u_3}{\partial y}+\frac{\partial U_2}{\partial X}+H(y)\frac{\partial^2 U_1}{\partial X^2}+P(y)\frac{\partial^3 u_0}{\partial X^3})\right)=\\&\left(E_0H(y)\theta(y)-E(y)(H(y)+\frac{\partial P(y)}{\partial y})\right)\frac{\partial^3 u_0}{\partial X^3}+E_0(\theta(y)-1)\frac{\partial^2 U_1}{\partial X^2}\end{aligned}\tag{2.43}$$

By analogy, the general solution of u_3 is as follows:

$$u_3(X,y)=U_3(X)+H(y)\frac{\partial U_2}{\partial X}+P(y)\frac{\partial^2 U_1}{\partial X^2}+Q(y)\frac{\partial^3 u_0}{\partial X^3}\tag{2.44}$$

where $Q(y)$ remains to be determined.

Substituting the above expression into equation (2.43), the left side of the equation becomes:

$$\begin{aligned}\frac{\partial}{\partial y}\Big(&E(y)(\frac{\partial H(y)}{\partial y}+1)\frac{\partial U_2}{\partial X}+E(y)(\frac{\partial P(y)}{\partial y}+H(y))\frac{\partial^2 U_1}{\partial X^2}\\&+E(y)(\frac{\partial Q(y)}{\partial y}+P(y))\frac{\partial^3 u_0}{\partial X^3}\Big)\end{aligned}$$

According to equation (2.33) , we have

$$\frac{\partial}{\partial y}\left(E(y)(\frac{\partial P(y)}{\partial y}+H(y))\right)=E_0(\theta(y)-1)$$

Beside $(E(y)(1+H(y)_{,y})_{,y}=0$, the equation (2.61) can be simplified as:

$$\frac{\partial}{\partial y}\left(E(y)(\frac{\partial Q(y)}{\partial y}+P(y))\right)=E_0H(y)\theta(y)-E(y)(H(y)+\frac{\partial P(y)}{\partial y})\tag{2.45}$$

Then following the same calculate process which is shown in the last section, we can get the following expression:

$$P(y)+\frac{\partial Q(y)}{\partial y}=\begin{cases}a_{3a}(\frac{y^2}{2}-\frac{\alpha L}{2}y)+b_{3a} & 0<y<\alpha L\\ a_{3b}(\frac{y^2}{2}-\frac{(1+\alpha)L}{2}y)+b_{3b} & \alpha L<y<L\end{cases}\tag{2.46}$$

with

$$\begin{cases} a_{3a} = \dfrac{E_0^2(1-\alpha)}{\rho_0 E_a^2 E_b}\left(E_a(-2\rho_a+\rho_0)+E_b(\rho_a+\rho_b-\rho_0)\right) \\ a_{3a} = \dfrac{E_0^2\alpha}{\rho_0 E_a E_b^2}\left(E_a(\rho_a+\rho_b-\rho_0)+E_b(-2\rho_b+\rho_0)\right) \\ b_{3a} = a_{3a}\dfrac{\alpha^3 L^2}{12} - a_{3b}\dfrac{L^2}{12}(\alpha^3-3\alpha^2+3\alpha-1) \\ b_{3b} = a_{3a}\dfrac{\alpha^3 L^2}{12} - a_{3b}\dfrac{L^2}{12}(\alpha^3-3\alpha^2-3\alpha-1) \end{cases}$$

And further calculations gives the exact expression of $Q(y)$. Some helpful conclusions should be noted:

$$\begin{aligned} &< E(y)(P(y)+\frac{\partial Q(y)}{\partial y}) > \\ &= -\frac{\alpha(1-\alpha)E_0L^2}{12\rho_0}\left(\frac{(E_b-E_a)(\alpha^2\rho_a-(1-\alpha)^2\rho_2)+E_0\rho_0}{(1-\alpha)E_a+\alpha E_b}-\rho_0\right) \end{aligned} \tag{2.47}$$

The $\mathrm{O}(\epsilon^2)$ order stress:

$$\begin{aligned} &E(y)(\frac{\partial u_2}{\partial X}+\frac{\partial u_3}{\partial y}) \\ =&E_0\frac{\partial U_2}{\partial X}+E(y)(H+\frac{\partial P}{\partial y})\frac{\partial^2 U_1}{\partial X^2}+E(y)(P+\frac{\partial Q}{\partial y})\frac{\partial^3 U_0}{\partial X^3} \end{aligned} \tag{2.48}$$

2.4.5 Asymptotic calculation of $\mathrm{O}(\epsilon^2)$ order equation

At $O(\epsilon^2)$, the wave equation is:

$$\frac{\partial}{\partial X}\left(E(y)(\frac{\partial u_2}{\partial X}+\frac{\partial u_3}{\partial y})\right)+\frac{\partial}{\partial y}\left(E(y)(\frac{\partial u_3}{\partial X}+\frac{\partial u_4}{\partial y})\right)=\rho(y)\frac{\partial^2 u_2}{\partial t^2} \tag{2.49}$$

Applying the averaging operator to the equation (2.49), and because of the periodic stress condition $\sigma_3(0)=\sigma_3(L)$, the above equation becomes:

$$\frac{1}{L}\int_0^L\left(\frac{\partial}{\partial X}\left(E(y)(\frac{\partial u_2}{\partial X}+\frac{\partial u_3}{\partial y})\right)\right)dy=\frac{1}{L}\int_0^L\rho(y)\frac{\partial^2 u_2}{\partial t^2}\,dy \tag{2.50}$$

Replacing the u_2, u_3 in equation (2.50), the left side becomes:

$$\begin{aligned}
&\frac{1}{L}\int_0^L \left(\frac{\partial}{\partial X}\left(E(y)(\frac{\partial u_2}{\partial X}+\frac{\partial u_3}{\partial y})\right)\right) dy \\
=&\frac{1}{L}\int_0^L \left(\frac{\partial}{\partial X}\left(E(y)(1+\frac{\partial H(y)}{\partial y})\frac{\partial U_2}{\partial X}+E(y)(H(y)+\frac{\partial P(y)}{\partial y})\frac{\partial^2 U_1}{\partial X^2}\right.\right. \\
&\left.\left.+E(y)(P(y)+\frac{\partial Q(y)}{\partial y})\frac{\partial^2 u_0}{\partial X^3}\right)\right) dy \\
=&< E(y)(1+\frac{\partial H(y)}{\partial y}) > \frac{\partial^2 U_2}{\partial X^2}+< E(y)(H(y)+\frac{\partial P(y)}{\partial y}) > \frac{\partial^3 U_1}{\partial X^3} \\
&+< E(y)(P(y)+\frac{\partial Q(y)}{\partial y}) > \frac{\partial^4 u_0}{\partial X^4}
\end{aligned}$$

As is shown in the previous section:

$$E(y)(1+\frac{\partial H(y)}{\partial y}) = E_0$$

$$< E(y)(H(y)+\frac{\partial P(y)}{\partial y}) >= 0$$

$$\begin{aligned}
&< E(y)(P(y)+\frac{\partial Q(y)}{\partial y}) > \\
=&-\frac{\alpha(1-\alpha)E_0L^2}{12\rho_0}\left(\frac{(E_b-E_a)(\alpha^2\rho_a-(1-\alpha)^2\rho_2)+E_0\rho_0}{(1-\alpha)E_a+\alpha E_b}-\rho_0\right)
\end{aligned}$$

The right side term of equation (2.50) becomes:

$$\begin{aligned}
&\frac{1}{L}\int_0^L \rho(y)\frac{\partial^2 u_2}{\partial t^2}\,dy \\
=&\frac{1}{L}\int_0^L \rho(y)\,dy\frac{\partial^2 U_2}{\partial t^2}+\frac{1}{L}\int_0^L \rho(y)H(y)\,dy\frac{\partial^2}{\partial t^2}\left(\frac{\partial U_1}{\partial X}\right) \\
+&\frac{1}{L}\int_0^L \rho(y)P(y)\,dy\frac{\partial^2}{\partial t^2}\left(\frac{\partial^2 u_0}{\partial X^2}\right) \\
=&\rho_0\frac{\partial^2 U_2}{\partial t^2}+< \rho(y)H(y) > \frac{\partial^2}{\partial t^2}\left(\frac{\partial U_1}{\partial X}\right)+< \rho(y)P(y) > \frac{\partial^2}{\partial t^2}\left(\frac{\partial^2 u_0}{\partial X^2}\right)
\end{aligned}$$

Knowing the expression of $p(y)$, one can calculate:

$$< \rho(y)P(y) >= \frac{\alpha^2(1-\alpha)^2(\rho_b-\rho_a)(E_a\rho_a-E_b\rho_b)E_0L^2}{12\rho_0E_aE_b} \tag{2.51}$$

Besides, we have obtained that $< \rho(y)H(y) >= 0$. With all these calculations, the equation (2.50) becomes:

$$E_0\frac{\partial^2 U_2}{\partial X^2}+ < E(y)(P(y)+\frac{\partial Q(y)}{\partial y}) > \frac{\partial^4 u_0}{\partial X^4} = \rho_0\frac{\partial^2 U_2}{\partial t^2}+ < \rho(y)P(y) > \frac{\partial^2}{\partial t^2}\left(\frac{\partial^2 u_0}{\partial X^2}\right)$$

Again, according to equation (2.27), we have

$$\frac{\partial^2 u_0}{\partial t^2} = \frac{E_0}{\rho_0}\frac{\partial^2 u_0}{\partial X^2}$$

Hence,

$$\frac{\partial^2}{\partial t^2}\left(\frac{\partial^2 u_0}{\partial X^2}\right) = \frac{\partial^2}{\partial X^2}\left(\frac{\partial^2 u_0}{\partial t^2}\right) = \frac{\partial^2}{\partial X^2}\left(\frac{E_0}{\rho_0}\frac{\partial^2 u_0}{\partial X^2}\right) = \frac{E_0}{\rho_0}\frac{\partial^4 u_0}{\partial X^4}$$

Equation (2.50) can be further simplified as:

$$E_0\frac{\partial^2 U_2}{\partial X^2} + (< E(y)(P(y)+\frac{\partial Q(y)}{\partial y}) > -\frac{E_0}{\rho_0} < \rho(y)P(y) >)\frac{\partial^4 u_0}{\partial X^4} = \rho_0\frac{\partial^2 U_2}{\partial t^2}$$

Substituting the two averaging expression, one can obtain the final homogenized equation of u_2

$$E_0\frac{\partial^2 U_2}{\partial X^2} + \frac{1}{\epsilon^2}E_d\frac{\partial^4 u_0}{\partial X^4} = \rho_0\frac{\partial^2 U_2}{\partial t^2} \tag{2.52}$$

with

$$E_d = \frac{\alpha^2(1-\alpha)^2(E_a\rho_a - E_b\rho_b)^2 E_0 l^2}{12\rho_0^2((1-\alpha)E_a + \alpha E_b)^2}$$

Then, the solution of u_4, which is indispensable to obtain the homogenized equation at the $O(\epsilon^3)$ order, should also be deduced by similar manipulations as before. However, as the homogenization process stops at the $O(\epsilon^2)$ order, u_4 is no longer needed.

Observing all the homogenized equations obtained by multi-scale asymptotic method and HPDM, it can be found that these homogenized wave equations for various orders are the same, which proves the accuracy of the homogenized models in another way.

2.4.6 Global homogenised equation

After all these manipulations, a summary about all the homogenized equations at various orders is needed:

At $O(\epsilon^0)$ Eq. (2.27) :

$$E_0\frac{\partial^2 U_0}{\partial X^2} = \rho_0\frac{\partial^2 U_0}{\partial t^2}$$

At $O(\epsilon^1)$ Eq. (2.42) :

$$E_0 \frac{\partial^2 U_1}{\partial X^2} = \rho_0 \frac{\partial^2 U_1}{\partial t^2}$$

At $O(\epsilon^2)$ Eq. (2.52) :

$$E_0 \frac{\partial^2 U_2}{\partial X^2} + \frac{1}{\epsilon^2} E_d \frac{\partial^4 U_0}{\partial X^4} = \rho_0 \frac{\partial^2 U_2}{\partial t^2}$$

As the displacement $u(X, y)$ has been expanded as

$$u(X, y) = u_0(X, y) + \epsilon u_1(X, y) + \epsilon^2 u_2(X, y) + ...$$

the global or the mean displacement is straightforwardly defined as:

$$U(X) =< u(X, y) >= U_0(X) + \epsilon U_1(X) + \epsilon^2 U_2(X) + ... \tag{2.53}$$

Combining these homogenized equations (2.27) $\times \epsilon^0$ + (2.42) $\times \epsilon^1$ + (2.52) $\times \epsilon^2$, then neglecting the $O(\epsilon^3)$ order and higher leads to a homogenized equation for the mean displacement:

$$E_0 \frac{\partial^2 U}{\partial X^2} + E_d \frac{\partial^4 U_0}{\partial X^4} = \rho_0 \frac{\partial^2 U}{\partial t^2} \tag{2.54}$$

Observing the coefficient E_d, one can notice that E_d is proportional to l^2. Thus,

$$E_d \frac{\partial^2}{\partial X^2} \propto O(\frac{l^2}{L^2}) \propto O(\epsilon^2)$$

For the second term in equation (2.54), neglecting the $O(\epsilon^3)$ order and higher means only the $O(\epsilon^0)$ order term of U can be considered. Thus, under the 'neglecting' hypotheses, we have:

$$E_d \frac{\partial^2 U_0}{\partial X^2} = E_d \frac{\partial^2 U}{\partial X^2} \tag{2.55}$$

Hence, two different ideas are available to do further approximation.

First idea(HOH1)

Applying directly the relation in (2.55) to (2.54) leads to:

$$E_0 \frac{\partial^2 U}{\partial X^2} + E_d \frac{\partial^4 U}{\partial X^4} = \rho_0 \frac{\partial^2 U}{\partial t^2} \tag{2.56}$$

Different from the original second order wave equation (2.1), an intuitively obtained fourth order PDE serves as the equivalent wave equation. In this homogenized equation,

E_0, ρ_0 can no longer be treated as the effective parameters of a homogeneous structure. And higher order means more boundary conditions are needed in the finite case. This model is referred as HOH1 for higher order homogenization model one.

Second idea(HOH2)

According to (2.27)

$$\frac{\partial^2 U_0}{\partial X^2} = \frac{\rho_0}{E_0}\frac{\partial^2 U_0}{\partial t^2}$$

Then

$$E_d\frac{\partial^4 U_0}{\partial X^4} = E_d\frac{\partial^2}{\partial X^2}(\frac{\rho_0}{E_0}\frac{\partial^2 U_0}{\partial t^2}) = \frac{\rho_0}{E_0}\frac{\partial^2}{\partial t^2}(E_d\frac{\partial^2 U_0}{\partial X^2}) = \frac{\rho_0}{E_0}\frac{\partial^2}{\partial t^2}(E_d\frac{\partial^2 U}{\partial X^2})$$

In this case, equation (2.54) becomes:

$$E_0\frac{\partial^2 U}{\partial X^2} + \rho_0\frac{E_d}{E_0}\frac{\partial^2}{\partial X^2}(\frac{\partial^2 U}{\partial t^2}) = \rho_0\frac{\partial^2 U}{\partial t^2} \tag{2.57}$$

A second order PDE comprising a time-space coupling term is deduced as the effective wave equation. In this model, the periodic structure can not be considered as a homogeneous one, neither. This model is referred as HOH2 for higher order homogenization model two.

With these models being obtained, the next important step will be the validation. In order to validate these models, the new dispersion relations of these models will be compared with the analytical dispersion relation. Furthermore, these homogenized models are applied to finite structures. The frequency response function of these new homogenized models are also compared with the numerical WFEM result. The valid frequency ranges in both cases of the homogenized models are established.

2.5 Validation in the infinite case

In this section, the dispersion relation obtained by higher order homogenized models will be compared with the analytical dispersion relation. At the same time, the traditional homogenized model (TH), which is actually the $O(\epsilon^0)$ order homogenization model, will also be illustrated to demonstrate a better accuracy of the higher order homogenized model. We have assumed that $\epsilon = l/L << 1$, and the homogenization

process is under long-wave approximation. The investigated frequency range is limited to the first propagating zone.

2.5.1 Dispersion relation

Supposing all the wave solutions are harmonic:

$$U(X,t) = A\ exp[i(\omega t - kX)] \tag{2.58}$$

where A is the amplitude, ω is the frequency, and k is the wavenumber. Then the dispersion relation is the relation between ω and k, which characterises the wave propagation in a waveguide. For the periodic structure, the analyse of the whole structure can be converted to a unit cell (figure 2.4). l_{a} and l_{b} denote respectively the length of material A and B.

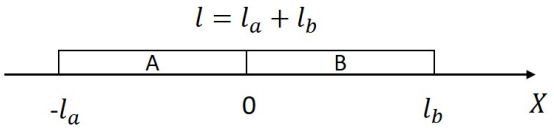

FIGURE 2.4: unit cell of the periodic rod

Analytical exact dispersion relation For the piecewise unit cell, a classical longitudinal wave equation can be written for part A and part B:

$$E_a\frac{\partial^2 U}{\partial X^2} - \rho_a\frac{\partial^2 U}{\partial t^2} = 0; \quad E_b\frac{\partial^2 U}{\partial X^2} - \rho_b\frac{\partial^2 U}{\partial t^2} = 0 \tag{2.59}$$

The periodic conditions obtained by Floquet-Bloch theory are:

$$U(l_{\mathrm{b}},t) = exp(-ikl)U(-l_{\mathrm{a}},t)$$

$$\frac{\partial U(l_{\mathrm{b}},t)}{\partial X} = exp(-ikl)\frac{\partial U(-l_{\mathrm{a}},t)}{\partial X}$$

The continuity conditions at the interface are:

$$U(0^-,t) = U(0^+,t)$$

$$\frac{\partial U(0^-,t)}{\partial X} = \frac{\partial U(0^+,t)}{\partial X}$$

These conditions lead to a four linear equations system. This equation system has a non-trivial solution if and only if the associated matrix's determinant is zero. Then the exact dispersion relation is obtained:

$$cos(kl) = cos(\frac{\omega}{c_\mathrm{a}}l_\mathrm{a})cos(\frac{\omega}{c_\mathrm{b}}l_\mathrm{b}) - \frac{1}{2}(\frac{\rho_\mathrm{a}c_\mathrm{a}}{\rho_\mathrm{b}c_\mathrm{b}} + \frac{\rho_\mathrm{b}c_\mathrm{b}}{\rho_\mathrm{a}c_\mathrm{a}})sin(\frac{\omega}{c_\mathrm{a}}l_\mathrm{a})sin(\frac{\omega}{c_\mathrm{b}}l_\mathrm{b}) \tag{2.60}$$

where $c_\mathrm{a} = \sqrt{E_\mathrm{a}/\rho_\mathrm{a}}$, $c_\mathrm{b} = \sqrt{E_\mathrm{b}/\rho_\mathrm{b}}$

TH model Substituting (2.58) into (2.27), we obtain the dispersion relation:

$$\omega = \sqrt{\frac{E_0}{\rho_0}}k \tag{2.61}$$

HOH1 model Substituting (2.58) into (2.56),we obtain the dispersion relation:

$$\omega = \sqrt{\frac{E_0}{\rho_0}}k\sqrt{\frac{E_0 - E_\mathrm{d}k^2}{E_0}} \tag{2.62}$$

HOH2 model Substituting (2.58) into (2.57),we obtain the dispersion relation:

$$\omega = \sqrt{\frac{E_0}{\rho_0}}k\sqrt{\frac{E_0}{E_0 + E_\mathrm{d}k^2}} \tag{2.63}$$

In the comparison, the analytical exact dispersion equation performs as the benchmark. The valid domain is defined as follows:

For each frequency f, if

$$\frac{|k_{ref} - k_{homo}|}{k_{ref}} < 1\%$$

then $f \in (0, f_{lim})$. Where k_{homo}, k_{ref} are the wavenumber obtained respectively by homogenized models and the reference model. The valid domain is $(0, f_{lim})$, f_{lim} is the limit of the valid domain.

A numerical example is presented: material A is Epoxy with $E_\mathrm{a} = 4.35GPa$, $\rho_\mathrm{a} = 1180kg/m^3$, $l_\mathrm{a} = 1m$; and material B is Aluminium with $E_\mathrm{b} = 77.56GPa$, $\rho_\mathrm{b} = 2730kg/m^3$, $l_\mathrm{b} = 1m$. With these parameters, one can calculate $E_0 = 8.238GPa$, $E_\mathrm{d} = 1.1428GPa$ and $\rho_0 = 1955kg/m^3$. The dispersion curves obtained by the four different models are depicted in figure (2.5).

From figure (2.5), it can be seen that the first band gap frequency $f_{gap} = 373$Hz. If a relative error of 1% is tolerated, the valid frequency of TH, HOH1 and HOH2 are

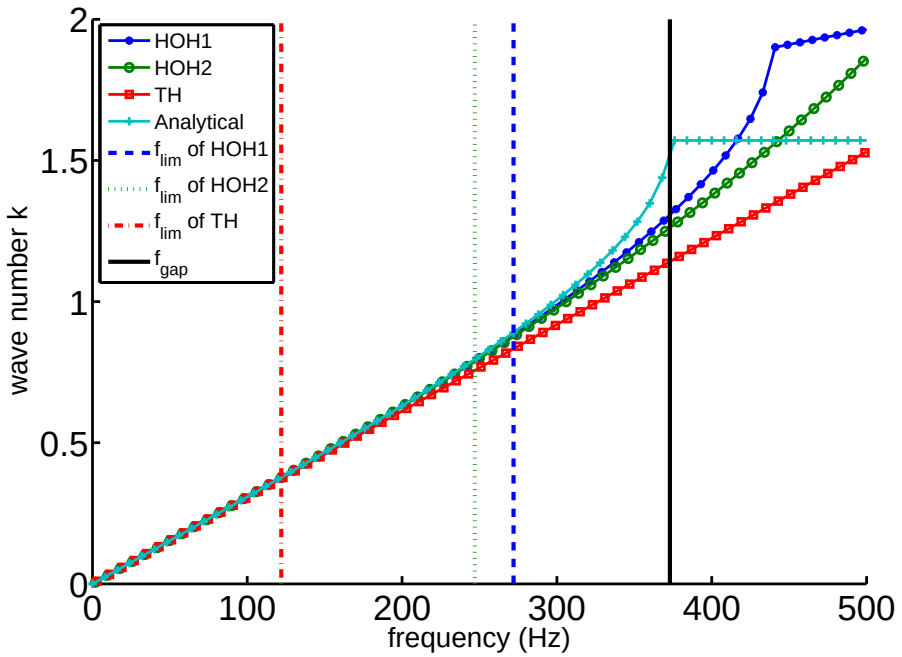

FIGURE 2.5: dispersion curve of the Ep-Al periodic rod obtained by different models

respectively (0, 122Hz), (0, 272Hz), (0, 247Hz). HOH1 performs a little better than HOH2, but they both provide a larger validity range. In this case, a more precise homogenized model is offered by the HOH1 and HOH2.

In the binary periodic structure, wave reflects at the interface of two materials due to the impedance mismatch. Thus, the dispersion curve of periodic structures behaves differently from the homogeneous structures where impedance mismatch doesn't exist. The biggest difference is the presence of the Bragg band gap in the periodic structure. The higher order homogenized wave propagation equations, deduced from the multi-scale asymptotic development, are the motion equations describing the periodic structure's dynamics. As the heterogeneity is taken into account during the homogenization process, the wave reflection caused by the heterogeneity is also considered in the homogenized wave equation. However, when the periodic structure is homogenized, the impedance mismatch disappears. That is another reason why the validity range is limited to the first propagating zone. The current results show that the higher order models are more accurate models than the classical model. However, further studies are still needed to investigate the convergence of this method.

It is obvious that three parameter contrasts $(l_b/l_a, E_b/E_a, \rho_b/\rho_a)$ play important roles in these models. In the next section, a parametric study concerning these three

contrasts has been made to verify the robustness of higher order homogenization models.

2.5.2 Parametric study: contrast of length fraction

The first contrast is the length fraction l_b/l_a. For simplicity, $l_a = \alpha l, l_b = (1-\alpha)l$, where $\alpha \in (0,1)$ reminds the same as in figure (2.1). In this case, the material A is Epoxy, whilst the material B is Aluminium. The properties of A and B remain the same as before, α is the only variable. Then, the first band gap frequency f_{gap} and the limit of the valid frequency range f_{lim} of these three different homogenized models are shown in figure (2.6).

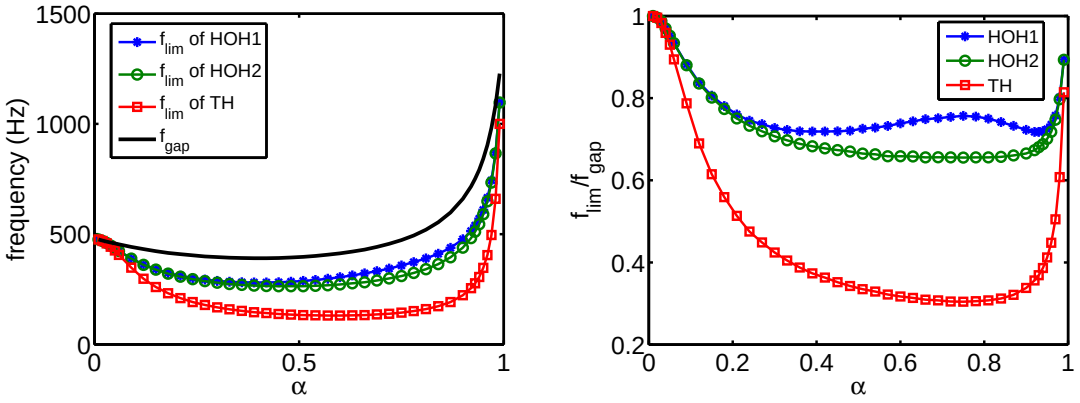

(a) valid frequency range f_{lim}

(b) relative valid frequency range f_{lim}/f_{gap}

FIGURE 2.6: different homogenized models in the fraction of α

When $\alpha \to 0$ ($l_a \to 0$), or when $\alpha \to 1$ ($l_a \to l$), the unit cell becomes almost a homogeneous rod with only material A or material B. Under this condition, the figure (2.6(a)) depicts that these three models all provide good approximation. But, for a more heterogeneous unit cell with α far from 0 and 1, the preponderance of HOH1 and HOH2 comes out. They both offer a larger valid frequency range compared to TH model. For instance, when $\alpha = 0.5$, which is the first studied case, from the figure (2.6(b)) one can deduce that the relative f_{lim} of HOH1 model and the HOH2 model are respectively about 72% and 67% which are almost twice larger then the TH model (34%). This result agrees with the detailed dispersion curve depicted in figure (2.5). In conclusion, for $\alpha \in (0.06, 0.98)$, the HOH1 and HOH2 provide a more precise description about the dispersion relation.

2.5.3 Parametric study: contrast of Young's modulus

The second contrast is the Young's modulus $\beta = E_b/E_a$. In this case, the material A is still Epoxy, whilst the properties of material B change. The properties of A and B are shown in table (2.1). Then, the first band gap frequency f_{gap} and the limit of the valid frequency range f_{lim} of these three different homogenized models are shown in figure (2.7).

Material	A(Epoxy)	B
Mass density (kg/m^3)	$\rho_a = 1180$	$\rho_b = \rho_a$
Young's Modulus (Pa)	$E_a = 4.35e9$	$E_b = \beta E_a$
Length (m)	$l_a = 1$	$l_b = l_a$

TABLE 2.1: Material properties

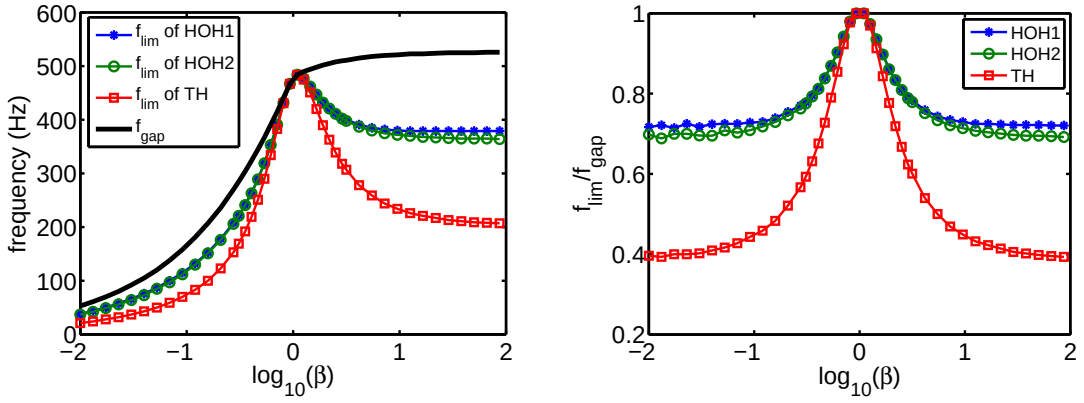

(a) valid frequency range f_{lim} (b) relative valid frequency range f_{lim}/f_{gap}

FIGURE 2.7: different homogenized models in the fraction of β

According to the figure (2.7(a)), when $\beta \to 1$, $E_b \approx E_a$, the unit cell becomes almost a homogeneous rod with only material A. All the three homogenized models provide good approximation before the f_{gap}. But for a more heterogeneous unit cell, the preponderance of HOH1 and HOH2 appears. A larger valid frequency range is acquired by the two models. Figure (2.7(b)) depicts that both the HOH1 model and the HOH2 model reach at least a 70% validity range before f_{gap} which is almost twice larger then the TH model. In conclusion, for $\beta \in (-\infty, 0.5) \cup (2, +\infty)$, the HOH1 and HOH2 are amended homogenization models.

2.5.4 Parametric study: contrast of mass density

The third contrast is the mass density $\gamma = \rho_b/\rho_a$. In this case, the material A is always Epoxy, whilst the material B's properties change. The properties of A and B are shown in table (2.2). Likewise, the first band gap frequency f_{gap} and the limit of the valid frequency range f_{lim} of these three different homogenized models are shown in figure (2.8).

Material	A(Epoxy)	B
Mass density (kg/m^3)	$\rho_{\mathrm{a}} = 1180$	$\rho_{\mathrm{b}} = \gamma\rho_{\mathrm{a}}$
Young's Modulus (Pa)	$E_{\mathrm{a}} = 4.35e9$	$E_{\mathrm{b}} = E_{\mathrm{a}}$
Length (m)	$l_{\mathrm{a}} = 1$	$l_{\mathrm{b}} = l_{\mathrm{a}}$

TABLE 2.2: Material properties

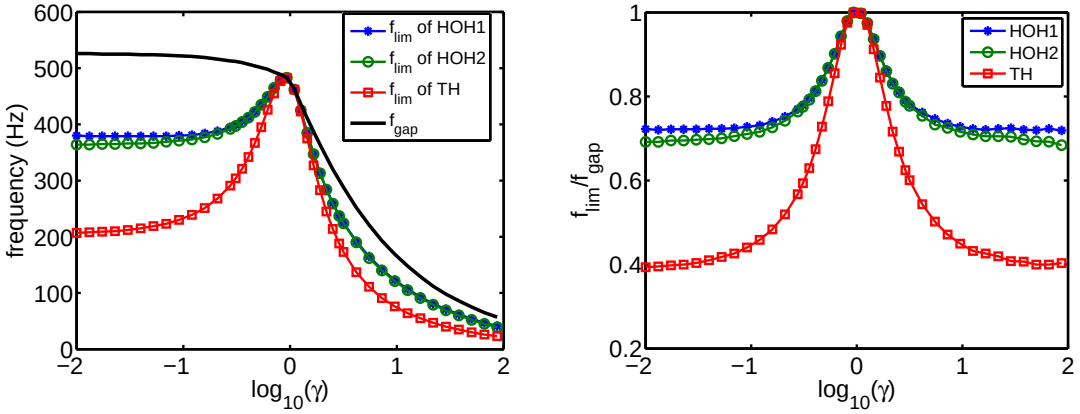

(a) valid frequency range f_{lim}

(b) relative valid frequency range f_{lim}/f_{gap}

FIGURE 2.8: different homogenized models in the fraction of γ

Similar conclusions can be draw from figure (2.8(a)). At low contrast, i.e. $\gamma \to 1$, $\rho_{\mathrm{b}} \approx \rho_{\mathrm{a}}$, all the three homogenized model are close to the benchmark before f_{gap}. At high contrast, the advantage of HOH1 and HOH2 arises. A larger valid frequency range is always ensured by the two models. Figure (2.8(b)) depicts again that almost twice larger validity range are derived by the HOH1 model and the HOH2 model compared to the TH model. In conclusion, for $\gamma \in (-\infty, 0.5) \cup (2, +\infty)$, HOH1 and HOH2 trun out again to be ameliorated homogenization models for dispersion relation. It is interesting that the results of β is similar to the results of γ.

2.6 Implementation in the finite case

The study of finite periodic structures is always associated with boundary condition problems. In this section, the variational approach is applied to each model to find the associated weak form boundary conditions. With these boundary conditions, the dynamic response of finite periodic structures is investigated. As the analytical frequency response function of the heterogeneous structure is no longer explicit, the response function obtained by WFEM is chosen as benchmark. In addition, the analytical or semi-analytical response functions obtained by the TH model, HOH1 model and HOH2 model are presented and compared.

2.6.1 Boundary conditions

In order to formulate the appropriate boundary conditions of the different models, the variational approach will be taken. As $U(X,t)$ is harmonic, the weak forms of different models in the domain $X \in [0, L]$ are as follows:

HOH1 model

In this model, the wave equation (2.56) is a fourth order PDE. The weak form of equation (2.56) reads:

$$\begin{aligned} &-\int_0^L E_0(\frac{\partial U}{\partial X})^2 dX + \int_0^L E_d(\frac{\partial^2 U}{\partial X^2})^2 dX + \int_0^L \rho_0\omega^2 U^2 dX \\ =&-\left[(E_0\frac{\partial U}{\partial X} + E_d\frac{\partial^3 U}{\partial X^3})U\right]_0^L + \left[E_d\frac{\partial^2 U}{\partial X^2}\frac{\partial U}{\partial X}\right]_0^L \end{aligned} \tag{2.64}$$

The right-hand-side of equation (2.64) reveals the format of the boundary conditions, namely:

$$\begin{aligned} &either \quad U(X) \qquad or \quad E_0\frac{\partial U(X)}{\partial X} + E_d\frac{\partial^3 U(X)}{\partial X^3} \\ &either \quad \frac{\partial U(X)}{\partial X} \qquad or \quad E_d\frac{\partial^2 U(X)}{\partial X^2} \end{aligned} \tag{2.65}$$

HOH2 model

According to wave equation (2.57), the weak form writes:

$$\begin{aligned}&\int_0^L (E_0 - \rho_0 \frac{E_d}{E_0}\omega^2)(\frac{\partial U}{\partial X})^2 dX - \int_0^L \rho_0 \omega^2 U^2 dX \\ &= \left[(E_0 - \rho_0 \frac{E_d}{E_0}\omega^2)\frac{\partial U}{\partial X} U\right]_0^L\end{aligned} \tag{2.66}$$

The right-hand-side of equation (2.66) reveals the format of the boundary conditions, namely:

$$either \quad U(X) \qquad or \quad (E_0 - \rho_0 \frac{E_d}{E_0}\omega^2)\frac{\partial U(X)}{\partial X} \tag{2.67}$$

With these weak forms, the dynamic comportment of finite structures is discussed through frequency response function. The key point is concentrated on the resonance frequency. For finite structures, the validity range is defined as:

For each resonance frequency f, if

$$\frac{|f_{ref} - f_{homo}|}{f_{ref}} < 2\%$$

then $f \in (0, f_{lim})$. Where f_{homo}, f_{ref} are the resonance frequency obtained respectively by homogenized models and the reference model.

2.6.2 Clamped-free boundary condition

The first case is the clamped-free boundary condition depicted in figure (2.9). The material A and B are Epoxy and Aluminium respectively, whose material properties remain the same as in the first studied case. $l_a = l_b = 1m$ and the length of the whole structure $L = 20$, which means 10 unit cells are considered. The cross-section is a circle with radius $r = 0.0644m$, and the amplitude of the excitation $F_0 = 100N$. In this case, WFEM is used to obtain the reference of frequency response function. For each unit cell, 100 rod elements are used to ensure the accuracy.

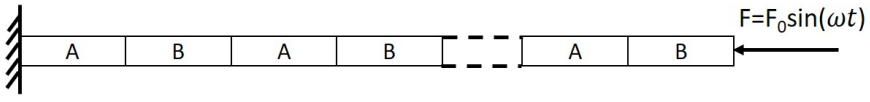

FIGURE 2.9: A clamped-free periodic structure with a harmonic excitation

TH model

In this model, the wave equation is equation (2.27):

$$E_0\frac{\partial^2 U}{\partial X^2}-\rho_0\frac{\partial^2 U}{\partial t^2}=0$$

As the force is applied only at the free tip, the boundary conditions read:

$$U(0)=0; \qquad E_0\frac{\partial U(L)}{\partial X}=\frac{F}{S} \tag{2.68}$$

where $S=\pi r^2$ is the cross-section area. With the mode superposition method, one can readily deduce the movement of the structure as:

$$U(X,t)=\frac{2F_0 sin(\omega t)}{\rho_0 SL}\sum_i^{\infty}\frac{1}{\omega_i^2-\omega^2}sin(p_i L)sin(p_i X) \tag{2.69}$$

where $i=1,2,3...$ denotes the integer, $\omega_i=p_i c_0$ denotes the eigen frequency of the homogenized structure, and $p_i=(2i-1)\pi/2L$, $c_0=\sqrt{E_0/\rho_0}$.

HOH1 model

According to (2.65), the boundary conditions are:

$$\begin{aligned} U(0)&=0; \qquad E_0\frac{\partial U(L)}{\partial X}+E_d\frac{\partial^3 U(L)}{\partial X^3}=\frac{F}{S}\\ \frac{\partial U(0)}{\partial X}&=0; \qquad E_d\frac{\partial^2 U(L)}{\partial X^2}=0 \end{aligned} \tag{2.70}$$

As $E_0>0, E_d>0$, the general solution of equation (2.56) is:

$$U(X)=c_1 sin(z_1 X)+c_2 cos(z_1 X)+c_3 sin(z_2 X)+c_4 cos(z_2 X) \tag{2.71}$$

where c_1, c_2, c_3, c_4 are constants, $-z_1^2, -z_2^2$ are roots of associated characteristic equation of equation (2.56). Then with these boundary conditions in (2.70), the displacement of the whole structure can be deduced by solving the four linear equations.

HOH2 model

According to (2.67), the format of the boundary conditions reads:

$$U(0)=0; \qquad (E_0-\rho_0\frac{E_d}{E_0}\omega^2)\frac{\partial U(L)}{\partial X}=\frac{F}{S} \tag{2.72}$$

In fact, the boundary conditions in (2.72) are similar to the boundary conditions in (2.68). Using the mode superposition method, one can deduce the movement of the structure:

$$U(X,t) = \frac{2F_0 sin(\omega t)}{\rho_0 SL} \sum_i^{\infty} \frac{1}{\omega_i^2 - \omega^2(1 + \frac{E_d}{E_0} p_i^2)} sin(p_i L) sin(p_i X) \tag{2.73}$$

where $i = 1, 2, 3...$ denotes the integer, and $\omega_i = p_i c_0$, $p_i = (2i-1)\pi/2L$ are the same as in (2.69). Equation (2.73) is similar to equation (2.69), or it is a modification of (2.69) with the modified eigen frequency $\Omega_i = \omega_i / \sqrt{1 + \frac{E_d}{E_0} p_i^2}$.

A comparison of frequency response function at excitation point ($X = L$) derived by different models is shown in figure (2.10). It can be seen that the TH model and the HOH1 model perform well till the 3rd resonance frequency, where the relative error are respectively 1.3% and 0%, the validity range is (0, 127HZ). The HOH2 model proves a better approximation till the 5th resonance frequency, where the relative error is 0.7%, and the validity range is (0, 222HZ).

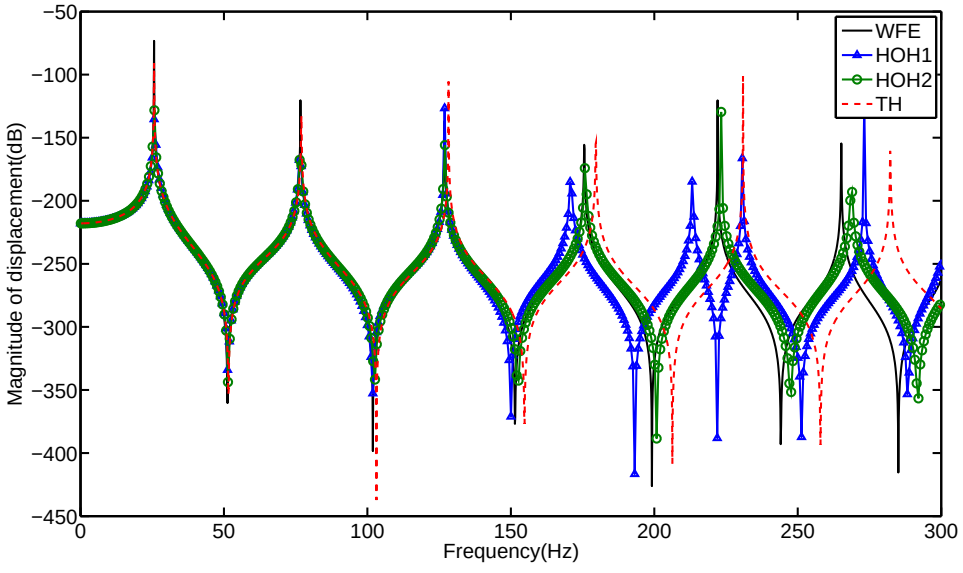

FIGURE 2.10: Frequency response function at excitation point derived by different models (10 unit cells)

In order to find out whether the valid frequency range is sensible to unit cell number, structures with larger unit cell numbers are also studied and illustrated. Figure (2.11) depictes the comparison when the unit cell number is 15. For clarity, only the HOH2 model is presented. It can be seen that the HOH2 model keeps the accuracy till the 7th

resonance, where the relative error is 0.4%, and the validity range is (0, 214Hz). For the TH model and HOH1 model, the validity ranges are relatively (0, 118HZ) (4th resonance frequency), (0,51Hz)(2nd resonance frequency) and the relative errors at that peak are respectively 1.1%, 0.3%. Another cases are shown in table (2.3). In a word, with the augment of the unit cell number, the valid frequency range of TH model and HOH2 model remain almost unchanged, whilst the HOH1 model are sensible to the number of unit cell. The main reason may lies in the boundary conditions introduced for HOH1. Intuitively deduced, the HOH1 model (fourth order PDE) is associated to four boundary conditions. Two of them (the first two in equation (2.70)) are physical while the other two are artificial. As for the HOH2 model (second order PDE), the two associated boundary conditions are all physical. That is why HOH2 model is proposed. The reason why HOH1 is sensible to the unit cell number may be related to the two artificial boundary conditions. Compared to HOH1, HOH2 model is recommended to simulate periodic structure. It is robust and valid in a larger frequency range independent of the unit cell number.

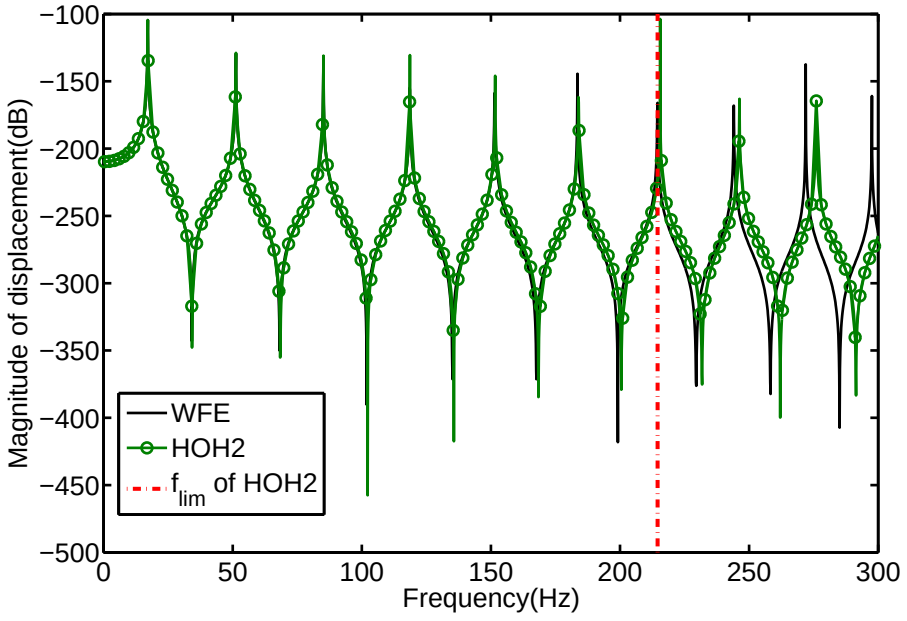

FIGURE 2.11: Frequency response function at excitation point for a structure with 15 unit cells

Unit cell number	10	15	20	25	30
TH	127	118	139	133	127
HOH1	127	51	139	51	127
HOH2	222	214	233	227	222

TABLE 2.3: Valid frequency range f_{lim} (Hz) for different structure

2.6.3 Clamped-clamped boundary condition

The second case is the clamped-clamped boundary condition depicted in figure (2.12). The material properties are kept the same as in the previous section except for the boundary conditions. In this case, the excitation is applied at point $X = 7l$ (the interface between the 7th and 8th unit cell) and the frequency response function at point $X = 9l$ (the interface between 9th and 10th unit cell) is presented.

TH model

The wave equation remains unchanged, whilst the boundary conditions become:

$$U(0) = 0; \qquad U(L) = 0 \tag{2.74}$$

It is readily to derive the response function by using mode superposition method.

$$U(X,t) = \frac{2F_0 sin(\omega t)}{\rho_0 SL} \sum_i^{\infty} \frac{1}{\omega_i^2 - \omega^2} sin(p_i L) sin(p_i X) \tag{2.75}$$

where $i = 1, 2, 3...$ denotes the integer, $\omega_i = q_i c_0$ denotes the eigen frequency of the homogenized structure, and $q_i = i\pi/L$, $c_0 = \sqrt{E_0/\rho_0}$.

HOH1 model

According to the weak formulation (2.65), the appropriate boundary conditions read:

$$\begin{aligned} U(0) &= 0; \qquad U(L) = 0 \\ \frac{\partial U(0)}{\partial X} &= 0; \qquad \frac{\partial U(L)}{\partial X} = 0 \end{aligned} \tag{2.76}$$

In order to obtain the forced response, the whole structure is considered as two parts: left side of excitation point and right side of excitation point. Then the response of the two parts can be obtained by satisfying the boundary conditions in (2.76) together with the continuity conditions (force, displacement) at point $X = 7l$. Numerical calculation is used to solve the linear equation system.

	1st	2nd	3rd	4th	5th	6th
WFEM	51	102	152	199	244	285
TH	51	103	154	205	257	308
HOH1	51	102	151	192	219	255
HOH2	51	102	152	200	246	291

TABLE 2.4: Resonance frequencies obtained by different models (10 unit cells)

HOH2 model

According to the weak formulation (2.67), the appropriate boundary conditions read:

$$U(0) = 0; \qquad U(L) = 0 \tag{2.77}$$

The forced response of this model can also be deduced by the same calculation used in the HOH1 model.

The resonance frequencies obtained by different models are shown in table (2.4), and the various frequency response functions are shown in figure(2.13). To ensure the accuracy of the WFEM result, 100 rod elements are used to simulate the unit cell. Similar conclusions can be drawn: for TH model and HOH1 model, the first three resonances are well predicted; for HOH2 model, the accuracy is ensured till the 5th resonance frequency. These results are accordant with the conclusions in clamped-free case.

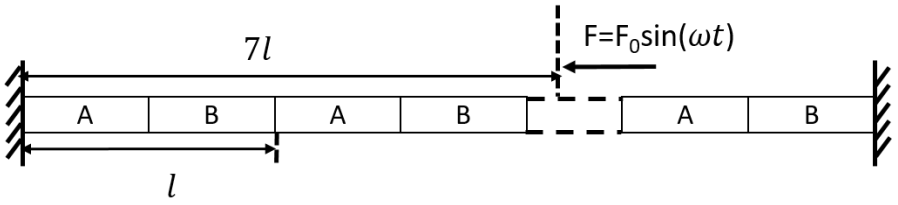

FIGURE 2.12: A clamped-clamped periodic structure

The same investigation is also made for a periodic structure composed of 15 unit cells. In this case, the excitation point is $X = 11l$ (the interface between the 11th and 12th unit cell), while the observation point is $X = 4l$ (the interface between the 4th and 5th unit cell). The HOH2 model and the WFEM are depicted in figure (2.14). It can be seen that the first seven resonance frequencies are well predicted by HOH2 model, which suggests that the validity range is (0,229Hz). The validity range of HOH1 and TH are relatively (0, 68Hz) and (0,135Hz). All these results are accordant with the results in

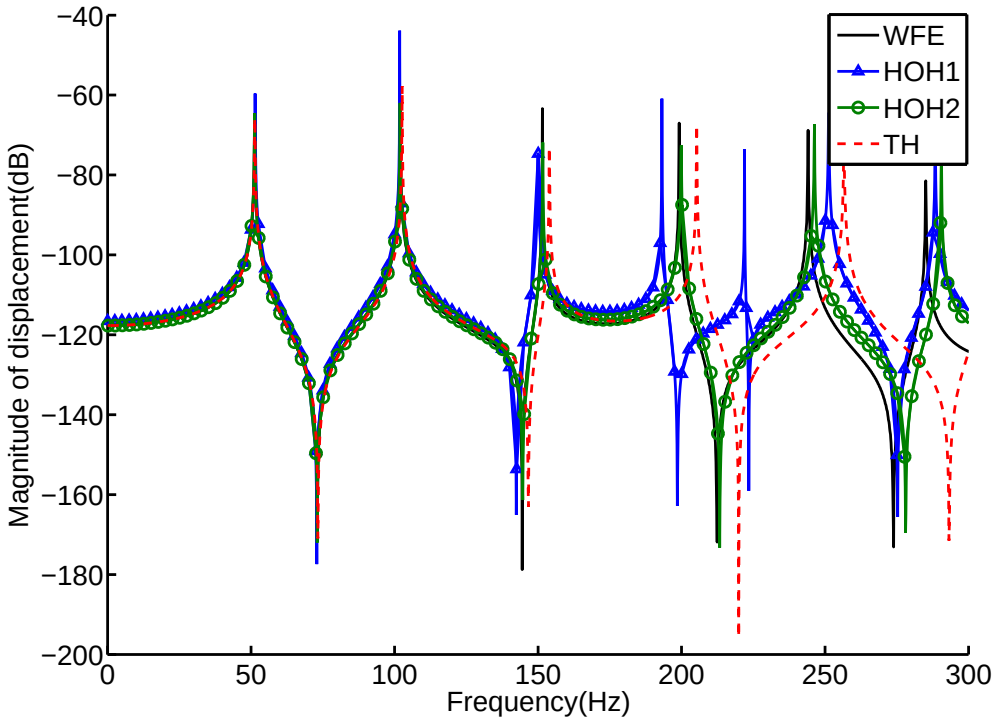

FIGURE 2.13: Frequency response function at $X = 9l$ obtained by different models (10 unit cells)

the clamped-free case shown in table (2.3). The HOH2 model always turns out to be a better model.

Some attentions should be paid to the choice of the finite periodic structure configuration when the WFEM is used to obtain the reference data. For an infinite periodic structure depicted in (2.1), there exists diverse possible configurations of a unit cell which make no difference for the study of dispersion relation. But for a finite structure, these different configurations lead to different structures, which possess different frequency response function under the same boundary conditions. According to the idea of homogenization, after the homogenization process, the heterogeneous periodic structure becomes kind of a symmetry homogeneous structure. It is reasonable that a symmetry configuration is used to derive the benchmark for the study of a finite structure.

2.7 Conclusions

In this chapter, detailed formulations of the two-scale asymptotic expansion method are presented and higher order homogenized models are established to predict the free

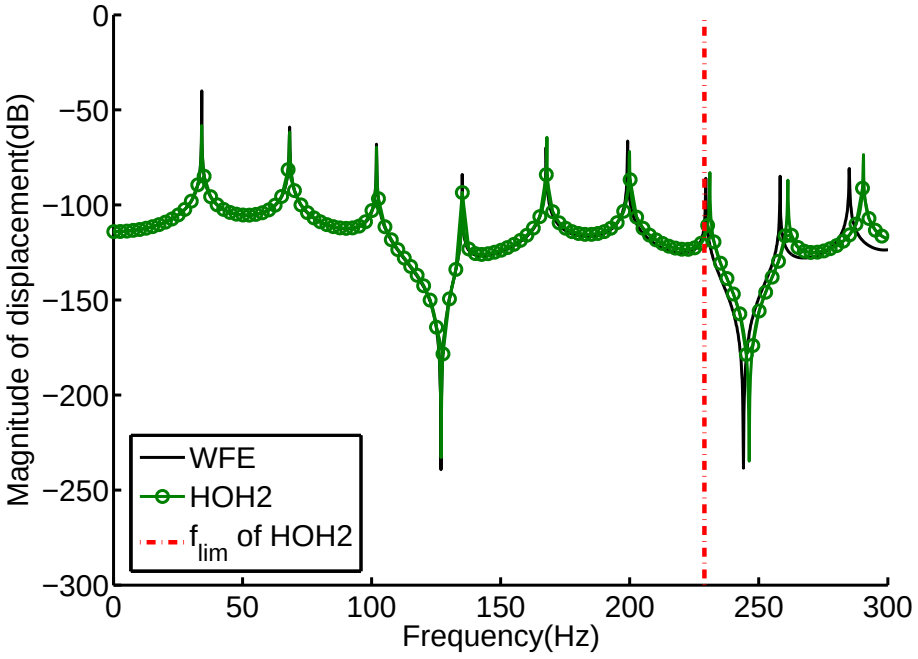

FIGURE 2.14: Frequency response function at $X = 4l$ for a structure with 15 unit cell

vibration and forced vibration of a periodic rod. All these models are based on the long-wave assumption, which means the studied frequency range is limited to the first propagating zone. The analytical method (dispersion relation), and numerical method WFEM (frequency response function) have been chosen as the benchmark, and the traditional homogenization model is also illustrated to demonstrate the higher order homogenization model's superiority.

In the infinite case, the dispersion relation is investigated. The HOH1 model and the HOH2 model exhibit similar results, and they turn out to be more accurate models by enlarging about twice the validity range compared to the TH model.

In the finite case, the frequency response function is investigated. HOH2 model turns out to be an amended model which is not sensible to the unit cell number.

As a result, the HOH2 model is recommended to simulate binary periodic structures. In this work, the homogenization process stops at the $O(\epsilon^2)$ order. Further calculations may induce more complicated homogenized equations which predict more precisely the behaviour of heterogeneous structures. Being validated in the longitudinal wave case, the higher order model may also perform well in the transversal wave case.

Chapter 3

Homogenization of transversal waves in 1 dimensional periodic structures

3.1 Introduction

Periodic structures, such as sandwich panels, stiffened plates, and truss beam, are widely used in various industry domains. The main reason to explain the increasing interests in periodic structures is that their dynamic behaviour is very rich. They are known for the frequency stop bands which indicate the non propagating frequency interval and can be detected by Floquet-Bloch theory[69, 71]. Periodicity effects caused by wave propagation in various structures have been studied in [66–68]. According to Floquet-Bloch theory, the study of a periodic structure equals to the study of its unit cell. Several methods, such as receptance method [72], transfer matrix method (TMM) [73] and space-harmonic method [74] have been developed on account of this theory. As for complex periodic structures, the unit cell's finite element model will be considered and the wave finite element method (WFEM) will be used [75–77]. The analysis of periodic structures are relatively more difficult and onerous due to anisotropy and heterogeneity when compared with isotropic and homogeneous structures. That is the reason whey homogenization method is another broadly discussed option.

In order to apply the homogenization process in a studied case, the wavelength should be larger than the unit cell length and the valid frequency range is limited in the first propagating zone. For traditional homogenization method, the primary object is to find out homogenized equivalent parameters of periodic structures. At low frequency where the wave length is very large, the original periodic structure can be considered as a homogeneous one equipping these effective parameters. With the frequency increasing, the wavelength shortens to, for instance, the characteristic length of the heterogeneity. In this case, the traditional homogenized model is no longer accurate because of the amplied dispersion effect, and the real valid frequency range of far less than the limit. Consequently, more accurate homogenized models with larger validity range are needed. In the classical continuum mechanics, similar limitation appears and various enriched continuum models have been developed from the gradient elasticity theory [78–82] to overcome the deficiency. Analogous to the gradient elasticity theory, multi-scale asymptotic homogenization method is considered to handle this limitation. Firstly proposed in [83–85], more recently in [86, 87], multi-scale homogenization method is an averaging tool to study the dynamic behaviour of periodic media. Apart from the method in this paper, a broad range of periodic structures models, based on the idea of multi-scale asymptotic expansion, have been explored in the literature [88] [89] [90].

Rather than find out the effective parameters, the studied method aims at a homogenized wave equation to describe the dynamic behaviour of the heterogeneous structure. As far as the author knows, few works have foucused on the application of this method on flexural wave. Some implementations on longitudinal wave can be found in [91–93]. In [91, 92], an initial excitation in displacement sets the clamped-free periodic strucutrue on free vibration. Then, the method is validated by studying the time-varying displacement of the structure. Factors related to the validity range have been identified. In [93], dispersion relations of infinite periodic structures are presented. In the author's previous work, a more abundant discussion is presented: the influence of material property contrasts on dispersion relation; the determination of valid domain; explanations of boundary conditions for different models; the forced response of finite structure under various boundary conditions.

In this paper, the higher order homogenized models of flexural waves in one-dimensional periodic beams are established by multi-scale expansion method. The detailed homogenization process description offers a clear understanding of the principle.

A parametric study of the dispersion relation serves as a validation of these models, and leads to a further discussion about the validity range. With the boundary conditions obtained by a vibrational approach, these models are applied on the finite periodic structures. The study of forced response under various boundary conditions confirms a fortiori the robustness of these homogenized models by comparing with the reference results obtained by WFEM. This paper is divided into 7 sections. The Euler-Bernoulli equation about flexural waves is gave in section 3.2. In section 3.3, the application of HPDM on periodic beam is discussed. Then, the principles and some details of multi-scale asymptotic homogenization method applied to periodic structures is presented in section 3.4. In section 3.5, the validation of higher order homogenized models through dispersion relations is discussed. Section 3.6 tells about some further implementations in finite case. At last, some conclusions are made in section 3.7.

3.2 Problem statement

The main object is to simulate the behaviour of transversal wave in a periodic beam by asymptotic homogenization method. In the studied case, material A together with B makes up the periodic beam (figure 3.1), and the governing wave equation is a fourth order PDE:

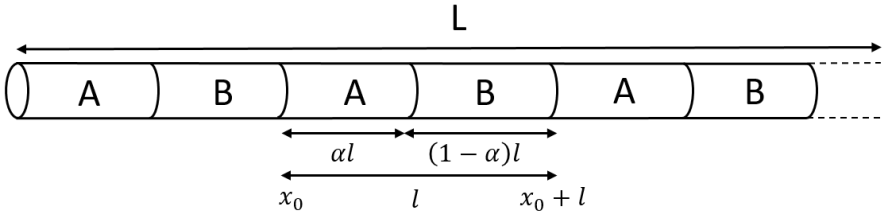

FIGURE 3.1: A bi-laminate periodic beam

$$\frac{\partial^2}{\partial x^2}\left(E(\frac{x}{\epsilon})I\frac{\partial^2 u(x,t)}{\partial x^2}\right)+\rho(\frac{x}{\epsilon})S\frac{\partial^2 u(x,t)}{\partial t^2}=0 \tag{3.1}$$

where the $u(x,t)$ denotes the displacement field, $\rho(x/\epsilon)$ the mass density, $E(x/\epsilon)$ the Young's Modulus. I is the inertia moment, S is the cross section area. The section is a circle with radius r, which indicates that $I=\pi r^4/4$, $S=\pi r^2$ are constants. $\epsilon=l/L$, with l the period of the structure, and L the characteristic length. Two scales are required to achieve the multi-scale homogenization: the macroscale $X=x$, representing the structure's global behaviour, and the microscale $y=x/\epsilon$, describing the heterogeneity

or the periodicity of the structure. Based on the multi-scale asymptotic approximation, an effective wave equation involving only the macroscale X is to be established.

3.3 HDPM homogenization process

In this section, the implementation of HPDM on the periodic beam will be discussed. The first step of HPDM is the discretization of the element dynamic balance, which is shown in figure (3.2). The dynamic balance will be verified by considering the displacement and rotation at $x = -\alpha l$ and $x = (1-\alpha)l$ as known boundary conditions. Together with the continuity conditions at $x = 0$, the moment and the shear force at the endpoints will be deduced.

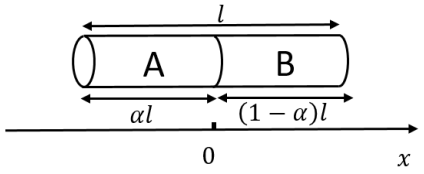

FIGURE 3.2: Beam element chosen for HPDM

The wave equations for material A and material B are :

$$E_a I \frac{\partial^4 u}{\partial x^4} + \rho_a S \frac{\partial^2 u}{\partial t^2} = 0; \quad E_b I \frac{\partial^4 u}{\partial x^4} + \rho_b S \frac{\partial^2 u}{\partial t^2} = 0$$

where E_a, E_b, ρ_a, ρ_b are the Young's modulus and the density of material A and B, I is the inertia moment and S is the section area. As the studied displacement is harmonic, the wave equation becomes:

$$u'''' - k_a^4 u = 0; \quad u'''' - k_b^4 u = 0$$

with $k_a = \sqrt[4]{\rho_a S\omega^2/E_a I}, k_b = \sqrt[4]{\rho_b S\omega^2/E_b I}$. The solution is in the following form:

$$u = \begin{cases} c_1 sin(k_a x) + c_2 cos(k_a x) + c_3 sinh(k_a x) + c_4 cosh(k_a x) & -\alpha l < x < 0 \\ c_5 sin(k_b x) + c_6 cos(k_b x) + c_7 sinh(k_b x) + c_8 cosh(k_b x) & 0 < x < (1-\alpha)l \end{cases}$$

with the associated conditions:

$$u(-\alpha l) = u^B; \quad u(0^-) = u(0^+); \quad u((1-\alpha)l) = u^E$$
$$u'(-\alpha l) = \theta^B; \quad u'(0^-) = u'(0^+); \quad u((1-\alpha)l) = \theta^E$$
$$E_a I u''(0^-) = E_b I u''(0^+);$$
$$E_a I u'''(0^-) = E_b I u'''(0^+);$$

As the rotation, the moment and the shear force in the transversal vibration case are defined as:

$$\theta = \frac{\partial u}{\partial x}; \quad M = -EI\frac{\partial^2 u}{\partial x^2}; \qquad T = EI\frac{\partial^3 u}{\partial x^3}$$

then the state vector for material A can be obtained by the following formulation:

$$\begin{pmatrix} u(x) \\ \theta(x) \\ M(x) \\ T(x) \end{pmatrix} = N_a(x) \begin{pmatrix} c_1 \\ c_2 \\ c_3 \\ c_4 \end{pmatrix}$$

with

$$N_a(x) = \begin{bmatrix} sin(k_a x) & cos(k_a x) & sinh(k_a x) & cosh(k_a x) \\ cos(k_a x) & -sin(k_a x) & cosh(k_a x) & sinh(k_a x) \\ E_a I k^2 sin(k_a x) & E_a I k^2 cos(k_a x) & -E_a I k^2 sinh(k_a x) & -E_a I k^2 cosh(k_a x) \\ -E_a I k^3 cos(k_a x) & E_a I k^3 sin(k_a x) & E_a I k^3 cosh(k_a x) & -E_a I k^3 sinh(k_a x) \end{bmatrix}$$

Then the transfer matrix between the state vectors of the two extremities of material A are in the following form:

$$\begin{pmatrix} u^B \\ \theta^B \\ M^B \\ T^B \end{pmatrix} = \begin{pmatrix} v(-\alpha l) \\ \theta(-\alpha l) \\ M(-\alpha l) \\ T(-\alpha l) \end{pmatrix} = N_a(-\alpha l) \begin{pmatrix} c_1 \\ c_2 \\ c_3 \\ c_4 \end{pmatrix} = N_a(-\alpha l) N_a(0)^{-1} \begin{pmatrix} u(0) \\ \theta(0) \\ M(0) \\ T(0) \end{pmatrix}$$

Note $R_a = N_a(-\alpha l)N_a(0)^{-1}$, and the transfer matrix for material B, R_b can also be deduced by replacing the associated properties of A with B.

$$\begin{pmatrix} u(0) \\ \theta(0) \\ M(0) \\ T(0) \end{pmatrix} = N_b(0)N_b((1-\alpha)l)^{-1} \begin{pmatrix} u((1-\alpha)l) \\ \theta((1-\alpha)l) \\ M((1-\alpha)l) \\ T((1-\alpha)l) \end{pmatrix} = R_b \begin{pmatrix} u^E \\ \theta^E \\ M^E \\ T^E \end{pmatrix}$$

At the junction, the continuity of moment, rotation, moment and shear force have to be preserved. Then the relationship between the left endpoint and right endpoint of the unit cell can be expressed in the following manner:

$$\begin{pmatrix} u^B \\ \theta^B \\ M^B \\ T^B \end{pmatrix} = R_a R_b \begin{pmatrix} u^E \\ \theta^E \\ M^E \\ T^E \end{pmatrix}$$

As $u^B, u^E, \theta^B, \theta^E$ are known, the moment and the shear force at the extremities can be yielded by solving the linear system equation. The expanded solution with respect to ϵ are as follows, some details are presented in the appendix.

$$\begin{aligned}
M^B &= m_1(u^B - u^E)\frac{1}{\epsilon^2 L^2} + (m_2\theta^B + m_3\theta^E)\frac{1}{\epsilon L} + (m_4 u^B + m_5 u^E)\epsilon^2 L^2 \\
&\quad + (m_6\theta^B + m_7\theta^E)\epsilon^3 L^3 + O(\epsilon^4) \\
M^E &= m_8(u^B - u^E)\frac{1}{\epsilon^2 L^2} + (m_9\theta^B + m_{10}\theta^E)\frac{1}{\epsilon L} + (m_{11} u^B + m_{12} u^E)\epsilon^2 L^2 \\
&\quad + (m_{13}\theta^B + m_{14}\theta^E)\epsilon^3 L^3 + O(\epsilon^4) \\
T^B &= t_1(u^B - u^E)\frac{1}{\epsilon^3 L^3} + (t_2\theta^B + t_3\theta^E)\frac{1}{\epsilon^2 L^2} + (t_4 u^B + t_5 u^E)\epsilon L \\
&\quad + (t_6\theta^B + t_7\theta^E)\epsilon^2 L^2 + O(\epsilon^3) \\
T^E &= t_8(u^B - u^E)\frac{1}{\epsilon^3 L^3} + (t_9\theta^B + t_{10}\theta^E)\frac{1}{\epsilon^2 L^2} + (t_{11} u^B + t_{12} u^E)\epsilon L \\
&\quad + (t_{13}\theta^B + t_{14}\theta^E)\epsilon^2 L^2 + O(\epsilon^3)
\end{aligned}$$

where $m_1, ..., m_{14}, t_1, ..., t_{14}$ are constant coefficients obtained by the linear equation system. With the element dynamic balance being verified, the homogenized wave equation are obtained by the nodal balance equations: $M_n^E = M_{n+1}^B, T_n^E = T_{n+1}^B$. Under the long-wave assumption, the scale ratio $\epsilon = l/L \ll 1$ is introduced to homogenize the periodic

structure. And according to the HPMD, the displacement at node n, n-1 and n+1 are expanded as equation (1.134), (1.135), (1.136). Inserting the expanded moment, shear force and displacement into the nodal balance equation, and identifying the terms with equal power of ϵ, a series of equations for v_i are obtained.

Moment balance equation: $M_n^E = M_{n+1}^B$

Order $O(\epsilon^1)$, noted as eq_{m1}

$$u'_{n0} - \theta_{n0} = 0$$

Order $O(\epsilon^2)$, noted as eq_{m2}

$$u'_{n1} - \theta_{n1} + \frac{L}{2} u''_0 \frac{m_1 + m_8}{m_1 - m_8} = 0$$

Order $O(\epsilon^3)$, noted as eq_{m3}

$$u'_{n2} - \theta_{n2} + \frac{L}{2} u''_{n1} \frac{m_1 + m_8}{m_1 - m_8} + \frac{L^2}{6} u'''_{n0} + \frac{L^2}{2} \theta''_{n0} \frac{m_9 - m_3}{m_1 - m_8} = 0$$

Order $O(\epsilon^4)$, noted as eq_{m4}

$$\begin{aligned} u'_{n3} - \theta_{n3} + \frac{L}{2} u''_2 \frac{m_1 + m_8}{m_1 - m_8} + \frac{L^2}{6} u'''_{n1} + \frac{L^2}{2} \theta''_{n1} \frac{m_9 - m_3}{m_1 - m_8} \\ + \frac{L^3}{24} u^{(4)}_{n0} \frac{m_1 + m_8}{m_1 - m_8} u_{n0} L^3 \frac{m_{11} + m_{12} - m_4 - m_5}{m_1 - m_8} = 0 \end{aligned}$$

Order $O(\epsilon^5)$, noted as eq_{m5}

$$\begin{aligned} u'_{n4} - \theta_{n4} + \frac{L}{2} u''_3 \frac{m_1 + m_8}{m_1 - m_8} + \frac{L^2}{6} u'''_{n2} + \frac{L^2}{2} \theta''_{n2} \frac{m_9 - m_3}{m_1 - m_8} \\ + \frac{L^3}{24} u^{(4)}_{n1} \frac{m_1 + m_8}{m_1 - m_8} + u_{n1} L^3 \frac{m_{11} + m_{12} - m_4 - m_5}{m_1 - m_8} \\ + \frac{L^4}{120} u^{(5)}_{n0} + \frac{L^4}{24} \theta^{(4)}_{n0} \frac{m_9 - m_3}{m_1 - m_8} - u'_{n0} L^4 \frac{m_{11} + m_5}{m_1 - m_8} + \theta_{n0} L^4 \frac{m_{13} + m_{14} - m_6 - m_7}{m_1 - m_8} = 0 \end{aligned}$$

Shear force balance equation: $T_n^E = T_{n+1}^B$

Order $O(\epsilon^2)$, noted as eq_{t2}

$$u''_{n0} - \theta'_{n0} = 0$$

Order $O(\epsilon^3)$, noted as eq_{t3}

$$u''_{n1} - \theta'_{n1} + \frac{L}{2} \theta''_0 \frac{t_9 - t_3}{t_9 + t_3} = 0$$

Order $O(\epsilon^4)$,noted as eq_{t4}

$$u''_{n2} - \theta'_{n2} + \frac{L}{2}\theta''_{n1}\frac{t_9 - t_3}{t_9 + t_3} - \frac{L^2}{6}\theta'''_{n0} + \frac{L^2}{12}u^{(4)}_{n0} + L^2 u_{n0}\frac{t_{11} + t_{12} - t_4 - t_5}{t_9 + t_3} = 0$$

Inserting $eq'_{m3}, eq''_{m2}, eq'''_{m1}$ into the above equation, the homogenized wave equation becomes:

$$u^{(4)}_{n0} - \frac{\rho_0 S}{E_0 I}\omega^2 u_{n0} = 0 \tag{3.2}$$

where $E_0 = E_a E_b/\alpha E_b + (1-\alpha)E_a, \rho_0 = \alpha\rho_a + (1-\alpha)\rho_b$. This is the homogenized wave equation for u_{n0}.

Order $O(\epsilon^5)$, noted as eq_{t5}

$$\begin{aligned} u''_{n3} - \theta'_{n3} + \frac{L}{2}\theta''_{n2}\frac{t_9 - t_3}{t_9 + t_3} - \frac{L^2}{6}\theta'''_{n1} + \frac{L^2}{12}u^{(4)}_{n1} + L^2 u_{n1}\frac{t_{11} + t_{12} - t_4 - t_5}{t_9 + t_3} \\ + \frac{L^3}{24}\theta^{(4)}_{n0}\frac{t_9 - t_3}{t_9 + t_3} + L^3\theta_{n0}\frac{t_{13} + t_{14} - t_6 - t_7}{t_9 + t_3} = 0 \end{aligned}$$

Inserting $eq'_{m4}, eq''_{m3}, eq'''_{m2}, eq^{(4)}_{m1}$ into the above equation leads to the homogenized wave equation for u_{n1}:

$$u^{(4)}_{n1} - \frac{\rho_0 S}{E_0 I}\omega^2 u_{n1} = 0 \tag{3.3}$$

Order $O(\epsilon^6)$

$$\begin{aligned} u''_{n4} - \theta'_{n4} + \frac{L}{2}\theta''_{n3}\frac{t_9 - t_3}{t_9 + t_3} - \frac{L^2}{6}\theta'''_{n2} + \frac{L^2}{12}u^{(4)}_{n2} + L^2 u_{n2}\frac{t_{11} + t_{12} - t_4 - t_5}{t_9 + t_3} \\ + \frac{L^3}{24}\theta^{(4)}_{n1}\frac{t_9 - t_3}{t_9 + t_3} + L^3\theta_{n1}\frac{t_{13} + t_{14} - t_6 - t_7}{t_9 + t_3} \\ + \frac{L^4}{360}u^{(6)}_{n0} - \frac{L^4}{120}\theta^{(5)}_{n0} + \frac{L^4}{2}u''_{n0}\frac{t_{11} - t_5}{t_9 + t + 3} - L^4\theta'_{n0}\frac{t_{13} + t_7}{t_9 + t_3} = 0 \end{aligned}$$

The homogenized wave equation for u_{n2} can be yielded by inserting $eq'_{m5}, eq''_{m4}, eq'''_{m3}, eq^{(4)}_{m2}, eq^{(5)}_{m1}$ into the above equation:

$$u^{(4)}_{n2} - \frac{\rho_0 S}{E_0 I}\omega^2 u_{n2} + \frac{E_d}{E_0}u^{(6)}_{n0} = 0 \tag{3.4}$$

with

$$E_d = -\frac{E_0}{\rho_0}\frac{\alpha^2(1-\alpha)^2(E_\mathrm{a} - E_\mathrm{b})(\rho_\mathrm{a} - \rho_\mathrm{b})L^2}{6((1-\alpha)E_\mathrm{a} + \alpha E_\mathrm{b})}$$

From these results, it can be seen that eq_{m1} is equivalent to eq_{t2} and eq_{m2} is equivalent

to eq_{t3}. Then, the shear force balance equations at various orders give the homogenized wave equation by using the relation obtained by the associated moment balance equations.

3.4 Multi-scale asymptotic homogenization process

An assumption that the macro length of the structure L is much larger than the period l, i.e. $\epsilon = l/L << 1$, is necessary to obtain the effective wave equation. With the macroscale $X = x$ and the microscale $y = x/\epsilon$, the asymptotic homogenization starts with the expansion of displacement u:

$$u(x,t) \equiv u(X,y,t) = u_0(X,y,t) + \epsilon u_1(X,y,t) + \epsilon^2 u_2(X,y,t) + ... \tag{3.5}$$

where $x \in [0,L]$, $X \in [0,L]$, $y \in [0,L/\epsilon]$.

The derivatives of x become:

$$\begin{aligned} \frac{\partial}{\partial x} &= \frac{\partial}{\partial X} + \frac{1}{\epsilon}\frac{\partial}{\partial y} \\ \frac{\partial^2}{\partial x^2} &= \frac{\partial^2}{\partial X^2} + \frac{2}{\epsilon}\frac{\partial^2}{\partial y \partial X} + \frac{1}{\epsilon^2}\frac{\partial^2}{\partial y^2} \end{aligned} \tag{3.6}$$

The wave equation (3.1) becomes:

$$\left(\frac{\partial^2}{\partial X^2} + \frac{2}{\epsilon}\frac{\partial^2}{\partial y \partial X} + \frac{1}{\epsilon^2}\frac{\partial^2}{\partial y^2}\right)\left(E(y)I\left(\frac{\partial^2}{\partial X^2} + \frac{2}{\epsilon}\frac{\partial^2}{\partial y \partial X} + \frac{1}{\epsilon^2}\frac{\partial^2}{\partial y^2}\right)u(X,y,t)\right) + \rho(y)S\frac{\partial^2 u(X,y,t)}{\partial t^2} = 0 \tag{3.7}$$

New periodic conditions with respect to y are:

Displacement:

$$u(X,0,t) = u(X,L,t)$$

Rotation:

$$\frac{\partial u}{\partial x}(X,0,t) = \frac{\partial u}{\partial x}(X,L,t)$$

Moment:

$$E(y)I\frac{\partial^2 u(X,0,t)}{\partial x^2} = E(y)I\frac{\partial^2 u(X,L,t)}{\partial x^2}$$

Shear force:

$$\frac{\partial}{\partial x}\left(E(y)I\frac{\partial^2 u(X,0,t)}{\partial x^2}\right)=\frac{\partial}{\partial x}\left(E(y)I\frac{\partial^2 u(X,L,t)}{\partial x^2}\right)$$

Then inserting the expansion of u into equation (3.7), and identifying the terms with equal power of ϵ, a sequence of equations for u_i starting with ϵ^{-4} order are obtained. At order $O(\epsilon^n)$, where $n<0$, the dynamic term does not exist in the wave equations. The main object is to obtain the affiliated displacement u_{n+4}. When $n\geqslant 0$, the dynamic term emerges, both the displacement and the homogenized equation are deduced. During the calculation, a_m, b_m, c_m ..., where $m=1,2,3...$ are associated integration constants. And for simplicity, the dependence of time is omitted.

3.4.1 Asymptotic calculation of O(ϵ^{-4}) order equation

At $O(\epsilon^{-4})$, the wave equation reads:

$$\frac{\partial^2}{\partial y^2}\left(E(y)I\frac{\partial^2 u_0}{\partial y^2}\right)=0 \tag{3.8}$$

Integrating twice equation (3.8) with respect to y leads to:

$$E(y)I\frac{\partial^2 u_0}{\partial y^2}=a_0(X)y+b_0(X) \tag{3.9}$$

In fact, the left hand side of equation (3.9) is the ϵ^{-2} order moment, which satisfies the periodic condition: $E(0)Iu_{0,yy}(X,0)=E(L)Iu_{0,yy}(X,L)$. $u_{,y}$ means the derivative with respect to y. The specific periodic condition results in $a_0(X)=0$, then

$$E(y)I\frac{\partial^2 u_0}{\partial y^2}=b_0(X) \tag{3.10}$$

Another integral gives:

$$\frac{\partial u_0}{\partial y}=\frac{b_0(X)}{I}\int_0^y\frac{1}{E(\tau)}d\tau+c_0(X) \tag{3.11}$$

Again, the left hand side of equation (3.11) is the ϵ^{-1} order rotation, which is also periodic. Then

$$c_0(X) = \frac{b_0(X)}{I}\int_0^L \frac{1}{E(\tau)}d\tau + c_0(X) \Rightarrow b_0(X) = 0$$

Equation (3.11) becomes:

$$\frac{\partial u_0}{\partial y} = c_0(X) \tag{3.12}$$

Thus, the general solution of u_0 is:

$$u_0 = c_0(X)y + d_0(X) \tag{3.13}$$

And because of the periodicity of u_0, $c_0(X)$ vanishes. At last, the solution of u_0 is obtained:

$$u_0(X, y) = d_0(X) = U_0(X) \tag{3.14}$$

u_0 the leading order displacement depends only on the macroscale X.

3.4.2 Asymptotic calculation of O(ϵ^{-3}) order equation

At $O(\epsilon^{-3})$, the wave equation becomes:

$$2\frac{\partial^2}{\partial y \partial X}\left(E(y)I\frac{\partial^2 u_0}{\partial y^2}\right) + \frac{\partial^2}{\partial y^2}\left(E(y)I\left(2\frac{\partial^2 u_0}{\partial y \partial X} + \frac{\partial^2 u_1}{\partial y^2}\right)\right) = 0 \tag{3.15}$$

As $u_0(X, y) = U_0(X)$, the above equation can be simplified as:

$$\frac{\partial^2}{\partial y^2}\left(E(y)I\frac{\partial^2 u_1}{\partial y^2}\right) = 0 \tag{3.16}$$

which is the same as equation (3.8). Then integrating twice with respect to y gives:

$$E(y)I\frac{\partial^2 u_1}{\partial y^2} = a_1(X)y + b_1(X) \tag{3.17}$$

The ϵ^{-1} order moment writes:

$$E(y)I\left(2\frac{\partial^2 u_0}{\partial y \partial X} + \frac{\partial^2 u_1}{\partial y^2}\right)$$

With $u_0(X,y) = U_0(X)$, the periodicity of ϵ^{-1} order moment ensures the periodicity of $E(y)Iu_{1,yy}$, which indicates that $a_1(X) = 0$. Then similar result can be obtained:

$$\frac{\partial u_1}{\partial y} = \frac{b_1(X)}{I}\int_0^y \frac{1}{E(\tau)}d\tau + c_1(X) \tag{3.18}$$

The ϵ^0 order rotation writes:

$$\frac{\partial u_0}{\partial X} + \frac{\partial u_1}{\partial y}$$

Hence, due to $u_0(X,y) = U_0(X)$, the periodicity of $u_{1,y}$ should be derived by the periodicity of ϵ^0 order rotation, and the periodicity leads to $b_1(X) = 0$. The general solution of u_1 turns out to be similar form to u_0:

$$u_1 = c_1(X)y + d_1(X) \tag{3.19}$$

At last, the periodicity of u_1 makes $c_1(X) = 0$ and the final solution of u_1 reads:

$$u_1(X,y) = d_1(X) = U_1(X) \tag{3.20}$$

u_1 the ϵ^1 order displacement depends only on the macroscale X.

3.4.3 Asymptotic calculation of O(ϵ^{-2}) order equation

At $O(\epsilon^{-2})$, the wave equation is:

$$\begin{aligned}&\frac{\partial^2}{\partial X^2}\left(E(y)I\frac{\partial^2 u_0}{\partial y^2}\right) + 2\frac{\partial^2}{\partial y \partial X}\left(E(y)I\left(\frac{\partial^2 u_0}{\partial y \partial X} + \frac{\partial^2 u_1}{\partial y^2}\right)\right)\\ &+ \frac{\partial^2}{\partial y^2}\left(E(y)I\left(\frac{\partial^2 u_0}{\partial X^2} + 2\frac{\partial^2 u_1}{\partial y \partial X} + \frac{\partial^2 u_2}{\partial y^2}\right)\right) = 0\end{aligned} \tag{3.21}$$

With (3.14) and (3.20), the above equation can be simplified as:

$$\frac{\partial^2}{\partial y^2}\left(E(y)I\left(\frac{\partial^2 U_0}{\partial X^2} + \frac{\partial^2 u_2}{\partial y^2}\right)\right) = 0 \tag{3.22}$$

Integrating (3.22) twice with respect to y:

$$E(y)I\left(\frac{\partial^2 U_0}{\partial X^2} + \frac{\partial^2 u_2}{\partial y^2}\right) = a_2(X)y + b_2(X) \tag{3.23}$$

Observing the ϵ^0 order moment:

$$E(y)I\left(\frac{\partial^2 u_0}{\partial X^2}+2\frac{\partial^2 u_1}{\partial y \partial X}+\frac{\partial^2 u_2}{\partial y^2}\right)$$

Considering (3.14), (3.20), it can be found that the left hand side of equation (3.23) is exactly the ϵ^0 order moment, whose periodicity derives that $a_2(X)=0$. Then

$$E(y)I\left(\frac{\partial^2 U_0}{\partial X^2}+\frac{\partial^2 u_2}{\partial y^2}\right)=b_2(X) \tag{3.24}$$

Another integral of (3.24) gives:

$$\frac{\partial u_2}{\partial y}=\frac{b_2(X)}{I}\int_0^y \frac{1}{E(\tau)}\,d\tau-\frac{\partial^2 U_0}{\partial X^2}(y+c_2)+d_2(X) \tag{3.25}$$

According to the periodicity of ϵ^1 order rotation, $u_{2,y}$ is periodic. In order to simplify the notation, an averaging operator $<>$ is defined as:

$$<f>=\frac{1}{L}\int_0^L f(y)dy \tag{3.26}$$

Then the periodicity of $u_{2,y}$ indicates that:

$$\begin{aligned}-\frac{\partial^2 U_0}{\partial X^2}c_2+d_2(X)&=\frac{b_2(X)}{I}\int_0^L\frac{1}{E(\tau)}\,d\tau-\frac{\partial^2 U_0}{\partial X^2}(L+c_2)+d_2(X)\\ \Rightarrow b_2(X)&=E_0 I U_{0,XX}\end{aligned} \tag{3.27}$$

where in the studied case figure (3.1)

$$E_0=\frac{1}{<\frac{1}{E(y)}>}=\frac{E_{\mathrm{a}}E_{\mathrm{b}}}{(1-\alpha)E_{\mathrm{a}}+\alpha E_{\mathrm{b}}}$$

E_{a}, E_{b} denotes respectively the Young's Modulus of material A and B. Substituting b_2 into (3.25),

$$\begin{aligned}u_{2,y}(X,y)&=E_0U_{0,XX}\int_0^y\frac{1}{E(\tau)}\,d\tau-U_{0,XX}(y+c_2)+d_2(X)\\&=d_2(X)+\left(E_0\int_0^y\frac{1}{E(\tau)}\,d\tau-y-c_2\right)U_{0,XX}\\&=d_2(X)+H(y)U_{0,XX}\end{aligned} \tag{3.28}$$

where

$$H(y) = E_0 \int_0^y \frac{1}{E(\tau)}\, d\tau - y - c_2$$

and $H(y)$ remains to be determined. For the material A

$$\begin{aligned} H_a(y) &= E_0 \frac{y}{E_a} - y - c_{2a} \\ &= \frac{E_b y}{(1-\alpha)E_a + \alpha E_b} - y - c_{2a} \\ &= \frac{(1-\alpha)(E_b - E_a)}{(1-\alpha)E_a + \alpha E_b} y - c_{2a} \end{aligned}$$

For the material B

$$\begin{aligned} H_b(y) &= E_0 \frac{y}{E_b} - y - c_{2b} \\ &= \frac{E_a y}{(1-\alpha)E_a + \alpha E_b} - y - c_{2b} \\ &= \frac{\alpha(E_a - E_b)}{(1-\alpha)E_a + \alpha E_b} y - c_{2b} \end{aligned}$$

In order to determine the two constant c_{2a}, c_{2b}, some conditions are needed:

Periodicity condition: $u_{2,y}(X,0) = u_{2,y}(X,L) \Rightarrow H_a(0) = H_b(L)$

Continuity condition: $u_{2,y}(X,\alpha L^-) = u_{2,y}(X,\alpha L^+) \Rightarrow H_a(\alpha L^-) = H_b(\alpha L^+)$

The periodicity condition has been used before in equation (3.27). Thus one extra normalization condition are needed to make sure the uniqueness of the two constant, which gives us: $< u_{2,y}(X,y) >= d_2(X) \Rightarrow < H(y) >= 0$. With these conditions, the associated equation system is yielded:

$$\begin{aligned} H_a(\alpha L^-) = H_b(\alpha L^+) &\Rightarrow \frac{(1-\alpha)(E_b - E_a)}{(1-\alpha)E_a + \alpha E_b}\alpha L - c_{2a} = \frac{\alpha(E_a - E_b)}{(1-\alpha)E_a + \alpha E_b}\alpha L - c_{2b} \\ &\Rightarrow c_{2b} = c_{2a} + \frac{E_a - E_b}{(1-\alpha)E_a + \alpha E_b}\alpha L \end{aligned}$$

$$\begin{aligned} < H(y) >= 0 &\Rightarrow \frac{1}{L}\left(\int_0^{\alpha L} H_a(y)\, dy + \int_{\alpha L}^{L} H_b(y)\, dy\right) = 0 \\ &\Rightarrow \frac{(1-\alpha)(E_b - E_a)}{(1-\alpha)E_a + \alpha E_b}\frac{(\alpha L)^2}{2} - c_{2a}\alpha L \\ &+ \frac{\alpha(E_a - E_b)}{(1-\alpha)E_a + \alpha E_b}\frac{(1-\alpha^2)L^2}{2} - c_{2b}(1-\alpha)L = 0 \\ &\Rightarrow c_{2b} = -\frac{\alpha}{1-\alpha}c_{2a} + \frac{E_a - E_b}{2((1-\alpha)E_a + \alpha E_b)}\alpha L \end{aligned}$$

With these two equations, c_{2a}, c_{2b} are deduced:

$$\begin{cases} c_{2a} = \dfrac{(1-\alpha)(E_b - E_a)}{(1-\alpha)E_a + \alpha E_b}\dfrac{\alpha L}{2} \\ c_{2b} = \dfrac{\alpha(E_a - E_b)}{(1-\alpha)E_a + \alpha E_b}\dfrac{(1+\alpha)L}{2} \end{cases} \tag{3.29}$$

Therefore, the expression of $H(y)$ are in the following form:

$$H(y) = \frac{(E_\mathrm{b} - E_\mathrm{a})}{(1-\alpha)E_\mathrm{a} + \alpha E_\mathrm{b}} \begin{cases} (1-\alpha)\left(y - \dfrac{\alpha L}{2}\right) & 0 < y < \alpha L \\ (-\alpha)\left(y - \dfrac{(1+\alpha)L}{2}\right) & \alpha L < y < L \end{cases} \tag{3.30}$$

At last, the solution of u_2 is obtained by integrating (3.28) with respect to y:

$$u_2 = d_2(X)y + \int_0^y H(\tau)d\tau U_{0,XX} + e_2(X)$$

According to the periodicity of u_2,

$$\begin{aligned} e_2(X) &= d_2(X)L + \int_0^L H(\tau)d\tau U_{0,XX} + e_2(X) \\ \Rightarrow d_2(X) &= -<H(\tau)>U_{0,XX} = 0 \end{aligned}$$

Then the final formula of u_2 is:

$$u_2(X,y) = e_2(X) + \int_0^y H(\tau)d\tau U_{0,XX} = U_2(X) + M(y)U_{0,XX} \tag{3.31}$$

where $M(y)$ reminds to be determined.

The periodicity condition $u_2(X,0) = u_2(X,L) \Rightarrow M(0) = M(L)$;

the continuity condition $u_2(X,\alpha L^-) = u_2(X,\alpha L^+) \Rightarrow M(\alpha L^-) = M(\alpha L^+)$;

together with the normalization condition $< u_2(X,y) >= U_2(X) \Rightarrow < M(y) >= 0$;

give the unique solution of $M(y)$:

$$M(y) = \frac{(E_\mathrm{b} - E_\mathrm{a})}{(1-\alpha)E_\mathrm{a} + \alpha E_\mathrm{b}} \begin{cases} (1-\alpha)\left(\dfrac{y^2}{2} - \dfrac{\alpha L}{2}y + f_{2\mathrm{a}}\right) & 0 < y < \alpha L \\ (-\alpha)\left(\dfrac{y^2}{2} - \dfrac{(1+\alpha)L}{2}y + f_{2\mathrm{b}}\right) & \alpha L < y < L \end{cases} \tag{3.32}$$

with two constants

$$\begin{cases} f_{2\mathrm{a}} = \dfrac{2\alpha^2 - \alpha}{12} L^2 \\ f_{2\mathrm{b}} = \dfrac{2\alpha^2 + 3\alpha + 1}{12} L^2 \end{cases} \tag{3.33}$$

The outline of the calculation about u_{n+4} is shown in figure (3.3), the manipulation is mainly composed of four integrals accompanied with some simplifications using existing periodic or continuity conditions. Some useful conclusions should be summarized:

$$\begin{aligned} &E(y)I\left(\frac{\partial^2 u_0}{\partial X^2} + \frac{\partial^2 u_2}{\partial y^2}\right) = E_0 I \frac{\partial^2 U_0}{\partial X^2} \\ &E(y)(1 + M_{yy}) = E_0 \end{aligned} \tag{3.34}$$

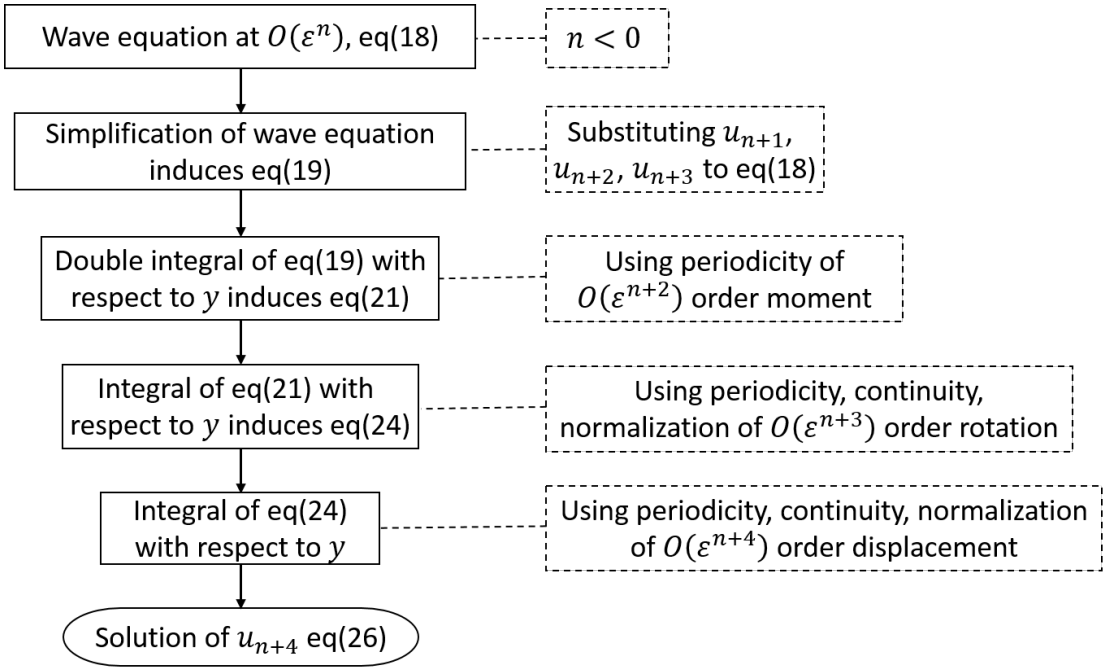

FIGURE 3.3: Outline of calculation about u_{n+4} at order $O(\epsilon^n)$

3.4.4 Asymptotic calculation of O(ϵ^{-1}) order equation

At $O(\epsilon^{-1})$, the wave equation becomes more complicated:

$$\begin{aligned}&\frac{\partial^2}{\partial X^2}\left(E(y)I\left(\frac{\partial^2 u_0}{\partial y \partial X}+\frac{\partial^2 u_1}{\partial y^2}\right)\right)\\&+2\frac{\partial^2}{\partial y \partial X}\left(E(y)I\left(\frac{\partial^2 u_0}{\partial X^2}+2\frac{\partial^2 u_1}{\partial y \partial X}+\frac{\partial^2 u_2}{\partial y^2}\right)\right)\\&+\frac{\partial^2}{\partial y^2}\left(E(y)I\left(\frac{\partial^2 u_1}{\partial X^2}+2\frac{\partial^2 u_2}{\partial y \partial X}+\frac{\partial^2 u_3}{\partial y^2}\right)\right)=0\end{aligned} \tag{3.35}$$

The calculation process reminds unchanged as shown in figure (3.3). By analogy, the solution of u_3 is in the following form:

$$u_3(X,y)=U_3(X)+M(y)U_{1,XX}+N(y)U_{0,XXX} \tag{3.36}$$

where $N(y)$ remains to be determined. Firstly, with existing conclusion (3.14),(3.20),(3.34), equation (3.35) can be simplified as:

$$\frac{\partial^2}{\partial y^2}\left(E(y)I\left(\frac{\partial^2 u_1}{\partial X^2}+2\frac{\partial^2 u_2}{\partial y \partial X}+\frac{\partial^2 u_3}{\partial y^2}\right)\right)=0 \tag{3.37}$$

Secondly, double integral of equation (3.37) yields:

$$E(y)I\left(\frac{\partial^2 u_1}{\partial X^2}+2\frac{\partial^2 u_2}{\partial y \partial X}+\frac{\partial^2 u_3}{\partial y^2}\right)=a_3(X)y+b_3(X)$$

The left hand side in the above equation is the ϵ^1 order moment, and its periodicity indicates $a_3(X)=0$. Then

$$E(y)I\left(\frac{\partial^2 u_1}{\partial X^2}+2\frac{\partial^2 u_2}{\partial y \partial X}+\frac{\partial^2 u_3}{\partial y^2}\right)=b_3(X) \tag{3.38}$$

Thirdly, with equation (3.31), the ϵ^2 order rotation writes:

$$\frac{\partial u_2}{\partial X}+\frac{\partial u_3}{\partial y}=\frac{\partial U_2}{\partial X}+M(y)\frac{\partial^3 U_0}{\partial X^3}+\frac{\partial u_3}{\partial y}$$

The periodicity of ϵ^2 order rotation, together with the periodicity of $M(y)$, ensures the periodicity of $u_{3,y}$. From equation (3.38), it can be deduced that:

$$\frac{\partial^2 u_3}{\partial y^2}=\frac{b_3(X)}{E(y)I}-\frac{\partial^2 U_1}{\partial X^2}-2\frac{\partial M}{\partial y}\frac{\partial^3 U_0}{\partial X^3}$$

Then the periodicity of $u_{3,y}$ indicates that $< u_{3,yy} >= 0$, i.e.

$$\frac{b_3(X)}{I}\int_0^L \frac{1}{E(\tau)}\,d\tau - \frac{\partial^2 U_1}{\partial X^2}L - 2M(L)\frac{\partial^3 U_0}{\partial X^3} = -2M(0)\frac{\partial^3 U_0}{\partial X^3}$$
$$\Rightarrow b_3(X) = E_0 I U_{1,XX}$$

Then,

$$E(y)I\left(\frac{\partial^2 u_1}{\partial X^2} + 2\frac{\partial^2 u_2}{\partial y \partial X} + \frac{\partial^2 u_3}{\partial y^2}\right) = E_0 I\frac{\partial^2 U_1}{\partial X^2} \tag{3.39}$$

Then substituting (3.14), (3.20), (3.36) into (3.39) derives the relation to determine $N(y)$:

$$2M_y + N_{yy} = 0 \Rightarrow N = -2\int_0^y M(\tau)d\tau + d_3 y + e_3 \tag{3.40}$$

Fourthly, the periodicity condition $u_3(X,0) = u_3(X,L) \Rightarrow N(0) = N(L)$;
the continuity condition $u_3(X,\alpha L^-) = u_3(X,\alpha L^+) \Rightarrow N(\alpha L^-) = N(\alpha L^+)$;
together with the normalization condition $< u_3(X,y) >= U_3(X) \Rightarrow < N(y) >= 0$ guarantee an unique solution of $N(y)$:

$$N(y) = \frac{-2(E_\mathrm{b} - E_\mathrm{a})}{(1-\alpha)E_\mathrm{a} + \alpha E_\mathrm{b}}\begin{cases}(1-\alpha)\left(\dfrac{y^3}{6} - \dfrac{\alpha L}{4}y^2 + c_{3\mathrm{a}}y + d_{3\mathrm{a}}\right)\\ (-\alpha)\left(\dfrac{y^3}{6} - \dfrac{(1+\alpha)L}{4}y^2 + c_{3\mathrm{b}}y + d_{3\mathrm{a}}\right)\end{cases} \tag{3.41}$$

with four constants

$$\begin{cases} c_{3\mathrm{a}} = \dfrac{2\alpha^2 - \alpha}{12}L^2\\ c_{3\mathrm{b}} = \dfrac{2\alpha^2 + 3\alpha + 1}{12}L^2\\ d_{3\mathrm{a}} = \dfrac{\alpha^2(1-\alpha)}{24}L^3\\ d_{3\mathrm{b}} = -\dfrac{\alpha(1+\alpha)^2}{24}L^3\end{cases} \tag{3.42}$$

As $N(y)$ is determined, the solution of $u_3(X,y)$ appears automatically. Similar to previous section, some useful conclusions are noted:

$$\begin{aligned} &u_3(X,y) = U_3(X) + M(y)U_{1,XX} + N(y)U_{0,XXX}\\ &E(y)I\left(\frac{\partial^2 u_1}{\partial X^2} + 2\frac{\partial^2 u_2}{\partial y \partial X} + \frac{\partial^2 u_3}{\partial y^2}\right) = E_0 I\frac{\partial^2 U_1}{\partial X^2}\\ &2M_y + N_{yy} = 0\end{aligned} \tag{3.43}$$

3.4.5 Asymptotic calculation of O(ϵ^0) order equation

As mentioned above, at $O(\epsilon^0)$, in the homogenized wave equation, dynamic term emerges. Then two primary objects, the homogenized wave equation and the solution of u_{n+4}, are to be achieved during the calculation.

$$\begin{aligned}&\frac{\partial^2}{\partial X^2}\left(E(y)I\left(\frac{\partial^2 u_0}{\partial X^2}+2\frac{\partial^2 u_1}{\partial y\partial X}+\frac{\partial^2 u_2}{\partial y^2}\right)\right)\\&+2\frac{\partial^2}{\partial y\partial X}\left(E(y)I\left(\frac{\partial^2 u_1}{\partial X^2}+2\frac{\partial^2 u_2}{\partial y\partial X}+\frac{\partial^2 u_3}{\partial y^2}\right)\right)\\&+\frac{\partial^2}{\partial y^2}\left(E(y)I\left(\frac{\partial^2 u_2}{\partial X^2}+2\frac{\partial^2 u_3}{\partial y\partial X}+\frac{\partial^2 u_4}{\partial y^2}\right)\right)+\rho(y)S\frac{\partial^2 u_0}{\partial t^2}=0\end{aligned}\tag{3.44}$$

The first object: homogenized wave equation. It can be noticed that the $O(\epsilon^n)$ order moment is:

$$E(y)I\left(\frac{\partial^2 u_n}{\partial X^2}+2\frac{\partial^2 u_{n+1}}{\partial y\partial X}+\frac{\partial^2 u_{n+2}}{\partial y^2}\right)\tag{3.45}$$

Equation (3.45) is periodic in y, and its derivative is also periodic. Then applying the averaging operator $<>$ to (3.44) leads to:

$$<\frac{\partial^2}{\partial X^2}\left(E(y)I\left(\frac{\partial^2 u_0}{\partial X^2}+2\frac{\partial^2 u_1}{\partial y\partial X}+\frac{\partial^2 u_2}{\partial y^2}\right)\right)>+<\rho(y)S\frac{\partial^2 u_0}{\partial t^2}>=0\tag{3.46}$$

Substituting (3.14), (3.20), (3.24) into (3.46), the $O(\epsilon^0)$ order homogenized equation is deduced in the following form:

$$E_0I\frac{\partial^4 U_0}{\partial X^4}+\rho_0S\frac{\partial^2 U_0}{\partial t^2}=0\tag{3.47}$$

where $\rho_0 =<\rho(y)>= \alpha\rho_{\mathrm{a}}+(1-\alpha)\rho_{\mathrm{b}}$, ρ_{a}, ρ_{b} denote respectively the mass density of material A and B. The outline of the calculation about homogenized equation is concluded in figure (3.4).

The second object: solution of u_4, which can be deduced according to figure (3.3). Firstly, substituting (3.34), (3.39), (3.47) into (3.44), the wave equation can be simplified as:

$$\frac{\partial^2}{\partial y^2}\left(E(y)I\left(\frac{\partial^2 u_2}{\partial X^2}+2\frac{\partial^2 u_3}{\partial y\partial X}+\frac{\partial^2 u_4}{\partial y^2}\right)\right)+(1-\frac{\rho(y)}{\rho_0})E_0I\frac{\partial^4 U_0}{\partial X^4}=0\tag{3.48}$$

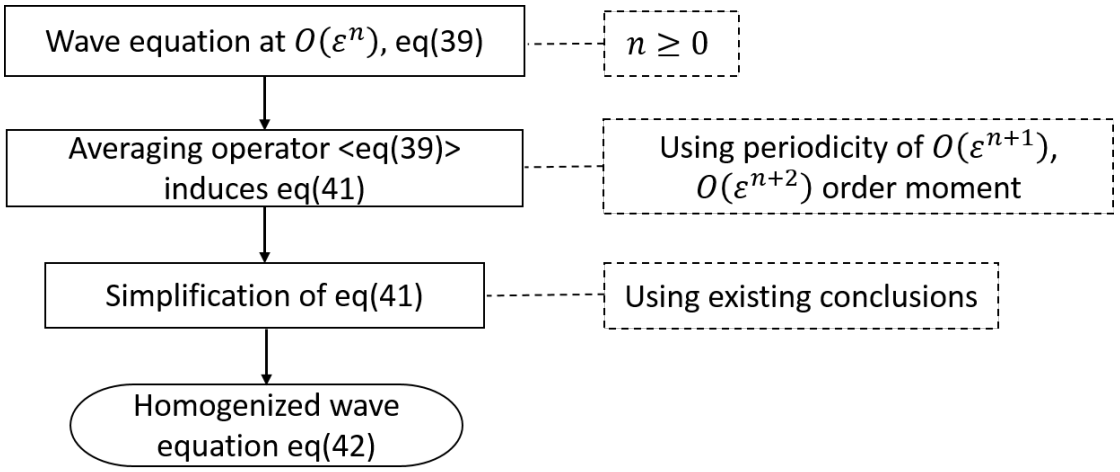

FIGURE 3.4: Outline of calculation about homogenized equation at order $O(\epsilon^n)$

By analogy, u_4 is in the following form:

$$u_4(X,y) = U_4(X) + M(y)U_{2,XX} + N(y)U_{1,XXX} + P(y)U_{0,XXXX} \tag{3.49}$$

where $P(y)$ reminds to be determined. According to (3.31), (3.36), (3.49), the second order moment becomes:

$$\begin{aligned} &E(y)I\left(\frac{\partial^2 u_2}{\partial X^2} + 2\frac{\partial^2 u_3}{\partial y \partial X} + \frac{\partial^2 u_4}{\partial y^2}\right) \\ =&E(y)I(1+M_{yy})\frac{\partial^2 U_2}{\partial X^2} + E(y)I(2M_y + N_{yy})\frac{\partial^3 U_1}{\partial X^3} + E(y)I(M + 2N_y + P_{yy})\frac{\partial^4 U_0}{\partial X^4} \end{aligned}$$

As $E(y)(1+M_{,yy}) = E_0$, $2M_{,y} + N_{,yy} = 0$, the first term in left hand side of equation (3.48) becomes:

$$\frac{\partial^2}{\partial y^2}\left(E(y)I\left(\frac{\partial^2 u_2}{\partial X^2} + 2\frac{\partial^2 u_3}{\partial y \partial X} + \frac{\partial^2 u_4}{\partial y^2}\right)\right) = \frac{\partial^2}{\partial y^2}\left(E(y)I(M + 2N_y + P_{yy})\right)\frac{\partial^4 U_0}{\partial X^4}$$

And the equation (3.48) becomes:

$$\frac{\partial^2}{\partial y^2}\left(E(y)(M + 2N_y + P_{yy})\right) = \left(\frac{\rho(y)}{\rho_0} - 1\right)E_0 \tag{3.50}$$

Secondly, by observing the ϵ^1 order shear force:

$$\begin{aligned}
&\frac{\partial}{\partial X}\left(E(y)I\left(\frac{\partial^2 u_1}{\partial X^2}+2\frac{\partial^2 u_2}{\partial y\partial X}+\frac{\partial^2 u_3}{\partial y^2}\right)\right)+\frac{\partial}{\partial y}\left(E(y)I\left(\frac{\partial^2 u_2}{\partial X^2}+2\frac{\partial^2 u_3}{\partial y\partial X}+\frac{\partial^2 u_4}{\partial y^2}\right)\right)\\
=&\frac{\partial}{\partial X}\left(E_0 I\frac{\partial^2 U_1}{\partial X^2}\right)+\frac{\partial}{\partial y}\left(E_0 I\frac{\partial^2 U_2}{\partial X^2}+E(y)I(M+2N_y+P_{yy})\frac{\partial^4 U_0}{\partial X^4}\right)\\
=&E_0 I\frac{\partial^3 U_1}{\partial X^3}+\frac{\partial}{\partial y}\left(E(y)I(M+2N_y+P_{yy})\right)\frac{\partial^4 U_0}{\partial X^4}
\end{aligned}$$

it can be seen that the periodicity of ϵ^1 order shear force ensures the periodicity of $\frac{\partial}{\partial y}\left(E(y)I(M+2N_y+P_{yy})\right)$. Then by observing the ϵ^2 order moment:

$$E(y)I\left(\frac{\partial^2 u_2}{\partial X^2}+2\frac{\partial^2 u_3}{\partial y\partial X}+\frac{\partial^2 u_4}{\partial y^2}\right)=E_0 I\frac{\partial^2 U_2}{\partial X^2}+E(y)I(M+2N_y+P_{yy})\frac{\partial^4 U_0}{\partial X^4}$$

the periodicity of ϵ^2 order moment indicates the periodicity of $E(y)I(M+2N_y+P_{yy})$, which means $<\frac{\partial}{\partial y}\left(E(y)I(M+2N_y+P_{yy})\right)>=0$. With these conditions, the integral of (3.50) is deduced in the following form:

$$\frac{\partial}{\partial y}\left(E(y)(M+2N_y+P_{yy})\right)=E_0\frac{\rho_{\mathrm{a}}-\rho_{\mathrm{b}}}{\rho_0}\begin{cases}(1-\alpha)(y-\dfrac{\alpha}{2}L)\\(-\alpha)(y-\dfrac{1+\alpha}{2}L)\end{cases}\tag{3.51}$$

Thirdly, observing the ϵ^3 order rotation:

$$\frac{\partial u_4}{\partial y}+\frac{\partial u_3}{\partial X}=\frac{\partial U_3}{\partial X}+\frac{\partial M(y)}{\partial y}\frac{\partial^2 U_2}{\partial X^2}+(\frac{\partial N(y)}{\partial y}+M(y))\frac{\partial^3 U_1}{\partial X^3}+(\frac{\partial P(y)}{\partial y}+N(y))\frac{\partial^4 U_0}{\partial X^4}$$

the periodicity of $P_{,y}+N$ is verified. Thus

$$<(M+2N_y+P_{yy})>=<M>+<N_y>+<N_y+P_{yy}>=0$$

Besides, $E(y)(M+2N_y+P_{yy})$ has been proved to be periodic. Hence, the integral of (3.51) is yielded:

$$E(y)(M+2N_y+P_{yy})=E_0\frac{\rho_{\mathrm{a}}-\rho_{\mathrm{b}}}{\rho_0}\begin{cases}(1-\alpha)(\dfrac{y^2}{2}-\dfrac{\alpha}{2}Ly+c_{4\mathrm{a}})\\(-\alpha)(\dfrac{y^2}{2}-\dfrac{1+\alpha}{2}Ly+c_{4\mathrm{b}})\end{cases}\tag{3.52}$$

with two constants

$$\begin{cases} c_{4\mathrm{a}} = \alpha \dfrac{-(1-\alpha)^2 E_a + \alpha^2 E_b}{12((1-\alpha)E_a + \alpha E_b)} L^2 \\ c_{4\mathrm{b}} = \dfrac{(1-\alpha)(\alpha^2+4\alpha+1)E_a + \alpha^2(\alpha+5)E_b}{12((1-\alpha)E_a + \alpha E_b)} L^2 \end{cases} \tag{3.53}$$

Then, the expression of $P(y)$ and u_4 can be obtained by further integrals.

3.4.6 Approximation calculate of $O(\epsilon^1)$ order equation

At $O(\epsilon^1)$, the wave equation is:

$$\begin{aligned} &\frac{\partial^2}{\partial X^2}\left(E(y)I\left(\frac{\partial^2 u_1}{\partial X^2} + 2\frac{\partial^2 u_2}{\partial y \partial X} + \frac{\partial^2 u_3}{\partial y^2}\right)\right) \\ &+2\frac{\partial^2}{\partial y \partial X}\left(E(y)I\left(\frac{\partial^2 u_2}{\partial X^2} + 2\frac{\partial^2 u_3}{\partial y \partial X} + \frac{\partial^2 u_4}{\partial y^2}\right)\right) \\ &+\frac{\partial^2}{\partial y^2}\left(E(y)I\left(\frac{\partial^2 u_3}{\partial X^2} + 2\frac{\partial^2 u_4}{\partial y \partial X} + \frac{\partial^2 u_5}{\partial y^2}\right)\right) + \rho(y)S\frac{\partial^2 u_1}{\partial t^2} = 0 \end{aligned} \tag{3.54}$$

According to figure (3.4), applying averaging operator <> to (3.54) leads to:

$$< \frac{\partial^2}{\partial X^2}\left(E(y)I\left(\frac{\partial^2 u_1}{\partial X^2} + 2\frac{\partial^2 u_2}{\partial y \partial X} + \frac{\partial^2 u_3}{\partial y^2}\right)\right) > + < \rho(y)S\frac{\partial^2 u_1}{\partial t^2} >= 0 \tag{3.55}$$

Substituting (3.20), (3.39) into (3.55), the $O(\epsilon^1)$ order homogenized equation is deduced in the following form:

$$E_0 I \frac{\partial^4 U_1}{\partial X^4} + \rho_0 S \frac{\partial^2 U_1}{\partial t^2} = 0 \tag{3.56}$$

In our studied case, the approximation process stops at $O(\epsilon^2)$ order, where the solution of u_4 is enough to deduce the homogenized equation. Therefore, the calculation of u_5 is no longer needed.

3.4.7 Approximation calculate of $O(\epsilon^2)$ order equation

At $O(\epsilon^2)$, the wave equation is:

$$\begin{aligned}&\frac{\partial^2}{\partial X^2}\left(E(y)I\left(\frac{\partial^2 u_2}{\partial X^2}+2\frac{\partial^2 u_3}{\partial y\partial X}+\frac{\partial^2 u_4}{\partial y^2}\right)\right)\\&+2\frac{\partial^2}{\partial y\partial X}\left(E(y)I\left(\frac{\partial^2 u_3}{\partial X^2}+2\frac{\partial^2 u_4}{\partial y\partial X}+\frac{\partial^2 u_5}{\partial y^2}\right)\right)\\&+\frac{\partial^2}{\partial y^2}\left(E(y)I\left(\frac{\partial^2 u_4}{\partial X^2}+2\frac{\partial^2 u_5}{\partial y\partial X}+\frac{\partial^2 u_6}{\partial y^2}\right)\right)+\rho(y)S\frac{\partial^2 u_2}{\partial t^2}=0\end{aligned} \tag{3.57}$$

Applying averaging operator $<>$ to (3.57) leads to:

$$<\frac{\partial^2}{\partial X^2}\left(E(y)I\left(\frac{\partial^2 u_2}{\partial X^2}+2\frac{\partial^2 u_3}{\partial y\partial X}+\frac{\partial^2 u_4}{\partial y^2}\right)\right)>+<\rho(y)S\frac{\partial^2 u_2}{\partial t^2}>=0 \tag{3.58}$$

Substituting (3.31), (3.36), (3.47), (3.49) into (3.58), the $O(\epsilon^2)$ order homogenized equation is deduced in the following form:

$$E_0 I\frac{\partial^4 U_2}{\partial X^4}+I(<E(y)(M+2N_y+P_{yy})>-\frac{E_0}{\rho_0}<\rho M>)\frac{\partial^6 U_0}{\partial X^6}+\rho_0 S\frac{\partial^2 U_2}{\partial t^2}=0 \tag{3.59}$$

Knowing the expression of $E(y)(M+2N_y+P_{yy})$ and $M(y)$, one can deduce:

$$<E(y)(M+2N_y+P_{yy})>-\frac{E_0}{\rho_0}<\rho M>=-\frac{E_0}{\rho_0}\frac{\alpha^2(1-\alpha)^2(E_{\mathrm{a}}-E_{\mathrm{b}})(\rho_{\mathrm{a}}-\rho_{\mathrm{b}})L^2}{6((1-\alpha)E_{\mathrm{a}}+\alpha E_{\mathrm{b}})}$$

And the $O(\epsilon^2)$ order homogenized equation becomes:

$$E_0 I\frac{\partial^4 U_2}{\partial X^4}+\frac{1}{\epsilon^2}E_d I\frac{\partial^6 U_0}{\partial X^6}+\rho_0 S\frac{\partial^2 U_2}{\partial t^2}=0 \tag{3.60}$$

with

$$E_d=-\frac{E_0}{\rho_0}\frac{\alpha^2(1-\alpha)^2(E_{\mathrm{a}}-E_{\mathrm{b}})(\rho_{\mathrm{a}}-\rho_{\mathrm{b}})l^2}{6((1-\alpha)E_{\mathrm{a}}+\alpha E_{\mathrm{b}})}$$

Observing all the homogenized equations obtained by multi-scale asymptotic method and HPDM in section 3.3, it can be found that these homogenized wave equations for various orders are the same, which proves the accuracy of the homogenized models in another way.

3.4.8 Global homogenized wave equation

In these previous sections, three homogenized equations of U_0, U_1, U_2 are obtained:

At $O(\epsilon^0)$ Eq. (3.47)

$$E_0 I \frac{\partial^4 U_0}{\partial X^4} + \rho_0 S \frac{\partial^2 U_0}{\partial t^2} = 0$$

At $O(\epsilon^1)$ Eq. (3.56)

$$E_0 I \frac{\partial^4 U_1}{\partial X^4} + \rho_0 S \frac{\partial^2 U_1}{\partial t^2} = 0$$

At $O(\epsilon^2)$ Eq. (3.60)

$$E_0 I \frac{\partial^4 U_2}{\partial X^4} + \frac{1}{\epsilon^2} E_d I \frac{\partial^6 U_0}{\partial X^6} + \rho_0 S \frac{\partial^2 U_2}{\partial t^2} = 0$$

In order to proceed the asymptomatic homogenization, the displacement $u(X, y)$ has been expanded as:

$$u(X, y) = u_0(X, y) + \epsilon u_1(X, y) + \epsilon^2 u_2(X, y) + ...$$

Applying the averaging operator $<>$ to $u(X, y)$ derives the global displacement:

$$U(X) =< u(X, y) >= U_0(X) + \epsilon U_1(X) + \epsilon^2 U_2(X) + ... \tag{3.61}$$

Adding the three equations in the following way: (3.47) + (3.56) $\times \epsilon$ + (3.60) $\times \epsilon^2$ and neglecting the $O(\epsilon^3)$ order and higher leads to a global homogenized equation for $U(X)$:

$$E_0 I \frac{\partial^4 U}{\partial X^4} + E_d I \frac{\partial^6 U_0}{\partial X^6} + \rho_0 S \frac{\partial^2 U}{\partial t^2} = 0 \tag{3.62}$$

According to equation (3.60), E_d is proportional to l^2, which induces:

$$E_d \frac{\partial^2}{\partial X^2} \propto O(\frac{l^2}{L^2}) \propto O(\epsilon^2)$$

Then, the second term in (3.62) is an $O(\epsilon^2)$ order term. Neglecting the $O(\epsilon^3)$ order and higher means only the $O(\epsilon^0)$ order of U can be considered. Thus, an approximation for the second term is established:

$$E_d \frac{\partial^2 U_0}{\partial X^2} = E_d \frac{\partial^2 U}{\partial X^2} \tag{3.63}$$

With the approximation in (3.63), two different models are obtained by two different application ideas.

First model (HOH1)

Applying directly the relation in (3.63) to (3.62) leads to:

$$E_0 I \frac{\partial^4 U}{\partial X^4} + E_d I \frac{\partial^6 U}{\partial X^6} + \rho_0 S \frac{\partial^2 U}{\partial t^2} = 0 \tag{3.64}$$

This is a sixth order effective equation for flexural wave. Different from the original fourth order wave equation (3.1), higher order terms appears to capture the behaviour of periodic structure, and E_0, ρ_0 are no longer effective parameters. This model is referred as HOH1 for higher order homogenization model one.

Second model (HOH2)

According to (3.47)

$$\frac{\partial^4 U_0}{\partial X^4} = -\frac{\rho_0 S}{E_0 I} \frac{\partial^2 U_0}{\partial t^2}$$

Then

$$E_d \frac{\partial^6 U_0}{\partial X^6} = E_d \frac{\partial^2}{\partial X^2}(-\frac{\rho_0 S}{E_0 I} \frac{\partial^2 U_0}{\partial t^2}) = -\frac{\rho_0 S}{E_0 I} \frac{\partial^2}{\partial t^2}(E_d \frac{\partial^2 U_0}{\partial X^2}) = -\frac{\rho_0 S}{E_0 I} \frac{\partial^2}{\partial t^2}(E_d \frac{\partial^2 U}{\partial X^2})$$

With this conclusion, the equation (3.62) becomes:

$$E_0 I \frac{\partial^4 U}{\partial X^4} - \rho_0 S \frac{E_d}{E_0} \frac{\partial^2}{\partial t^2}(\frac{\partial^2 U}{\partial X^2}) + \rho_0 S \frac{\partial^2 U}{\partial t^2} = 0 \tag{3.65}$$

This is a fourth order homogenized wave equation. A term coupling time and space appears to reveal the periodicity of the structure. And the periodic structure is not considered as a traditional homogeneous one, neither. This model is referred as HOH2 for higher order homogenization model two.

In the next section, the validation of these homogenized models will be discussed. In infinite periodic structure case, the new dispersion relations of these models will be compared with the dispersion relation obtained by WFEM. Furthermore, in finite case, the frequency response function of these new homogenized models are also compared with the numerical WFEM result. The valid frequency ranges of the homogenized models in both cases are established.

3.5 Validation in the case of infinite structure

For the infinite structure, the dispersion relation characterises the essential relation between its physical properties and the propagating wave properties. In this section, the dispersion relation obtained by different models, such as traditional homogenized model (TH), which is actually the $O(\epsilon^0)$ order equation, HOH1 model and HOH2 model, are compared to the numerical dispersion relation obtained by WFEM. To satisfy the feasibility of homogenization, $\epsilon = l/L$ must be small enough to ensure the scale separation, and the studied domain is limited to the frequency before the first band gap.

3.5.1 Dispersion relation

To obtain the dispersion relation of the various models, a trial solution $U(X,t) = Aexp(i(\omega t - kx))$ is substituted into different homogenized equations. Here, A is the amplitude, ω is the angular frequency and k is the wavenumber.

TH model

Substituting the trial solution into (3.47) results in:

$$\omega = \sqrt{\frac{E_0 I}{\rho_0 S}} k^2 \tag{3.66}$$

HOH1 model

Substituting the trial solution into (3.64) results in:

$$\omega = \sqrt{\frac{E_0 I}{\rho_0 S}} k^2 \sqrt{\frac{E_0 - E_d k^2}{E_0}} \tag{3.67}$$

HOH2 model

Substituting the trial solution into (3.65) results in:

$$\omega = \sqrt{\frac{E_0 I}{\rho_0 S}} k^2 \sqrt{\frac{E_0}{E_0 + E_d k^2}} \tag{3.68}$$

For the transversal wave propagating in periodic structure, there exist propagating waves, where k is pure real, and evanescent waves, where k is pure imaginary. Then the

investigation is carried out separately for the two different waves. The valid domain is defined as follows:

For each frequency $f = \omega/2\pi$, if

$$\frac{|k_{\text{WFEM}} - k_{\text{homo}}|}{k_{\text{WFEM}}} < 1\%$$

then $f \in (0, f_{\text{lim}})$. Where k_{homo}, k_{WFEM} are the wavenumber obtained respectively by homogenized model and the WFEM method. The valid domain is $(0, f_{\text{lim}})$, and f_{lim} is the limit of the valid domain. A numerical example is presented: material A is Epoxy while B is Aluminium. The properties of A and B are shown in table (3.1). And the cross-section radius is $r = 0.025m$. According to the table, one can calculate $E_0 = 8.238e9Pa$, $\rho_0 = 1955kg/m^3$, $E_d = -4.865e8Pa$. In all numerical examples studied in this paper, 100 beam elements are used for each unit cell to ensure the WFEM method's accuracy. Then the dispersion relations of different models are plotted in figure (3.5) and figure (3.6).

Material	A(Epoxy)	B(Aluminium)
Mass density (kg/m^3)	$\rho_a = 1180$	$\rho_b = 2730$
Young's Modulus (Pa)	$E_a = 4.35e9$	$E_b = 77.56e9$
Length (m)	$l_a = 1$	$l_b = l_a$

TABLE 3.1: Material properties

In figure (3.5), the real part of k is presented. It can be seen that the first band gap frequency $f_{\text{gap}} = 9.4$Hz. According to the valid domain definition, the valid frequency of TH, HOH1 and HOH2 are respectively (0, 2.6Hz), (0, 8.4Hz), (0, 8.2Hz). In figure (3.6), the imaginary part of k is presented. The first band gap frequency $f_{\text{gap}} = 9,4Hz$ remains the same as before, and the valid frequency of TH, HOH1 and HOH2 are respectively (0, 3.5Hz), (0, 5.9Hz), (0, 6.7Hz). From the two figures, it can be seen that no matter for propagating wave or for evanescent wave, HOH1 and HOH2 turn out to be a more precise homogenized model and a larger valid range is provided.

For periodic structures, as the impedance varies at the interface of different components, the waves propagating in the structure have reflection effect. Thus, the Bragg band gap appears in the dispersion curve of periodic structures, which is the primary difference from the homogeneous case without impedance mismatch. According to the multi-scale asymptotic development, new homogenized higher order wave equations are

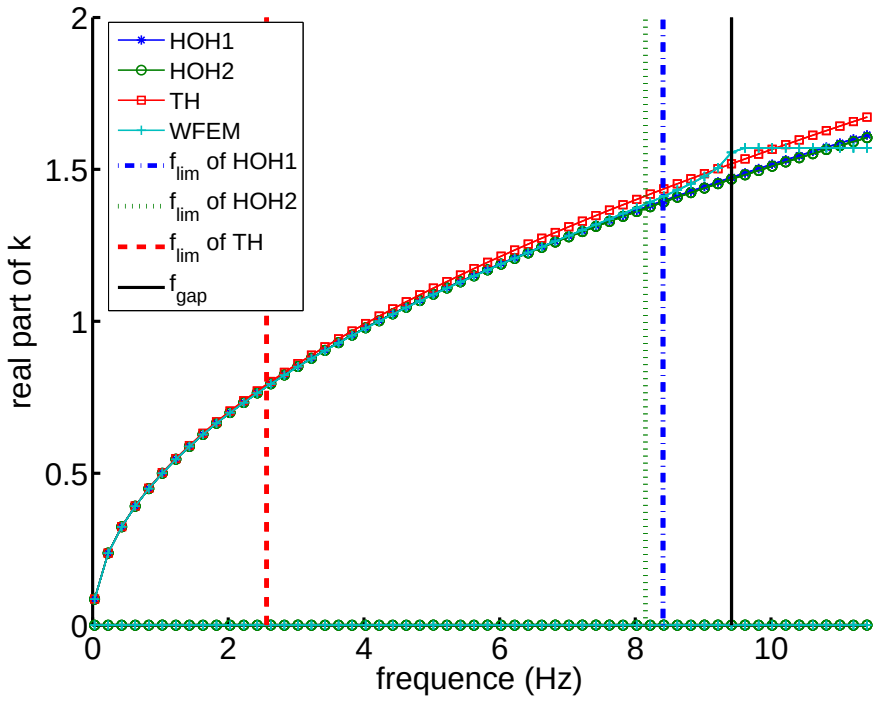

FIGURE 3.5: dispersion curve real(k) of the Ep-Al periodic beam obtained by different models

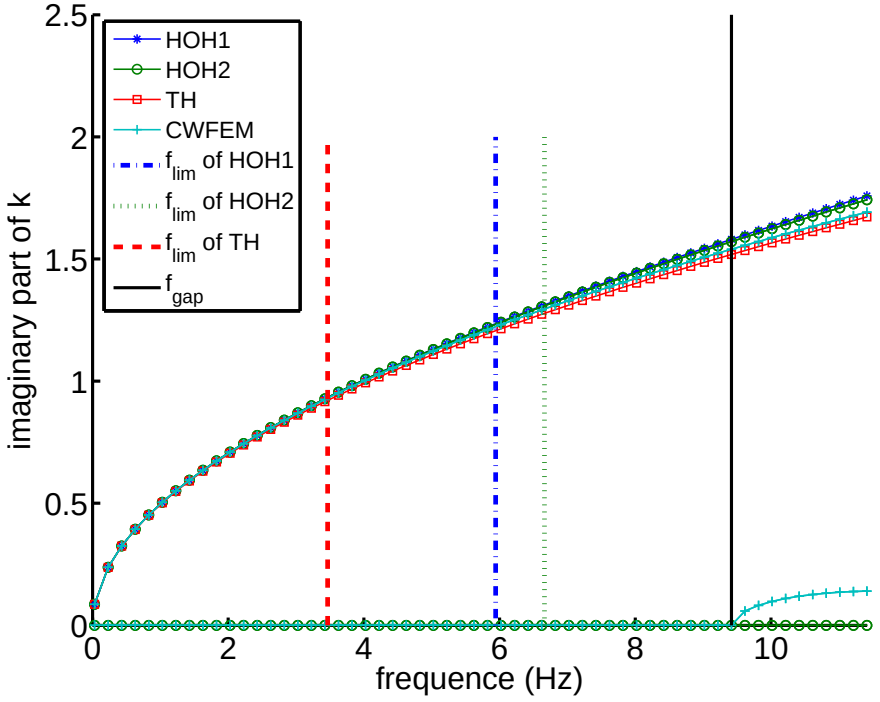

FIGURE 3.6: dispersion curve imag(k) of the Ep-Al periodic beam obtained by different models

derived to describe the periodic structure's behaviour. During the homogenization process, the heterogeneity has been taken into considered and is presented by a new homogenized term in the wave equation. That is the new homogenized model's superiority compared to traditional homogenization model. However, when the periodic structure is homogenized, the impedance mismatch disappears. Thus, the Bragg band gap can no longer be predicted by homogenized models, and the validity range is limited to the first propagating zone. The current results show that the higher order models are more accurate models than the classical model in the first propagating zone.

According to the formula, the dispersion relation is characterised by three parameter contrasts $(l_b/l_a, E_b/E_a, \rho_b/\rho_a)$. Thus, a parametric study concerning these three contrasts are presented in the following sections to demonstrate the superiority of the higher order models.

3.5.2 Parametric study: contrast of length fraction

In this case, the material A is Epoxy and the material B is Aluminium. The length of A, $l_\mathrm{a} = \alpha l$ and the length of B, $l_\mathrm{b} = (1-\alpha)l$. The length fraction α is the parameter to be studied. The f_gap and f_lim based on real(k) and imag(k) of these three different homogenized models are respectively shown in figure(3.7) and (3.8).

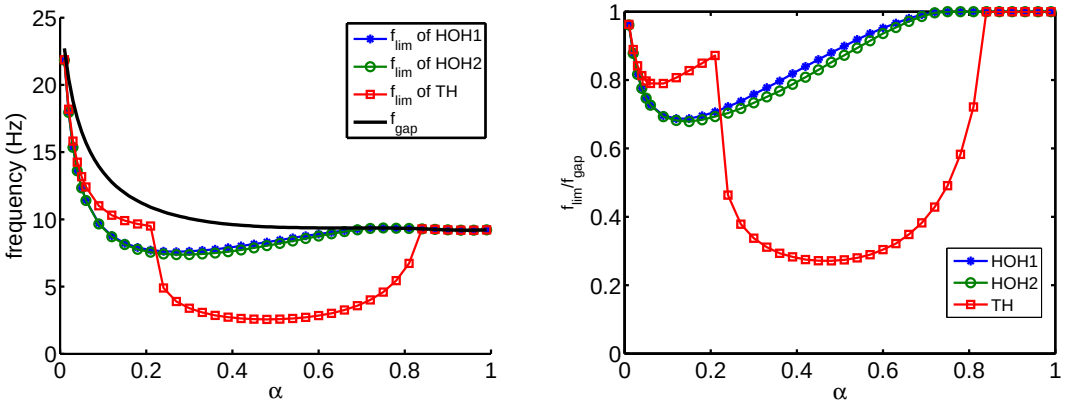

(a) valid frequency range f_{lim} (b) relative valid frequency range f_{lim}/f_{gap}

FIGURE 3.7: real(k) of different homogenized models in the fraction of α

When $\alpha \to 0$ ($l_a \to 0$), or $\alpha \to 1$ ($l_a \to l$), the periodic structure becomes a homogeneous beam made of material B or material A. As the periodicity becomes negligible,

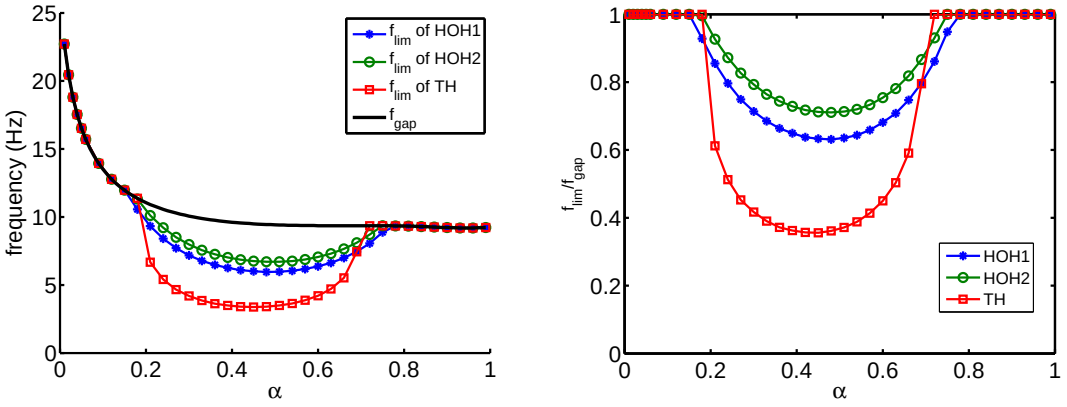

(a) valid frequency range f_{lim}

(b) relative valid frequency range f_{lim}/f_{gap}

FIGURE 3.8: imag(k) of different homogenized models in the fraction of α

the results in figure (3.7) and (3.8) depict that these three models all provide good approximation. Meanwhile, for a more heterogeneous structure with α far from 0 and 1, HOH1 and HOH2 are amended models. A larger valid frequency range is ensured by these two models compared to TH model. For instance, when $\alpha = 0.5$, which is the first studied case, according to the propagating wave in figure (3.7(b)), one can deduce that the HOH1 model and the HOH2 model provide respectively about 90% and 87% valid range before f_{gap} which is almost thrice larger then the TH model (27%); according to the evanescent wave in figure (3.8(b)), 63% and 71% valid range before f_{gap} are respectively achieved by HOH1 model and HOH2 model, which are twice larger then TH model (37%). These results agree with the detailed dispersion curve depicted in figure (3.5) and (3.6). Some contrary cases exist in the propagating wave, for example $\alpha = 0.2$. The reason is not clear, but for most other cases $\alpha \in (0.3, 0.9)$, the HOH1 and HOH2 provide a more precise description about the dispersion behaviour of an infinite periodic beam.

3.5.3 Parametric study: contrast of Young's modulus

The second contrast is the Young's modulus $\beta = E_b/E_a$. In this case, the material A is still Epoxy, whilst the properties of material B change. The properties of A and B are shown in table (3.2). The relevant results are shown in figure (3.9).

According to the figure (3.9), when $\beta \to 1$, $E_a \approx E_b$, all the three homogenized models provide good approximation before the f_{gap} for propagating waves (3.9(a))and

Material	A(Epoxy)	B
Mass density (kg/m^3)	$\rho_a = 1180$	$\rho_b = 5\rho_a$
Young's Modulus (Pa)	$E_a = 4.35e9$	$E_b = \beta E_a$
Length (m)	$l_a = 1$	$l_b = l_a$

TABLE 3.2: Material properties

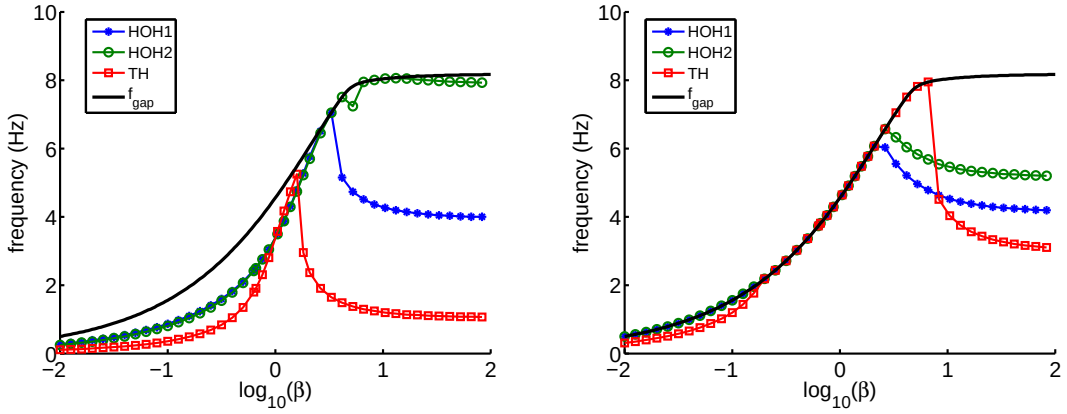

(a) real(k) valid frequency range f_{lim} (b) imag(k) valid frequency range f_{lim}

FIGURE 3.9: different homogenized models in the fraction of β

evanescent waves (3.9(b)). But for the most other cases, compared to TH model, a twice or more larger valid frequency range is acquired by the HOH1 model and HOH2 model. For different Young's modulus contrast $\beta \in (-\infty, 0.5) \cup (2, +\infty)$, the preponderance of the HOH1 and HOH2 are confirmed.

3.5.4 Parametric study: contrast of mass density

The last contrast is the mass density $\gamma = \rho_b/\rho_a$. The properties of A and B are shown in table (3.3). Similarly, the first band gap f_{gap} and the valid frequency range f_{lim} deduced by propagating waves and evanescent waves of these three different homogenized models are shown in figure (3.10).

Material	A(Epoxy)	B
Mass density (kg/m^3)	$\rho_a = 1180$	$\rho_b = \gamma\rho_a$
Young's Modulus (Pa)	$E_a = 4.35e9$	$E_b = 10E_a$
Length (m)	$l_a = 1$	$l_b = l_a$

TABLE 3.3: Material properties

From figure (3.10), it can be observed that at low contrast, i.e. $\gamma \to 1$, $\rho_a \approx \rho_b$, the dispersion curve of all the three homogenized model stay close to the benchmark before

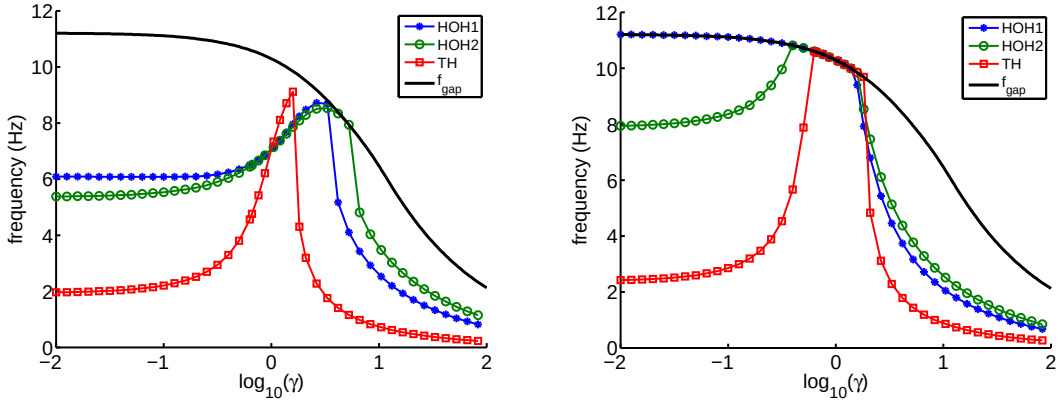

(a) real(k) valid frequency range f_{lim} (b) imag(k) valid frequency range f_{lim}

FIGURE 3.10: different homogenized models in the fraction of γ

the f_{gap}. At high contrast, a much more larger valid frequency range is always ensured by higher order models. In conclusion, for most cases $\gamma \in (-\infty, 0.5) \cup (2, +\infty)$, the HOH1 and HOH2 trun out again to be ameliorated homogenization model for infinite periodic beams.

3.6 Implementation in the finite case

The boundary condition is an essential element for the study of finite structures. In general, it performs as Dirichlet boundary condition or Neumann boundary condition. In the studied cases, in order to formulate the consistent boundary conditions, a variational approach will be applied to each model to deduce the associated boundary conditions in weak form. With these boundary conditions, the dynamic response of finite periodic structures is investigated. Then, the forced response function obtained by TH model, HOH1 model and HOH2 model are presented and compared with the numerical result obtained by WFEM.

3.6.1 Boundary conditions

In the studied cases, $U(X,t)$ is harmonic and the domain is $X \in [0, L]$. Then the associated boundary conditions of different models are as follows:

HOH1 model

The weak form of equation (3.64) reads:

$$\begin{aligned}&\int_0^L E_0 I(\frac{\partial^2 U}{\partial X^2})^2 dX - \int_0^L E_d I(\frac{\partial^3 U}{\partial X^3})^2 dX - \int_0^L \rho_0 S\omega^2 U^2 dX \\ =&-\left[(E_0 I\frac{\partial^3 U}{\partial X^3} + E_d I\frac{\partial^5 U}{\partial X^5})U\right]_0^L + \left[(E_0 I\frac{\partial^2 U}{\partial X^2} + E_d I\frac{\partial^4 U}{\partial X^4})\frac{\partial U}{\partial X}\right]_0^L \\ &-\left[E_d I\frac{\partial^3 U}{\partial X^3}\frac{\partial^2 U}{\partial X^2}\right]_0^L\end{aligned} \tag{3.69}$$

The right-hand-side of equation (3.69) exposes the format of the boundary conditions, namely:

$$\begin{aligned}&either \quad U(X) \qquad or \quad E_0 I\frac{\partial^3 U(X)}{\partial X} + E_d I\frac{\partial^5 U(X)}{\partial X^5} \\ &either \quad \frac{\partial U(X)}{\partial X} \qquad or \quad E_0 I\frac{\partial^2 U(X)}{\partial X^2} + E_d I\frac{\partial^4 U(X)}{\partial X^4} \\ &either \quad \frac{\partial^2 U(X)}{\partial X^2} \qquad or \quad E_d I\frac{\partial^3 U(X)}{\partial X^3}\end{aligned} \tag{3.70}$$

HOH2 model

The wave equation is (3.65), and the weak form reads:

$$\begin{aligned}&\int_0^L E_0 I(\frac{\partial^2 U}{\partial X^2})^2 dX - \int_0^L \frac{E_d}{E_0}\rho_0 S\omega^2(\frac{\partial U}{\partial X})^2 dX - \int_0^L \rho_0 S\omega^2 U^2 dX \\ =&\left[E_0 I\frac{\partial^2 U}{\partial X^2}\frac{\partial U}{\partial X}\right]_0^L - \left[(E_0 I\frac{\partial^3 U}{\partial X^3} + \frac{E_d}{E_0}\rho_0 S\omega^2\frac{\partial U}{\partial X})U\right]_0^L\end{aligned} \tag{3.71}$$

By analogy, the boundary conditions are:

$$\begin{aligned}&either \quad U(X) \qquad or \quad E_0 I\frac{\partial^3 U(X)}{\partial X^3} + \frac{E_d}{E_0}\rho_0 S\omega^2\frac{\partial U(X)}{\partial X} \\ &either \quad \frac{\partial U(X)}{\partial X} \qquad or \quad E_0 I\frac{\partial^2 U(X)}{\partial X^2}\end{aligned} \tag{3.72}$$

With boundary conditions being ready, the response function and affiliated resonance frequency, which characterise the dynamic comportment of finite structures, will be investigated in the following section to affirm the robustness of higher order models. For finite structures, the valid range is defined as:

For each resonance frequency f, if

$$\frac{|f_{\text{WFEM}} - f_{\text{homo}}|}{f_{\text{WFEM}}} < 1\%$$

then $f \in (0, f_{\text{lim}})$. Where f_{homo}, f_{WFEM} are the resonance frequency obtained respectively by homogenized model and WFEM method.

3.6.2 Clamped-free boundary condition

The first investigated case is depicted in figure (3.11). The left extremity of the periodic beam is clamped, while the right extremity is free. In order to obtain the dynamic response of the structure, a harmonic excitation with an amplitude of $F_0 = 100N$ is applied to the right extremity. The properties of components A and B are shown in table (3.4). The whole structure is composed of 10 unit cells, then $L = 20m$. The radius of the cross-section is $r = 0.025m$, and the area $S = \pi r^2$.

Material	A	B
Mass density (kg/m^3)	$\rho_a = 1180$	$\rho_b = 5\rho_a$
Young's Modulus (Pa)	$E_a = 4.35e9$	$E_b = 10E_a$
Length (m)	$l_a = 1$	$l_b = l_a$

TABLE 3.4: Material properties

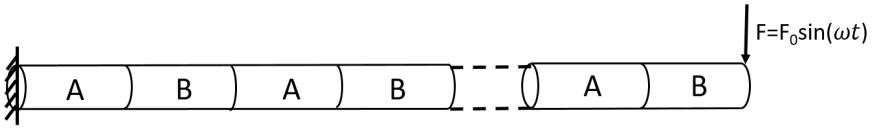

FIGURE 3.11: clamped-free periodic beam with a harmonic excitation

For TH model, the wave equation is a typical Euler-Bernoulli equation with four natural boundary conditions:

$$\begin{aligned} U(0) &= 0; & E_0 I \frac{\partial^3 U(L)}{\partial X^3} &= F \\ \frac{\partial U(0)}{\partial X} &= 0; & E_0 I \frac{\partial^2 U(L)}{\partial X^2} &= 0 \end{aligned} \tag{3.73}$$

For HOH1 model, a sixth order PDE is used to describe the structure comportment. According to (3.70), the appropriate boundary conditions are:

$$\begin{aligned} U(0) &= 0; & E_0 I \frac{\partial^3 U(L)}{\partial X} + E_d I \frac{\partial^5 U(L)}{\partial X^5} &= F \\ \frac{\partial U(0)}{\partial X} &= 0; & E_0 I \frac{\partial^2 U(L)}{\partial X^2} + E_d I \frac{\partial^4 U(L)}{\partial X^4} &= 0 \\ \frac{\partial^2 U(0)}{\partial X^2} &= 0; & E_d I \frac{\partial^3 U(L)}{\partial X^3} &= 0 \end{aligned} \tag{3.74}$$

By analogy, for HOH2 model, equation (3.72) provides the format of the affiliated boundary conditions:

$$\begin{aligned} U(0) &= 0 \qquad & E_0 I \frac{\partial^3 U(L)}{\partial X^3} + \frac{E_d}{E_0}\rho_0 S\omega^2 \frac{\partial U(L)}{\partial X} &= F \\ \frac{\partial U(0)}{\partial X} &= 0 \qquad & E_0 I \frac{\partial^2 U(L)}{\partial X^2} &= 0 \end{aligned} \tag{3.75}$$

With the corresponding boundary conditions, the displacement solution of different models can be deduced by solving associated linear equations.

A comparison of frequency response functions at excitation point ($X = L$) derived by different models is shown in figure (3.12). As the periodic structure is composed of 10 unit cells, 10 resonance frequencies appear before the first band gap. By observing the pic in the figure, it can be concluded that the TH model performs well till the 5th resonance frequency, where the relative error is 1.9%, the valid range is (0, 1.5HZ). The HOH1 and HOH2 model prove a better approximation till the 9th (or even the 10th) resonance frequency, where the relative error is 0.8% and 0.1% , and the valid range is (0, 5.8HZ).

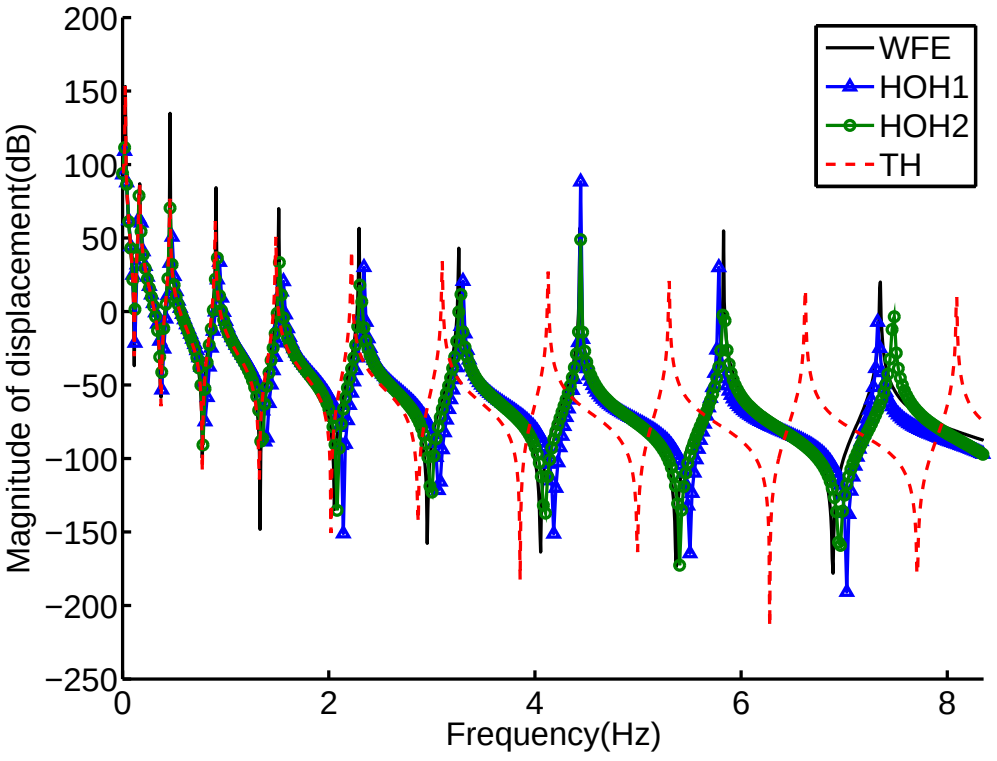

FIGURE 3.12: frequency response function at $x = L$ obtained by different models(10 unit cells)

Other cases, where the unit cell number varies, are also investigated to exhibit the robustness of these amended models. Figure (3.13) shows a result when the unit cell number is 20. In this case, 20 resonance frequencies exist before the first band gap. For clarity, only the HOH2 model is presented. It can be seen that the HOH2 model keeps the accuracy till the 18th resonance, where the relative error is 0.9%, and the valid range is (0, 6,2Hz). For the TH model, the valid frequency range is (0, 1.4HZ) and the affiliated relative error at that limit is 1.8%. For HOH1 models, the corresponding result are (0, 5,5Hz) and 1.2%. Table (3.5) presents some other results. In a word, with the augment of the unit cell number the valid range frequency varies little. HOH1 and HOH2 models provide better simulation.

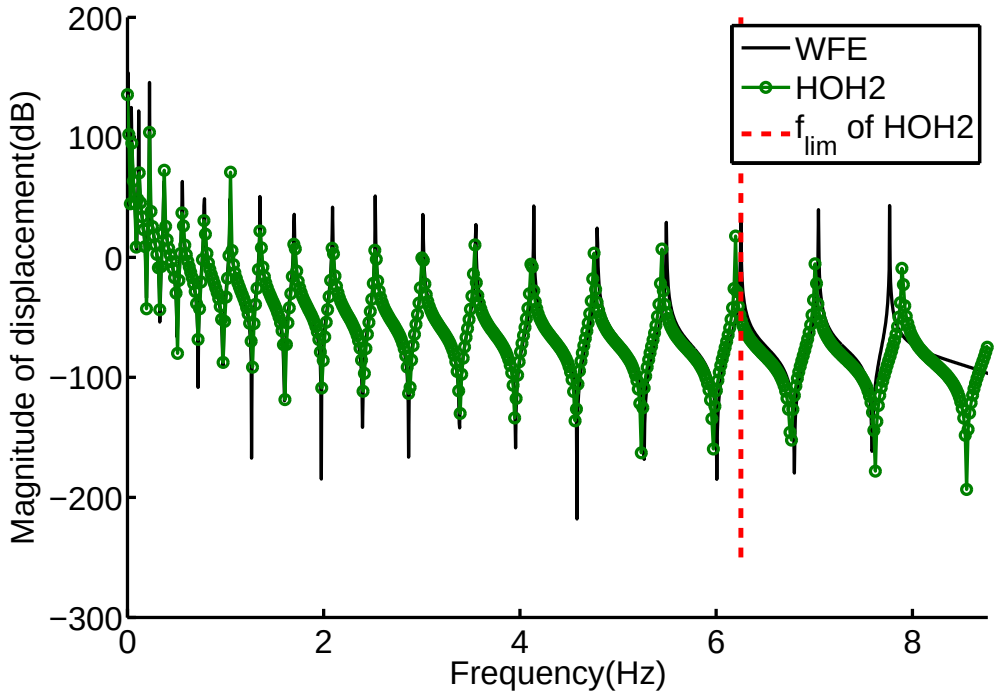

FIGURE 3.13: frequency response function at $x = L$ obtained by different models(20 unit cells)

Unit cell number	10	20	30	50
TH	1.5	1.4	1.3	1.4
HOH1	5.8	5.5	4.4	4.2
HOH2	5.8	6.2	6.4	6.2

TABLE 3.5: Valid frequency range f_{lim} (Hz) for different structure

3.6.3 Simple supported boundary condition

In this case, the structure is simple supported at the extremities, depicted in figure (3.14). The material properties remains the same as the previous section. At point $X = 7l$ (the interface between the 7th and 8th unit cell), a harmonic excitation is applied to the structure and the frequency response function at point $X = 9l$ (the interface between 9th and 10th unit cell) will be investigated.

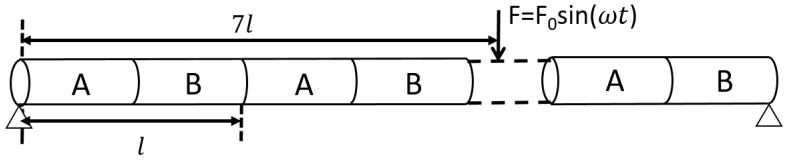

FIGURE 3.14: A simple supported periodic structure

The boundary conditions for different models are as follows:

TH model:

$$\begin{aligned} U(0) &= 0; \qquad & U(L) &= 0 \\ \frac{\partial^2 U(0)}{\partial X^2} &= 0; \qquad & \frac{\partial^2 U(L)}{\partial X^2} &= 0 \end{aligned} \tag{3.76}$$

This typical problem can be solved by mode superposition method.

HOH1 model:

$$\begin{aligned} U(0) &= 0; \qquad & U(L) &= 0 \\ E_0 I \frac{\partial^2 U(0)}{\partial X^2} + E_d I \frac{\partial^4 U(0)}{\partial X^4} &= 0; \qquad & E_0 I \frac{\partial^2 U(L)}{\partial X^2} + E_d I \frac{\partial^4 U(L)}{\partial X^4} &= 0 \\ \frac{\partial^2 U(0)}{\partial X^2} &= 0; \qquad & \frac{\partial^2 U(L)}{\partial X^2} &= 0 \end{aligned} \tag{3.77}$$

In order to obtain the displacement filed, the whole structure is considered as two parts: left side of excitation point and right side of excitation point. Then the response of the two parts can be obtained by satisfying the boundary conditions in (3.77) together with the continuity conditions (force, moment, rotation, displacement...) at point $X = 7l$. Numerical calculation is used to solve the linear equation system.

HOH2 model:

$$\begin{aligned} U(0) &= 0; \qquad & U(L) &= 0 \\ \frac{\partial^2 U(0)}{\partial X^2} &= 0; \qquad & \frac{\partial^2 U(L)}{\partial X^2} &= 0 \end{aligned} \tag{3.78}$$

Similarly, the method used in HOH1 model gives the forced response of HOH2 model.

The resonance frequencies obtained by different methods are shown in table (3.6), and the forced response function is plotted in figure(3.15). The TH model describes correctly the first six resonances. Meanwhile, the HOH1 and HOH2 model, they provide an accurate estimation of the first nine or even ten resonances. These conclusions agree with the conclusions obtained in the clamped-free case. In summary, the TH model is an underestimated model; whilst the higher order homogenized models are amended models and provide more accurate estimation.

	1st	2nd	3rd	4th	5th	6th	7th	8th	9th
WFEM	0.1	0.3	0.7	1.2	1.9	2.8	3.9	5.2	6.7
TH	0.1	0.3	0.7	1.2	1.8	2.6	3.6	4.7	5.9
HOH1	0.1	0.3	0.7	1.2	1.9	2.8	3.8	5.0	6.5
HOH2	0.1	0.3	0.7	1.2	1.9	2,8	3.8	5.1	6.6

TABLE 3.6: Resonance frequencies (Hz) obtained by different models (10 unit cells)

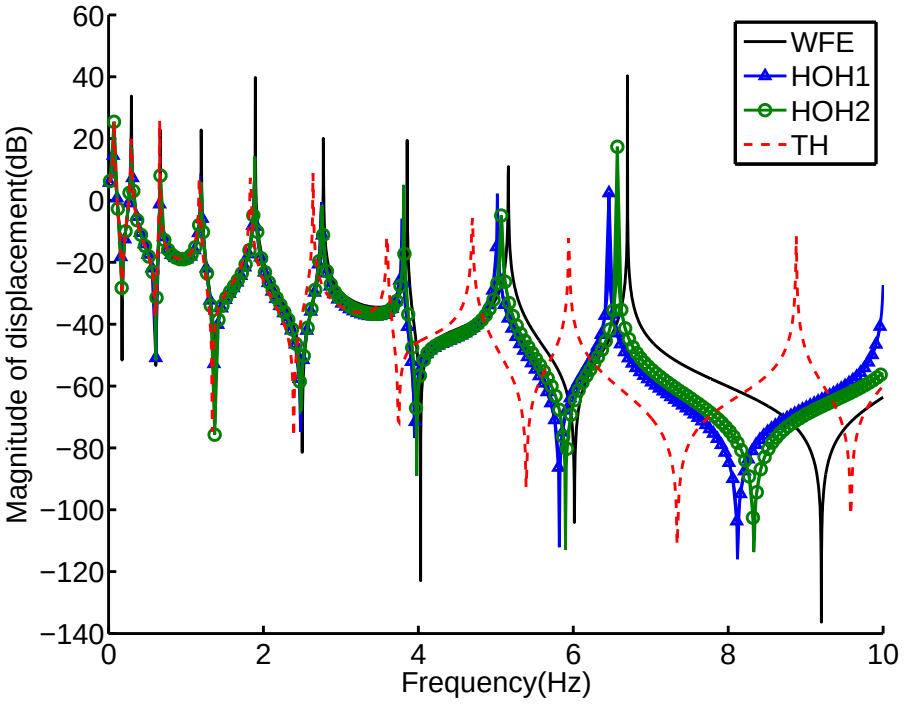

FIGURE 3.15: Frequency response function at $X = 9l$ obtained by different models (10 unit cells)

Another case where the periodic structure is composed of 20 unit cells has also been investigated. In this case, the excitation is located at $X = 14l$, and the response

function of HOH2 model and WFEM at point $X = 18l$ is illustrated in figure (3.16). It can be seen that the validity range of HOH2 model is (0, 5.9Hz). The validity range of HOH1 and TH in this case are relatively (0, 5.2Hz) and (0, 1.5Hz). All these results are accordant with these results in the clamped-free case shown in table (3.5). With the unit cell number changing, the valid domain of these models keeps almost unchanged.

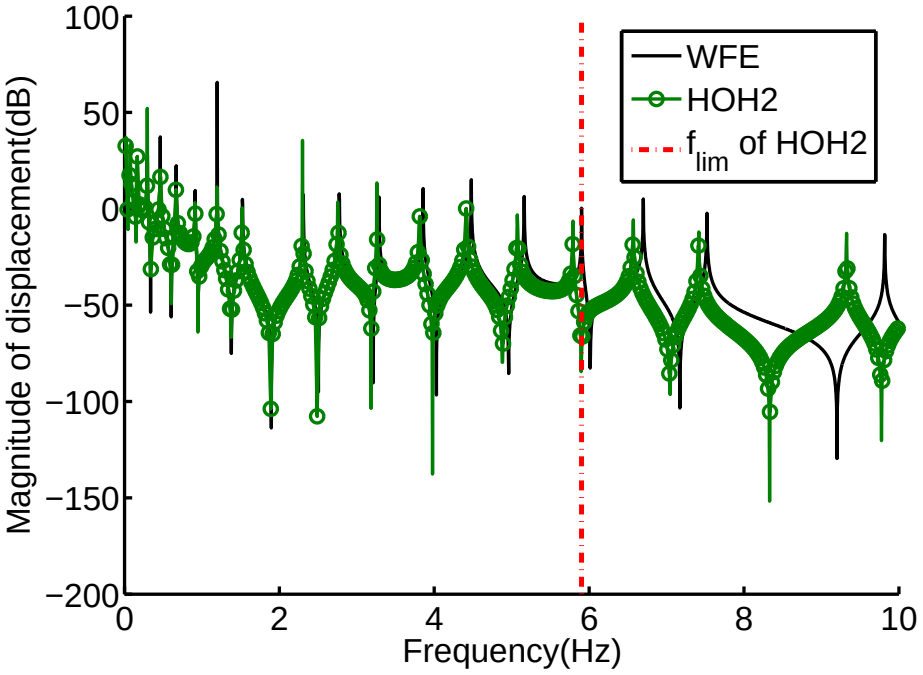

FIGURE 3.16: Frequency response function at $X = 18l$ obtained by different models (20 unit cells)

When choosing the WFEM as the benchmark method, some attentions should be paid to the structure configuration. Many different unit cell configurations can be chosen to form the infinite periodic structure depicted in (3.1). These different configurations make no difference for the study of dispersion relation. But for finite structures, different configurations lead to different finite structures, which possess different dynamic behaviour under the same boundary conditions. After homogenization, the heterogeneous periodic structure becomes kind of an uniform structure, which is of course symmetry. Thus, a symmetry configuration is a reasonable choice for the study of a finite structure.

3.7 Conclusions

In this paper, two higher order homogenization models are deduced by asymptotic expansion method to describe the free vibration and forced vibration of a periodic beam. And some detailed formulations of the two-scale asymptotic expansion method are presented. According to the homogenization theory, the wave length should be larger then the unit cell length. Thus, the considered frequency is limited to the first propagating zone. The numerical method WFEM has been chosen as the reference to validate these models, and the traditional homogenization model is also compared.

In the infinite case, the dispersion relation is investigated. The HOH1 model and the HOH2 model are more accurate models by enlarging the validity range compared to the TH model. In the finite case, the frequency response function is investigated. The higher order models turn out to be robust to the boundary conditions and unit cell number. And in all these cases, HOH2 model performs a little better than HOH1 model.

As a result, the HOH1 and HOH2 are both more accuracy models and the HOH2 is even better. In this work, the homogenization process stops at the $O(\epsilon^2)$ order, their ability to describe the finite structure's dynamic behaviour have totally exceed the traditional model. Further development may induce more accurate homogenized models. Being validated in the beam, this method may also work in more complicated structures.

Chapter 4

Homogenization of 1 dimensional framed structures

4.1 Introduction

Periodic reticulated materials and structures are widely employed in various industries, such as aeronautics (lattice beams), civil engineering (building), materials science (mechanics of foam and glass wool) and biomechanics (vegetable tissue or bones). Numerous studies aiming to find their homogenised models have been carried out [94]. The homogenization approaches lie in obtaining an analytical continuous description for the periodic structures. Several approaches have been developed: The first methods were based on the finite difference operator and used the beam theory of the resistance of material [95]. Methods based on homogenization of periodic heterogeneous media [96] with multiple parameters and scale changes were developed by Cioranescu [97] and used the continuum mechanics at the micro-scale. The homogenization method of Periodic Discrete Media (HPDM), considered in this paper, were elaborated by Caillerie *et al.* [98] and recently completed by Boutin and his co-authors [99–101].

Another category of the approaches consists in modelling directly one unit cell of the periodic structures. Thanks to the Floquet-Bloch theorem [102, 103], one can model only a unit cell to deduce the dynamics of the whole structure. Among these methods we shall focus on the numerical Wave Finite Element Method (WFEM). WFEM utilises conventional FE software packages to model the unit cell. This means that structures

with complex cell geometries or material distributions can be analysed with relative ease [104–106]. An enhanced WFEM – CWFEM for Condensed Wave Finite Element Method is proposed and employed in the work [107–109]. CWFEM adds the model order reduction which allows to compute more efficiently when the unit cell contains large number of internal nodes.

In this chapter, both analytical HPDM and numerical CWFEM are employed to study a periodic discrete framed structure. The principal objective of this chapter is to re-evaluate the validity of the HPDM using the wave characteristics identified by CWFEM. In the aforementioned studies, the validity of the HPDM were often evaluated in terms of modes (natural frequency) of finite structures [100, 101], while it is known that the response of a vibrating system can be viewed either in terms of modes or in terms of elastic wave motion [110]. Based on the wave characteristics, one can give a quick evaluation of homogenised model without considering the problem of a finite structure. Therefore the problem of unit cell number and the boundary conditions may be omitted. This consideration comes from the following 3 points: Firstly, in the first stage of design, it may be encountered that the homogenised model sought is for some periodic structures without knowing exactly the unit cell number. Secondly, the boundary condition for a real structure may be not perfectly determined. Thirdly, it might be difficult to express the boundary conditions for the equivalent homogenised equations, especially the additional boundary conditions for a higher order differential equation.

Focusing on this objective, the chapter is organized as follows: In section 4.2, the analytical method HPDM to study the longitudinal and transverse vibrations of a reticulated beam is briefly explained. Subsequently, in section 4.3, an overview of the numerical CWFEM is given. Then in section 4.4, a specified structure is studied by both HPDM and CWFEM. Finally, the concluding remarks and perspectives are presented in section 4.5.

4.2 Implementation of HPDM on one-dimensionnal framed structures

The analytical formulations of HPDM to study the longitudinal [101] and transverse [100] vibrations are explained in this section.

4.2.1 Studied structures and kinematic descriptors

The studied structures are composed by a pile of a large number of unbraced identical frames called unit cells. Each cell is made of a floor supported by two walls (see Fig. 4.1). The walls and the floors are beams or plates which behave as Euler-Bernoulli beams. They are linked by perfectly stiff and massless nodes. The characteristics of the floors ($j = f$) and the walls ($j = w$) are: l_j length, a_j in-plane thickness, h depth in the out-of-plane direction, $A_j = a_j h$ cross-section area, $I_j = a_j^3 h/12$ the in-plane bending cross-section inertia, ρ_j density, E_j elastic modulus. The HPDM begins with the discrete nodal force and momentum balance. The study of the momentum balance of the whole structure is represented by the study of the momentum balance of the nodes. The motions of the nodes can be used as kinematic descriptors of the motions of the structure. Fig. 4.1 shows that each level n contains two nodes: n_1 on the left and n_2 on the right. Their motion in the plane $(\mathbf{e_x}, \mathbf{e_y})$ is described by three kinematic variables: v_{n_j} for the displacement in direction $\mathbf{e_x}$ and u_{n_j} for the displacement in direction $\mathbf{e_y}$ and θ_{n_j} for the rotation with $j = 1$ or 2.

Because of the longitudinal symmetry of the structure, it is possible to uncouple the transverse (anti-symmetric) and longitudinal (symmetric) kinematics thanks to the change of variable. Six variables describing the motions of the two nodes of the level n can be found. Among which three variables are associated to the rigid motion and three correspond to the deformation.

• three variables for the rigid body motion of the level n

$$U_n = \frac{u_{n_1} + u_{n_2}}{2} \qquad \text{mean transverse displacement} \tag{4.1a}$$

$$V_n = \frac{v_{n_1} + v_{n_2}}{2} \qquad \text{mean longitudinal displacement} \tag{4.1b}$$

$$\alpha_n = \frac{v_{n_1} - v_{n_2}}{l_f} \qquad \text{global rotation} \tag{4.1c}$$

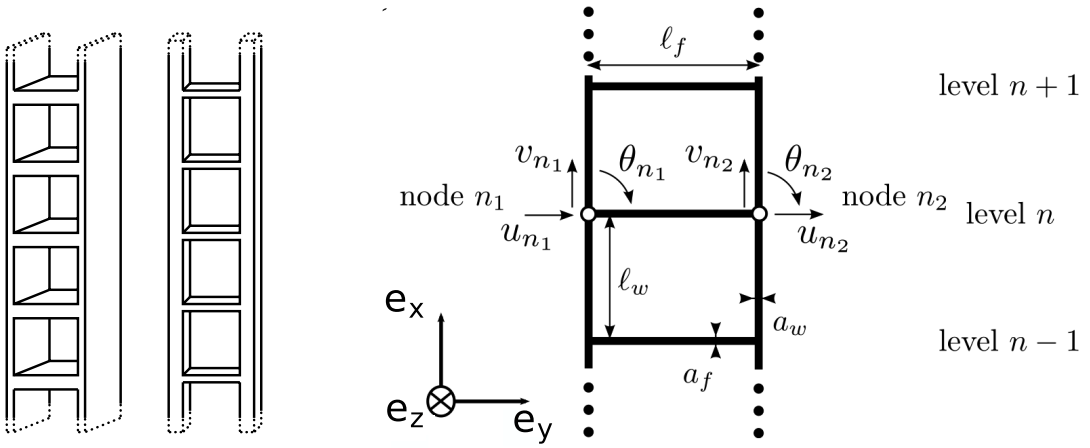

(a) An example (b) Notations

FIGURE 4.1: Schema of the studied structures [101]

• three variables for the deformation of the level n

$$\theta_n = \frac{\theta_{n_1} + \theta_{n_2}}{2} \qquad \text{mean rotation of the nodes} \tag{4.2a}$$

$$\Phi_n = \theta_{n_2} - \theta_{n_1} \qquad \text{differential rotation of the nodes} \tag{4.2b}$$

$$\Delta_n = u_{n_2} - u_{n_1} \qquad \text{transverse dilatation} \tag{4.2c}$$

Then the discrete description is transformed into a continuous beam description. The kinematic descriptors are considered as the discrete values of continuous functions of the space variable x. For example for the mean longitudinal displacement, we have $V(x = x_n) = V_n$. The key assumption of HPDM is that the cell size in the direction of the periodicity l_w is small compared to the characteristic size L of the vibration of the structure. When the scale ratio $\epsilon = l_w/L$ approaches to zero, all the continuous functions can be expanded in the power of ϵ, such as follows:

$$V_\epsilon(x) = V^0(x) + \epsilon V^1(x) + \epsilon^2 V^2(x) + ... \tag{4.3}$$

4.2.2 The analytical continuous formulation for studied discrete framed structure

Based on the asymptotic expansion, HPDM determines equivalent continuous equations on different orders of ϵ. The method is described briefly as follows, while the details of the development can be found in the appendix of [100] and [101]. The method is summed up in two steps: discretization and homogenization. The discretization step starts with the local balance of each beam element. The forces/moments at the endpoints are expressed by the displacement/rotation at these points. The balance equations with discreted variables defined in Eqs.(4.1) - (4.2) are then derived from the nodal force balance equations. The homogenization step switches discreted description to continuous description by considering the discrete dynamic variables at each node as specific values of a continuous function. Since the scale ratio is small enough, the variation in variables between neighbouring nodes is expressible using Taylor's Series. This in turn leads to the macroscopic derivatives. With all these dynamic variables developed in Taylor's Series with respect to the scale ratio, a sequence of balance equation at various orders can be derived by nodal balance equation.

The element local balance has been verified in the Introduction, the nodal balance in this case is in the following form:
for node n_1, the nodal balance in directions x, y, z are respectively:

$$N^E_{wn1}(v_{(n-1)1}, v_{n1}) - N^B_{w(n+1)1}(v_{n1}, v_{(n+1)1}) + T^B_{fn}(v_{n1}, v_{n2}, \theta_{n1}, \theta_{n2}) = 0 \tag{4.4a}$$

$$T^E_{wn1}(u_{(n-1)1}, u_{n1}, \theta_{(n-1)1}, \theta_{n1}) - T^B_{w(n+1)1}(u_{n1}, u_{(n+1)1}, \theta_{n1}, \theta_{(n+1)1}) - N^B_{fn}(u_{n1}, u_{n2}) = 0 \tag{4.4b}$$

$$\begin{aligned} &M^E_{wn1}(u_{n1}, u_{(n+1)1}, \theta_{n1}, \theta_{(n+1)1}) - M^B_{w(n+1)1}(u_{n1}, u_{(n+1)1}, \theta_{n1}, \theta_{(n+1)1}) \\ &- M^B_{fn}(v_{n1}, v_{n2}, \theta_{n1}, \theta_{n2}) = 0 \end{aligned} \tag{4.4c}$$

for node n_2, the nodal balance in directions x, y, z are respectively:

$$N^E_{wn2}(v_{(n-1)2}, v_{n2}) - N^B_{w(n+1)2}(v_{n2}, v_{(n+1)2}) - T^E_{fn}(v_{n1}, v_{n2}, \theta_{n1}, \theta_{n2}) = 0 \tag{4.5a}$$

$$T^E_{wn2}(u_{(n-1)2}, u_{n2}, \theta_{(n-1)2}, \theta_{n2}) - T^B_{w(n+1)2}(u_{n2}, u_{(n+1)2}, \theta_{n2}, \theta_{(n+1)2}) + N^E_{fn}(u_{n1}, u_{n2}) = 0 \tag{4.5b}$$

$$M^E_{wn2}(u_{n2}, u_{(n+1)2}, \theta_{n2}, \theta_{(n+1)2}) - M^B_{w(n+1)2}(u_{n2}, u_{(n+1)2}, \theta_{n2}, \theta_{(n+1)2}) + M^E_{fn}(v_{n1}, v_{n2}, \theta_{n1}, \theta_{n2}) = 0 \tag{4.5c}$$

Then the equation system for longitudinal vibration (4.6) and transversal vibration (4.7) are obtained by these nodal balance equations:

$$\begin{cases} (4.5a) + (4.4a) \\ (4.5b) - (4.4b) \\ (4.5c) - (4.4c) \end{cases} \tag{4.6}$$

$$\begin{cases} (4.5a) - (4.4a) \\ (4.5b) + (4.4b) \\ (4.5c) + (4.4c) \end{cases} \tag{4.7}$$

For the structures studied in this chapter, the scaling for both the longitudinal and transverse vibrations is as follow:

$$\frac{E_f}{E_w} = O(1); \quad \frac{\rho_f}{\rho_w} = O(1); \quad \frac{l_f}{l_w} = O(1) \tag{4.8}$$

For the longitudinal vibration without internal resonance, the equivalent formulation determined by Chesnais *et al.* using HPDM is given as [101] :

$$\Lambda\omega^2 V + 2E_w A_w V'' = 0 \tag{4.9}$$

As for transverse vibration, the formulation for the generic model deduced by Hans and Boutin [100] is as follow:

$$\frac{2E_w^2 I_w I}{K} U'''''' - (2E_w I_w + E_w I) U'''' - \frac{E_w I}{K} \Lambda\omega^2 U'' + \Lambda\omega^2 U = 0 \tag{4.10}$$

The macroscopic parameters in Eqs. (4.9) and (4.10) are:

- The linear mass of the cell $\Lambda = 2\rho_w A_w + \rho_f A_f l_f / l_w$.
- The bending stiffnesses of the two walls. Inner bending: $2E_w I_w$. Global bending: $E_w I = E_w A_w l_f^2/2$.
- The shear stiffnesses of the cell $K^{-1} = K_w^{-1} + K_f^{-1}$, with $K_w = 24E_w I_w/l_w^2$, $K_f = 12E_f I_f/(l_w l_f)$;

$I_i = a_i^3 h/12$ is the moment of inertia, with $i = f$ for the floor and $i = w$ for the walls. With these analytical formulations, the dispersion relation can be easily deduced when supposing the harmonic vibration $V(x,t) = V\exp(j\omega t - kx)$.

4.2.3 Boundary condition equations

The generic model of the transverse vibration involves all three kinematic variables in Eq. (4.1): U, α, θ. The behaviour laws are defined as follows:

$$\begin{cases} \text{shear force} & T = -K(U' + \alpha) \\ \text{bending moment} & M = E_w I \alpha' \\ \text{inner moment} & \mathscr{M} = 2E_w I_w U'' \end{cases} \tag{4.11}$$

The force and moment balance equations, associated with the inner kinematic of the section are:

$$(T + \mathscr{M}')' = \Lambda\omega^2 U, \quad M' = -T, \quad K_w(U' + \theta) + K_f(\theta - \alpha) = 0 \tag{4.12}$$

The weak formulation of 1st equation in Eq. (4.12) gives:

$$\underbrace{\int_0^H \Lambda\omega^2 U^2 dx}_{\text{kinetic energy}} = \underbrace{\int_0^H (\frac{T^2}{K} + \frac{M^2}{E_w I} + \frac{\mathscr{M}^2}{2E_w I_w})dx}_{\text{Elastic energy}} + \underbrace{[(T + \mathscr{M}')U]_0^H - [M\alpha]_0^H - [\mathscr{M}U']_0^H}_{\text{Work of boundary conditions}} \tag{4.13}$$

This equation presents the equality of the kinetic energy with the elastic energy and the energy provided at the boundaries. The last three terms correspond to the work of the boundary, which can define appropriate boundary conditions. The boundary conditions for clamped, free and simply-supported side are listed in Tab. 4.1. Using Eqs. (4.11) and (4.12), one can deduce boundary conditions on U to solve its differential equation in Eq. (4.10), which are given in C.

TABLE 4.1: Equations for different boundary conditions

	Clamped	Free	Simply-supported
$(T+\mathscr{M}')U$	$U=0$	$T+\mathscr{M}'=0$	$U=0$
$M\alpha$	$\alpha=0$	$M=0$	$M=0$
$\mathscr{M}U'$	$U'=0$	$\mathscr{M}=0$	$\mathscr{M}=0$

4.3 Overview of the numerical condensed wave finite element method

The outline of the numerical CWFEM is given hereafter. For a more detailed formulation, the reader is referred to [107]. Since the framed structure is periodic, one can obtain the whole framed structure (Fig. 4.2(c)) only by repeating a single unit cell (Fig. 4.2(a)) in the propagation direction. Coordinates $\mathbf{q}_{\mathtt{R}}$, $\mathbf{q}_{\mathtt{L}}$, $\mathbf{q}_{\mathtt{I}}$ represent the physical DOFs of the left boundary, right boundary and internal nodes, as shown in Fig 4.2(a). However the choice of the unit cell can be various, the unit cell in Fig. 4.2(a) is used which minimizes the number of coupling co-ordinates, so as to decrease the computational cost.

4.3.1 Modelling of the unit cell

The method begins with establishing the equation of motion of the unit cell for free vibration. The mass and stiffness matrices $\mathbf{M}$ and $\mathbf{K}$ can be extracted from conventional FE packages.

$$\tilde{\mathbf{M}}\begin{pmatrix}\ddot{\mathbf{q}}_{\mathtt{L}}\\ \ddot{\mathbf{q}}_{\mathtt{R}}\\ \ddot{\mathbf{q}}_{\mathtt{I}}\end{pmatrix}+\tilde{\mathbf{K}}\begin{pmatrix}\mathbf{q}_{\mathtt{L}}\\ \mathbf{q}_{\mathtt{R}}\\ \mathbf{q}_{\mathtt{I}}\end{pmatrix}=\begin{pmatrix}\tilde{\mathbf{F}}_{\mathtt{L}}\\ \tilde{\mathbf{F}}_{\mathtt{R}}\\ \mathbf{0}\end{pmatrix} \tag{4.14}$$

The Craig-Bampton method, known as fixed interface component mode synthesis, is applied to carry out the model order reduction on the unit cell. The physical DOFs $\mathbf{q}_{\mathtt{I}}$ are then reformulated to a reduced modal basis of modal DOFs, with generalized coordinate $\mathbf{P}_{\mathtt{C}}$. We have

$$\begin{pmatrix}\mathbf{q}_{\mathtt{L}}\\ \mathbf{q}_{\mathtt{R}}\\ \mathbf{q}_{\mathtt{I}}\end{pmatrix}=\begin{bmatrix}\mathbf{I_n} & \mathbf{0} & \mathbf{0}\\ \mathbf{0} & \mathbf{I_n} & \mathbf{0}\\ \mathbf{\Psi}_{\mathtt{L}} & \mathbf{\Psi}_{\mathtt{R}} & \mathbf{\Psi}_{\mathtt{C}}\end{bmatrix}\begin{pmatrix}\mathbf{q}_{\mathtt{L}}\\ \mathbf{q}_{\mathtt{R}}\\ \mathbf{P}_{\mathtt{C}}\end{pmatrix}=\mathbf{B}\begin{pmatrix}\mathbf{q}_{\mathtt{L}}\\ \mathbf{q}_{\mathtt{R}}\\ \mathbf{P}_{\mathtt{C}}\end{pmatrix} \tag{4.15}$$

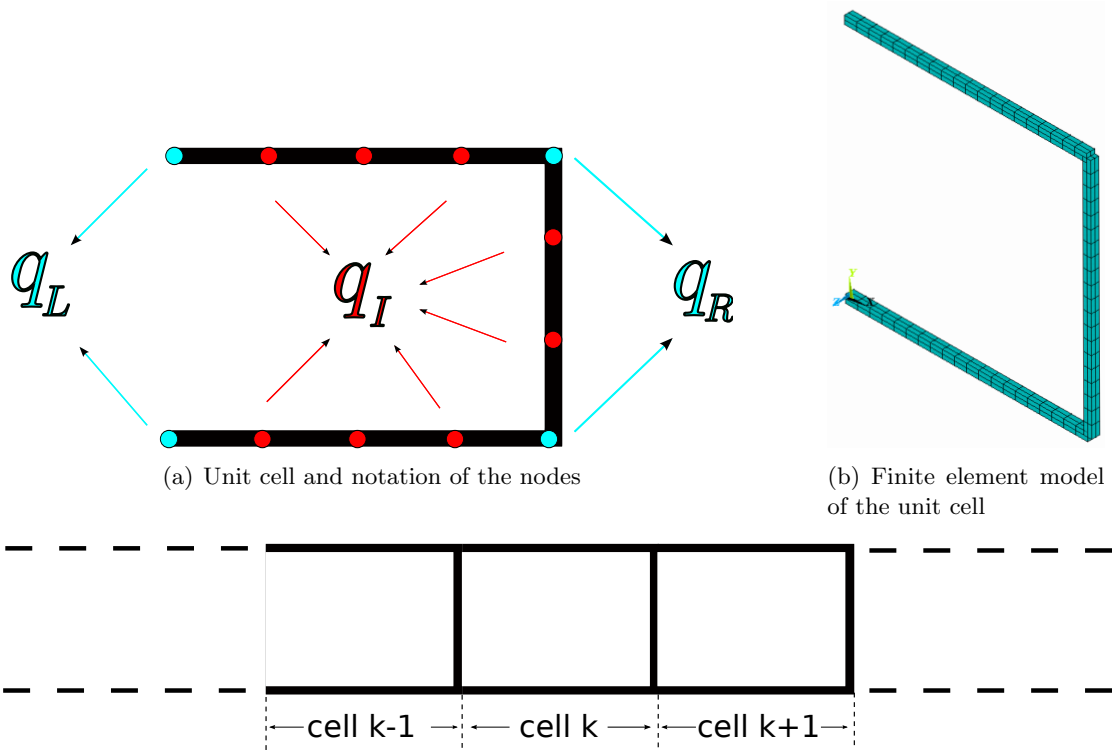

(a) Unit cell and notation of the nodes

(b) Finite element model of the unit cell

(c) An infinite framed structure

FIGURE 4.2: Framded structures and its unit cell in CWFEM

with $[\boldsymbol{\Psi}_{\mathtt{L}} \quad \boldsymbol{\Psi}_{\mathtt{R}}]$ representing the constraint modes of the boundary. Matrix $\boldsymbol{\Psi}_{\mathtt{C}}$ is a set of truncated modes in $\boldsymbol{\Psi}_{\mathtt{I}}$, which are the fixed interface modes of the unit cell obtained with $\mathbf{q}_{\mathtt{L}} = \mathbf{q}_{\mathtt{R}} = \mathbf{0}$. Among $\boldsymbol{\Psi}_{\mathtt{I}}$, it is suggested to retain in $\boldsymbol{\Psi}_{\mathtt{C}}$ at least the modes under 3 times maximum investigated frequency [107]. Then the equation of motion of the reduced model can be written into the following form:

$$\mathbf{M}^* \begin{pmatrix} \ddot{\mathbf{q}}_{\mathtt{L}} \\ \ddot{\mathbf{q}}_{\mathtt{R}} \\ \ddot{\mathbf{P}}_{\mathtt{C}} \end{pmatrix} + \mathbf{K}^* \begin{pmatrix} \mathbf{q}_{\mathtt{L}} \\ \mathbf{q}_{\mathtt{R}} \\ \mathbf{P}_{\mathtt{C}} \end{pmatrix} = \begin{pmatrix} \mathbf{F}_{\mathtt{L}} \\ \mathbf{F}_{\mathtt{R}} \\ \mathbf{0} \end{pmatrix} \tag{4.16}$$

The new mass matrix as well as the stiffness matrix can then be written in the following manner:

$$\mathbf{M}^* = \mathbf{B}^{\mathtt{T}}\tilde{\mathbf{M}}\mathbf{B} \tag{4.17}$$

The generalized force remains the same value as before:

$$\begin{pmatrix} \mathbf{F}_{\mathtt{L}} \\ \mathbf{F}_{\mathtt{R}} \\ \mathbf{0} \end{pmatrix} = \mathbf{B}^{\mathtt{T}} \begin{pmatrix} \tilde{\mathbf{F}}_{\mathtt{L}} \\ \tilde{\mathbf{F}}_{\mathtt{R}} \\ \mathbf{0} \end{pmatrix} = \begin{pmatrix} \tilde{\mathbf{F}}_{\mathtt{L}} \\ \tilde{\mathbf{F}}_{\mathtt{R}} \\ \mathbf{0} \end{pmatrix} \tag{4.18}$$

Assuming harmonic response, the equation can be written with the dynamic stiffness matrix $\mathbf{D}^* = \mathbf{K}^* - \omega^2\mathbf{M}^*$

$$\begin{bmatrix} \mathbf{D}^*_{\mathtt{LL}} & \mathbf{D}^*_{\mathtt{LR}} & \mathbf{D}^*_{\mathtt{LC}} \\ \mathbf{D}^*_{\mathtt{RL}} & \mathbf{D}^*_{\mathtt{RR}} & \mathbf{D}^*_{\mathtt{RC}} \\ \mathbf{D}^*_{\mathtt{CL}} & \mathbf{D}^*_{\mathtt{CR}} & \mathbf{D}^*_{\mathtt{CC}} \end{bmatrix} \begin{pmatrix} \mathbf{q}_{\mathtt{L}} \\ \mathbf{q}_{\mathtt{R}} \\ \mathbf{P}_{\mathtt{C}} \end{pmatrix} = \begin{pmatrix} \mathbf{F}_{\mathtt{L}} \\ \mathbf{F}_{\mathtt{R}} \\ \mathbf{0} \end{pmatrix} \tag{4.19}$$

From the third line of Eq. (4.19), internal DOFs can be removed using dynamic condensation. The Eq. (4.19) becomes

$$\begin{bmatrix} \mathbf{D}_{\mathtt{LL}} & \mathbf{D}_{\mathtt{LR}} \\ \mathbf{D}_{\mathtt{RL}} & \mathbf{D}_{\mathtt{RR}} \end{bmatrix} \begin{pmatrix} \mathbf{q}_{\mathtt{L}} \\ \mathbf{q}_{\mathtt{R}} \end{pmatrix} = \begin{pmatrix} \mathbf{F}_{\mathtt{L}} \\ \mathbf{F}_{\mathtt{R}} \end{pmatrix} \tag{4.20}$$

where

$$\mathbf{D}_{\alpha\beta} = \mathbf{D}^*_{\alpha\alpha} - \mathbf{D}^*_{\alpha\mathtt{C}}(\mathbf{D}^*_{\mathtt{CC}})^{-1}\mathbf{D}^*_{\mathtt{C}\beta} \quad \alpha, \beta \in \{\mathbf{L}, \mathbf{R}\} \tag{4.21}$$

$\mathbf{D}^*_{\mathtt{CC}}$ is a diagonal matrix and of smaller size than $\mathbf{D}^*_{\mathtt{II}}$. $\mathbf{D}^*_{\mathtt{CC}}$ is much easier to be inverted and the poor conditioned problem can be avoided.

4.3.2 The spectral problem on the reduced model of the unit cell

For the unit cell $\mathtt{k}$, Eq. (4.20) can be reformed into

$$\mathbf{u}^{(\mathtt{k})}_{\mathtt{R}} = \mathbf{S}\mathbf{u}^{(\mathtt{k})}_{\mathtt{L}}, \tag{4.22}$$

where $\mathbf{u}^{(\mathtt{k})}_{\mathtt{L}} = ((\mathbf{q}^{(\mathtt{k})}_{\mathtt{L}})^{\mathtt{T}}(-\mathbf{F}^{(\mathtt{k})}_{\mathtt{L}})^{\mathtt{T}})^{\mathtt{T}}$ and $\mathbf{u}^{(\mathtt{k})}_{\mathtt{R}} = ((\mathbf{q}^{(\mathtt{k})}_{\mathtt{R}})^{\mathtt{T}}(\mathbf{F}^{(\mathtt{k})}_{\mathtt{R}})^{\mathtt{T}})^{\mathtt{T}}$ represent the left and right state vectors for the unit cell $\mathtt{k}$. The wave basis and wavenumbers are associated to the

eigen solution of the following problem:

$$\mathbf{S}\mathbf{\Phi}_i = \gamma_i \mathbf{\Phi}_i \quad , \quad |\mathbf{S} - \gamma_i \mathbf{I}| = \mathbf{0}. \tag{4.23}$$

where $\mathbf{I}$ represents the identity matrix. However, matrix $\mathbf{S}$ is often ill conditioned, the eigenvalue problem in Eq. (4.23) is often reformulated as follows:

$$[\mathbf{N}]\mathbf{\Phi}' = \gamma[\mathbf{L}]\mathbf{\Phi}', \tag{4.24}$$

where

$$\mathbf{\Phi}' = \begin{pmatrix} \mathbf{q}_{\mathrm{L}} \\ \mathbf{q}_{\mathrm{R}} \end{pmatrix} \tag{4.25}$$

and

$$[\mathbf{N}] = \begin{bmatrix} \mathbf{0} & \mathbf{I_n} \\ \mathbf{D}_{\mathrm{RL}} & \mathbf{D}_{\mathrm{RR}} \end{bmatrix} \quad , [\mathbf{L}] = \begin{bmatrix} \mathbf{I_n} & \mathbf{0} \\ -\mathbf{D}_{\mathrm{LL}} & -\mathbf{D}_{\mathrm{LR}} \end{bmatrix} \tag{4.26}$$

For the state vector $\mathbf{\Phi}$, it is related using matrix $\mathbf{L}$.

$$\mathbf{\Phi} = \begin{pmatrix} \mathbf{q}_{\mathrm{L}} \\ -\mathbf{F}_{\mathrm{L}} \end{pmatrix} = \mathbf{L} \begin{pmatrix} \mathbf{q}_{\mathrm{L}} \\ \mathbf{q}_{\mathrm{R}} \end{pmatrix} = \mathbf{L}\mathbf{\Phi}' \tag{4.27}$$

The eigenvalues γ_i and wavenumbers k_i are linked through the relation $\gamma_i = e^{-jk_i l_w}$, while l_w denotes the length of the unit cell in propagation direction and $j^2 = -1$. The waves are then classified according to their propagation direction and their attenuation so as to proceed the forced response calculation. For the formulations of the Forced-CWFEM the reader can refer to [105, 107, 111] for the details.

4.4 Framed structures by the numerical and analytical approaches

The same structure is studied as in [100]. The characteristics of the structure are listed in Tab. 4.2. Free vibration of the infinite structure is investigated firstly in this section, a finite structure with a fixed number of unit cells is studied afterwards. To ensure the convergence of the mesh, the two walls and the floor are both discretized into 20 finite elements. Each unit cell contains 183 DOFs, among which 171 are internal

TABLE 4.2: Characteristics of the studied structure

l_w (m)	l_f (m)	a_w (m)	a_f (m)	ρ (kg m^{-3})	E (GPa)	μ
3	3	0.1	0.1	7600	200	0.3

DOFs. In the CWFEM, the first 20 fixed interface modes are conserved in $\mathbf{\Psi}_\mathrm{C}$. So instead of inverting a non-diagonal matrix of 171×171 at each frequency, a diagonal matrix of 20 × 20 is inverted in the dynamic condensation (Eq. (4.21)), which improves the computation efficiency. The thickness of the walls a_w and the floor a_f is smaller compared to their lengths l_w and l_f, the beam model is therefore employed in the simulation. In our simulation, the out-of-plane DOFs are blocked so as to study only the in-plane waves.

4.4.1 Free vibration in an infinite structure

The dispersion relation of an infinite structure is given in Fig. 4.3. Here only the propagative waves in x positive direction are illustrated. Up to 20 Hz, 3 types of wave are identified. Their shapes are given in Fig. 4.4.

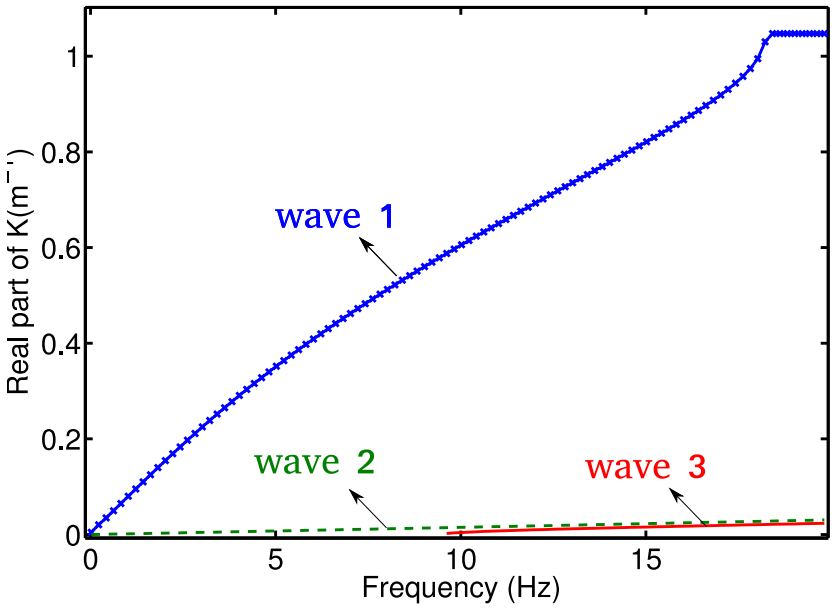

FIGURE 4.3: The dispersion relation from 0-20 Hz

It can be seen from its wave shape that wave 1 (Fig. 4.4(a)) corresponds to the transverse vibration. Due to the periodicity of the structure, Bragg type [112] stop band appears at around 18 Hz. As for the wave 2 (Fig. 4.4(b)), it corresponds to the

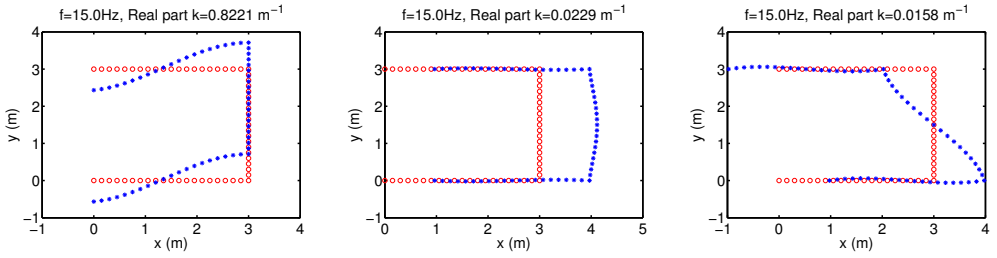

(a) Wave 1 (b) Wave 2 (c) Wave 3

FIGURE 4.4: Wave shapes (∗) Undeformed unit cell (o)

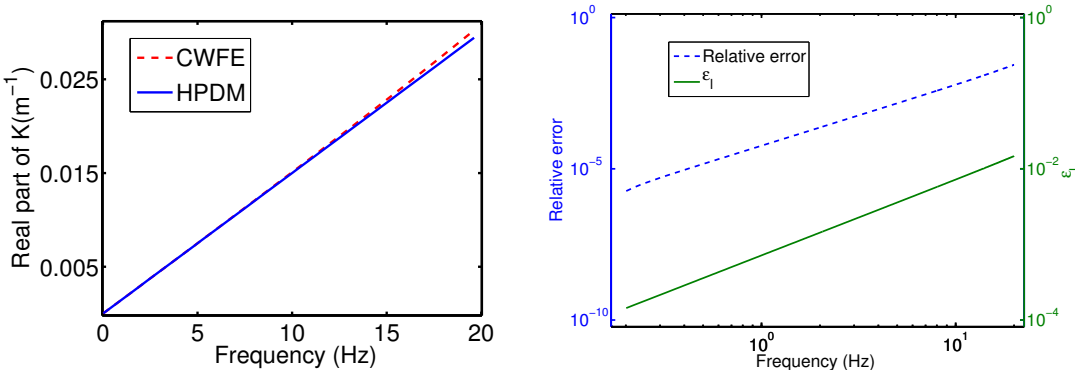

(a) The dispersion relation

(b) Relative error and scale ratio in the function of frequency

FIGURE 4.5: Dispersion relation by CWFEM and HPDM for wave 2

traction-compression motion in the propagation direction. Another type of longitudinal wave cuts on around 10 Hz. Its wave shape is given in Fig. 4.4(c). Contrary to the wave shape 2 with small deformation of the floor, in wave 3, the deformation of the floor is larger and the two walls move in opposite directions in x axis. Wave 3 corresponds to the atypical gyration modes studied in [113]. It is evanescent at 0 Hz and becomes propagative at around 10 Hz.

4.4.1.1 For longitudinal vibration (wave 2)

The longitudinal wave studied corresponds to the wave which propagates from 0 Hz, i.e. wave 2. The dispersion relation determined by HPDM and by CWFEM is illustrated in Fig. 4.5(a). In Fig. 4.5(b), the relative error between the wavenumbers k_{HPDM} and k_{CWFEM} is given with y-axis labelling on the left. The scale ratio ϵ_l in the function of frequency is also included in this figure with y-axis labelling on the right. It should be noted that both curves are plotted with a logarithmic scale for x-axis and y-axis.

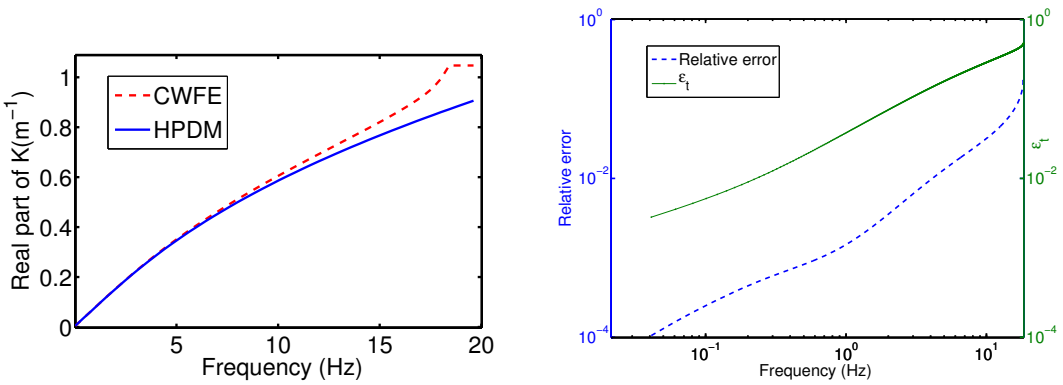

(a) The dispersion relation

(b) Relative error and scale ratio in the function of frequency

FIGURE 4.6: Dispersion relation by CWFEM and HPDM for wave 1

The scale ratio ϵ_l for an infinite periodic structure is defined as $\epsilon_l = l_w/\lambda_l$, with λ_l the wavelength of wave 2. In addition, the wavelength can be determined using the relation $\lambda_l = 2\pi/k_{\text{CWFEM}}$. At 20 Hz ($\epsilon_l = 0.015$), HPDM determines quite well the wavenumber with only a relative error of 2.5%.

4.4.1.2 For transverse vibration (wave 1)

Here we focus on the transverse vibration of the structure. It corresponds to the wave 1 identified previously. The dispersion relations determined by the two methods are given in Fig. 4.6(a). Good correlation is obtained between k_{HPDM} and k_{CWFEM} until 10 Hz. And they differ largely when we approach the stop band around 18 Hz since this homogenised model is developed considering the situations without internal resonance. In a similar way to longitudinal wave, the relative error between k_{HPDM} and k_{CWFEM} as well as the scale ratio ϵ_t are given in Fig. 4.6(b). It can be seen that up to 20 Hz, ϵ_t varies between 10^{-3} and 0.5, while a relative error around 0.5% is obtained for $\epsilon_t = 0.1$.

4.4.2 Parametric study on dispersion relations with respect to the thickness

A parametric study on the dispersion relation with respect to the thickness a_w (a_f) of the wall (floor) is given here. The model studied before is referred as model 1, with the thickness $a_w = a_f = 0.1$ m. For model 2, we have $a_w = a_f = 0.05$ m and for model

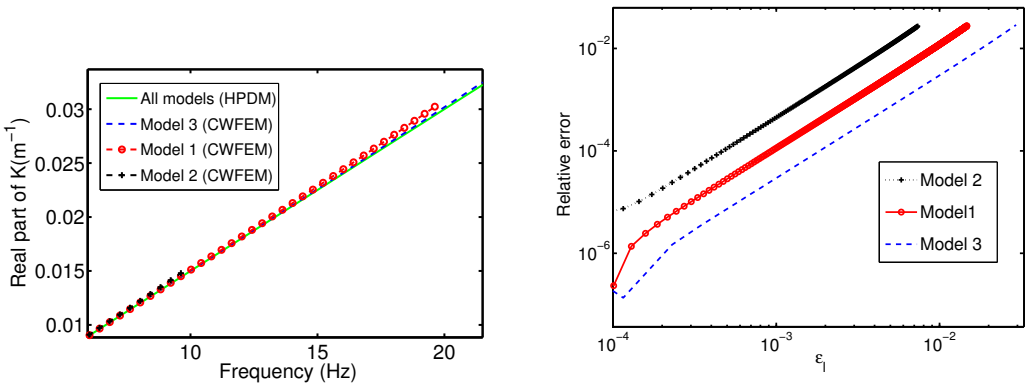

(a) The dispersion relation

(b) Relative error between k_{HPDM} and k_{CWFEM} in the function of scale ratio

FIGURE 4.7: Wave 2 (longitudinal wave) for the three models

3, $a_w = a_f = 0.2$ m. Other parameters such as the length of the wall (floor) and the material properties remain the same as model 1.

The dispersion relation as well as the relative error of k_{HPDM} in the function of scale ratio are given for the different models. For the longitudinal wave (Fig. 4.7), HPDM determines the same dispersion relation for all the three models since it predicts a non-dispersive behaviour for longitudinal wave. When the thickness of the wall and the floor are multiplied by 1/2 (for model 2) or 2 (for model 3), the equivalent mass are multiple by 1/2 or 2, so as the equivalent stiffness. The relative error in the function of scale ratio is plotted in Fig. 4.7(b), which shows that the relative errors decrease when the thickness increase. It can be explained as follows: the thicker the wall (floor) is, the more the studied framed structure approaches a homogeneous rod. As for the homogeneous rod, the homogenized non-dispersive model by HPDM is indeed the precise solution.

As for the transverse wave (Fig. 4.8), the stiffness per unit mass increases with the thickness. Hence the frequency range before the 1st stop band increases with the thickness. The relative errors for different models converge when ϵ_t exceeds 10^{-1}.

4.4.3 Free and forced transverse vibration in a finite structure

In this section, the transverse vibration of a finite structure will be investigated. The natural frequencies of free vibration are calculated firstly. Then the forced response is studied by the analytical HPDM as well as the numerical FEM and CWFEM.

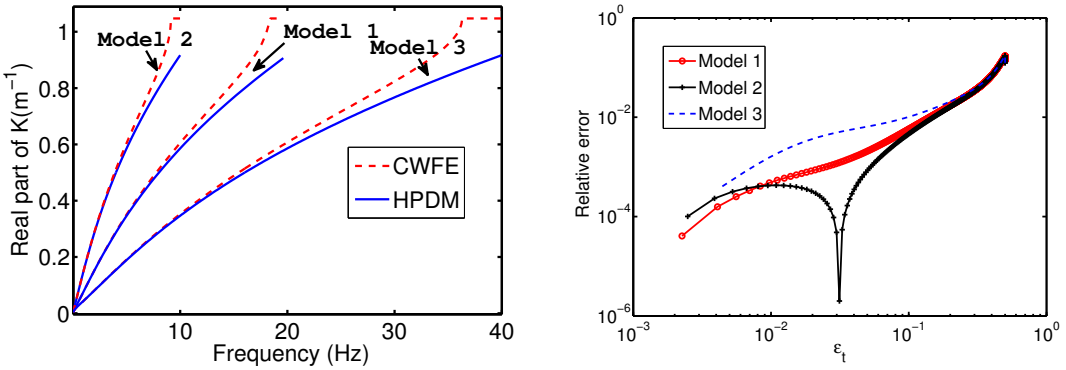

(a) The dispersion relation

(b) Relative error between k_{HPDM} and k_{CWFEM} in the function of scale ratio

FIGURE 4.8: Wave 1 (transverse wave) for the three models

TABLE 4.3: The natural frequencies (Hz) under clamped-free boundary condition

	1st mode	2nd mode	3rd mode	4th mode
Hans [100]	0.70	2.12	3.76	5.57
HPDM	0.70	2.15	3.76	5.56
FEM	0.68	2.09	3.63	5.33
CWFEM	0.68	2.09	3.63	5.33
Error HPDM	2.9%	2.9%	3.6%	4.3%

4.4.3.1 Natural frequency of a finite structure

A finite structure consisted of 10 unit cells is modelled by HPDM, CWFEM and FEM. The comparison of these frequencies given by different methods is given below. Tab. 4.3 illustrates the natural frequencies of the structure under clamped-free boundary condition, while those under the clamped-simply supported are presented in Tab. 4.4. The natural frequencies calculated by HPDM in our studies correlate well with those given by Hans [100]. The results issue from the FEM are used as reference to calculte the error of HPDM in Tab. 4.3 and Tab. 4.4. The HPDM predicts fairly well the natural frequencies until the 4th mode for both boundary conditions. Contrary to the dispersion relation, where a good correlation is obtained until almost 10 Hz. The valid frequency range of HPDM is more restricted for the finite structure compared to the infinite structure. It can be explained by the fact that the natural modes are not totally determined by the propagating wave. The evanescent waves, which may be less well predicted in the model of HPDM, play also an important role.

TABLE 4.4: The natural frequencies (Hz) under clamped-simply supported boundary condition

	1st mode	2nd mode	3rd mode	4th mode
HPDM	1.42	2.96	4.69	6.68
FEM	1.44	2.97	4.66	6.55
CWFEM	1.44	2.97	4.66	6.55
Error HPDM	1.4%	0.3%	0.6%	2.0%

4.4.3.2 Forced response

Similar as the 10 unit cells under clamped-free boundary condition, a transverse harmonic force is applied on the free side of the finite structure, as shown in Fig. 4.9.

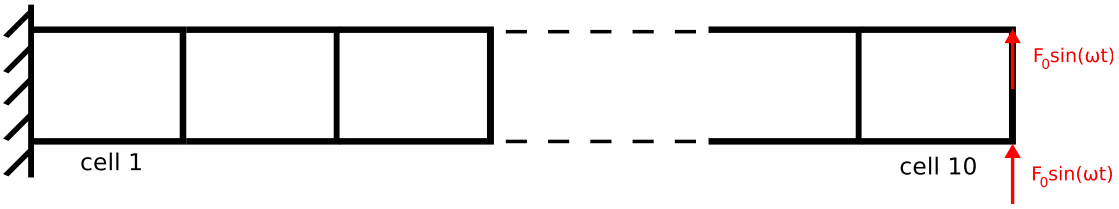

FIGURE 4.9: Clamped-free structure with excitation at free side

The structure is studied using the HPDM, CWFEM and FEM. The result calculated by ANSYS is employed as reference. The response at $x = 10l_w$ is illustrated in Fig. 4.10, with the amplitude of the force fixed to be 1 N.

CWFEM gives accurate result compared to ANSYS, while bigger discrepancies are found for HPDM. The conclusion is similar to the precedent section for the natural frequencies of free vibration. The first four resonance frequencies are fairly predicted, while the error becomes larger when we approach higher frequencies.

4.5 Conclusion

This chapter investigates the wave propagation feature in an infinite discrete framed structures by both HPDM and CWFEM. The dynamics of a finite structure is investigated by CWFEM and FEM. The main conclusions of this work can be drawn as follows:

1. The analytical continuous descriptions for longitudinal and transverse vibrations in framed structure are given by the HPDM. When the proprieties (material, length

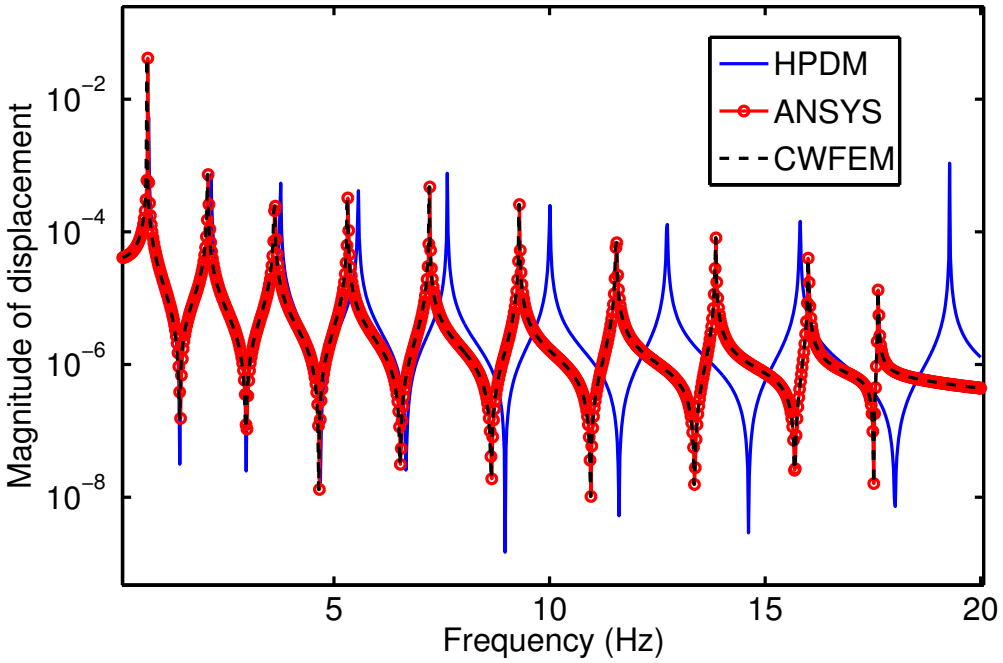

FIGURE 4.10: Forced response at the excitation point

and thickness) of the floor and the wall are of the same order, the homogenized equation of motion for the longitudinal wave is a second order differential equation, the same as a typical longitudinal wave in a homogeneous rod, as for the transverse vibrations, the homogenized equation of motion is a sixth order differential equation, contrary to the typical Euler-Bernoulli beam. The method allows to study and highlight the mechanism of the structure.

2. Numerical CWFEM is able to deduce all the waves propagating in the framed structure and the forced response of these structures. It gives accurate results on a specified structure with determined parameters.

3. When the scale ratio reaches 0.01, the HPDM predicts correctly the dispersion relation compared to the CWFEM with a error of less than 5%. For the studied case, a relative error of 2.5% is found for longitudinal wave with ϵ_l around 0.01 and a relative error of 0.5% for transverse wave with ϵ_t around 0.1.

4. The valid frequency range of HPDM for a finite structure is evaluated using the forced response and the natural frequency as the criteria. The validity range is smaller compared to the dispersion relation in an infinite structure. The evanescent

waves may be badly predicted in HPDM and play an important role in the finite case.

Further investigation will extend the study to the braced framed structure. It may be also interesting to study the contribution of the evanescent wave in the finite case to evaluate the error of the HPDM.

Chapter 5

Homogenization of 2 dimensional framed structures

5.1 Introduction

The periodic framed structure means the repetition of interconnected beam unit cells in one or multi-directions. Because of its abundant dynamic properties, the periodic framed structure is widely used in sandwich panels, truss beams, buildings, foam, plants,... The most known characteristic is the existence of band gap which indicates the frequency range without propagating waves [66, 114]. The band gap are mostly Bragg type which appears when the wavelength is on the order of the unit cell length. In other cases where the wavelength is much greater than the unit cell length, the band gap can also appear because of the local resonance [5, 115, 116]. In addition, due to the anisotropy in 2D framed structures, waves in pass bands propagate in preferred directions [117–119]. In order to simplify the study of periodic structure, a number of researches have been motivated to find their homogenised models [94]. According to the homogenization theory, an analytical continuous description is used to simulate the structure's dynamic behaviour. Based on the theory, several ideas have been developed: the beam theory of the material resistance [95], homogenization of periodic heterogeneous media [96], multi-scale separation and continuum mechanics [97], and the homogenization method of Periodic Discrete Media (HPDM), considered in this chapter, elaborated in [98] and recently completed in [99–101].

Instead of considering the whole structure, the study of periodic media can be converted to its unit cell. According to the Floquet-Bloch theorem [102, 103], the direct modelling of one unit cell can provide full descriptions of the whole structure's dynamic behaviour. Based on the theory, the most used method is the Wave Finite Element Method (WFEM), which utilises conventional FE software packages to model the unit cell. In this method, structures with complex geometries or material distributions can be analysed with relative ease [104–106]. Based on WFEM, an enhenced method, Condensed Wave Finite Element Method (CWFEM), is proposed and employed in [107–109]. The enhanced method combines the WFEM with the model order reduction technique. This combination makes the compute more efficient when the unit cell contains large number of internal nodes.

In this work, HPDM and CWFEM are employed to study a 2D infinite periodic framed structure. The principal objective of this chapter is to re-evaluate the efficiency of the HPDM theory using the wave characteristics identified by CWFEM. In most cases, the HPDM model is validated through eigen modes (natural frequencies). According to the wave-mode duality[110], the response of a vibrating system can also be explained in terms of elastic wave motions. Hence, a quick evaluation of the homogenised model can be presented with the wave characteristics obtained by CWFEM. Focusing on this objective, the chapter is organized as follows: In Sec. 2, the analytical method HPDM implemented on 2D framed structures is presented. Two different characterise frequency ranges are discussed. Subsequently, in Sec. 3, an overview of the numerical CWFEM on 2D case is given. Then in Sec. 4, a specified infinite structure is studied by both HPDM and CWFEM. Specific waves are identified and discussed through wave shapes and dispersion relations. Finally, the concluding remarks and perspectives are presented in Sec. 5.

5.2 Implementation of HPDM on two-dimensional framed structure

The associated theory and formulations of HPDM applied on two-dimensional framed structures [120] are explainedn in this section.

5.2.1 The studied structure

The infinite studied structures are composed by repeating the unit cell, shown in (Fig. 5.1) in the x and y directions. The horizontal elements (walls) and the vertical elements (floors) are all considered as Euler-Bernoulli beams, and they are linked by perfectly stiff and massless nodes. The characteristics of the floors ($j = f$) and the walls ($j = w$) are: l_j length, a_j in-plane thickness, h depth in the out-of-plane direction, $A_j = a_j h$ cross-section area, $I_j = a_j^3 h/12$ the in-plane bending cross-section inertia, ρ_j density, E_j elastic modulus.

The implementation of HPDM is composed of two parts: the discretization of the continuum dynamic balance and the homogenization process. As the studied structure is composed of interconnected beams, the dynamic balance of the whole structure can be expressed in a discrete form by the element balance and nodal balance. The discretization consists in expressing explicitly the forces and moments at the endpoints of an element as functions of the nodal kinematic variables by using Euler-Bernoulli theory. Then, the nodal balance equations at the endpoints give the discrete description of the whole structure. Figure 5.2 shows that the position of the node is located by the floor number and the wall number (w, f), their displacements in the plan (x, y) is described by $U_x^{(w,f)}, U_y^{(w,f)}$ and the rotation is presented by $\theta^{(w,f)}$. As the considered solution are harmonic, the dependence of time will be omitted during the homogenization. The material properties of floor and wall are as follows:

$$\frac{E_f}{E_w} = O(1), \quad \frac{\rho_f}{\rho_w} = O(1), \quad \frac{l_f}{l_w} = O(1)$$

$$\frac{h_f}{h_w} = O(1), \quad \frac{a_w}{l_w} = O(\epsilon), \quad \frac{a_f}{l_w} = O(\epsilon)$$

The element dynamic balance has been satisfied in the Introduction, it remains to write the nodal balance. As no external force is applied on the structure, the dynamic balance of node (w, f) is composed of four nodes connected to it. The nodal balance equation of node (w, f) in the direction x, y, z are respectively:

$$T_w^E(U_x^{(w,f-1)}, U_x^{(w,f)}, \theta^{(w,f-1)}, \theta^{(w,f)}) - T_w^B(U_x^{(w,f)}, U_x^{(w,f+1)}, \theta^{(w,f)}, \theta^{(w,f+1)}) + N_f^E(U_x^{(w-1,f)}, U_x^{(w,f)}) - N_f^B(U_x^{(w+1,f)}, U_x^{(w,f)}) = 0 \quad (5.1)$$

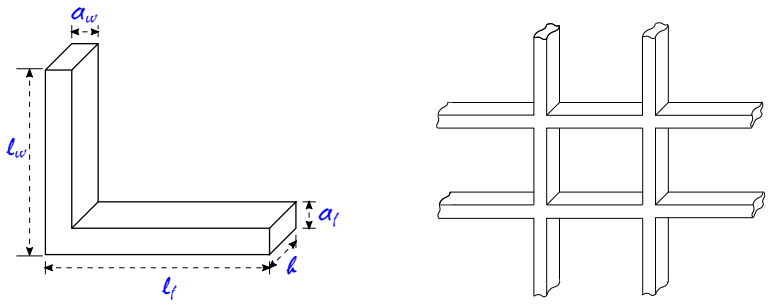

(a) The unit cell and its dimension

(b) The unit cell and geometric parameters

FIGURE 5.1: The unit cell of 2D framed structure

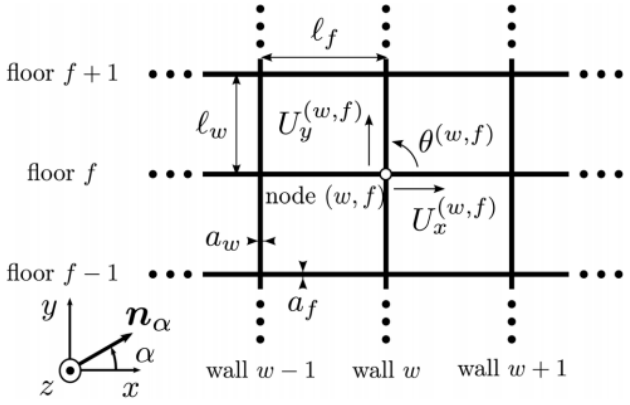

FIGURE 5.2: Structure notations

$$T_f^B(U_y^{(w,f)}, U_y^{(w+1,f)}, \theta^{(w,f)}, \theta^{(w+1,f)}) - T_f^E(U_y^{(w-1,f)}, U_y^{(w,f)}, \theta^{(w-1,f)}, \theta^{(w,f)}) + N_w^E(U_y^{(w,f-1)}, U_y^{(w,f)}) - N_w^B(U_y^{(w,f)}, U_y^{(w,f+1)}) = 0 \quad (5.2)$$

$$M_w^E(U_x^{(w,f-1)}, U_x^{(w,f)}, \theta^{(w,f-1)}, \theta^{(w,f)}) - M_w^B(U_x^{(w,f)}, U_x^{(w,f+1)}, \theta^{(w,f)}, \theta^{(w,f+1)}) + M_f^E(U_y^{(w-1,f)}, U_y^{(w,f)}, \theta^{(w-1,f)}, \theta^{(w,f)}) - M_f^B(U_y^{(w,f)}, U_y^{(w+1,f)}, \theta^{(w,f)}, \theta^{(w+1,f)}) = 0 \quad (5.3)$$

According to the homogenization theory, the scale separation is necessary, which means the characteristic length L of the structure is much greater then the periodicity l. Thus, the scale ratio $\epsilon = l/L \ll 1$ is a small parameter, and the associated variables can be expanded in the power of ϵ. Besides, as $l \ll L$, the variables at one node vary slowly to the node connected to it. Therefore, the variables at the node can be considered as discrete values of continuous functions and the nodes can be connected by Taylor's

series:

$$X^{(w,f+1)} = X^0(wl_f, fl_w) + \epsilon \left(X^1(wl_f, fl_w) + L\frac{X^0}{y}(wl_f, fl_w) \right) + ...$$

Then, substituting the associated expansion series and the Taylor's series into the nodal balance equation, the homogenized model will be obtained by identifying the leading order equations.

5.2.2 Shear wave at $\omega = O(\epsilon\omega_r)$

At very low frequency, the wave length of both bending and compression waves propagating in the elements is much larger than the unit cell length. The reference frequency is defined by convention as:

$$\omega_r = \frac{1}{L}\sqrt{\frac{E_w}{\rho_w}}$$

The case $\omega = O(\epsilon\omega_r)$ verifies that the scale separation is satisfied for bending waves and compression waves. Then, applying the expansion series of axial forces, shear force and moment to the nodal balance equation provides the corresponding equations in the direction x, y, z:

$$\begin{cases} E_x \dfrac{\partial^2 \tilde{U}_x^0}{\partial x^2} = 0 \\ E_x \dfrac{\partial^2 \tilde{U}_x^1}{\partial x^2} = 0 \\ E_x \dfrac{\partial^2 \tilde{U}_x^2}{\partial x^2} + G_w(\dfrac{\partial \tilde{\theta}^0}{\partial y} + \dfrac{\partial^2 \tilde{U}_x^0}{\partial y^2}) + M_s\omega^2\tilde{U}_x^0 = 0 \end{cases} \tag{5.4}$$

$$\begin{cases} E_y \dfrac{\partial^2 \tilde{U}_y^0}{\partial y^2} = 0 \\ E_y \dfrac{\partial^2 \tilde{U}_y^1}{\partial y^2} = 0 \\ E_y \dfrac{\partial^2 \tilde{U}_y^2}{\partial y^2} + G_f(\dfrac{\partial \tilde{\theta}^0}{\partial x} + \dfrac{\partial^2 \tilde{U}_y^0}{\partial x^2}) + M_s\omega^2\tilde{U}_y^0 = 0 \end{cases} \tag{5.5}$$

$$G_w(\tilde{\theta}^0 + \frac{\partial \tilde{U}_x^0}{\partial y}) + G_f(\tilde{\theta}^0 + \frac{\partial \tilde{U}_y^0}{\partial x}) = 0 \tag{5.6}$$

with

$$\begin{cases} M_w = \frac{\rho_w A_w}{l_f} : & \text{mass per unit surface of wall} \\ M_f = \frac{\rho_f A_f}{l_w} : & \text{mass per unit surface of floor} \\ M_s = M_w + M_f : & \text{mass per unit surface of the structure} \\ E_x = \frac{E_f A_f}{l_w} : & \text{elastic modulus in the x direction} \\ E_y = \frac{E_w A_w}{l_f} : & \text{elastic modulus in the y direction} \\ G_w = 12\frac{E_w I_w}{l_w^2 l_f} : & \text{shear modulus of wall} \\ G_f = 12\frac{E_f I_f}{l_w l_f^2} : & \text{shear modulus of floor} \end{cases}$$

As waves can be expressed as a superposition of plane waves, the wave travelling in the direction $\mathbf{n}_\alpha$ writes in the following form:

$$\mathbf{U}(\epsilon, x) = \mathbf{U}^0(x) + \epsilon \mathbf{U}^1(x) + \epsilon^2 \mathbf{U}^2(x) + ...$$

$$\mathbf{U}^0(x) = \begin{pmatrix} \tilde{U}_x^0 \\ \tilde{U}_y^0 \end{pmatrix} = \begin{pmatrix} \tilde{u}_x^0 \\ \tilde{u}_y^0 \end{pmatrix} exp[-ik(\alpha)\mathbf{n}_\alpha \mathbf{x}]$$

where $\tilde{u}_x^0, \tilde{u}_y^0$ are amplitude in the direction x, y; $k(\alpha)$ is the wavenumber in direction $\mathbf{n}_\alpha$.

Substituting $\mathbf{U}^0(x)$ into Equ. (5.4), (5.5):

$$\begin{cases} -E_x k^2(\alpha) cos^2(\alpha) \tilde{u}_x^0 exp[-ik(\alpha)\mathbf{n}_\alpha \mathbf{x}] = 0 \\ -E_y k^2(\alpha) sin^2(\alpha) \tilde{u}_y^0 exp[-ik(\alpha)\mathbf{n}_\alpha \mathbf{x}] = 0 \end{cases} \tag{5.7}$$

In order to obtain non zero solution ($\mathbf{u}^0 \neq 0$), $sin(\alpha)$ or $cos(\alpha)$ has to be zero, which means the wave can only propagate in the direction x or y. In the case $\alpha = 0$, the wave propagates in the x direction. According to equation (5.7), $\tilde{u}_x^0 = 0$ which means the travelling wave is a pure shear wave with the polarization in y. As the medium is infinite, the invariance of macroscopic field $\mathbf{U}^0$ under a translation perpendicular to the direction of propagation implies the invariance of its correctors in higher orders. Then,

$$\frac{\partial^2 \tilde{U}_x^2}{\partial x^2} = 0$$

Eliminating $\tilde{\theta}^0$ in equation (5.4) by using equation (5.6), the wavenumber of the shear wave can be obtained:

$$k(0) = \omega\sqrt{\frac{M_s}{G}}; \quad \text{with} \quad \frac{1}{G} = \frac{1}{G_w} + \frac{1}{G_f}$$

The same results can be obtained in the case $\alpha = \pi/2$. In conclusion, at low frequency $\omega = O(\epsilon\omega_r)$, only pure shear waves travelling in the direction x or y exist.

5.2.3 Compressional waves at $\omega = O(\omega_r)$

Another case discussed here is $\omega = O(\omega_r)$. In this case, the wavelength of bending waves is the same order as the unit length. Local resonance caused by the bending of wall appears, and the expansion series for shear force and bending moment can not be used. Thus, the new homogenized equations in the direction x, y become:

$$E_x \frac{\partial^2 \tilde{U}_x^0}{\partial x^2} + (M_f + M_w f(\hat{\omega}_w))\omega^2 \tilde{U}_x^0 = 0 \tag{5.8}$$

$$E_y \frac{\partial^2 \tilde{U}_y^0}{\partial y^2} + (M_w + M_f f(\hat{\omega}_f))\omega^2 \tilde{U}_y^0 = 0 \tag{5.9}$$

with

$$\begin{cases} \hat{\omega}_w = \omega \left(\dfrac{2l_w}{3\pi}\right)^2 \sqrt{\dfrac{\rho_w A_w}{E_w l_w}} \\ \hat{\omega}_f = \omega \left(\dfrac{2l_f}{3\pi}\right)^2 \sqrt{\dfrac{\rho_f A_f}{E_f l_f}} \\ f(\hat{\omega}) = \dfrac{8}{3\pi\sqrt{\hat{\omega}} g(\hat{\omega})} sin(\dfrac{3\pi}{4}\sqrt{\hat{\omega}}) sinh(\dfrac{3\pi}{4}\sqrt{\hat{\omega}}) \\ g(\hat{\omega}) = sin(\dfrac{3\pi}{4}\sqrt{\hat{\omega}}) cosh(\dfrac{3\pi}{4}\sqrt{\hat{\omega}}) + sinh(\dfrac{3\pi}{4}\sqrt{\hat{\omega}}) cos(\dfrac{3\pi}{4}\sqrt{\hat{\omega}}) \end{cases}$$

In equation (5.8), it can de seen that an effective mass depending on the frequency in stead of the real mass is used to describe the local resonance of wall bending. The same analysis is carried out in this case: introducing the $\mathbf{U}^0(x)$ into equation (5.8), (5.9).

$$\begin{cases} \left(-E_x k^2(\alpha) cos^2(\alpha) + M^w(\hat{\omega}_w)\omega^2\right) \tilde{u}_x^0 exp[-ik(\alpha)\mathbf{n}_\alpha \mathbf{x}] = 0 \\ \left(-E_y k^2(\alpha) sin^2(\alpha) + M^f(\hat{\omega}_f)\omega^2\right) \tilde{u}_y^0 exp[-ik(\alpha)\mathbf{n}_\alpha \mathbf{x}] = 0 \end{cases} \tag{5.10}$$

with $M^w(\hat{\omega}_w) = M_f + M_w f(\hat{\omega}_w), M^f(\hat{\omega}_f) = M_w + M_f f(\hat{\omega}_f)$. The existence of a non-zero solution implies that:

$$-E_x k^2(\alpha) cos^2(\alpha) + M^w(\hat{\omega}_w)\omega^2 = 0 \tag{5.11a}$$

$$\text{or} \quad -E_y k^2(\alpha) sin^2(\alpha) + M^f(\hat{\omega}_f)\omega^2 = 0 \tag{5.11b}$$

When equation (5.11a) is satisfied, $\tilde{u}_y^0 = 0$, all nodes move in the x direction. And equation (5.11a) shows that $cos(\alpha) \neq 0$. In this case, waves propagate in all directions except the y direction ($\alpha = \pi/2$). For waves in the x direction ($\alpha = 0$), the propagation direction is the same as the polarization direction, which implies that only pure compressional waves travel in the x direction. The associated wavenumber can be obtained from equation (5.11a):

$$k(0) = \omega \sqrt{\frac{M^w(\hat{\omega}_w)}{E_x}}$$

The wavenumber is similar to the one of a compressional wave in a classical elastic medium. The real mass is replaced by the effective mass, and the local bending resonance can be predicted when the effective mass becomes infinite and changes its sign. For the other directions, the waves are shear-compression waves. Because of the orientation of the elements, the polarization of these waves are fixed in the x direction, and the wavenumber is:

$$k(\alpha) = \frac{k(0)}{|cos(\alpha)|}$$

The wavelength of macroscopic waves in the direction $\mathbf{n}_\alpha$ is the projection of waves travelling in the x direction on to the direction $\mathbf{n}_\alpha$. For the other case of equation (5.11b), the roles of the floors and walls are reversed. Waves can travail in all directions except for the x direction. Pure compression waves propagate in the y direction, and the shear-compression waves travail in the other direction. And the wavelength of diagonal waves is the projection of waves in y direction.

5.3 Overview of the numerical CWFEM en 2D

The outline of the numerical CWFEM implemented en 2D structures is given hereafter. The unit cell that forms the periodic structures is discretized by the Finite Element (FE) method. The mass and stiffness matrices $\mathbf{M}$ and $\mathbf{K}$ of the unit cell are extracted

from commercial FE package. The nodal DOFs are defined as in Fig. 5.3(a), which are divided into: boundary DOFs (three corners $\mathbf{q}_1 \quad \mathbf{q}_2 \quad \mathbf{q}_3$) and internal DOFs ($\mathbf{q}_\mathtt{I}$). They are classified as $[\mathbf{q}_1 \quad \mathbf{q}_2 \quad \mathbf{q}_3 \quad \mathbf{q}_\mathtt{I}]$. The boundary nodal DOFs are denoted $\mathbf{q}_\mathtt{bd}$. The nodal forces are classified in the same way, the boundary nodal forces are represented by $\mathbf{f}_\mathtt{bd}$. It should be noted that the choice of the unit cell can be various, the unit cell in Fig. 5.3 is used since it minimizes the number of boundary DOFs, so as to decrease the computational cost.

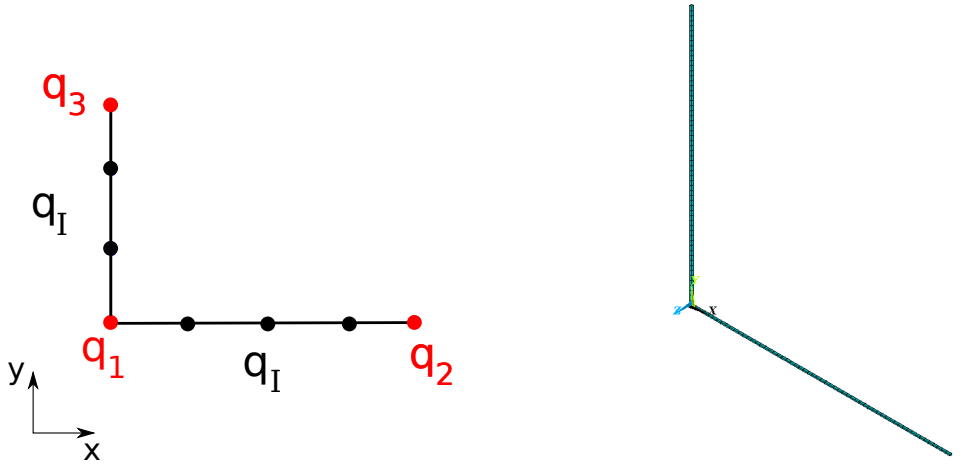

(a) Nodes definition of the unit cell (b) The FE model of the unit cell

FIGURE 5.3: An unit cell of the periodic frame structure

5.3.1 Modelling of the unit cell with model order reduction

The nodal DOFs of the unit cell are written as $[\mathbf{q}_\mathtt{bd} \quad \mathbf{q}_\mathtt{I}]$. In the free wave propagation case, $\mathbf{f}_\mathtt{I} = \mathbf{0}$. Assuming time-harmonic behaviour and neglecting damping, the unit cell's motion equation becomes

$$\left(\begin{bmatrix} \tilde{\mathbf{K}}_{\mathtt{bdbd}} & \tilde{\mathbf{K}}_{\mathtt{bdI}} \\ \tilde{\mathbf{K}}_{\mathtt{Ibd}} & \tilde{\mathbf{K}}_{\mathtt{II}} \end{bmatrix} - \omega^2 \begin{bmatrix} \tilde{\mathbf{M}}_{\mathtt{bdbd}} & \tilde{\mathbf{M}}_{\mathtt{bdI}} \\ \tilde{\mathbf{M}}_{\mathtt{Ibd}} & \tilde{\mathbf{M}}_{\mathtt{II}} \end{bmatrix} \right) \begin{pmatrix} \mathbf{q}_\mathtt{bd} \\ \mathbf{q}_\mathtt{I} \end{pmatrix} =$$

$$[\tilde{\mathbf{K}} - \omega^2 \tilde{\mathbf{M}}] \begin{pmatrix} \mathbf{q}_\mathtt{bd} \\ \mathbf{q}_\mathtt{I} \end{pmatrix} = \begin{pmatrix} \mathbf{f}_\mathtt{bd} \\ \mathbf{0} \end{pmatrix} \tag{5.12}$$

where matrix $[\tilde{\mathbf{K}} - \omega^2 \tilde{\mathbf{M}}]$ is the dynamic stiffness matrix of the unit cell. According to the work [108], model order reduction is proposed in the unit cell modelling. The hybrid coordinates $[\mathbf{q}_\mathtt{bd} \quad \mathbf{P}_\mathtt{c}]$ of reduced model are related to the physical coordinates $[\mathbf{q}_\mathtt{bd} \quad \mathbf{q}_\mathtt{I}]$

by the transfer matrix $\mathbf{B}$ as shown below:

$$\begin{pmatrix} \mathbf{q}_{\mathtt{bd}} \\ \mathbf{q}_{\mathtt{I}} \end{pmatrix} = \begin{bmatrix} \mathbf{I_n} & \mathbf{0} \\ \mathbf{\Psi}_{\mathtt{bd}} & \mathbf{\Psi}_{\mathtt{C}} \end{bmatrix} \begin{pmatrix} \mathbf{q}_{\mathtt{bd}} \\ \mathbf{P}_{\mathtt{C}} \end{pmatrix} = \mathbf{B} \begin{pmatrix} \mathbf{q}_{\mathtt{bd}} \\ \mathbf{P}_{\mathtt{C}} \end{pmatrix} \tag{5.13}$$

where $[\mathbf{\Psi}_{\mathtt{bd}}]$ represents the static constraint modes which associate physical displacements at the boundary $\mathbf{q}_{\mathtt{bd}}$ to physical displacements of elastic DOFs $\mathbf{q}_{\mathtt{I}}$.

$$\mathbf{\Psi}_{\mathtt{bd}} = -\tilde{\mathbf{K}}_{\mathtt{II}}^{-1}\tilde{\mathbf{K}}_{\mathtt{Ibd}} \tag{5.14}$$

The fixed boundary modes are denoted $[\mathbf{\Psi}_{\mathtt{I}}]$, which are obtained by fixing the boundary DOFs:

$$[\tilde{\mathbf{K}}_{\mathtt{II}} - \omega_0^2\tilde{\mathbf{M}}_{\mathtt{II}}]\mathbf{\Psi}_{\mathtt{I}} = 0 \tag{5.15}$$

$[\mathbf{\Psi}_{\mathtt{C}}]$ represents a set of truncated modes in $[\mathbf{\Psi}_{\mathtt{I}}]$. Among $[\mathbf{\Psi}_{\mathtt{I}}]$, it is suggested to retain in $[\mathbf{\Psi}_{\mathtt{C}}]$ at least the modes under 3 times maximum investigated frequency [108]. Then the equilibrium equation of the reduced model is written as:

$$[\mathbf{K}^* - \omega^2\mathbf{M}^*] \begin{pmatrix} \mathbf{q}_{\mathtt{bd}} \\ \mathbf{P}_{\mathtt{C}} \end{pmatrix} = \begin{pmatrix} \mathbf{f}_{\mathtt{bd}} \\ \mathbf{0} \end{pmatrix} \tag{5.16}$$

with

$$\mathbf{K}^* = \mathbf{B}^{\mathbf{T}}\tilde{\mathbf{K}}\mathbf{B} \quad , \quad \mathbf{M}^* = \mathbf{B}^{\mathbf{T}}\tilde{\mathbf{M}}\mathbf{B} \tag{5.17}$$

More details about this method can be found in [108].

5.3.2 Formulation of the WFEM (frequency and direction of wave propagation known)

Since the frequency is fixed, we can express Eq. (5.16) using the dynamic matrix of the reduced model:

$$\begin{bmatrix} \mathbf{D}^*_{\mathtt{bdbd}} & \mathbf{D}^*_{\mathtt{bdc}} \\ \mathbf{D}^*_{\mathtt{cbd}} & \mathbf{D}^*_{\mathtt{cc}} \end{bmatrix} \begin{pmatrix} \mathbf{q}_{\mathtt{bd}} \\ \mathbf{P}_{\mathtt{C}} \end{pmatrix} = \begin{pmatrix} \mathbf{f}_{\mathtt{bd}} \\ 0 \end{pmatrix} \tag{5.18}$$

Eliminating the internal DOFs in equation (5.18) provides the dynamic condensed matrix $\mathbf{D}_{\mathtt{bdbd}}$. and Eq. (5.18) becomes:

$$\begin{bmatrix} \mathbf{D}_{11} & \mathbf{D}_{12} & \mathbf{D}_{13} \\ \mathbf{D}_{21} & \mathbf{D}_{22} & \mathbf{D}_{23} \\ \mathbf{D}_{31} & \mathbf{D}_{32} & \mathbf{D}_{33} \end{bmatrix} \begin{pmatrix} \mathbf{q}_1 \\ \mathbf{q}_2 \\ \mathbf{q}_3 \end{pmatrix} = \begin{pmatrix} \mathbf{f}_1 \\ \mathbf{f}_2 \\ \mathbf{f}_3 \end{pmatrix} \tag{5.19}$$

According to periodic structures theory of the Floquet and Bloch [102, 103], the DOFs are related as follows:

$$\mathbf{q}_2 = \lambda_x \mathbf{q}_1, \mathbf{q}_3 = \lambda_y \mathbf{q}_1 \tag{5.20}$$

In addition, for free wave propagation, the sum of nodal forces of all the elements connected to nodes 1 is zero, which leads to:

$$\mathbf{f}_1 + \lambda_x^{-1}\mathbf{f}_2 + \lambda_y^{-1}\mathbf{f}_3 = \mathbf{0} \tag{5.21}$$

Remind the relation between λ_x, λ_y, the wavenumbers k_x, k_y and propagation constants μ_x, μ_y are as follows:

$$\lambda_x = e^{-i\mu_x}, \quad \lambda_y = e^{-i\mu_y}, \quad \mu_x = l_f k_x, \quad \mu_y = l_w k_y \tag{5.22}$$

For the specified direction of propagation θ, we have

$$\frac{k_y}{k_x} = \tan\theta, \quad \frac{\mu_y}{\mu_x} = \frac{l_w k_y}{l_f k_x} = \frac{l_w}{l_f}\tan\theta \tag{5.23}$$

where μ_x and μ_y might be complex, but their ratio is real and given. Supposing the ratio $\mu_y/\mu_x = m_y/m_x$, where m_x and m_y are integers without common divisor, then one can note that $\mu_x = \mu m_x, \mu_y = \mu m_y$ and $\gamma = e^{-i\mu}$, and the relation in equation (5.22) becomes:

$$\lambda_x = e^{-i\mu m_x} = \gamma^{m_x}, \quad \lambda_y = e^{-i\mu m_y} = \gamma^{m_y} \tag{5.24}$$

Based on Eqs. (5.19), (5.20) and (5.24), Eq (5.21) becomes

$$\begin{aligned}[\mathbf{D}_{31}\gamma^{m_x} + \mathbf{D}_{32}\gamma^{2m_x} + (\mathbf{D}_{11} + \mathbf{D}_{22} + \mathbf{D}_{33})\gamma^{m_x+m_y} + \mathbf{D}_{12}\gamma^{2m_x+m_y} \\ + \mathbf{D}_{13}\gamma^{m_x+2m_y} + \mathbf{D}_{21}\gamma^{m_y} + \mathbf{D}_{33}\gamma^{2m_y}]\mathbf{q}_1 = \mathbf{0}\end{aligned} \tag{5.25}$$

If m is the highest order of γ, equation (5.25) is then a m order polynomial eigenvalue problem which has $2mn$ solutions for γ. Here, n is the length of the vector $\mathbf{q_1}$. So the equation (5.25) can be recast as the standard linear eigenvalue problem.

$$(\mathbf{Q} - \gamma\mathbf{I})\mathbf{Z} = \mathbf{0} \tag{5.26}$$

where

$$\mathbf{Q} = \begin{bmatrix} -\mathbf{A}_{\mathtt{m}}^{-1}\mathbf{A}_{\mathtt{m}-1} & \cdots & -\mathbf{A}_{\mathtt{m}}^{-1}\mathbf{A}_1 & -\mathbf{A}_{\mathtt{m}}^{-1}\mathbf{A}_0 \\ \mathbf{I} & \cdots & \mathbf{0} & \mathbf{0} \\ \vdots & \ddots & \vdots & \vdots \\ \mathbf{0} & \cdots & \mathbf{I} & \mathbf{0} \end{bmatrix}, \mathbf{Z} = \begin{pmatrix} \gamma^{m-1}\mathbf{q_1} \\ \vdots \\ \gamma\mathbf{q_1} \\ \mathbf{q_1} \end{pmatrix} \tag{5.27}$$

The order of the eigenvalue problem might be very large and hence there will be many solutions. Surely, for an arbitrary angle θ, we can't always have $\mu_y/\mu_x = m_y/m_x$. Sometimes it maybe obliged to solve a transcendental eigenvalue problem [121]. But here in our case, only some specified directions ($\theta = 0°, 45°$) are investigated, in addition with a small size of $\mathbf{q_1}$, the wave propagation characteristics are calculated with relative ease. Once γ is calculated, the wavenumber is obtained according to:

$$k = \sqrt{k_x^2 + k_y^2} = \sqrt{|log(\gamma) * m_x/l_f|^2 + |log(\gamma) * m_y/l_w|^2} \tag{5.28}$$

Once the eigenvector $\mathbf{q_1}$ is calculated, the wave shape with all the physical DOFs can be calculated using the following relation:

$$\begin{pmatrix} \mathbf{q}_1 \\ \mathbf{q}_2 \\ \mathbf{q}_3 \\ \mathbf{q}_{\mathtt{I}} \end{pmatrix} = \begin{bmatrix} \mathbf{I} & \cdots & \mathbf{0} \\ \vdots & \ddots & \vdots \\ \mathbf{0} & \cdots & \mathbf{I} \\ \boldsymbol{\Psi}_{\mathtt{bd}} & & \boldsymbol{\Psi}_{\mathtt{C}} \end{bmatrix} \begin{bmatrix} \mathbf{I} \\ (\mathbf{D}^*_{\mathtt{cc}})^{-1}\mathbf{D}^*_{\mathtt{cbd}} \end{bmatrix} \begin{bmatrix} \mathbf{I} & \lambda_x\mathbf{I} & \lambda_y\mathbf{I} \end{bmatrix} \mathbf{q}_1$$

At last the waves are tracked by the correlation between complex wave shape using the Modal Assurance Criterion (MAC) [122].

TABLE 5.1: Characteristics of the studied structure

l_w (m)	l_f (m)	a_w (mm)	a_f (mm)	ρ (kg m^{-3})	E (Pa)	ν
3	3	21	21	2300	3e10	0.2

5.4 Investigation of 2D framed structures by the numerical and analytical approaches

A framed structure with the wall equals to floor is studied here. The material properties of the structure are listed in Tab. (5.1). The wave propagation characteristics in x (or y) direction is investigated firstly by both CWFEM and HPDM. The validity range of the HPDM is discussed, the interpretation of the results is given as well. Then the characteristics of the wave motion in a diagonal direction (45° direction) is studied afterwards. To ensure the convergence of the mesh, the wall and the floor are both discretized into 200 finite elements. Beam 4 under Euler-Bernoulli theory assumption in ANSYS is employed to generate the FEM model of the unit cell. Since only the in-plane waves are studied, the DOFs related to the out-of-plane motion are fixed to simply the problem. Each unit cell contains hence 1203 DOFs, among which 1194 are internal Dofs and only 9 DOFs are at the boundary. The studied frequency range is between 0 – 800 Hz. In the CWFEM, the first 54 fixed interface modes (until 2.4k Hz) are conserved in $\mathbf{\Psi_C}$. So instead of inverting a non-diagonal matrix of 1194×1194 at each frequency, a diagonal matrix of 54 × 54 is inverted in the dynamic condensed equation (5.18). Compared to the classical WFEM, the computation efficiency of CWFEM is greatly improved.

5.4.1 wave propagation in x direction

The wave propagation in x direction is investigated at first. This case corresponds to $m_x = 1, m_y = 0$ in Eq. (5.25). Since the proprieties of the wall are the same as those of floor, and the unit cell is square with $l_w = l_f$, the wave characteristics in y direction is expected to be the same as those in x direction.

The dispersion relation of waves in x direction is given in Fig.(5.4). Here only the propagative waves in x positive direction are illustrated. Up to 20 Hz, 2 types of wave are identified. Their shapes are given in Fig.(5.5). It can be seen that wave 1

(Fig. 5.5(a)) corresponds to the transverse vibration (shear wave). Due to the periodicity of the structure, Bragg type [112] stop band appears at around 2.2 Hz. As for wave 2 (Fig. 5.5(b)), it corresponds to the traction-compression motion (longitudinal wave) in the propagation direction. A stop band at around 8.6 – 10.7 Hz occurs due to the local resonance in bending of the vertical element in the y direction. More discussion will be given in section 5.4.1.2.

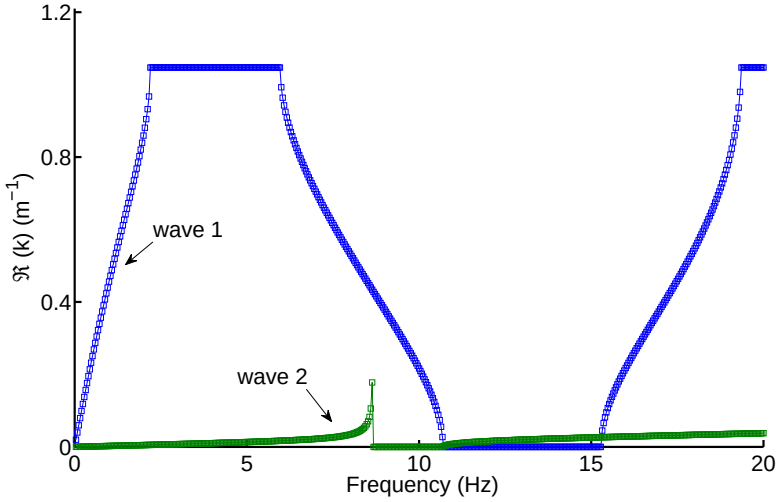

(a) The real part of the wavenumber

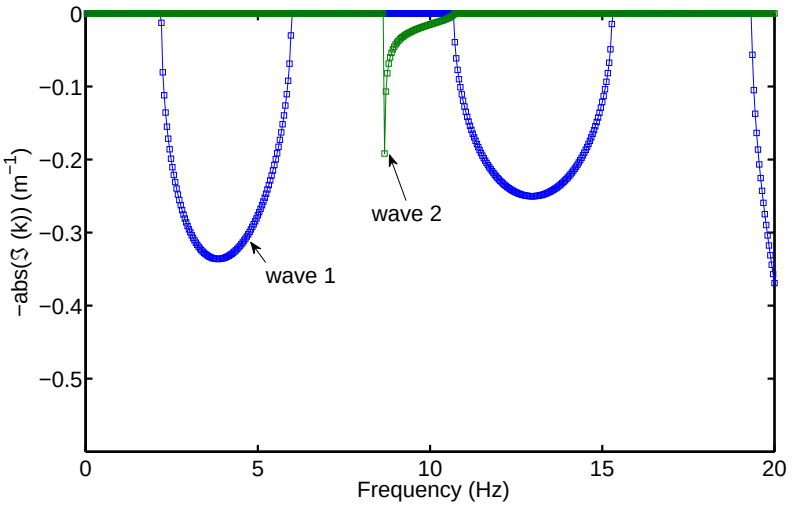

(b) The imaginary part of the wavenumber

FIGURE 5.4: Wave propagation characteristics in x direction

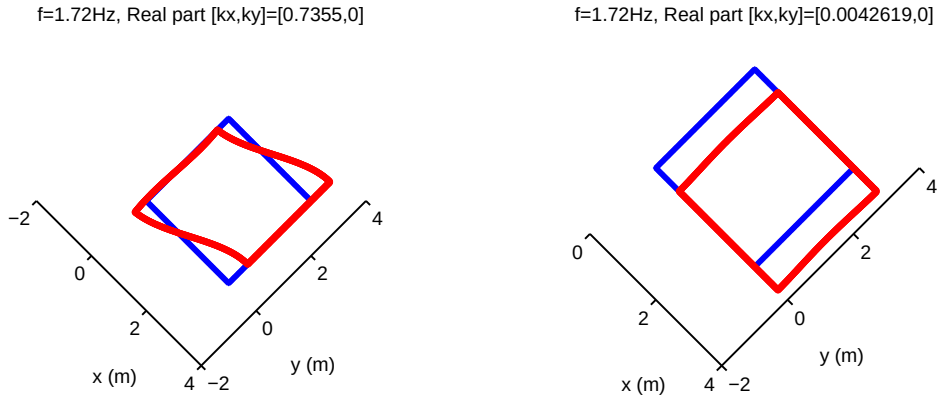

(a) Wave 1 (b) Wave 2

FIGURE 5.5: Wave shapes (o) Undeformed unit cell (∗)

5.4.1.1 The shear wave

From the wave shape in Fig. 5.5(a), it can be seen that the polarization direction (y) is perpendicular to the wave propagation direction (x). The dispersion relation determined by HPDM and by CWFEM is illustrated in Fig. 5.6(a). In Fig. 5.6(b), the relative error between the wavenumbers determined by the two methods is given with y-axis labelling on the left. The scale ratio ϵ_s in the function of frequency is also included in this figure with y-axis labelling on the right. The scale ratio ϵ_s is defined as $\epsilon_s = l_x/\lambda_s$, with λ_s the wavelength of flexural wave in the homogeneous wall/floor: $\lambda_s = 2\pi\sqrt[4]{EI/(\rho A\omega^2)}$. It can be seen that at low frequency, only slight discrepancy is found between two methods. The error increases with the frequency, however, when we approach the stop band at 2.2 Hz, the error decreases. A possible explanation is given using the ratio between the deformation in two directions $|U_y|/|U_x|$, which is plot in Fig. 5.7.

Since HPDM assumes that for the pure shear wave determined by the Eq. (5.7), the polarization direction should be strictly perpendicular to the propagation direction. So for shear wave in x direction, the ratio $|U_y|/|U_x|$ should be infinite. The bigger the ratio is, the better the assumption is satisfied. It can be seen at low frequency, the ratio is between 100 – 1000. Then the ratio decreases with the frequency, and when approaching the stop band, the ratio re-increases and attains the maximum at 2.2 Hz where the stop band begins.

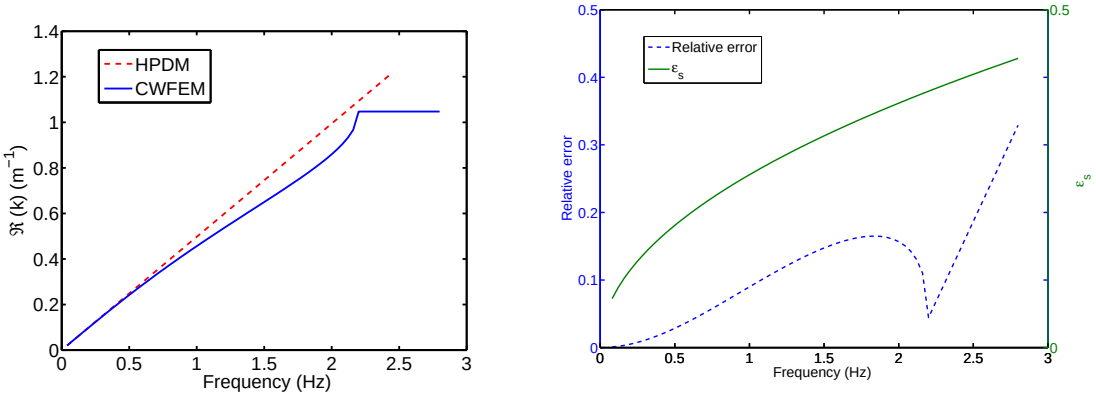

(a) The dispersion relation

(b) Relative error and scale ratio in the function of frequency

FIGURE 5.6: Wavenumber of shear waves in x direction determined by CWFEM and HPDM

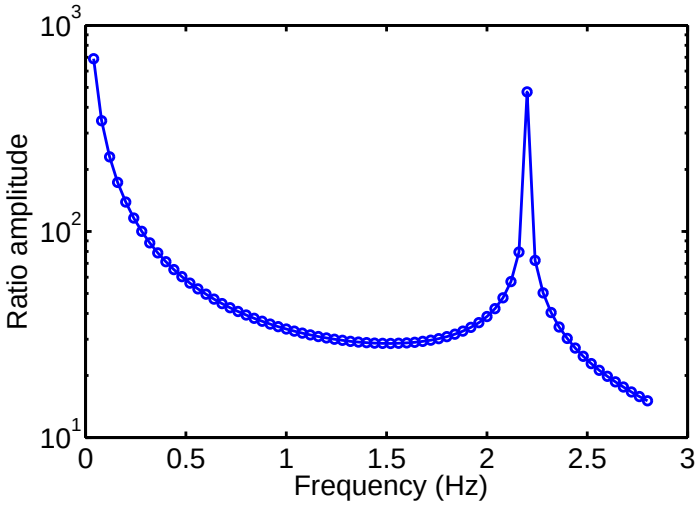

FIGURE 5.7: The ratio between the deformation in two directions $|U_y|/|U_x|$

5.4.1.2 The longitudinal wave

The longitudinal wave in the frequency range 0 – 800 Hz is studied here. From the wave shape at a fixed frequency given in Fig. 5.5(b), it can be seen that the polarisation is mainly in the x direction, which is the same as the propagation direction. The wavenumber determined by HPDM and CWFEM is illustrated in Fig.(5.8). A frequency range between 0 Hz and 800 Hz is studied here. HPDM captures well not only the real part of wavenumber, but also its imaginary part until 400 Hz. All the stop bands due to the local resonances (around 8 Hz, 47 Hz, 115 Hz, 342 Hz) are correctly predicted by the HPDM. Between 488 Hz – 505 Hz, a larger local resonance stop band influenced by the Bragg scattering shows up. A bigger discrepancy is found between HPDM and CWFEM

for this stop band. Then we have a not very evident Bragg stop band in 581 Hz — 602 Hz, as it can be seen from the real part of wavenumber (Fig. 5.8(a)) and its imaginary part (Fig. 5.8(b)). HPDM fails to predict the presence of this stop band. After 602 Hz, the two curves seem to diverge from each other. But they are almost symmetric to the $k = \pi/L_x$. In fact, if the CWFEM is not plotted only in the first Brillouin zone with $k_x \in [-\pi/L_x, \pi/L_x]$ and $k_y \in [-\pi/L_y, \pi/L_y]$, the two curves should be very close to each other. According to the Floquet-Bloch theorem [102, 103], the wavenumber is periodic of period $2\pi/L_x$ for k_x and $2\pi/L_y$ for k_y. In addition, for a periodic structure with symmetric unit cell, the wavenumber is also symmetric to $k_x = 0$ and $k_y = 0$.

Thanks to HPDM, we know the local resonances occur when the frequency approaches the odd modes of the wall with two extremities fixed. The wave shape near these local resonance frequencies can be determined by CWFEM. In Fig. (5.9) the wave shapes around the first three local resonances frequencies are given. It can be seen that two floors are in traction-compression and deform a little and the two walls is under flexion with the two extremities fixed. The wave shapes correspond indeed to the first three odd modes.

5.4.2 Wave propagation in 45° direction

Since big anisotropy appears in the periodic frame, it is also interesting to study the wave propagation in a diagonal direction. Here the wave propagation in 45° direction is studied. The relevant values taken in equation (5.25) are $m_x = 1, m_y = 1$. The dispersion relation is given in Fig (5.10). It can be seen that three waves are identified in the range 0 – 20 Hz. The wave 1 is evanescent at low frequency and becomes propagative around 3.8 Hz. The wave 2 seems to have a polarisation direction (135°) perpendicular to the propagation direction (45°). The wave 3 corresponds to the longitudinal wave, with the polarisation direction parallel to the propagation direction. The first local resonance appear at 8.6 Hz, which is almost the same frequency as the first local resonance in x direction.

According to HPDM, for the shear-compressive wave travelling in direction $\mathbf{n}_\alpha$, the wavenumber is $k(\alpha) = k(0)/|cos(\alpha)|$, and the polarization is in the x direction. It is compared with the compressive/longitudinal wave (wave 3 in Fig.5.10) identified by CWFEM. The frequency range until 300 Hz is studied, as shown in Fig (5.13). It can be

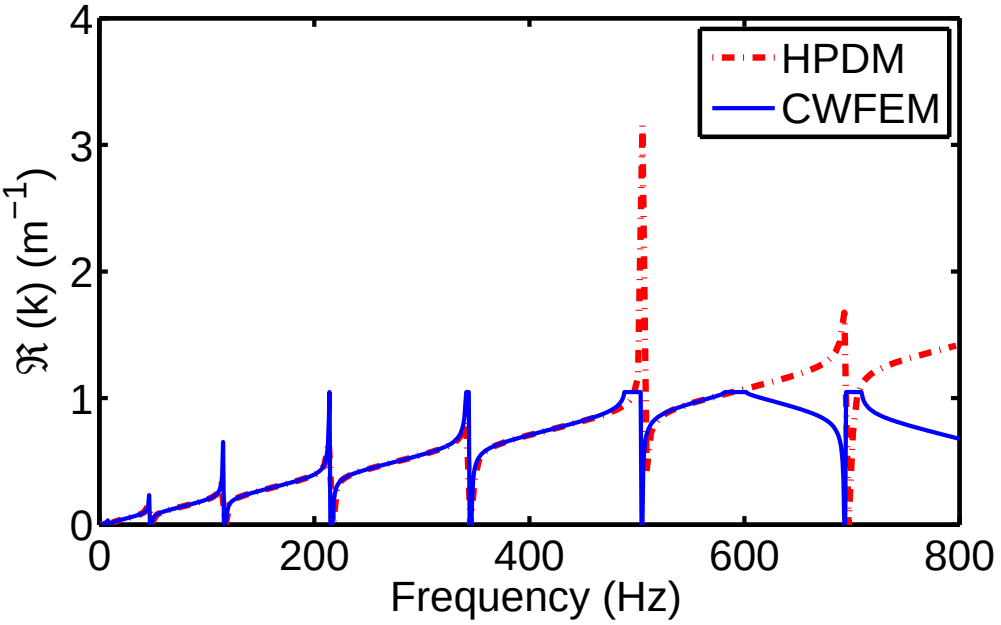

(a) The real part of wavenumber

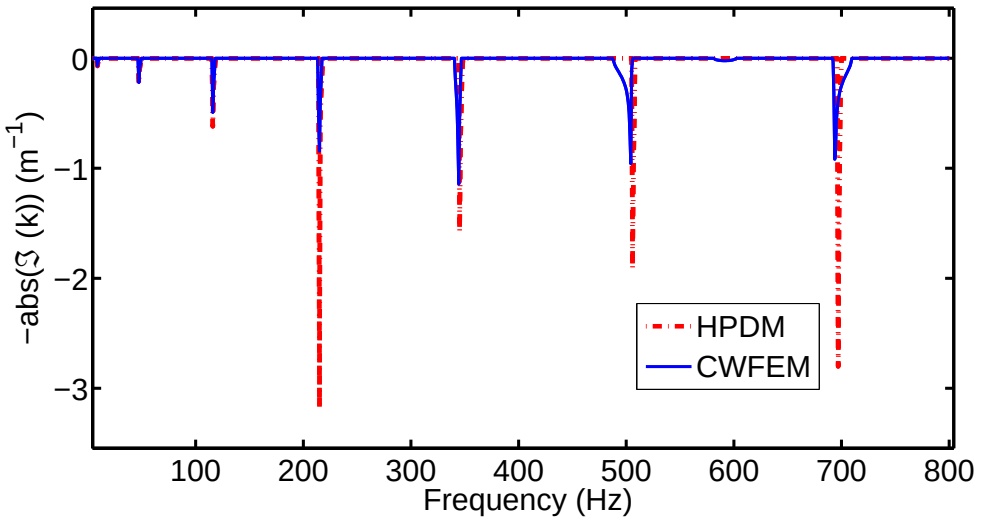

(b) The imaginary part of wavenumber

FIGURE 5.8: Wavenumber of longitudinal wave in x direction determined by CWFEM and HPDM

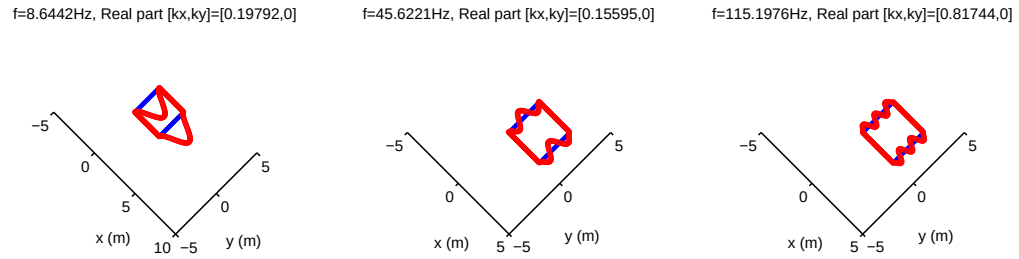

(a) 1st local resonance (b) 2nd local resonance (c) 3rd local resonance

FIGURE 5.9: Wave shapes (o) Undeformed unit cell (∗)

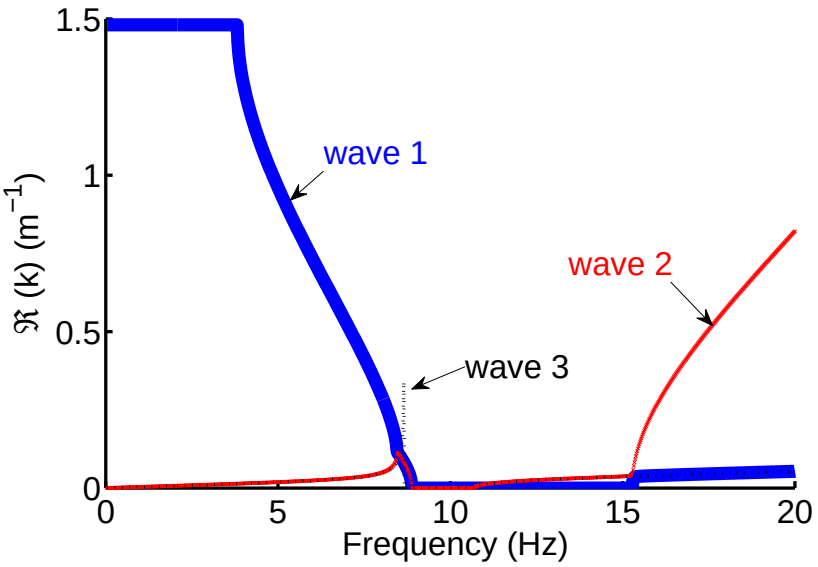

(a) The real part of the wavenumber

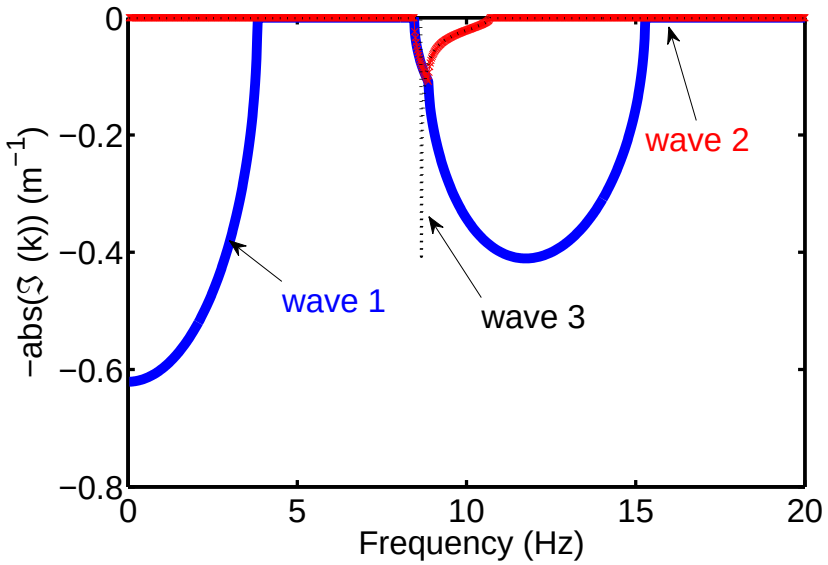

(b) The imaginary part of the wavenumber

FIGURE 5.10: Wave propagation characteristics in 45° direction

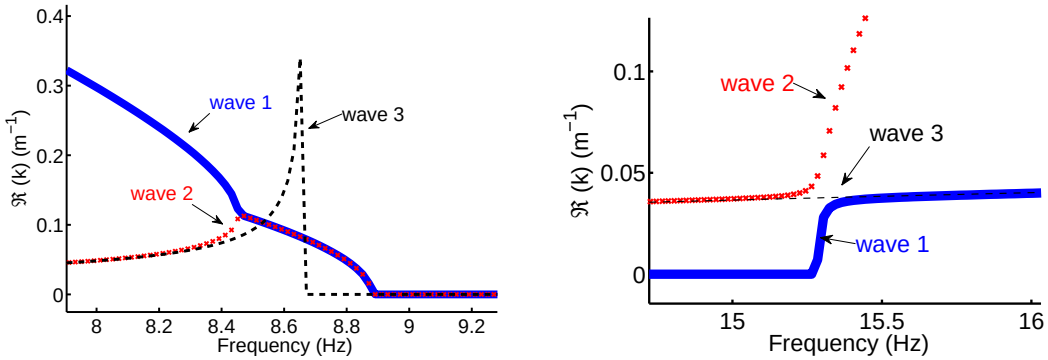

(a) Zoom around 8.6 Hz (b) Zoom around 15.3 Hz

FIGURE 5.11: Two zoom of dispersion relation of Fig. 5.10(a)

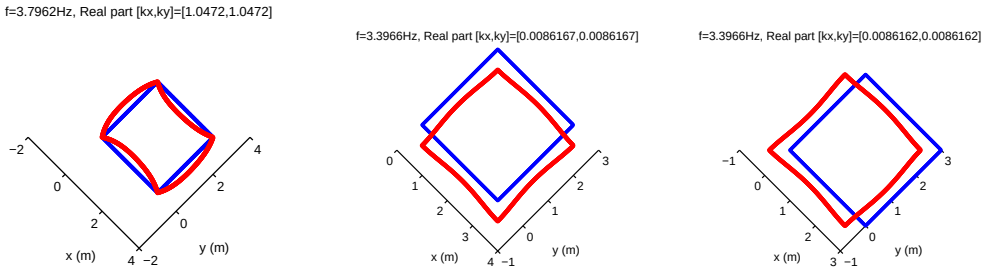

(a) Wave 1 (b) Wave 2 (c) Wave 3

FIGURE 5.12: Wave shapes (o) Undeformed unit cell (∗) for 45° direction (Fig. 5.10)

seen that the two results correlate surprisingly well except on certain local resonances. An possible explanation is given: for the low frequency before the first local resonances, the wave 2 and 3 have the same wavenumber (eigenvalue). Thus, they form a subspace. The polarisation (eigenvector) of wave 2 is in 135° (same as $-45°$) while the polarisation of wave 3 is in 45°. Their polarisation together leads to the polarisation of the global wave in direction x. According to Fig (5.10), (5.13), the local resonances determined by HPDM for the diagonal wave is the same as the pure compressive wave in x direction. According to CWFEM, the even modes and odd modes both lead to local resonances for diagonal waves. However, the HPDM can only deduce the resonance corresponding to the odd modes of the wall with two extremities fixed. And the wave 1 is not predicted by HPDM.

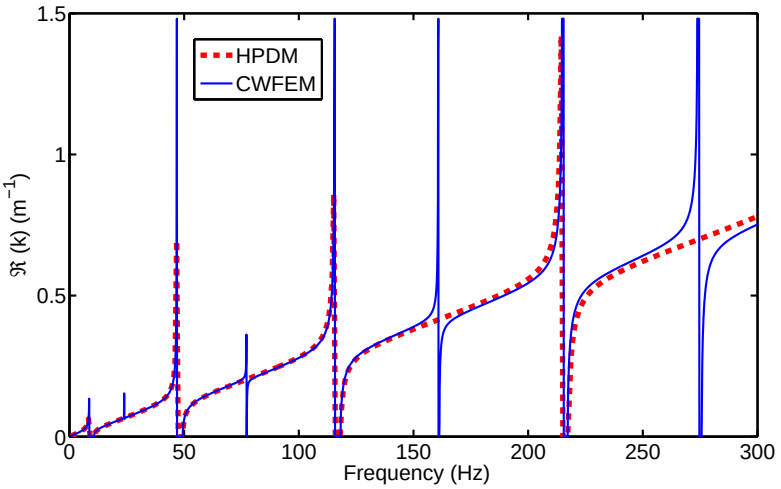

FIGURE 5.13: Wavenumber of longitudinal wave in 45° direction

5.5 Conclusion

This chapter investigates the wave propagation feature in a 2D infinite framed structure by both HPDM and CWFEM. As the element beam is oriented only according two directions, the studied structure is highly anisotropic. Thus, the wave properties depends on the direction. In this work, as the vertical element and the horizontal element have the same material properties, the wave travailing in the direction x is studied. The behaviour of the wave propagating in the y direction is supposed to be the same as the waves in x direction. At last, another wave in 45^o is also investigated and presented.

At low frequency $\omega = O(\epsilon\omega_r)$, the element have a quasi-static behaviour. The wavelength of bending and tension-compression are both larger than the unit cell length. The expanded series of axial force, shear force and moment are applied to the nodal balance equation. According to HPDM, only shear waves travailing in direction x or y exist. The pure shear wave is identified by CWFEM through the dispersion relation and the wave shape. The relative error of wavenumber determined by the two methods shows that HPMD gives a quite precise simulation of the low frequency behaviour.

Another studied frequency range is $\omega = O(\omega_r)$. In this case, the wavelength of bending is no longer larger than the unit cell length. The associated expanded series of shear force and moment are no longer applicable. New homogenization procedure is adapted to simulate the local resonance of the structure. According to HPDM, pure compression waves exits in the x or y direction, while the shear-compression wave travail

in the other direction. The pure compression wave is well identified by the CWFEM. The local resonance obtained by the two methods corresponds to each other. The presented wave shape verifies that the resonances appear at the odd modes of the wall with two endpoints fixed.

For the waves travelling in 45^o direction. Shear-compression waves with polarization in x direction are predicted by the HPDM. The wavenumber of the shear-compression wave varies with frequency and direction, and the local resonance of the diagonal wave correspond to the compression wave in x direction. However, according to CWFEM, three kinds of waves are identified. The shear-compression wave can be considered as the superposition of wave 2 and wave 3. The wave 1 is not predicted by HPDM. The local resonance obtained by CWFEM corresponds to all the modes of the wall with the endpoints fixed, while the only odd mode local resonance is predicted by HPDM.

Further investigation will extend the study to the braced framed structure or the wall different from the floor structure. It may be also interesting to study the contribution of the evanescent wave in the finite case to evaluate the error of the HPDM.

Chapter 6

Conclusions and Perspectives

6.1 Conclusions

The main contributions of the conducted work are summarized below:

- The asymptotic expansion method is used to deduce homogenized models for periodic structures. According to the classical homogenization theory, the dynamic behaviour of periodic structures at low frequency can be homogenized into an uniform structure, where the effective properties of the homogenized models are the mean values of the periodic structure. Taking mean values as effective values is an intuitionist approach to find homogenized models. However, the validity range of this model is very limited. In the opinion of asymptotic expansion method, the scale separation being satisfied, all the associated variables can be expanded into infinite series. It has been proved in the Introduction that the mean value homogenized model is, in fact, the wave equation obtained at leading order of the expanded displacement. Since the leading order model is very limited, higher order models are needed to give enriched models with larger validity range. Thus, the multi-scale asymptotic expansion method and the HPDM is used to find the 'more precise' homogenized models.

- In chapter 2, both methods are implemented on the typical case, the longitudinal waves travelling in bi-periodic rods. The same higher order homogenized models (HOH1 and HOH2) are deduced by the two method. Compared to traditional

model (TH), a higher order term (HOH1) or a time-space coupling term (HOH2) appears in the homogenized equation. The local behaviour caused by the periodicity is somehow presented by the additional term. In order to formulated the appropriate boundary conditions, the variational approach is used. Then investigations on dispersion relations and frequency response function are carried out to validate the higher order models. The periodicity of the structure has been considered in the homogenization process. Consequently, the investigation results show that the validity range in infinite case is enlarge by HOH1 and HOH2 models. As to finite case, HOH2 proves to be a more robust homogenized model.

- Following the longitudinal case, the transversal vibration of the bi-periodic beams is discussed in chapter 3. More periodicity conditions, displacement, rotation, moment, shear force, are considered, and higher order homogenized models (HOH1 and HOH2)for flexural waves are deduced by multi-scale expansion method and HPDM. In this case, both evanescent waves and propagating waves contribute to the dynamic behaviour of the structure. In order to deduce the reliable reference results, the WFEM method is used to deduce the dispersion relation and the frequency response functions. More accurate simulation results have been yielded by HOH1 and HOH for propagating waves and evanescent waves through the investigation of dispersion relations and the frequency response functions.

- In chapter 4, the studied subject is the 1D framed structure, which is a periodic structure composed by interconnected beams. The HPDM is used to provide homogenized models at leading order for longitudinal vibrations and transverse vibrations. The typical longitudinal wave equation serves as the continuous description of the structure's longitudinal vibration, while a sixth order wave equation is used for the continuous description of the transverse movement. By investigating the dispersion relation, the forced response and the natural frequency, the valid frequency range of HPDM homogenized model is re-evaluated by the CWFEM and ANSYS.

- The 2D framed structures case is discussed in chapter 5. In the 2D case, the waveguide is highly anisotropic, and waves propagate in preferred directions. According to the HPDM model, the discussed frequency range is divided by two characteristic frequencies: $\omega = O(\epsilon\omega_r)$, where the compressive wave and bending

wave can both be homogenized, and $\omega = O(\omega_r)$, where only the compressive wave can be homogenized. At the first frequency range, pure shear waves exist only in the element orientation direction. At the second frequency range, pure compressive waves propagate in the orientation direction, while the diagonal waves are shear-compressive type. The predicted shear waves at very low are identified by CWFEM. At $\omega = O(\omega_r)$, for the compressive wave in orientation direction, the local resonance caused by bending in wall are confirmed by CWFEM. But for diagonal waves, not all the wave identified by CWFEM are predicted by HPDM.

6.2 Perspectives

The periodic structure has attracted much attentions in both theory research and experiential fields. Apart form the direct simulation of the structure, multi-scale homogenization provides an approximated but analytical description of the periodic structure's dynamic behaviour. The continuous analytical formulation helps the understanding of the mechanisms governing the global behaviour. The suggested ideas for future studies are:

- The convergence of higher order models. In our studied rod or beam case, it has been proved that the higher order homogenized model (obtained at second order of expansion) decries more precisely the dynamic behaviour of periodic structure than the classical homogenized model (obtained at leading order). According to the expansion series, the higher order terms is a correction for the leading order. The higher order it takes, the better model it will deduce. However, whether it exits the limit of approximation or the exact dynamic behaviour will be fully described with all expansion considered. A convergence theory about the approximation limit needs to be discussed.

- The choice of the appropriate boundary conditions. In our studied case, the homogenized boundary conditions are formulated by the variational approach which keeps the energy conservation. However, some of the artificial boundary conditions have no physical explanations. The use of homogenised boundary conditions instead of real boundary conditions could introduce significant perturbations, which

appears in the HOH1 model of longitudinal case. More physical and reasonable explanations about the boundary conditions are needed.

- For the framed structure, the homogenized models are obtained at leading order. As there is no theoretical difficulty to derive them by carrying on further the same process, the study of the higher order terms would be interesting for a more accurate description, especially when the scale separation is weak. This approach can also be extended without theoretical difficulty to investigate more realistic structures, such as the braced framed structures, and the building where walls are different from walls and form different geometries.

- Including all the homogenized models, even if the local resonance can be predicted, the validity range is limited to the Bragg band gap. The researches on the expansion of homogenization on higher frequency is still not completed. The convergence study of the present homogenized theory may yield new enriched homogenization models which are capable of describing correctly the existence of the Bragg band gap.

Appendix A

Expansions in longitudinal periodic case

The axial force in longitudinal vibration of periodic rod are:

$$N^B = -Sp\frac{qu^E + (psin(ml)sin(nl) - qcos(ml)cos(nl))u^B}{pcos(ml)sin(nl) + qsin(ml)cos(nl)}$$
$$N^E = -Sq\frac{-pu^B + (pcos(ml)cos(nl) - qsin(ml)sin(nl))u^E}{pcos(ml)sin(nl) + qsin(ml)cos(nl)}$$

Series expansions of the associated coefficient in the axial force:

$$\frac{1}{pcos(ml)sin(nl) + qsin(ml)cos(nl)} = \frac{1}{(qm+pn)\,l} + \frac{\left(qm^3 + 3pm^2n + 3qmn^2 + pn^3\right)l}{6\,(qm+pn)^2} + O\left(l^3\right)$$

$$\frac{psin(ml)sin(nl) - qcos(ml)cos(nl)}{pcos(ml)sin(nl) + qsin(ml)cos(nl)} = -\frac{q}{(mq+np)\,l} + \frac{\left(m^3q^2 + 3\,m^2npq + 3\,mn^2p^2 + n^3pq\right)l}{3\,(mq+np)^2} + O\left(l^3\right)$$

$$\frac{pcos(ml)cos(nl) - qsin(ml)sin(nl)}{pcos(ml)sin(nl) + qsin(ml)cos(nl)} = \frac{p}{(mq+np)\,l} - \frac{(m^3pq + 3\,m^2nq^2 + 3\,mn^2pq + n^3p^2)l}{3\,(mq+np)^2} + O\left(l^3\right)$$

Then using $l = \epsilon L$, the series expansions with respect to ϵ are obtained.

Appendix B

Expansions in transversal periodic case

Linear equation system to deduce the moment and shear force.

$$\begin{pmatrix} u^B \\ \theta^B \\ M^B \\ T^B \end{pmatrix} = R \begin{pmatrix} u^E \\ \theta^E \\ M^E \\ T^E \end{pmatrix} \Rightarrow \begin{bmatrix} -1 & 0 & R_{33} & R_{34} \\ 0 & -1 & R_{43} & R_{44} \\ 0 & 0 & R_{13} & R_{14} \\ 0 & 0 & R_{23} & R_{24} \end{bmatrix} \begin{pmatrix} M^B \\ T^B \\ M^E \\ T^E \end{pmatrix} = \begin{pmatrix} -(R_{31}u^E + R_{32}\theta^E) \\ -(R_{41}u^E + R_{42}\theta^E) \\ u^B - (R_{11}u^E + R_{12}\theta^E) \\ \theta^B - (R_{21}u^E + R_{22}\theta^E) \end{pmatrix}$$

with $R = R_a R_b$. As $l = \epsilon L$ and $\epsilon \ll 1$, the moment and shear force can be expanded with respect to ϵ. Here are the coefficients in the series expanded.
For the moment, we have:

$$m_1 = \frac{-6E_aE_bI\,\left(\left(\alpha^2-1\right)E_a - E_b\,\alpha^2\right)}{\left(-1+\alpha\right)^4 {E_a}^2 - 2\,E_b\,\alpha\,\left(-1+\alpha\right)\left(\alpha^2-\alpha+2\right)E_a + {E_b}^2\alpha^4}$$

$$m_2 = \frac{-4E_aE_bI\left(\left(E_a-E_b\right)\alpha^3 - E_a\right)}{\left(E_a-E_b\right)^2\alpha^4 - 4E_a\left(E_a-E_b\right)\alpha^3 + 6E_a\left(E_a-E_b\right)\alpha^2 - 4E_a\left(E_a-E_b\right)\alpha + {E_a}^2}$$

$$m_3 = \frac{-E_aE_bI\left(-4\left(E_a-E_b\right)\alpha^3 + 6\left(E_a-E_b\right)\alpha^2 - 2E_a\right)}{\left(E_a-E_b\right)^2\alpha^4 - 4E_a\left(E_a-E_b\right)\alpha^3 + 6E_a\left(E_a-E_b\right)\alpha^2 - 4E_a\left(E_a-E_b\right)\alpha + {E_a}^2}$$

$$m_8 = \frac{-6E_aE_bI\left(\left(E_a-E_b\right)\alpha^2 + \left(-2\,E_a+2\,E_b\right)\alpha + E_a\right)}{\left(E_a-E_b\right)^2\alpha^4 - 4\,E_a\,\left(E_a-E_b\right)\alpha^3 + 6\,E_a\,\left(E_a-E_b\right)\alpha^2 - 4\,E_a\,\left(E_a-E_b\right)\alpha + {E_a}^2}$$

$$m_9 = \frac{-E_aE_bI\left(4\left(E_a-E_b\right)\alpha^3 - 6\left(E_a-E_b\right)\alpha^2 + 2E_a\right)}{\left(E_a-E_a\right)^2\alpha^4 - 4E_a\,\left(E_a-E_b\right)\alpha^3 + 6E_a\left(E_a-E_b\right)\alpha^2 - 4E_A\left(E_a-E_b\right)\alpha + {E_a}^2}$$

$$m_{10} = \frac{-4E_aE_bI\left(-\left(E_a-E_b\right)\alpha^3+3\left(E_a-E_b\right)\alpha^2-3\left(E_a-E_b\right)\alpha+E_a\right)}{\left(E_a-E_b\right)^2\alpha^4-4E_a\left(E_a-E_b\right)\alpha^3+6E_a\left(E_a-E_b\right)\alpha^2-4E_a\left(E_a-E_b\right)\alpha+{E_b}^2}$$

The other coefficients of moment are too long to write, but here are some useful conclusions: $m_1 - m_8 = -(m_9 + m_{10} - m_3 - m_2), m_3 + m_9 = 0$

For the shear force, we have

$$t_1 = \frac{-12E_aE_bI\left(\left(-1+\alpha\right)E_a-E_b\alpha\right)}{\left(-1+\alpha\right)^4{E_a}^2-2E_b\alpha\left(-1+\alpha\right)\left(\alpha^2-\alpha+2\right)E_a+{E_b}^2\alpha^4}$$

$$t_2 = \frac{-6E_aE_bI\left(\left(E_a-E_b\right)\alpha^2-E_a\right)}{\left(E_a-E_b\right)^2\alpha^4-4E_a\left(E_a-E_b\right)\alpha^3+6E_a\left(E_a-E_b\right)\alpha^2-4E_a\left(E_a-E_b\right)\alpha+{E_a}^2}$$

$$t_3 = \frac{-6E_aE_bI\left(-\left(E_a-E_b\right)\alpha^2+2\left(E_a-E_b\right)\alpha-E_a\right)}{\left(E_a-E_b\right)^2\alpha^4-4E_a\left(E_a-E_b\right)\alpha^3+6E_a\left(E_a-E_b\right)\alpha^2-4E_a\left(E_a-E_b\right)\alpha+{E_a}^2}$$

$$t_8 = \frac{-12E_aE_bI\left(\left(-1+\alpha\right)E_a-E_b\alpha\right)}{\left(-1+\alpha\right)^4{E_a}^2-2E_b\alpha\left(-1+\alpha\right)\left(\alpha^2-\alpha+2\right)E_a+{E_b}^2\alpha^4}$$

$$t_9 = \frac{-6E_aE_bI\left(\left(E_a-E_b\right)\alpha^2-E_a\right)}{\left(E_a-E_b\right)^2\alpha^4-4E_a\left(E_a-E_b\right)\alpha^3+6E_a\left(E_a-E_b\right)\alpha^2-4E_a\left(E_a-E_b\right)\alpha+{E_a}^2}$$

$$t_{10} = \frac{-6E_aE_bI\left(-\left(E_a-E_b\right)\alpha^2+2\left(E_a-E_b\right)\alpha-E_a\right)}{\left(E_a-E_b\right)^2\alpha^4-4E_a\left(E_a-E_b\right)\alpha^3+6E_a\left(E_a-E_b\right)\alpha^2-4E_a\left(E_a-E_b\right)\alpha+{E_a}^2}$$

For the same reason, the other coefficients of shear force are not present, but here are some useful conclusions: $t_1 = t_8, t_2 = t_9, t_3 = t_{10}, t_8 + t_1 = 2(t_9 + t_3), t_{11} + t_5 = 0$

Appendix C

Appropriate boundary conditions for equation of U

For clamped boundary condition:

$$U = 0 \tag{C.1a}$$

$$U' = 0 \tag{C.1b}$$

$$2E_w I_w U'''' - \Lambda\omega^2 U' - KU''' = 0 \tag{C.1c}$$

For free boundary condition:

$$-2E_w^2 I I_w U'''' + \omega^2 E_w I \Lambda U' + E_w I K U''' + 2E_w I_w K U''' = 0 \tag{C.2a}$$

$$2E_w I_w U'''' - \Lambda\omega^2 U - KU'' = 0 \tag{C.2b}$$

$$U'' = 0 \tag{C.2c}$$

For simply-supported boundary condition:

$$U = 0 \tag{C.3a}$$

$$2E_w I_w U'''' - \Lambda\omega^2 U - KU'' = 0 \tag{C.3b}$$

$$U'' = 0 \tag{C.3c}$$

Bibliography

[1] MM Sigalas and EN Economou. Elastic and acoustic wave band structure. *Journal of sound and vibration*, 158(2):377–382, 1992.

[2] M Sigalas and EN Economou. Band structure of elastic waves in two dimensional systems. *Solid State Communications*, 86(3):141–143, 1993.

[3] Manvir S Kushwaha, P Halevi, L Dobrzynski, and B Djafari-Rouhani. Acoustic band structure of periodic elastic composites. *Physical Review Letters*, 71(13): 2022, 1993.

[4] Manvir S Kushwaha, P Halevi, G Martinez, L Dobrzynski, and B Djafari-Rouhani. Theory of acoustic band structure of periodic elastic composites. *Physical Review B*, 49(4):2313, 1994.

[5] Zhengyou Liu, Xixiang Zhang, Yiwei Mao, YY Zhu, Zhiyu Yang, CT Chan, and Ping Sheng. Locally resonant sonic materials. *Science*, 289(5485):1734–1736, 2000.

[6] NS Bakhvalov. Averaging of partial differential equations with rapidly oscillating coefficients. *Current problems of mathematical physics and computational mathematics.(A 83-20302 07-70) Moscow, Izdatel'stvo Nauka, 1982,*, pages 38–47, 1982.

[7] Alain Bensoussan, Jacques-Louis Lions, and George Papanicolaou. *Asymptotic analysis for periodic structures*, volume 374. American Mathematical Soc., 2011.

[8] Luc Tartar. Compensated compactness and applications to partial differential equations. In *Nonlinear analysis and mechanics, Heriot-Watt symposium*, volume 4, pages 136–211. Pitman, 1979.

[9] François Murat. Compacité par compensation. *Annali della Scuola Normale Superiore di Pisa-Classe di Scienze*, 5(3):489–507, 1978.

[10] Gabriel Nguetseng. A general convergence result for a functional related to the theory of homogenization. *SIAM Journal on Mathematical Analysis*, 20(3):608–623, 1989.

[11] Doina Cioranescu, Alain Damlamian, and Georges Griso. Periodic unfolding and homogenization. *Comptes Rendus Mathematique*, 335(1):99–104, 2002.

[12] Isaac Newton. *The Principia: mathematical principles of natural philosophy*. Univ of California Press, 1999.

[13] John William Strutt Baron Rayleigh. *The theory of sound*, volume 2. Macmillan, 1896.

[14] C-T Sun, JD Achenbach, and G Herrmann. Time-harmonic waves in a stratified medium propagating in the direction of the layering. *Journal of Applied Mechanics*, 35(2):408–411, 1968.

[15] S Nemat-Nasser. General variational methods for waves in elastic composites. *Journal of Elasticity*, 2(2):73–90, 1972.

[16] DJ Mead. A general theory of harmonic wave propagation in linear periodic systems with multiple coupling. *Journal of Sound and Vibration*, 27(2):235–260, 1973.

[17] DJ Ewins. Vibration characteristics of bladed disc assemblies. *Journal of Mechanical Engineering Science*, 15(3):165–186, 1973.

[18] JH Griffin and TM Hoosac. Model development and statistical investigation of turbine blade mistuning. *Journal of Vibration, Acoustics, Stress, and Reliability in Design*, 106(2):204–210, 1984.

[19] Matthew P Castanier, G Ottarsson, and Christophe Pierre. A reduced order modeling technique for mistuned bladed disks. *Journal of Vibration and Acoustics*, 119(3):439–447, 1997.

[20] VS Deshpande and NA Fleck. High strain rate compressive behaviour of aluminium alloy foams. *International Journal of Impact Engineering*, 24(3):277–298, 2000.

[21] Md Akil Hazizan and WJ Cantwell. The low velocity impact response of foam-based sandwich structures. *Composites Part B: Engineering*, 33(3):193–204, 2002.

[22] MOW Richardson and MJ Wisheart. Review of low-velocity impact properties of composite materials. *Composites Part A: Applied Science and Manufacturing*, 27 (12):1123–1131, 1996.

[23] NA Fleck and VS Deshpande. The resistance of clamped sandwich beams to shock loading. *Journal of Applied Mechanics*, 71(3):386–401, 2004.

[24] Jing Bao, Zhifei Shi, and Hongjun Xiang. Dynamic responses of a structure with periodic foundations. *Journal of Engineering Mechanics*, 138(7):761–769, 2011.

[25] Michele Brun, Alexander B Movchan, and Ian S Jones. Phononic band gap systems in structural mechanics: Finite slender elastic structures and infinite periodic waveguides. *Journal of Vibration and Acoustics*, 135(4):041013, 2013.

[26] Mahmoud I Hussein, Michael J Leamy, and Massimo Ruzzene. Dynamics of phononic materials and structures: Historical origins, recent progress, and future outlook. *Applied Mechanics Reviews*, 66(4):040802, 2014.

[27] Douglas Thorby. *Structural dynamics and vibration in practice: an engineering handbook*. Butterworth-Heinemann, 2008.

[28] Tao Chen and Ligang Wang. Suppression of bending waves in a periodic beam with timoshenko beam theory. *Acta Mechanica Solida Sinica*, 26(2):177–188, 2013.

[29] Dianlong Yu, Jianyu Fang, Li Cai, Xiaoyun Han, and Jihong Wen. Triply coupled vibrational band gap in a periodic and nonsymmetrical axially loaded thin-walled bernoulli–euler beam including the warping effect. *Physics Letters A*, 373(38): 3464–3469, 2009.

[30] Yan Gao, Michael J Brennan, and Fusheng Sui. Control of flexural waves on a beam using distributed vibration neutralisers. *Journal of Sound and Vibration*, 330(12):2758–2771, 2011.

[31] Yong Xiao, Brian R Mace, Jihong Wen, and Xisen Wen. Formation and coupling of band gaps in a locally resonant elastic system comprising a string with attached resonators. *Physics Letters A*, 375(12):1485–1491, 2011.

[32] L Houillon, MN Ichchou, and L Jezequel. Wave motion in thin-walled structures. *Journal of Sound and Vibration*, 281(3):483–507, 2005.

[33] TL Huang, MN Ichchou, OA Bareille, M Collet, and M Ouisse. Traveling wave control in thin-walled structures through shunted piezoelectric patches. *Mechanical Systems and Signal Processing*, 39(1):59–79, 2013.

[34] J-M Mencik and MN Ichchou. Wave finite elements in guided elastodynamics with internal fluid. *International Journal of Solids and Structures*, 44(7):2148–2167, 2007.

[35] WJ Zhou and MN Ichchou. Wave propagation in mechanical waveguide with curved members using wave finite element solution. *Computer Methods in Applied Mechanics and Engineering*, 199(33):2099–2109, 2010.

[36] DJ Mead. Wave propagation and natural modes in periodic systems: I. mono-coupled systems. *Journal of Sound and Vibration*, 40(1):1–18, 1975.

[37] DJ Mead. Wave propagation and natural modes in periodic systems: Ii. multi-coupled systems, with and without damping. *Journal of Sound and Vibration*, 40 (1):19–39, 1975.

[38] WX Zhong and FW Williams. On the direct solution of wave propagation for repetitive structures. *Journal of Sound and Vibration*, 181(3):485–501, 1995.

[39] Denis Duhamel, Brian R Mace, and Michael J Brennan. Finite element analysis of the vibrations of waveguides and periodic structures. *Journal of sound and vibration*, 294(1):205–220, 2006.

[40] Denys J Mead. The forced vibration of one-dimensional multi-coupled periodic structures: an application to finite element analysis. *Journal of Sound and Vibration*, 319(1):282–304, 2009.

[41] Brian R Mace, Denis Duhamel, Michael J Brennan, and Lars Hinke. Finite element prediction of wave motion in structural waveguides. *The Journal of the Acoustical Society of America*, 117(5):2835–2843, 2005.

[42] Y Waki, BR Mace, and MJ Brennan. Numerical issues concerning the wave and finite element method for free and forced vibrations of waveguides. *Journal of Sound and Vibration*, 327(1):92–108, 2009.

[43] CW Zhou, JP Lainé, MN Ichchou, and AM Zine. Numerical and experimental investigation on broadband wave propagation features in perforated plates. *Mechanical Systems and Signal Processing*, 75:556–575, 2016.

[44] CW Zhou, JP Lainé, MN Ichchou, and AM Zine. Multi-scale modelling for two-dimensional periodic structures using a combined mode/wave based approach. *Computers & Structures*, 154:145–162, 2015.

[45] J-M Mencik and MN Ichchou. A substructuring technique for finite element wave propagation in multi-layered systems. *Computer Methods in Applied Mechanics and Engineering*, 197(6):505–523, 2008.

[46] J-M Mencik. A model reduction strategy for computing the forced response of elastic waveguides using the wave finite element method. *Computer Methods in Applied Mechanics and Engineering*, 229:68–86, 2012.

[47] C Droz, J-P Lainé, MN Ichchou, and G Inquiété. A reduced formulation for the free-wave propagation analysis in composite structures. *Composite Structures*, 113: 134–144, 2014.

[48] C Droz, C Zhou, MN Ichchou, and J-P Lainé. A hybrid wave-mode formulation for the vibro-acoustic analysis of 2d periodic structures. *Journal of Sound and Vibration*, 363:285–302, 2016.

[49] Y Waki, BR Mace, and MJ Brennan. Free and forced vibrations of a tyre using a wave/finite element approach. *Journal of Sound and Vibration*, 323(3):737–756, 2009.

[50] CW Zhou, JP Lainé, MN Ichchou, and AM Zine. Wave finite element method based on reduced model for one-dimensional periodic structures. *International Journal of Applied Mechanics*, 7(02):1550018, 2015.

[51] Mervyn CC Bampton and Roy R CRAIG, JR. Coupling of substructures for dynamic analyses. *Aiaa Journal*, 6(7):1313–1319, 1968.

[52] D-M Tran. Component mode synthesis methods using interface modes. application to structures with cyclic symmetry. *Computers & Structures*, 79(2):209–222, 2001.

[53] GML Gladwell. Branch mode analysis of vibrating systems. *Journal of sound and vibration*, 1(1):41–59, 1964.

[54] S Nemat-Nasser, T Iwakuma, and M Hejazi. On composites with periodic structure. *Mechanics of materials*, 1(3):239–267, 1982.

[55] Gang Wang, Shaofan Li, Hoang-Nam Nguyen, and Nicholas Sitar. Effective elastic stiffness for periodic masonry structures via eigenstrain homogenization. *Journal of materials in civil engineering*, 19(3):269–277, 2007.

[56] Weihong Zhang, Fengwen Wang, Gaoming Dai, and Shiping Sun. Topology optimal design of material microstructures using strain energy-based method. *Chinese journal of aeronautics*, 20(4):320–326, 2007.

[57] KS Challagulla, AV Georgiades, and AL Kalamkarov. Asymptotic homogenization modeling of smart composite generally orthotropic grid-reinforced shells: Part i–theory. *European Journal of Mechanics-A/Solids*, 29(4):530–540, 2010.

[58] AV Georgiades, KS Challagulla, and AL Kalamkarov. Asymptotic homogenization modeling of smart composite generally orthotropic grid-reinforced shells: Part ii–applications. *European Journal of Mechanics-A/Solids*, 29(4):541–556, 2010.

[59] AL Kalamkarov, EM Hassan, AV Georgiades, and MA Savi. Asymptotic homogenization model for 3d grid-reinforced composite structures with generally orthotropic reinforcements. *Composite structures*, 89(2):186–196, 2009.

[60] Antonella Cecchi and Nicola L Rizzi. Heterogeneous elastic solids: a mixed homogenization-rigidification technique. *International journal of solids and structures*, 38(1):29–36, 2001.

[61] Myung-Jo Jhung and Jong-Chull Jo. Equivalent material properties of perforated plate with triangular or square penetration pattern for dynamic analysis. *Nuclear engineering and technology*, 38(7):689–696, 2006.

[62] W-C Wang and K-H Lai. Hybrid determination of equivalent characteristics of perforated plates. *Experimental mechanics*, 43(2):163–172, 2003.

[63] D Chronopoulos, B Troclet, O Bareille, and M Ichchou. Modeling the response of composite panels by a dynamic stiffness approach. *Composite Structures*, 96: 111–120, 2013.

[64] RV Craster, J Kaplunov, and AV Pichugin. High-frequency homogenization for periodic media. In *Proceedings of the Royal Society of London A: Mathematical, Physical and Engineering Sciences*, volume 466, pages 2341–2362. The Royal Society, 2010.

[65] RV Craster, J Kaplunov, and J Postnova. High-frequency asymptotics, homogenisation and localisation for lattices. *The Quarterly Journal of Mechanics and Applied Mathematics*, 63(4):497–519, 2010.

[66] D. Mead. Wave propagation in continuous periodic structures: research contributions from southampton, 1964–1995. *Journal of Sound and Vibration*, 190(3): 495–524, 1996.

[67] Léon Brillouin. *Wave propagation in periodic structures: electric filters and crystal lattices*. Courier Corporation, 2003.

[68] Changsheng Li, Dan Huang, Jierong Guo, and Jianjun Nie. Engineering of band gap and cavity mode in phononic crystal strip waveguides. *Physics Letters A*, 377 (38):2633–2637, 2013.

[69] Gaston Floquet. Sur les équations différentielles linéaires à coefficients périodiques. In *Annales scientifiques de l'École normale supérieure*, volume 12, pages 47–88, 1883.

[70] Charles Kittel. *Introduction to solid state*. John Wiley & Sons, 1966.

[71] Felix Bloch. Über die quantenmechanik der elektronen in kristallgittern. *Zeitschrift für physik*, 52(7-8):555–600, 1929.

[72] D Mead and S Lee. Receptance methods and the dynamics of disordered one-dimensional lattices. *Journal of Sound and Vibration*, 92(3):427–445, 1984.

[73] Yu-Kweng Lin and TJ McDaniel. Dynamics of beam-type periodic structures. *Journal of Manufacturing Science and Engineering*, 91(4):1133–1141, 1969.

[74] J-H Lee and J Kim. Analysis of sound transmission through periodically stiffened panels by space-harmonic expansion method. *Journal of Sound and Vibration*, 251 (2):349–366, 2002.

[75] Brian R Mace, Denis Duhamel, Michael J Brennan, and Lars Hinke. Finite element prediction of wave motion in structural waveguides. *The Journal of the Acoustical Society of America*, 117(5):2835–2843, 2005.

[76] M Kharrat, M.N Ichchou, O. Bareille, and W Zhou. Pipeline inspection using a torsional guided-waves inspection system. part 2: Defect sizing by the wave finite element method. *International Journal of Applied Mechanics*, 6(04):1450035, 2014.

[77] C. W. Zhou, J. P. Lainé, M. N. Ichchou, and a. M. Zine. Wave Finite Element Method Based on Reduced Model for One-Dimensional Periodic Structures. *International Journal of Applied Mechanics*, 07(02):1550018, 2015.

[78] Andrei V Metrikine and Harm Askes. One-dimensional dynamically consistent gradient elasticity models derived from a discrete microstructure: Part 1: Generic formulation. *European Journal of Mechanics-A/Solids*, 21(4):555–572, 2002.

[79] Harm Askes and Andrei V Metrikine. One-dimensional dynamically consistent gradient elasticity models derived from a discrete microstructure: Part 2: Static and dynamic response. *European Journal of Mechanics-A/Solids*, 21(4):573–588, 2002.

[80] Harm Askes, Andrei V Metrikine, Aleksey V Pichugin, and Terry Bennett. Four simplified gradient elasticity models for the simulation of dispersive wave propagation. *Philosophical Magazine*, 88(28-29):3415–3443, 2008.

[81] Harm Askes and Elias C Aifantis. Gradient elasticity in statics and dynamics: an overview of formulations, length scale identification procedures, finite element implementations and new results. *International Journal of Solids and Structures*, 48(13):1962–1990, 2011.

[82] Egor V Dontsov, Roman D Tokmashev, and Bojan B Guzina. A physical perspective of the length scales in gradient elasticity through the prism of wave dispersion. *International Journal of Solids and Structures*, 50(22):3674–3684, 2013.

[83] E Sanchez-Palencia. Homogenization method for the study of composite media. In *Asymptotic Analysis II—*, pages 192–214. 1983.

[84] Enrique Sanchez-Palencia and André Zaoui. Homogenization techniques for composite media. In *Homogenization Techniques for Composite Media*, volume 272, 1987.

[85] Alain Bensoussan, Jacques-Louis Lions, and George Papanicolaou. *Asymptotic analysis for periodic structures*, volume 374. American Mathematical Soc., 1978.

[86] Jean-Louis Auriault, Claude Boutin, and Christian Geindreau. *Homogenization of coupled phenomena in heterogenous media*, volume 1. Wiley Online Library, 2009.

[87] Vasilii Vasil'evich Jikov, Sergei M Kozlov, and Olga Arsen'evna Oleinik. *Homogenization of differential operators and integral functionals*. Springer Science & Business Media, 2012.

[88] Gabriel Nguetseng. A general convergence result for a functional related to the theory of homogenization. *SIAM Journal on Mathematical Analysis*, 20(3):608–623, 1989.

[89] Doina Cioranescu, Alain Damlamian, and Georges Griso. Periodic unfolding and homogenization. *Comptes Rendus Mathematique*, 335(1):99–104, 2002.

[90] Sebastien Guenneau, Richard Craster, Tryfon Antonakakis, Kirill Cherednichenko, and Shane Cooper. Homogenization techniques for periodic structures. *arXiv preprint arXiv:1304.7519*, 2013.

[91] Jacob Fish and Wen Chen. Higher-order homogenization of initial/boundary-value problem. *Journal of engineering mechanics*, 127(12):1223–1230, 2001.

[92] Jacob Fish, Wen Chen, and Gakuji Nagai. Non-local dispersive model for wave propagation in heterogeneous media: one-dimensional case. *International Journal for Numerical Methods in Engineering*, 54(3):331–346, 2002.

[93] Igor V Andrianov, Vladimir I Bolshakov, Vladyslav V Danishevs' kyy, and Dieter Weichert. Higher order asymptotic homogenization and wave propagation in periodic composite materials. In *Proceedings of the Royal Society of London A: Mathematical, Physical and Engineering Sciences*, volume 464, pages 1181–1201. The Royal Society, 2008.

[94] Ahmed K Noor. Continuum modeling for repetitive lattice structures. *Applied Mechanics Reviews*, 41(7):285–296, 1988.

[95] John D Renton. The beam-like behavior of space trusses. *AIAA journal*, 22(2): 273–280, 1984.

[96] Enrique Sánchez-Palencia. Non-homogeneous media and vibration theory. In *Non-homogeneous media and vibration theory*, volume 127, 1980.

[97] Doina Cioranescu and Jeannine Saint Jean Paulin. *Homogenization of reticulated structures*, volume 136. Springer Science & Business Media, 2012.

[98] D Caillerie, P Trompette, and P Verna. Homogenisation of periodic trusses. *congrès IASS*, pages 7139–7180, 1989.

[99] C Boutin and S Hans. Homogenisation of periodic discrete medium: Application to dynamics of framed structures. *Computers and Geotechnics*, 30(4):303–320, 2003.

[100] Stephane Hans and Claude Boutin. Dynamics of discrete framed structures: a unified homogenized description. *Journal of mechanics of materials and structures*, 3(9):1709–1739, 2008.

[101] C Chesnais, C Boutin, and S Hans. Effects of the local resonance on the dynamic behavior of periodic frame structures. *Wave Motion*, 57:3447–3454, 2015.

[102] Gaston Floquet. Sur les équations différentielles linéaires à coefficients périodiques. In *Annales scientifiques de l'École normale supérieure*, volume 12, pages 47–88, 1883.

[103] Felix Bloch. Über die quantenmechanik der elektronen in kristallgittern. *Zeitschrift für physik*, 52(7-8):555–600, 1929.

[104] C. Droz, J.-P. Lainé, M.N. Ichchou, and G. Inquiété. A reduced formulation for the free-wave propagation analysis in composite structures. *Composite Structures*, 113:134–144, jul 2014.

[105] Y. Fan, M. Collet, M. Ichchou, L. Li, O. Bareille, and Z. Dimitrijevic. Energy flow prediction in built-up structures through a hybrid finite element/wave and finite element approach. *Mechanical Systems and Signal Processing*, 67:137–158, 2015. ISSN 08883270.

[106] C. Droz, C. W. Zhou, M. N. Ichchou, and J. P. Lainé. A hybrid wave-mode formulation for the vibro-acoustic analysis of 2D periodic structures. *Journal of Sound and Vibration*, 363:285–302, 2016. ISSN 0022460X.

[107] C. W. Zhou, J. P. Lainé, M. N. Ichchou, and A. M. Zine. Wave Finite Element Method Based on Reduced Model for One-Dimensional Periodic Structures. *International Journal of Applied Mechanics*, 07(02):1550018, 2015. ISSN 1758-8251.

[108] C.W. Zhou, J.P. Lainé, M.N. Ichchou, and A.M. Zine. Multi-scale modelling for two-dimensional periodic structures using a combined mode/wave based approach. *Computers & Structures*, 154:145–162, 2015.

[109] C. W. Zhou, J. P. Lainé, M. N. Ichchou, and A. M. Zine. Numerical and experimental investigation on broadband wave propagation features in perforated plates. *Mechanical Systems and Signal Processing*, 75:556–575, 2016. ISSN 08883270.

[110] R.S Langley. Some perspectives on wave-mode duality in SEA. In *IUTAM Symposium on Statistical Energy Analysis*, pages 1–12. Springer, 1997.

[111] Y Fan, M Collet, M Ichchou, L Li, O Bareille, and Z Dimitrijevic. A wave-based design of semi-active piezoelectric composites for broadband vibration control. *Smart Materials and Structures*, 25(5):055032, 2016.

[112] Liao Liu and Mahmoud I Hussein. Wave motion in periodic flexural beams and characterization of the transition between bragg scattering and local resonance. *Journal of Applied Mechanics*, 79(1):011003, 2012.

[113] Celine Chesnais, S. Hans, and Claude Boutin. Dynamics of Reticulated Structures: Evidence of Atypical Gyration Modes. *International Journal for Multiscale Computational Engineering*, 9(5):515–528, 2011.

[114] Léon Brillouin. *Wave Propagation in Periodic Structures*. Dover Publication, New York, 2 edition, 2003.

[115] PG Martinsson and AB Movchan. Vibrations of lattice structures and phononic band gaps. *The Quarterly Journal of Mechanics and Applied Mathematics*, 56(1): 45–64, 2003.

[116] Ying Wu, Yun Lai, and Zhao-Qing Zhang. Effective medium theory for elastic metamaterials in two dimensions. *Physical Review B*, 76(20):205313, 2007.

[117] RS Langley. The response of two-dimensional periodic structures to point harmonic forcing. *Journal of sound and vibration*, 197(4):447–469, 1996.

[118] Massimo Ruzzene, Fabrizio Scarpa, and Francesco Soranna. Wave beaming effects in two-dimensional cellular structures. *Smart materials and structures*, 12(3):363, 2003.

[119] A Srikantha Phani, J Woodhouse, and NA Fleck. Wave propagation in two-dimensional periodic lattices. *The Journal of the Acoustical Society of America*, 119(4):1995–2005, 2006.

[120] Céline Chesnais, Claude Boutin, and Stéphane Hans. Effects of the local resonance on the wave propagation in periodic frame structures: Generalized newtonian mechanics. *The Journal of the Acoustical Society of America*, 132(4):2873–2886, 2012.

[121] B. R. Mace and E. Manconi. Modelling wave propagation in two-dimensional structures using finite element analysis. *Journal of Sound and Vibration*, 318 (4-5):884–902, December 2008.

[122] D. J. Ewins. *Modal Testing: Theory and Practice*. Johy Wiley & Sons Inc, New York, 1984.